The University of Maine
DigitalCommons@UMaine

Electronic Theses and Dissertations | Fogler Library

Summer 8-17-2018

Molecular Mechanisms Underlying Toxicant Effects on Mast Cell Signaling and Mitochondria

Juyoung Katherine Shim
University of Maine, juyoung.shim@maine.edu

Follow this and additional works at: https://digitalcommons.library.umaine.edu/etd

 Part of the Molecular Biology Commons, and the Toxicology Commons

Recommended Citation
Shim, Juyoung Katherine, "Molecular Mechanisms Underlying Toxicant Effects on Mast Cell Signaling and Mitochondria" (2018). *Electronic Theses and Dissertations*. 2909.
https://digitalcommons.library.umaine.edu/etd/2909

This Open-Access Thesis is brought to you for free and open access by DigitalCommons@UMaine. It has been accepted for inclusion in Electronic Theses and Dissertations by an authorized administrator of DigitalCommons@UMaine. For more information, please contact um.library.technical.services@maine.edu.

MOLECULAR MECHANISMS UNDERLYING TOXICANT EFFECTS ON MAST CELL SIGNALING AND MITOCHONDRIA

By

Juyoung K. Shim

B.A. Hankook University of Foreign Studies, 1994

B.S. Bates College, 2005

A DISSERTATION

Submitted in Partial Fulfillment of the

Requirements for the Degree of

Doctor of Philosophy

(in Biochemistry and Molecular Biology)

The Graduate School

The University of Maine

August 2018

Advisory Committee:

Julie A. Gosse, Associate Professor of Biochemistry; Advisor

John T. Singer, Professor of Microbiology

Paul J. Millard, Associate Professor of Chemical and Biological Engineering

Rebecca J. Van Beneden, Professor of Biochemistry and Marine Sciences, Director for School of Marine Sciences

Robert E. Gundersen, Chair of Molecular and Biomedical Sciences

© 2018 Juyoung Katherine Shim

All Rights Reserved

MOLECULAR MECHANISMS UNDERLYING TOXICANT EFFECTS ON MAST CELL SIGNALING AND MITOCHONDRIA

By Juyoung K. Shim

Dissertation Advisor: Dr. Julie A. Gosse

An Abstract of the Dissertation Presented
in Partial Fulfillment of the Requirements for the
Degree of Doctor of Philosophy
(in Biochemistry and Molecular Biology)
August 2018

Mast cells contribute to numerous physiological processes and diseases including immunological and neurological roles. Mast cells degranulate, releasing potent mediators, following signal transduction initiated by receptor crosslinking. Previously, we showed that the environmental toxicant arsenic and the antibacterial agent triclosan inhibit mast cell degranulation; thus, we have investigated the mechanisms underlying their inhibitory action. We have discovered that arsenic targets early steps in the mast cell signaling pathway: it inhibits phosphorylation of early tyrosine kinase Syk and of Syk's direct substrate PI3K. Arsenic's tyrosine phosphorylation inhibition causes inhibition of calcium influx into the cytosol, a key event necessary for degranulation.

Pharmaceutical agent triclosan also inhibits calcium influx but, in contrast to arsenic, does not inhibit early steps in the pathway. We have discovered that one of triclosan's targets in the mast cell signaling pathway is phospholipase D (PLD): PLD activity is decreased by triclosan. Triclosan does not inhibit activity of key enzyme protein kinase C but does delay its translocation to the plasma membrane and translocation of its substrate MARCKS to the cytosol. In addition, we have shown that another mechanism of triclosan toxicity, mitochondrial uncoupling, also occurs *in vivo*. We developed a high-throughput assay to measure bioenergetics

of living zebrafish embryos and showed that triclosan exposure decreases ATP production without causing mortality of zebrafish.

Finally, in preparation for comparative studies of toxicant effects on mast cells *in vivo* using zebrafish and *in vitro* using the mast cell model RBL-2H3, we aimed to develop a tryptase assay of mast cell degranulation that could be used in both systems. However, we discovered that RBL-2H3 cells express neither mRNA nor protein of several tryptase genes. Overall, the findings in this thesis provide biochemical and cellular explanations for known human health effects of triclosan and arsenic and set the stage for future comparative toxicology studies of mast cell function.

DEDICATION

To my husband, Changsu K. Lee and my daughter, Hana “Alexa” L. Lee

And to my parents and families

ACKNOWLEDGEMENTS

I feel very fortunate to have met, encountered, and acquainted myself with many amazing people during my graduate work, and though I may have missed some of the names here that deserve recognition, I would like to express my sincere thanks to all.

Foremost, I cannot give enough thanks to my advisor, Dr. Julie Gosse, for her guidance throughout my studies. She has provided tremendous support and timely (often-necessary) encouragement. She is one of the most dedicated teachers I have ever encountered and truly cares about her students' overall wellbeing. She taught me through experimental problem solving, critical thinking, and scientific writing more than I could give her credit for here. Thank you!

I would also like to thank my committee members, Drs. John Singer, Robert Gundersen, Rebecca Van Beneden, and Paul Millard for their extensive personal and professional guidance. You are the best (and the only) committee I could ever ask for. I also appreciate your congenial correspondence whenever I needed extra help.

My work here would not have been possible without colleagues and collaborators who have contributed to my research. Dr. Rachel Kennedy and Dr. Lisa Weatherly have been more than officemates, and who have been my best supporters and helpers to pull through scientific problems and personal hardships. I would also like to thank Suraj Sangroula and Siham Hattab for assisting me with confocal experiments. Richard Luc assisted me tremendously in zebrafish experiments, Tyler McGathey provided much moral support during my preparations for the comprehensive exam. I thank Atefeh Rajaei for her input in writing the tryptase paper and Andrew Hart for his help on the tubulin assay. Dr. Remi Gratacap also helped me greatly with

confocal experiments, zebrafish experiments, and the comprehensive exam. I would like to thank him especially for his sympathetic ear.

My collaborative works outside of my department have been successful thanks to these wonderful people: Dr. Heather Hamlin and her student Sarah Conlin (Department of Marine Biology) were a pleasure to work with. I am grateful for their part of the work to yield a publication. I also want to thank the Dr. Marie Hayes Laboratory for giving me an opportunity to work on an oxytocin project. Special thanks to Andy Neilson and Ryan Ng for providing me the equipment, reagents, and helpful advice for zebrafish bioenergetics experiments. Their assistance was indispensable to complete the project.

My time in the Gosse lab provided me the opportunity to work with many wonderful undergraduate students. I am grateful to all of them for their helping hands and hard work. Molly Caron, Logan Gerchman, and Talya Briana have worked together on the PKC and PLD activity experiments, which required lots of troubleshooting. I would not have completed this project without their help. Hina Hashmi was another great undergraduate who helped me with arsenic experiments. I would also like to thank Alan Baez for information on Sucralose, Maxwell Dorman for zebrafish work, Nicholas Doucette for the Oxytocin assay, and Saige McGinnis for purified PLD assay. I thank Bailey West, Grace Bagley, and Bridget Konitzer for help with laboratory equipment and maintenance.

I am very thankful for members of other labs in the department of Molecular and Biomedical Sciences. They are always willing to help me and share their resources. Thanks to Dr. Carol Kim and Dr. Con Sullivan for use of the Amaxa Nucleofector equipment, Dr. Robert Wheeler and his lab for the use of the Ibidi heating system, Dr. Melissa Maginnis and her lab for the use of refrigerated centrifuge, Dr. Joshua Kelly and his lab for the use of bacterial incubator,

Dr. Sally Molloy and her lab for the use of electrophoresis equipment, and Dr. Timothy Bowden for gel imaging system. Especially I would like to thank and acknowledge graduate students in other labs for necessary training and willingness to accommodate me in their lab space: Brittany Seman, Allison Scherer, Linda Archambault, Collen Mayberry, Audrey Bergeron, Magdalena Blaskiewicz, and William Simke.

A special thanks to Doreen Sanborn, Tammy Gosselin, and Roseann Cochrane for their administrative support and to Mark Nilan from for providing me zebrafish embryos.

I would like to acknowledge the kind generosity of Drs. David Holowka and Barbara Baird for the antigen, RBL-2H3 cells, and mRFP-MARCKS-ED plasmid; Dr. Michael Frohman and Yelena Altshuller at Stony Brook University and Dr. Shamshad Cockcroft at University College London for the PLD1-EGFP construct.

Thank you to the John Wiley & Sons, Journal of Applied Toxicology for permission to reuse material published in their journal. The full citation for the article in the Chapter 2 is: Shim, J., Kennedy, R. H., Weatherly, L. M., Hutchinson, L. M., Pelletier, J. H., Hashmi, H. N., Blais, K., Velez, A., and Gosse, J. A. (2016) Arsenic inhibits mast cell degranulation via suppression of early tyrosine phosphorylation events. *J. Appl. Toxicol.*, 36: 1446–1459. doi: 10.1002/jat.3300. The full citation for the article in the Chapter 5 is: Shim, J., Weatherly, L. M., Luc, R. H., Dorman, M. T., Neilson, A., Ng, R., Kim, C. H., Millard, P. J., and Gosse, J. A. (2016) Triclosan is a mitochondrial uncoupler in live zebrafish. *J. Appl. Toxicol*., 36: 1662–1667. doi: 10.1002/jat.3311.

Chapter 3 has been submitted to a journal for publication consideration, and the authors are listed as; Juyoung K. Shim, Molly A. Caron, Lisa M. Weatherly, Logan B. Gerchman, Suraj Sangroula, Siham Hattab, Alan Y. Baez, Talya J. Briana, and Julie A. Gosse.

Chapter 4 has also been submitted to a journal for publication consideration, and the authors are listed as; Juyoung K. Shim, Rachel H. Kennedy, Lisa M. Weatherly, Andrew V. Abovian, Hina N. Hashmi, Atefeh Rajaei, and Julie A. Gosse.

This work was financially supported by the National Institute of General Medical Sciences (NIH P20-GM103423), Maine Agricultural & Forest Experiment Station (Grant Number ME08004-10; Dr. Julie A. Gosse), the University of Maine ADVANCE Rising Tide Center (NSF Grant # 1008492), a Research Starter Grant in Pharmacology/Toxicology from the PhRMA foundation (Dr. Julie A. Gosse), the National Institute of Health under the Award Number R15ES24593, the E. Reeve Hitchner Memorial Grant (University of Maine), the 2014-2015 CUGR Fall Creative and Academic Achievement Fellowship supported through a PRE-VUE grant with additional funding from the Maine Economic Improvement Fund (MEIF), and by the Radke Research Fellowship (University of Maine). The author has been supported by the by the Michael J. Eckardt Dissertation Fellowship (University of Maine).

Lastly, I would like to thank my family here and in Korea for their love and support. My parents have shown me, by their example, what a good parent should be. Also thank my parents and siblings for sending me food and goodies from Korea. I cannot express my gratitude enough to my husband. He is my best friend and my best supporter. He cooked many (most) dinners and been incredibly patient with me during stressful times. His constant support and encouragement have made me who I am. I like to thank my daughter Hana for providing me unending inspiration and unending challenges as a parent. She has been a jewel to my journey and I feel lucky to have her in my life. Finally, real special thanks to my goldendoodle puppy, Eleanor "Ellie". Her sassiness and companionship gave me the laughs to overcome my stress during my last leg of my Ph.D. marathon.

TABLE OF CONTENTS

LIST OF TABLES

LIST OF FIGURES

LIST OF ABBREVIATIONS

4-MU	4-methylumbelliferyl-N-acetyl-b-D-glucosaminide
Ag	antigen
ANOVA	one-way analysis of variance
Arsenic	As
ATP	adenosine triphosphate
AUC	area under the curve
BAPNA	N-benzoyl D,L-arginine p-nitroanilide
BCA	bicinchoninic acid assay
BkgD	background
BSA	bovine serum albumin
BT	BSA-Tyrodes Buffer
Btk	Bruton's tyrosine kinase
BMMB	bone marrow-derived mast cell
C48/80	compound 48/80
CCCP	carbonyl cyanide 3-chlorophenylhydrazone
CTMC	connective tissue mast cells
CRAC	Ca^{2+} release-activated Ca^{2+}
DAG	diacylglycerol
DMSO	dimethy sulfoxide
DNP	2,4-dinitrophenol
EDC	endocrine disrupting chemical
ELISA	enzyme-linked immunosorbent assay
EPA	Environmental Protection Agency
ER	endoplasmic reticulum
ETC	electron transport chain
FBS	fetal bovine serum
FcεRI	Fc epsilon RI, the high-affinity receptor for the Fc region of IgE
FCCP	carbonyl cyanide-*4*-(trifluoromethoxy)phenylhydrazone
FIPI	5-Fluoro-2-indolyl des-chlorohalopemide
FPALM	fluorescence photoactivation localization microscopy
Gab2	Grb2-associated binder 2
Grb2	growth factor receptor-bound protein 2
H_2O_2	hydrogen peroxide
HMC	human mast cells
hpf	hour post fertilization
hps	hour post stimulation
IACUC	Institutional Animal Care and Use Committee
IgE	immunoglobulin E
IL	interleukin
IP_3	inositol 1,4,5-triphosphate
IP_3R	IP_3 receptor
ITAMS	immunoreceptor tyrosine-based activation motifs
Itk	IL-2-inducible T-cell kinase
LAT	linker for activated T cells

LDH	lactate dehydrogenase
MARCKS	Myristoylated alanine-rich C-kinase substrate
MC	mast cell
MC_T	connective tissue mast cells
MC_{TC}	mucosal type mast cells
MEM	minimum essential media
MMC	mucosal mast cell
MMP	mitochondrial membrane potential
OCR	oxygen consumption rate
PA	phosphatidic acide
PC	phosphatidylcholine
PCR	polymerase chain reaction
PH	pleckstrin homology
PI3K	Phosphoinositide 3-kinase
PIP_2	phosphatidylinositol 4,5-biphosphate
PIP_3	phosphatidylinositol 3,4,5-trisphosphate
PKC	protein kinase C
PLC	phospholipase C
PLD	phospholipase D
PMA	phorbol 12- myristate 13-acetate
PMSF	phenylmethanesulfonyl fluoride
pNA	p-nitroaniline
PTK	protein tyrosine kinase
RBL-2H3	rat basophilic leukemia mast cells, clone 2H3
ROS	reactive oxygen species
SCF	stem cell factor
SD	standard deviation
SEM	standard error of the mean
SERCA	sarco/endoplasmic reticulum calcium ATPase
SH2	Src homology 2
SIP	sphingosine-1-phosphate
SLP-76	SH2 domain-containing leukocyte protein of 76 kDa
SOCE	store-operated calcium entry
Sos	Son of Sevenless
spont.	spontaneous release of granules
STIM-1	stromal interaction molecule 1
Syk	Spleen tyrpsine kinase
TC	tissue culture
TCS	triclosan
TFHL	Tryptase from human lung
Tg	thapsigargin
TLR	toll-like receptor
TNF	tumor necrosis factor
TX	Triton X-100
ZF	zebrafish

CHAPTER 1

INTRODUCTION

1.1 Mast cell signaling pathway

1.1.1 Mast cell

Mast cells (MCs) are immune-effector cells that are well-known for their roles in allergic reactions. MCs are present in all chordates, which possess a notochord (Kuby, 1997; Prykhozhij and Berman, 2014). Chordates include the vertebrates, the urochordate (*e.g.* sea squirts), and the cephalochordates (*e.g*. lancelets), thus MCs are likely one of the most conserved immune cells, a fact which implies their crucial roles evolutionarily in an organisms' survival and function. In fact, not only are MCs found in most species, but also found in nearly every tissue (Kuby, 1997).

They are involved in myriad physiological and pathophysiological processes, including host defense against infectious agents, innate and acquired immunity, homeostatic responses, wound repair, tissue remodelling, allergy, asthma, autoimmunity, infectious disease, cancer, inflammatory bowel disease, and even central nervous system disorders such as autism, anxiety, and multiple sclerosis (Metcalfe *et al*., 1997; Williams and Galli, 2000; Galli *et al*., 2005a; Silver and Curley, 2013; Girolamo *et al*., 2017).

These diverse actions of MCs result from diverse mediators released from MCs. In response to a wide range of stimuli, MCs degranulate, secreting stored mediators in cytoplasmic granules, such as histamine, neutral protease (*e.g.* chymase, tryptase, carboxypeptidase), β-hexosaminidase, serotonin, heparin, and some cytokines (Schwartz and Austen, 1980). Also, activated MCs can synthesize cytokines, chemokines, lipid mediators, and other inflammatory mediators *de novo* (Galli *et al*., 2005a; Shelburne and Abraham, 2011). MCs derive from hematopoietic cells in the bone marrow and migrate to various tissues for maturation (Rodewald

et al., 1996; Chen *et al*., 2005). MCs are found in nearly all tissue types, including at interfaces with the environment, such as skin, gastrointestinal linings, oral mucosa, blood capillaries, lymphatic vessels, and near nerve terminals (Theoharides *et al*., 2012a; Blank and Benhamou, 2013). This positioning is advantageous for MCs to serve as a first line of defense to pathogens and to coordinate inflammatory reactions to outside stimuli (Abraham and St John, 2010).

MCs are phenotypically and functionally heterogeneous depending on the microenvironment in which they mature. Thus the ubiquity of MCs' presence among species and tissues have induced different MC subtypes, while some of basic constituents of MCs are still conserved (Baccari *et al*., 2011). For example, human MCS are subcategorized into MC_{TC} and MC_T, by the presence of proteases (Irani *et al*., 1986). Tryptase is often utilized as a granule-associated MC marker since it is presented all human MC subtypes.

Since the discovery of MC by Paul Ehrlich in 1878, many studies on MC biology and function have been reported. Because of difficulty in isolation and culturing primary mast cells, several immortalized mast cell models have been established, including rat basophilic leukemia-clone 2H3 (RBL-2H3), human HMC-1, and human LAD2. MCs contain several extracellular receptors including the FcεRI, Toll-like receptors, interleukin receptors, *c*-kit receptor, and more (Metcalfe, 2008; Passante *et al*., 2009). Among those mast cell models, RBL-2H3 cells are the most commonly utilized for over 40 years, since they are easy to grow, display mature mast cell characteristics, have robust expression of the high affinity receptor for IgE (FcεRI) on the plasma membrane, and most importantly encompass core signaling machinery of human mast cells (Barsumian *et al*., 1981). Therefore, RBL-2H3 ("RBL") cells have been extensively used to study interactions of IgE high affinity receptor FcεRI with its ligands and the signaling pathway leading to degranulation is well-described. Other mast cells also have been employed in MC

studies; however, each has its own limitations: HMC-1 cells are poorly granulated and lack FcεRI (Nilsson *et al*., 1994) and LAD2 cells require long doubling time (> 2 weeks). Measurement of degranulation from RBL cells is typically performed by quantifying the release of β-hex or histamine, which will be detailed later in this chapter.

1.1.2 Mast cell signaling

Degranulation is classically initiated by antigen (Ag)-crosslinking of immunoglobulin E (IgE)-bound FcεRI receptor (Kuby, 1997). FcεRI is a tetrameric receptor composed of one extracellularly-exposed α chain plus membrane-spanning β (one) and γ (two) chains (Metzger *et al*., 1982; Metzger *et al*., 1986; Ravetch and Kinet, 1991). FcεRI β and γ subunits possess cytoplasmic immunoreceptor tyrosine-based activation motifs (ITAMs) (Reth, 1989; Cambier, 1995; Daeron, 1997). Antigen crosslinking of FcεRI causes phosphorylation of ITAMs by non-receptor protein tyrosine kinase (PTK) Lyn (Xiao *et al*., 2005). Phosphorylated ITAMs bind proteins with Src-homology-2 (SH2) domains, leading to activation (Cohen *et al*., 1995; Furumoto *et al*., 2004; de Castro *et al*., 2010; Siraganian *et al*., 2010). Phosphorylated sites on γ become docking areas for another PTK spleen tyrosine kinase (Syk), which contains an SH2 domain (de Castro *et al*., 2010; Siraganian *et al*., 2010). Binding to FcεRIγ causes a conformational change in Syk, resulting in autophosphorylation (Benhamou *et al*., 1993; Minoguchi *et al*., 1994; Pribluda *et al*., 1994; Zhang *et al*., 2000) and results in Syk's phosphorylation/activation by Lyn.

In addition to the Lyn-propagated signaling pathway, the complementary PTK Fyn pathway is initiated upon FcεRI receptor aggregation (Rivera and Gilfillan, 2006). Fyn signaling leads to activation of the phosphatidylinositol-3-OH kinase (PI3K) pathway (Gu *et al*., 2001).

Importantly, Syk is essential for FcεRI-mediated signaling in mast cells since Syk is required for both Lyn-directed and Fyn-directed pathways (Costello *et al*., 1996; Zhang *et al*., 1996).

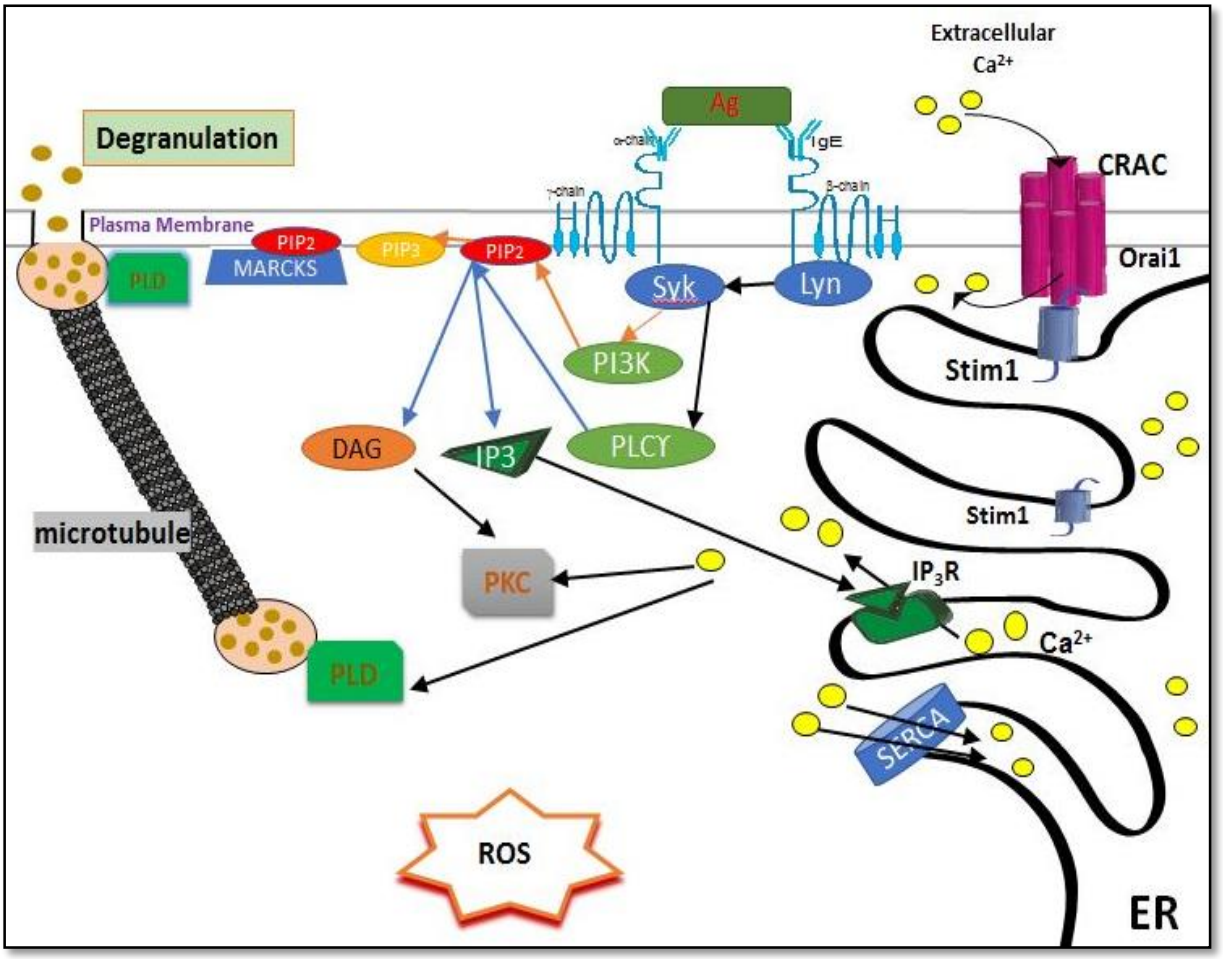

Figure 1. 1. Overview of the mast cell degranulation signaling pathway.
Crosslinking of IgE-bound FcεRI by multivalent antigen (Ag) results in phosphorylation cascade to activate several enzymes (Lyn, Syk, PI3K and PLCγ). Activated PI3K generates PIP_3 from PIP_2. PLCγ hydrolyzes PIP_2 to DAG and IP_3. IP_3 binds to its cognate receptor on the ER, causing depletion of Ca^{2+} from internal ER storage to the cytosol, resulting in STIM1 (calcium sensor in the ER membrane) interaction with Orai1 (subunit of CRAC channel) for influx of Ca^{2+} across plasma membrane into the cell. ER stores get replenished by reuptake of cytosolic Ca^{2+} into the ER through SERCA pump. Ca^{2+} and/or DAG activate PKC. Activated PKC translocates from cytosol to the plasma membrane where it phosphorylates substrates in its proximity, such as MARCKS, which tightly binds to PIP_2. Phosphorylated MARCKS dissociates from the plasma membrane and enters the cytosol, thus exposing PIP_2 to be accessible to other proteins. Another major target of PKC is PLD, which is localized either to cytoplasmic granules or at the plasma membrane, to facilitate granule translocation and fusion to the plasma membrane. Granules are mobilized along with microtubules for degranulation. Degranulation process generates and requires ROS.

Activated Syk phosphorylates the adaptor protein linker for activation of T cells (LAT) (Saitoh *et al*., 2003), which physically brings together proteins such as Grb2 (Growth factor receptor-bound protein 2), Gads, SLP-76, Vav, and the enzyme phospholipase C γ (PLC γ). Next, PLC γ1 is phosphorylated by Syk or by a Tec family tyrosine kinase, Itk (Interleukin-2-inducible T-cell kinase) or Btk (Bruton's tyrosine kinase) (Ishiai *et al*., 2000). Gads (Grb2-related adaptor downstream of Shc) binds SLP-76 (SH2 domain-containing leukocyte protein of 76) (Ishiai *et al*., 2000), which is phosphorylated by Syk and then which binds Btk and Vav (Kettner *et al*., 2003). Next, Lyn phosphorylates and activates Btk, which activates PLC γ1 (Benhamou *et al*., 1992; Beaven and Metzger, 1993) via its Pleckstrin Homology (PH) domain. Btk binds to plasma membrane lipids phosphatidylinositol 4, 5-bisphosphate (PIP_2) and phosphatidylinositol 3, 4, 5-trisphosphate (PIP_3) (Fluckiger *et al*., 1998; Scharenberg and Kinet, 1998).

Syk activates PI3K, which converts PIP_2 into PIP_3 (Kitaura *et al*., 2000). PIP_3 activates Rac/Rho GTPases resulting in remodeling of the actin cytoskeleton, also called membrane ruffling ("ruffles" of the polymerized actin cytoskeleton) (Hawkins *et al*., 1995; Parker, 1995). PI3K also activates sphingosine kinase-S1P (sphingosine-1-phosphate), which produces S1P, thus supporting Ca^{2+} mobilization (Choi *et al*., 1996; Melendez and Khaw, 2002; Urtz *et al*., 2004), protein kinase C (PKC) activation, and degranulation (Olivera *et al*., 2007).

PLC γ hydrolyzes PIP_2 to yield inositol-1, 4, 5-trisphosphate (IP_3) and diacylglycerol (DAG). IP_3 then binds to its receptor IP_3R in the endoplasmic reticulum (ER) membrane, thereby releasing Ca^{2+} from ER to the cytosol (Berridge, 1993; Taylor and Thorn, 2001). This emptying of ER Ca^{2+} leads to second influx of Ca^{2+} across the plasma membrane into the cytosol through calcium release-activated calcium (CRAC) channels. STIM-1 (Stromal interaction molecule 1) in

the ER membrane and Orai1 (the pore subunit of CRAC channels) are responsible for this event. When ER Ca^{2+} is depleted, STIM1 goes through a conformational change (Liou *et al*., 2005; Fahrner *et al*., 2013) and binds to Orai1(Feske *et al*., 2006; Vig *et al*., 2006). This interaction causes opening of CRAC channels, inducing a flood of extracellular Ca^{2+} coming into the cytosol (Roos *et al*., 2005; Hogan *et al*., 2010), which is termed "store operated calcium entry" (SOCE) (Putney, 1986; Putney, 1990; Clapham, 1995). Sarco/endoplasmic Ca^{2+}-ATPase (SERCA) pumps refill Ca^{2+} into the ER after cytosolic Ca^{2+} influx (Ma and Beaven, 2011), for later usage. Replenishment of the ER Ca^{2+} can be inhibited by selective SERCA inhibitor thapsigargin, which will be utilized in Chapter 2 for arsenic mechanism studies (Thastrup *et al*., 1990; Lytton *et al*., 1991).

Another of PLC γ's products, DAG, along with elevated Ca^{2+} and reactive oxygen species (ROS), are involved in activation of PKC. It has been known that intracellular ROS is generated as well as required during mast cell degranulation (Swindle et al., 2004; Min and Shin, 2009; Weatherly et al., 2018). PKC is family of Ser/Thr kinases, which is categorized into three subfamilies, classical (cPKC), novel (nPKC), and atypical (aPKC), based on their biochemical and structural properties of their bindings to DAG and/or Ca^{2+} (Ozawa *et al*., 1993b; Newton, 1995; Newton, 2001). The cPKC isoforms (PKC α, βI, βII, and γ) contain conserved functionally active C1 domains (which bind DAG) (Newton, 2001) as well as C2 domains (which bind Ca^{2+} and acidic phospholipids). The nPKC isoforms (PKC δ, ε, θ, and η) contain the C1 domain, but lack functional C2 domains, thus, are activated by DAG and unresponsive to Ca^{2+} (Newton, 1995).

PKC β (cPKC) and δ (nPKC) are particularly important in IgE–mediated degranulation and ruffling (Nechushtan *et al*., 2000; Cho *et al*., 2004). Activation of PKC changes its affinity

to the plasma membrane, causing to translocate to the plasma membrane. Translocated PKC is then fully active via conformational changes to reveal its active site (Newton, 2010). Stimulation of RBL-2H3 cells causes a rapid translocation of PKC δ from the cytosol to the plasma membrane (Cho *et al*., 2004). Also, PKC δ translocation and degranulation are inhibited by ROS attenuation (Cho *et al*., 2004). Myristoylated alanine-rich C-kinase substrate (MARCKS) is one of the abundant PKC substrate (Aderem, 1992). MARCKS tightly binds to PIP_2 at the plasma membrane in unstimulated cells (Heo *et al*., 2006). In stimulated MCs, translocated PKC phosphorylates MARCKS, which dissociates from the plasma membrane, thus exposing PIP_2 to be accessible to other proteins (e.g. PLC γ) for sustained signaling for degranulation (Gadi *et al*., 2011). Also, PIP_2 is necessary in assembly of the soluble N-ethylmaleimide–sensitive factor attachment protein receptor (SNARE) machinery required for degranulation (Tadokoro *et al*., 2015).

Another target of activated PKC is phospholipase D (PLD) in mast cells (Lin and Gilfillan, 1992) . PLD hydrolyzes phosphatidylcholine (PC) into phosphatidic acid (PA), which plays important roles as a second messenger for diverse cellular functions(Wakelam *et al*., 1997; Cockcroft, 2001; O'Luanaigh *et al*., 2002; Zeniou-Meyer *et al*., 2007). Also PA can be converted to DAG by PA phosphohydrolase, resulting in a secondary rise in DAG levels in the cells (Nakashima et al., 1991; Lin et al., 1992), important for the sustained activation of the DAG-dependent PKC isoforms (Baldassare *et al*., 1992; Nishizuka, 1995; Peng and Beaven, 2005). Additionally, PA plays a critical role in regulating mast cell morphology (Marchini-Alves *et al*., 2012). Structurally, mammalian PLD contains lipid (PIP_3 and PIP_2) -binding domains and a PKC-binding domain, but lacks a Ca^{2+} binding domain (Henage *et al*., 2006; Selvy *et al*., 2011). However, studies showed that Ca^{2+} and PIP_2 act as crucial cofactors for

mammalian PLD activation (Sciorra *et al*., 2002; Henage *et al*., 2006; Selvy *et al*., 2011), even though mammalian PLD activity is insensitive to changes in cytosolic Ca^{2+} concentration *in vitro* (Hammond *et al*., 1997).

Also several studies showed that PLD can be activated by agents to elicit intracellular Ca^{2+} rise, such as Ca^{2+} ionophore (Lin and Gilfillan, 1992), thapsigargin (Cissel *et al*., 1998) and PMA (Lin and Gilfillan, 1992). In addition, compound 48/80, a MC secretagogue, induces PLD activation (Chahdi *et al*., 2000).

Mammalian PLD is expressed as two isoforms: PLD1 has low basal activity and is located at the cytoplasmic granules. In stimulated MC, PLD1 undergoes translocation to the plasma membrane (Choi *et al*., 2002; Lee *et al*., 2006). PLD2 is constitutively expressed near the plasma membrane (Choi *et al*., 2002; Lee *et al*., 2006). These spatial distinctions of two isoforms have led scientists to postulate that PLD1 is involved in granule translocation to the plasma membrane while PLD2 is involved in membrane fusion of MC granules (Choi *et al*., 2002). However, a recent study using PLD1- and PLD2-knockout mice found that PLD1 is a positive regulator in MC degranulation, but PLD2 is a negative regulator, since PLD2 deficiency enhanced microtubule formation (Zhu *et al*., 2015).

MC granule transport is facilitated by microtubules, while granule docking and fusion to the plasma membrane is assisted by SNARE complexes (Guo et al., 1998; Baram et al., 1999; Paumet et al., 2000; Blank et al., 2002; Logan et al., 2003; Puri and Roche, 2008; Tiwari et al., 2008; Woska and Gillespie, 2012). Microtubule polymerization is indispensable for degranulation (Urata and Siraganian, 1985; Tasaka *et al*., 1991; Marti-Verdeaux *et al*., 2003; Smith *et al*., 2003). SNAREs are located on vesicular (v-SNAREs) and target membranes (t-SNAREs) (Woska and Gillespie, 2012) and mediates the final stages of priming, docking, and

fusion of granules with the plasma membrane (Puri and Roche, 2008). SNAREs form a complex by direct interaction with synaptotagmins (Syts) with help of PIP_2 (Dai *et al*., 2007a; Tadokoro *et al*., 2015). Syt is a Ca^{2+} sensor protein, which contains C2 calcium-binding domains (Dai *et al*., 2007a). Even though Syts were first characterized as a neuronal Ca^{2+} sensor in the pre-synaptic axon terminal, several studies have identified Syts homologs in MCs (Baram *et al*., 1998; Baram *et al*., 1999; Baram *et al*., 2001; Kimura *et al*., 2001). In addition, a study revealed that PIP_2 enhanced synaptotagmin- SNARE-mediated membrane fusion of MC granules only in the presence of Ca^{2+} (Tadokoro *et al*., 2015). Therefore, the components of a quaternary complex (SNARE- PIP_2- synaptotagmin- Ca^{2+}) are all necessary for granule docking, fusion and exocytosis.

The result of mast cell signaling is degranulation, but also causes F-actin polymerization simultaneously. PI3K activation of Rac/Rho GTPases leads to actin rearrangements, resulting in membrane "ruffling," or the rearrangement of the actin cytoskeleton. Lamellipodia that fail to establish stable adhesions become detached from the substrate and retracted toward the cell body; during this retraction process, actin-rich membrane protrusions, or membrane ruffles, are formed (Giannone *et al*., 2007). Ruffles are compartments of active actin reorganization (Borm *et al*., 2005). Actin cytoskeletal rearrangement is not an essential element of the degranulation pathway (degranulation occurs even when ruffling is stopped by actin inhibitor cytochalasin D (Holowka *et al*., 2000)), but the two share common events such as activation of PKC and influx of Ca^{2+} (Pfeiffer *et al*., 1985; Yanase *et al*., 2011). A recent study has shown that the use of inhibitors of PKCβ and PKCα inhibited both ruffling and degranulation. The Rho guanine nucleotide exchange factor Vav and also Cdc42 have been shown to be associated with mast cell degranulation and ruffling (Guillemot *et al*., 1997; Pivniouk *et al*., 2003; Zeng *et al*., 2003).

PLD2 also is important for membrane ruffle formation, in a mechanism involving PLD2 interactions with Grb2 and Rac (Mahankali *et al*., 2011).

1.1.3 Mast cell granule-associated mediators

Most of the physiological and pathophysiological functions of mast cells are closely associated with the actions of the myriad immunomodulatory granule mediators. The preformed and pre-activated compounds in the granules are released rapidly (~seconds to minutes) for immediate and acute reactions, such as alteration of vascular permeability, vasodilation, and adhesiveness (Metcalfe *et al*., 1997; Theoharides *et al*., 2012a). These mediators include histamine, proteases (tryptase, chymase, carboxypeptidase A and cathepsin G), β-hexosaminidase, proteoglycans (heparin), serotonin, and some cytokines (*e.g.* tumor necrosis factor-α [TNF-α] (Olszewski *et al*., 2006; Olszewski *et al*., 2007), Interleukin-4 [IL-4] (Wilson et al., 2000; Hines, 2002). Newly synthesized mediators are also released to the extracellular environment, such as leukotriene C_4 (LTC_4), prostaglandin D_2 (PGD_2), platelet-activating factor, chemokines, and other cytokines (Metcalfe *et al*., 1997; Galli *et al*., 2005b), which plays an immunoregulatory function by recruiting macrophages, neutophils, dendritic cells and T-cells to the site of infection (Abraham and St John, 2010).

Histamine is probably the most well-known pro-inflammatory granule-associated mediator, but it is not exclusively released by mast cells. The action of histamine is local and short-lived since it gets rapidly degraded upon release (Hines, 2002), which is modulated by binding to its receptors (H_1, H, H_3 and H_4), found in many cell types, such as smooth muscle, epithelia, and neurons, causing vasodilation, bronchoconstriction, and edema (Theoharides *et al*., 1982). Furthermore, these histamine receptors are expressed in other immune cells, including

neutrophils, eosinophils, lymphocytes, and macrophages, implying that histamine can modulate the function of these cells (Carlos *et al*., 2006).

Many MC granule constituents are proteases, in particular, tryptase and chymase. Positively charged granule proteases bind tightly to negatively charged proteoglycans, which serve as a scaffold for stable complexes of charged molecules (Pejler *et al*., 2007).

Mast cell tryptase is a family of trypsin-like serine proteases (Caughey, 2011) that cleave sites after basic amino acids such as Arg and Lys (Lehninger *et al*., 2005). Tryptase requires the proteoglycan heparin to be enzymatically active (Hallgren *et al*., 2001). In general, tryptases can be grouped into three main types, α (I-II), β (I-III), and γ (transmembrane). The main tryptases in humans are β-tryptases, which are the products of two genes, TPSB2 and TPSAB1 (Caughey, 2011). The orthologues of β-tryptases are found in mouse and rat, which are mMCP-6, mMCP-7, Tpsb2, and Tpsab1. Tryptase acts upon many substrates, receptors and zymogens (Schwartz, 1990), leading to host defense, tissue -remodeling/repair, pro-inflammatory as well as anti-inflammatory reactions (Caughey, 2007). For example, lung tryptase elicits bronchial constriction to protect airways from entry of pathogens or foreign substances, by degrading bronchodilating peptides (Tam and Caughey, 1990), cleaving extracellular matrix in the bronchial wall (Gruber *et al*., 1989), or activating protease-activated receptor (PAR)-2 which modulates inflammatory responses (Dai *et al*., 2007b). Another important role of tryptase is wound healing and tissue remodeling, by promoting the proliferation of fibroblasts and type 1 collagen production (Hartmann *et al*., 1992). Anti-inflammatory action of tryptase is also reported that tryptase destroys pro-inflammatory cytokines, such as IL-6, IL-13 and TNF-α, consequently reducing inflammation (Zhao *et al*., 2005). Intriguingly, tryptase is closely related to neurological diseases, such as schizophrenia and multiple sclerosis (MS). In MS, tryptase level

is remarkably elevated (Rozniecki *et al*., 1995). In murine models, β-tryptase expression is upregulated during the inflammatory reaction against a parasitic infection (Ide *et al*., 1995) and formation of keloid tissue (Ong *et al*., 2010). Overall, tryptase is a crucial player in inflammation, tissue homeostasis, and innate immunity.

Because MC tryptase is an abundant mediator unique to mast cells, it serves as a canonical biomarker for anaphylaxis, mastocytoma, and systemic mastocytosis. In clinical settings, tryptase level in the patient plasma is measured for diagnosis of MC diseases (Bussmann *et al*., 2007). In the laboratory, active tryptase can be measured by incubation with a substrate such as N-α-benzoyl-DL-Arg-p-nitroanilide (BAPNA) or tosyl-Gly-Pro-Lys-p-nitroanilide: tryptase cleaves the bond between the Arg or Lys and the p-nitroaniline (pNA), releasing chromogenic pNA, measurable in a plate reader (Lavens *et al*., 1993).

Another serine protease, chymase, also participates in anti- and pro-inflammatory reactions and host defense. It facilitates maintenance of gut barriers, bronchoconstriction, vasoconstriction, and defense against parasites (Nakano *et al*., 1997; Caughey, 2007). Chymase along with carboxypeptidase A3 play a prominent role in degrading venom-associated peptides and toxins (Akahoshi *et al.*, 2011). Carboxypeptidase A3 also controls systemic toxicity of endogenous vasoconstricting peptides during sepsis (Maurer *et al*., 2004).

β- hexosaminidase (β-hex) is an exoglycosidase that cleaves terminal sugars (Schwartz *et al*., 1979). β-hex enzyme catalyzes degradation of GM2 ganglioside, and mutations in this enzyme lead to neurodegenerative diseases (Bayleran *et al*., 1987; Tifft and Proia, 1997). β-hex has been successfully used as a MC function marker because it is released in parallel with canonical MC marker histamine (Schwartz *et al*., 1979). For many of the studies using RBL cells, degranulation has been quantified via measurement of released β-hex by incubating with

substrate resulting fluorescent product, easily detected in a microplate reader (Naal *et al*., 2004), but tryptase release has not typically been used as a RBL-2H3 degranulation marker.

1.2 Zebrafish as a model for mast cell and mitochondria

1.2.1 Zebrafish as models for toxicology

Zebrafish (*Danio rerio*) have emerged as a powerful vertebrate model organism for genetic and developmental biology because of their small size, low-cost maintenance, high fecundity, short generation time, easy gene manipulation, external transparent development, and availability of extensive genomic resources (Ward and Lieschke, 2002; Sullivan and Kim, 2008; Ellett and Lieschke, 2010). In addition, their physiological equivalence with mammalian systems provides an intriguing model of human disease (Ward and Lieschke, 2002; Yoder *et al*., 2002; Lieschke and Currie, 2007).

Zebrafish (ZF) are gaining popularity in toxicology as an attractive system as well, owing to their striking similarities to mammalian toxicity profiles, and their easily-monitored drug or toxicant effects (Spitsbergen and Kent, 2003; Link *et al*., 2006; Lieschke and Currie, 2007; Scholz *et al*., 2008; Oppedal and Goldsmith, 2010; Lam *et al*., 2012). Moreover, ZF are currently the best-suited vertebrate model for high-throughput toxicity screening, capable of bridging the *in vitro* cell-based systems and *in vivo* mammalian models (Sukardi *et al*., 2010; Tanguay, 2018).

ZF represent a more pertinent and valuable model organism for environmental toxicants (Bambino and Chu, 2017), especially toxicants that are detected in aquatic environments (Scholz *et al*., 2008) which provide information for both human health and aquatic toxicology and ecology, since aquatic pollution has become a serious global issue. For example, Mizell and

Romig utilized ZF embryos to monitor effects of common aquatic pollutants, such as dioxin (*e.g.* TCDD), benzene, and toluene (Mizell and Romig, 1997). The continuous observation of phenotypic changes upon toxicant exposure owing to transparent body and rapid growth are sure to provide significant advantages to developmental toxicologists.

Numerous studies have examined the effects of endocrine disruptor chemicals (EDCs), including bisphenol A (BPA), ethinyl estradiol (EE2), and polybrominated diphenyl ethers (PBDEs), using ZF embryos and larvae, on changes in gene transcription and hormonal levels (Chung *et al*., 2011; Velasco-Santamaria *et al*., 2011; Chen *et al*., 2012; Cardoso *et al*., 2017; Souder and Gorelick, 2018). Also, metal toxicology studies have employed ZF: those metal toxicants include mercury, zinc, cadmium, lead, and arsenic (Chan *et al*., 2006; Senger *et al*., 2010; Richetti *et al*., 2011; Wu *et al*., 2012). The rise of organic pollutants in the environment, mostly polyaromatic hydrocarbons (PAHs), has been reported as a serious health concern in recent years. The sources of PAHs include pesticides, naphthalene, benzopyrene, and dichlorophenol products. Many ZF studies have found adverse effects of PAHs on development, gene expression, nucleic acid, oxidative stress and endocrine systems of ZF embryos (Kienle *et al*., 2009; Hawliczek *et al*., 2012; Huang *et al*., 2012; Ma *et al*., 2012; Shao *et al*., 2012; Xing *et al*., 2012).

It is worth noting that the ZF model is equipped with genomic data [its genome has been fully sequenced and annotated (Howe *et al*., 2013)], numerous transgenic morphants, and easy genetic-manipulation. Since technologies in molecular/genetics/bioinformatics have advanced remarkably, recent toxicological studies have expanded the scope to elucidating molecular mechanisms and cellular targets, in addition to describing end-point toxicity to chemicals. Thus, the increased and augmented recognition and usage of ZF in toxicology is promising.

1.2.2 Zebrafish in mast cell studies

Despite the many advantages of ZF, utilizing ZF in mast cell studies has not been extensively explored yet, partly because of the lack of information on ZF mast cells up until recently. Only a decade ago, the Berman lab first characterized ZF mast cells (Dobson *et al*., 2008); thus, this area of ZF MC studies are still at an early but promising stage. In those studies, carboxypeptidase A5 (cpa5), which is homologous to human CPA1 and mouse Cpa3, was identified as a MC specific marker in ZF (Dobson *et al*., 2008; Da'as *et al*., 2012). Application of an anti-human FcεRI and anti-human tryptase antibody to ZF revealed FcεRI receptor-like and tryptase homologs in ZF (Da'as *et al*., 2011). Furthermore, techniques were developed to monitor MC degranulation in adult ZF by injecting c48/80 (MC stimulant) and quantifying the release of tryptase using a N-alpha-benzoyl-DL-arginine-p-nitroanilide (BAPNA), chromogenic synthetic tryptase substrate (Dobson *et al*., 2008; Da'as *et al*., 2011). A systemic mastocytois (SM) model has been developed in ZF, which is characterized by excessive accumulation of MCs, by inducing genetic mutaion in the *c*-Kit receptor to generate transgenic animal (Balci *et al*., 2011; Balci *et al*., 2014). Overall, these studies found that ZF MCs share similarities in innate and adaptive immune responses with humans (Dobson *et al*., 2008; Da'as *et al*., 2011; Da'as *et al*., 2015).

Additionally, the Berman laboratory has developed a mast cell degranulation assay using adult ZF to study by tryptase as a degranulation marker (Dobson *et al*., 2008; Da'as *et al*., 2011). After adult ZF were injected intraperitoneally with MC stimulant c48/80, blood samples are collected by cardiac puncture and incubated with BAPNA. This assay showed an increase in blood tryptase levels, ~60% above controls (Dobson *et al*., 2008). Later, this tryptase assay also

produced a significant readout for MC degranulation by injection of mouse IgE followed by DNP-BSA antigen injection in adult ZF (Da'as *et al*., 2011).

Although these studies done by the Berman lab (2018 and 2011) demonstrate the feasibility of using ZF as a model to study MCs *in vivo*, using adult ZF to measure MC degranulation has drawbacks: their small size (3-4 cm) precludes large-scale extraction of plasma where tryptase is detected. In addition, all the chemicals need to be injected intraperitoneally and blood samples are collected manually with frequent anesthetization of the animals. Therefore, this method is costly, labor-intensive and low-throughput. Recently, Yang *et al*.(2015) reported an *in vivo,* microplate-based colorimetric tryptase assay using ZF embryos (Yang *et al*., 2015), rather than adult ZF. In this method, all the drugs and reagents, including c48/80 and BAPNA, are directly added to the fish water and animals are arrayed in microplate for direct readout of signals in a microplate reader. Thus, this method can be utilized as a high-throughput assay.

β-hexosaminidase release as a MC degranulation marker has been utilized in the RBL-2H3 cell line, which is one of the most widely used *in vitro* MC systems. Thus, previous findings on ZF MCs have strongly motivated us to establish tryptase assay *in vitro* models using RBL mast cells, to be able to parallel studies of MCs *in vitro* and *in vivo*. However, in Chapter 4, we detail our finding that RBL cells do not express tryptase genes.

1.2.3 Zebrafish in mitochondrial studies

Mitochondria are often noted as powerhouses which generate energy (adenosine triphosphate, ATP) in all eukaryotic cells. Also, mitochondria are involved in regulation of calcium signaling since they can store and release calcium in concert with the ER (Pacher *et al*., 2000). During ATP synthesis, mitochondria also consume oxygen as the final electron acceptor;

thus, ATP production and oxygen consumption in mitochondria are tightly coupled, and this process is called oxidative phosphorylation (Lehninger *et al*., 2005).

Because of the important roles of mitochondria, they have been a subject of studies in various scientific fields. However, most of studies on mitochondria have been done in cell culture or mitochondria isolated from animal models (Newton *et al*., 2005; Ajao *et al*., 2015). Due to the unique features of ZF being transparent and possessing advanced genetic tools, scientists have utilized ZF to investigate mitochondria in a living, intact organism (Kim *et al*., 2008; Paquet *et al*., 2014; Noble *et al*., 2015; Bergamin *et al*., 2016; Zhou *et al*., 2018).

Our lab has previously showed that the antimicrobial agent triclosan (TCS) suppresses MC degranulation *in vitro* (Palmer *et al*., 2012; Weatherly *et al*., 2013). In our search of mechanisms underlying MC inhibition by TCS, we found that TCS is a proton ionophore mitochondrial uncoupler (MU) in multiple cell types (Weatherly *et al*., 2016). Proton ionophore MUs interfere with ATP synthesis by transporting hydrogen ions across the inner mitochondrial membrane, thus bypassing the proton channel of ATP synthase (Heytler and Prichard, 1962). Disruption of the proton gradient also causes the electron transfer chain to operate more vigorously, so oxygen consumption rate (OCR) is increased by proton ionophore MUs. Additionally, we and others have revealed that TCS inhibits mitochondrial membrane potential (Attene-Ramos *et al*., 2015; Weatherly *et al*., 2018).

To align with our *in vitro* studies, we developed a novel *in vivo* assay using ZF embryos in 96-well high-throughput format utilizing XF^{e} 96 Extracellular Flux Analyzer, to measure mitochondrial bioenergetics (Shim *et al*., 2016b)—see Chapter 5. As expected, ATP-linked respiration decreases and OCR increases on TCS exposure. There are other studies using zebrafish for mitochondrial bioenergetics; however, these studies employed relatively low-

throughput 24-well plates and required laborious placement of screens into each individual well to contain ZF within the well during the signal acquisition (Stackley *et al*., 2011; Bestman *et al*., 2015).

A recent study by Paquet *et al*. (2014) reported development of a transgenic ZF which is labeled with mitochondrial markers attached to fluorescent proteins ("MitoFish"). The authors used MitoFish to examine mitochondrial dynamics in real-time via *in vivo* imaging (Paquet *et al*., 2014). Similarly, another group generated the transgenic ZF line MTS-Kaede, in which mitochondria are labeled in neurons, to study mitochondrial transport (Bergamin *et al*., 2016). Dopaminergic neuron-specific (Noble *et al*., 2015) and neutrophil-specific (Zhou *et al*., 2018) mitochondria transgenic ZF lines have also established recently. Thus, the potential for use of zebrafish in toxicity testing of mitochondrial function is great and growing.

1.3 Arsenic and triclosan

1.3.1 Arsenic

Arsenic (As) exposure is a global concern since it is ubiquitously detected in soil, water, and air, from natural or anthropogenic sources (Abdul *et al.*, 2015). The major route of human exposure is diet, via foods or drinking water, with the additional concern of occupational-related arsenic exposure for certain groups (Arslan *et al*., 2017). In the United States, the allowed level of As in drinking water set by Environmental Protection Agency (EPA) is 10 ppb; however, there are many parts of the world (*e.g.* West Bengal, Bangladesh, Taiwan, and South America) which the As level in drinking water is very high: hundreds of ppb to ppm. Thus, across the world, hundreds of millions people are at risk of As exposure.

Many human epidemiological studies have reported strong association between populations exposed to high levels of As and prevalence of numerous disorders and diseases. The International Agency for Research on Cancer (IARC) has classified inorganic arsenic as a carcinogen. A study done in Argentina showed that inorganic As exposure is associated with high incidence of colorectal, lung, breast, prostate, and skin cancers (Bardach *et al*., 2015). Many other studies also reported that urinary arsenic concentration is positively correlated with frequency of lung cancer (Steinmaus *et al*., 2010; Melak *et al*., 2014), bladder cancer (Melak *et al*., 2014), squamous cell carcinoma (Gilbert-Diamond *et al*., 2013), basal cell carcinoma (Leonardi *et al*., 2012), and non-melanoma skin cancer (Kim *et al*., 2017). Also, a high As level detected in blood is also related to bladder cancer and renal cancer (Mostafa and Cherry, 2013).

Arsenic exposure is also correlated to diabetes (James *et al*., 2013; Grau-Perez *et al*., 2017), cardiovascular disease (Wade *et al*., 2015; Wu *et al*., 2015), skin lesions (Chung *et al*., 2006; Rahman *et al*., 2006; Mondal *et al*., 2016), chronic kidney diseases (Hsueh *et al*., 2009), hypertension (Guha Mazumder *et al*., 2012), and child pneumonia (George *et al*., 2015). Additionally, a study done by Wu *et al*. (2011) found a positive correlation between arsenic exposure and birth defects (Milton *et al*., 2010; Wu *et al*., 2011). Human health problems caused by As are reviewed in (Abdul *et al*., 2015).

Our lab has previously demonstrated that mast cell degranulation is dampened by inorganic Arsenite in Ag-stimulated RBL cells (Hutchinson *et al*., 2011). We then have sought out the mechanisms of arsenic's inhibitory action on MCs and revealed that early tyrosine kinase phosphorylation was significantly decreased by As exposure. Specifically, the levels of phosphorylation of Syk kinase and one of the Syk substrates, PI3K, are reduced upon As

exposure in activated RBL cells (Shim *et al*., 2016a). This mechanistic study is detailed in Chapter 2.

Interestingly, arsenic has been employed in traditional Chinese medicine over 5000 years to treat asthma. Our findings of inhibitory action of As on mast cells, which is a key player for asthma, might be the mechanism of this treatment. Moreover, As has shown to decrease asthma symptoms in mice (Chu *et al*., 2010) and to abrogate anaphylactic response in guinea pigs (Poriadin *et al*., 1977).

1.3.2 Triclosan

Triclosan (TCS) is a broad-spectrum antimicrobial agent that has been widely used in consumer products since its original usage in clinical settings in 1972. During 2003–2004, the National Health and Nutrition Examination Survey (NHANES) measured triclosan in urine and TCS was detected in approximately 75% of the people tested (Calafat *et al*., 2008). More recent survey studies in Korea, Denmark, and China reported 93% (Kim *et al*., 2011), 79% (Frederiksen *et al*., 2013) and 100% (Li *et al*., 2013) detection rates of TCS from 140-300 test subjects.

By the late 2000s, TCS was found in over 90% of soap products (FDA, 2013) until it was banned by the FDA in consumer soap products in 2016 (Kux, 2016) and hospital sterilizing products in 2017 (Fischer, 2017). However, TCS remains in other consumer products, such as toothpaste, and other household products (*e.g.* toys, kitchenware, bedding, fabric etc.).

Numerous emerging epidemiological studies report adverse human health consequences to TCS exposure. Since several studies have demonstrated that TCS is an endocrine disrupting chemical (Wang and Tian, 2015; Wang *et al*., 2015; Ruszkiewicz *et al*., 2017), and an epidemiological study showed prenatal TCS exposure affects thyroid hormone levels (Wang *et*

al., 2017). Also maternal TCS level is strongly associated with reproduction (Wang *et al*., 2015; Hua *et al*., 2017) and fetal growth and development, such as fatal abnormalities, birth weight, head circumference (Lassen *et al*., 2016; Etzel *et al*., 2017; Wei *et al*., 2017). Additionally, studies done in 2018 reported abnormalities of sperm morphology (Jurewicz *et al*., 2018), and lowered cognitive test scores in children (Jackson-Browne *et al*., 2018) linked to triclosan exposure. Intriguingly, while urinary TCS concentration level is inversely associated with body mass index and waist size (Li *et al*., 2015), one epidemiological study presented a positive correlation between TCS exposure and high risk of gestational diabetes (Ouyang *et al*., 2018).

Most of mechanisms causing these health consequences by TCS are not fully elucidated, however, several studies have provided molecular and biochemical data about TCS. TCS increases reactive oxygen species (ROS) generation, which leads to oxidative DNA damage (Lv *et al*., 2016), or tumorigenesis (Yueh *et al*., 2014). TCS alters gene expression in mice (Yueh *et al*., 2014; Marshall *et al*., 2015), which potentially induces cancer formation. Abnormal gene expression profiles were observed in TCS-exposed sea urchins (Hwang *et al*., 2017). Calcium homeostasis is also modulated by TCS exposure (Ahn *et al*., 2008; Cherednichenko *et al*., 2012; Weatherly *et al*., 2018). Finally, TCS's detrimental effects on mitochondrial function has been explored by us and others (Ajao *et al*., 2015; Shim *et al*., 2016b; Weatherly *et al*., 2016).

Our lab has investigated the effects of TCS on mast cell degranulation. First, we have developed the method to prepare TCS in aqueous buffer and determine the resultant concentration by spectrophotometer, to avoid unnecessary confounding effects of organic solvents (Weatherly *et al*., 2013). We found that TCS rapidly inhibits MC degranulation in Ag-mediated as well as Ca^{2+} ionophore-stimulated RBL cells (Palmer *et al*., 2012). This finding was replicated in human (HMC-1) mast cells (Weatherly *et al*., 2016). Inhibited MC degranulation by

TCS might be a potential explanation for the TCS usage as a treatment of atopic dermatitis (Tan *et al*., 2010).

We then endeavoured to elucidate the mechanisms by which TCS disrupts degranulation. Recently, we have demonstrated that TCS is a proton ionophore mitochondrial uncoupler (MU) in several cell types (RBL, HMC-1.2, NIH-3T3, and primary human keratinocytes) and in living zebrafish (Shim *et al*., 2016b). In both *in vitro* and *in vivo* models, TCS inhibits ATP production and increases OCR. We also revealed that TCS disrupts mitochondrial structure, mitochondrial membrane potential and calcium signaling (Weatherly *et al*., 2018). In addition, Popova *et al*. (2018) demonstrated that TCS acts as a protonophore, which permeates artificial bilayer lipid membranes, thus transporting protons across the membrane, resulting in membrane depolarization. Interestingly, TCS showed more potent protonophoric activity than carbonyl cyanide 3-chlorophenylhydrazone (CCCP), which is a canonical protonophore/MU. TCS's protonophoric activity was also tested using bacterial membrane and isolated rat liver mitochondria: TCS elicited bacterial membrane depolarization and induced mitochondria swelling in rat liver. This study also showed that TCS induces calcium efflux from mitochondria, leading to disruption of calcium homeostasis, in agreement with our previous data by Weatherly *et al*. (Popova *et al*., 2018; Weatherly *et al*., 2018). Thus, these studies strongly suggest that TCS disrupts mitochondrial function and membrane potential.

We further investigate the targets of triclosan's inhibitory action in the MC signaling transduction pathway, in particular, two key signaling molecules downstream of Ca^{2+} influx: protein kinase C (PKC) and phospholipase D (PLD). The detailed of mechanistic studies on these molecules will be discussed in Chapter 3.

1.4 Current studies

Mast cells are physiologically important cells, involved in myriad biological events as well as various diseases. Thus, disruption of mast cell function might trigger many unfavourable effects in an organism.

Arsenic exposure is a global concern since it is commonly detected in drinking water and food sources. While arsenic is known to inhibit MC function (Hutchinson *et al*., 2011), until now the underlying biochemical mechanisms were unknown. Chapter 2 describes the molecular mechanisms underlying inorganic Arsenite inhibition of MC degranulation: by hampering early tyrosine kinase Syk and its substrate PI3K.

Synthetic antimicrobial agent triclosan has also been shown to inhibit MC function, but the underlying molecular mechanisms were previously unknown. Chapter 3 reveals triclosan's molecular targets in the MC signaling pathway, which are very different from arsenic's targets. Since our previous findings on TCS effects on Ca^{2+} mobilization in stimulated MCs, we examined downstream key players post Ca^{2+} influx. We found that PLD activity was strongly impeded, and subcellular translocations of PKC and its substrate, MARCKS, were delayed by TCS.

In Chapter 4, we report that one of the most utilized MC cell culture model RBL-2H3 cells do not express the classical mast cell marker tryptase. We have developed and employed several assays to detect tryptase release from the RBL cell supernatant, but no measureable signals were detected. We also examined the expression of mRNA transcript of tryptase genes from RBL by PCR, but no tryptase mRNA was detected. Before this study, the question of why tryptase was not typically utilized in RBL-2H3 mast cell studies was unanswered for decades.

Finally, Chapter 5 depicts a novel *in vivo* high-throughput assay using zebrafish embryos to measure mitochondrial bioenergetics. Previously, TCS had been shown to be a proton ionophoric mitochondrial uncoupler in numerous cell lines (Ajao *et al*., 2015; Weatherly *et al*., 2016) and in isolated mitochondria (Newton *et al*., 2005), but this mitotoxicity had not yet been confirmed in an animal. Using this method, we have demonstrated that TCS is a mitochondrial uncoupler in a living organism, zebrafish.

CHAPTER 2

ARSENIC INHIBITS MAST CELL DEGRANULATION VIA SUPPRESSION OF EARLY TYROSINE PHOSPHORYLATION EVENTS[1]

2.1 Abstract

Exposure to arsenic (As) is a global health concern. We previously documented an inhibitory effect of inorganic Arsenite on IgE- mediated degranulation of RBL-2H3 mast cells (Hutchinson *et al*., 2011). Mast cells are tissue-resident cells that are positioned at the host-environment interface, thereby serving vital roles in many physiological processes and disease states, in addition to their well-known roles in allergy and asthma. Upon activation, mast cells secrete several mediators from cytoplasmic granules, in degranulation. The present study is an investigation of Arsenite's molecular target(s) in the degranulation pathway. Here, we report that arsenic does not affect degranulation stimulated by either the Ca^{2+}ionophore A23187 or thapsigargin, which both bypass early signaling events. As also does not alter degranulation initiated by another non-IgE-mediated mast cell stimulant, the G-protein activator compound 48/80. However, arsenic inhibits Ca^{2+} influx into antigen-activated mast cells. These results indicate that target of arsenic in the degranulation pathway is upstream of Ca^{2+} influx. Phospho-Syk and phospho-p85 phosphoinositide 3-kinase enzyme-linked immunosorbent assays data show that arsenic inhibits early phosphorylation events. Taken together, this evidence indicates that the mechanism underlying arsenic inhibition of mast cell degranulation occurs at the early tyrosine phosphorylation steps in the degranulation pathway.

[1] A portion (50%) of this work was performed by Rachel Kenndey (Kennedy, R.H., 2013. Effects of endocrine disrupting chemicals on mast cell function, Electronic Theses and Dissertations. University of Maine) with the remainder being performed by Juyoung Shim.

2.2 Short Abstract

Arsenite (As) inhibits IgE-mediated degranulation of RBL-2H3 mast cells. Mast cells serve vital roles in many physiological processes and diseases. Upon activation, mast cells secrete mediators from cytoplasmic granules, in degranulation. Here, we report that As does not affect degranulation stimulated by Ca^{2+} ionophore A23187, thapsigargin, or the G-protein activator compound 48/80, all of which bypass early signaling events. However, arsenic inhibits Ca^{2+}influx into antigen-activated mast cells. Syk and phosphoinositide 3-kinase ELISA data show that arsenic inhibits early phosphorylation events.

2.3 Introduction

Exposure to arsenic is a major human health concern according to both the World Health Organization and the Agency for Toxic Substances and Disease Registry (NRC, 2001; ATSDR, 2007). Millions of people worldwide are exposed to high levels of arsenic from a variety of natural and anthropogenic sources, including drinking water, various foods, pesticides, mining sites, and toxic waste sites. Many private water wells in the U.S., as well as those around the world (such as South America and Bangladesh) routinely contain levels of As well above 50 ppb (parts per billion; µg/L), and sometimes as high as 3000 ppb (ATSDR, 2007).

Chronic exposure to arsenic, in particular via drinking water, has been correlated to many diseases, including severe dermatological disorders (Smith *et al*., 2000; Xia *et al*., 2009; Paul *et al*., 2013), respiratory diseases (Smith *et al*., 1992; Hopenhayn-Rich *et al*., 1998; Putila and Guo, 2011), diabetes/obesity (Abernathy *et al*., 1999; Maull *et al*., 2012), and cardiovascular disease (Chen *et al*., 2009; Huang *et al*., 2009; Smith and Steinmaus, 2009; Abhyankar *et al*., 2012; Das *et al*., 2012). Arsenic exposure also inhibits hematopoietic and immune systems

(NRC, 2001) and causes neurological and cognitive impairments (Wasserman *et al*., 2004; Wasserman *et al*., 2007; Chen *et al*., 2009). Moreover, arsenic is a known human carcinogen, which affects almost all major organs including liver, kidney, bladder, skin and lung (Ferreccio *et al*., 2000; Chiu *et al*., 2004; Liaw *et al*., 2008; Heck *et al*., 2009; Putila and Guo, 2011; Liu-Mares *et al*., 2013; Mostafa and Cherry, 2013; Naujokas *et al*., 2013; Saint-Jacques *et al*., 2014).

We recently demonstrated that antigen-stimulated degranulation of the mast cell model rat basophilic leukemia cells (RBL-2H3) is inhibited by non-cytotoxic doses of inorganic Arsenite (Hutchinson *et al*., 2011). Mast cells are multi- effector immune cells that participate in the first line of defense against parasites. Mast cells, found in most human tissues (Kuby, 1997), are also major effectors in allergic responses, asthma, other innate immune processes, and carcinogenesis. Mast cells are also involved in neurological conditions such as multiple sclerosis, autism, and anxiety (Silver and Curley, 2013). The RBL-2H3 mast cell model is biologically very similar to human basophils and rodent mucosal mast cells (Fewtrell, 1979; Seldin *et al*., 1985; Metzger *et al*., 1986).

Arsenic can be detected in a variety of human samples, and urine and blood are usually the major materials that are monitored for arsenic exposure (Kraus *et al*., 2000). However, arsenic can be stored and concentrated in the tissues of many organs such as kidney, lung, skin, and liver (Benramdane *et al*., 1999), and mast cells are found in most human organs, as we discussed in Hutchinson, *et al*. (2011). In fact, the concentrations of arsenic found in tissue tend to be higher (up to ~7-350 fold higher) than in blood (Benramdane *et al*., 1999). In a previous article (Hutchinson *et al*., 2011), we noted several publications reporting human tissues containing between 100 and 6000 ppb arsenic. For example, one study examined tissue arsenic

concentrations in people who had regularly consumed drinking water containing 220-2000 ppb arsenic and found several hundred to several thousand ppb arsenic (Schroeder *et al*., 1968). Since mast cells function within tissues, it is necessary to study arsenic concentrations that are found within tissues. Thus, the 100-750 ppb arsenic concentrations employed in this study are biologically relevant.

Highly granulated, mast cells respond to various stimuli by partially or completely releasing the contents of their granules, which include a range of mediators such as histamine and serotonin. The mechanism underlying arsenic inhibition of the function of mast cell degranulation is not yet known. Given the complexity of the degranulation signal transduction pathway and the similarities to signaling pathways in other immune cells, such as T cells, there are many potential targets for arsenic inhibition.

Degranulation is a process that classically begins with antigen crosslinking of IgE-bound FcεRI receptors, which abound on the mast cell surface (Kuby, 1997). The physical aggregation of the receptors results in their tyrosine phosphorylation by the protein tyrosine kinase Lyn (Kinet, 1999; Xiao *et al*., 2005). Phosphorylation of the receptor causes the protein tyrosine kinase spleen tyrosine kinase (Syk) to be recruited to the receptor (Benhamou *et al*., 1993; On *et al*., 2004). The activation of Syk (Minoguchi *et al*., 1994; Zhang *et al*., 2000), leads to the activation of phospholipase C (PLC) γ (Benhamou *et al*., 1992; Beaven and Metzger, 1993) and results in Ca^{2+} mobilization (Ferris *et al*., 1989; Millard *et al*., 1989; Putney *et al*., 2001), which is essential to degranulation (Zhang *et al*., 1996).

PLC γ1 is an important player in Ag-receptor signaling: it catalyzes the hydrolysis of the membrane phospholipid phosphatidylinositol 4,5-bisphosphate (PIP_2) to generate second messengers inositol-1,4,5 - trisphosphate (IP_3) and diacylglycerol (DAG). IP_3 initiates the release

of Ca^{2+} from internal stores (*i.e.*, the endoplasmic reticulum [ER]), while DAG is responsible for activation of an assortment of protein kinase C (PKC) isoforms (Kalesnikoff and Galli, 2008). Activated PKC phosphorylates the cytoskeletal protein myosin, important for degranulation (Ludowyke *et al*., 1989).

A second signaling pathway resulting in IP_3 generation is initiated by phosphoinositide 3-Kinase (PI3K), which is activated by Syk (Okkenhaug and Vanhaesebroeck, 2003; Mocsai *et al*., 2010) and which phosphorylates inositol lipids to generate the signaling molecules PIP_2 and PIP_3 (Kitaura *et al*., 2000). PIP_2 is then used by PLC γ to generate IP_3. PH domains within PLC γ, Vav, Akt, Btk, and PDK1 mediate binding of these proteins to PIP_2 and to PIP_3, thus drawing these proteins to the plasma membrane for activation (Kitaura *et al*., 2000; Abramson and Pecht, 2007). For example, PDK1 activation leads to activation of PKC δ, important for degranulation. Overall, PI3K activates Ca^{2+} influx and degranulation of mast cells (Ching *et al*., 2001).

IP_3 is crucial for degranulation. Activation of IP_3 receptors initiates a biphasic increase in intracellular Ca^{2+} (Berridge, 1993; Taylor and Thorn, 2001). The binding of IP_3 to its receptors in the ER causes Ca^{2+} to be released from the internal ER stores, causing depletion of Ca^{2+} from the ER. IP_3 receptors are ion channels that allow for passive diffusion of Ca^{2+} from the ER (Scharenberg *et al*., 2007). Depletion of Ca^{2+} stores results in an influx of Ca^{2+} across the plasma membrane through calcium release-activated calcium (CRAC) channels (Hogan *et al*., 2010), which is referred to as "store operated calcium entry" (SOCE) (Putney, 1986; Putney, 1990; Clapham, 1995), producing an extracellular Ca^{2+} influx and calcium-release activated current (Kraft and Kinet, 2007). The major players in "store operated calcium entry" are STIM-1 (Liou *et al*., 2005; Zhang *et al*., 2005), an ER calcium sensor which interacts directly with Orai1 channels (Feske *et al*., 2006; Vig *et al*., 2006), the pore subunit of CRAC channels within the

plasma membrane, to couple depletion of ER Ca^{2+} with activation of CRAC channels. Influx of Ca^{2+} across the plasma membrane permits reuptake of Ca^{2+} into the ER through sarco/endoplasmic Ca^{2+}-ATPase (SERCA) pumps (Ma and Beaven, 2011), which actively pump Ca^{2+} from the cytosol into the ER to replenish internal stores (Scharenberg *et al*., 2007). Depletion of the ER pool of Ca^{2+} by either IP_3 or the compound thapsigargin (selective inhibition of SERCA) (Thastrup *et al*., 1990; Lytton *et al*., 1991) leads to entrance of Ca^{2+} into the cell (Ma and Beaven, 2011). Overall, the primary synergistic signals for secretion are an increase in intracellular Ca^{2+} as well as activation of PKC (Ozawa *et al*., 1993a).

Next, increases in intracellular Ca^{2+} and PKC translocation work in tandem to activate phospholipase D (PLD) (Lin and Gilfillan, 1992). In fact, PLD can be activated in RBL-2H3 cells via several means: FcεRI receptor crosslinkers (Dinh and Kennerly, 1991; Ali *et al*., 1996), thapsigargin (Cissel *et al*., 1998), Ca^{2+} ionophore (Lin and Gilfillan, 1992), and compound 48/80 (Chahdi *et al*., 2000). PLD hydrolyzes phosphatidylcholine into phosphatidic acid (PA), which has been shown to stimulate PLC γ (Nishizuka, 1995). PA is converted to DAG by PA phosphohydrolase, thus causing a secondary rise in intracellular DAG levels (Nakashima et al., 1991; Lin et al., 1992). These increases have been shown to be important for the translocation and activation of the DAG-dependent isoforms of PKC (Lin et al., 1992; Nishizuka, 1995; Peng and Beaven, 2005). PLD1 is involved in granule translocation, and PLD2 is involved in membrane fusion of the granules (Choi *et al*., 2002). Granules are transported from the cell interior to the plasma membrane with the help of microtubules, where they dock with the help of multiple soluble N-ethylmaleimide-sensitive factor attachment protein receptors (Guo et al., 1998; Baram et al., 1999; Paumet et al., 2000; Blank et al., 2002; Logan et al., 2003; Puri and Roche, 2008; Tiwari et al., 2008; Woska and Gillespie, 2012). The result of mast cell signaling

is fusion of intracellular granules with the plasma membrane, causing the release of histamine, serotonin, leukotrienes, cytokines, β-hexosaminidase, and enzymes that trigger the symptoms of allergy and asthma and that play many other crucial physiological roles (Kopeć *et al*., 2006). Simultaneously, F-actin polymerization causes membrane "ruffling."

Actin cytoskeletal rearrangement is not an essential element of the degranulation pathway (degranulation occurs even when ruffling is stopped by actin inhibitor cytochalasin D (Holowka *et al*., 2000)), but the two share common events such as activation of PKC and influx of Ca^{2+} (Pfeiffer *et al*., 1985; Yanase *et al*., 2011). In a recent paper by Yanase *et al*. (2011), it was shown that the use of inhibitors of PKC β and PKC α inhibit both ruffling and degranulation. PLD2 also is important for membrane ruffle formation.

As part of our investigation of arsenic's mechanism of mast cell inhibition, we utilized another non-IgE-mediated stimulating method, compound 48/80 (c48/80), a polybasic mast cell secretagogue which has potent anaphylactic properties *in vivo* (Lagunoff *et al*., 1983; Chahdi *et al*., 2000) and which effects degranulation from rat mast cells (Johnson and Moran, 1969). Compound 48/80 is believed to act by the stimulation of heterotrimeric G-proteins (Chahdi *et al*., 2000), in particular, via Gi-2 and Gi-3 in RBL-2H3 cells (Senyshyn *et al*., 1998). Pretreatment of RBL-2H3 cells with the flavonoid quercetin causes an increase in histamine-containing intracellular granules (Trnovsky *et al*., 1993) and an over-expression of Gi-3α and Gi-2α (Senyshyn *et al*., 1998; Chahdi *et al*., 2000), so pre-incubation of RBL-2H3 cells with quercetin is required prior to exposure with c48/80 in order to make the cells responsive to c48/80-induced degranulation (Galli *et al*., 2008). Phospholipase D (PLD) is stimulated by c48/80 in quercetin-treated RBL-2H3 cells (Aridor *et al*., 1990; Senyshyn *et al*., 1998; Chahdi *et al*., 2000). Compound 48/80 induces a Ca^{2+} -dependent degranulation response that releases Ca^{2+} from

intracellular pools (Aridor *et al*., 1990; Hirasawa *et al*., 1995; Senyshyn *et al*., 1998), and transiently activates phospholipase C (PLC), possibly through indirect activation of PLD (Ali *et al*., 1990; Aridor *et al*., 1990; Park *et al*., 1991; Yamada *et al*., 1992; Senyshyn *et al*., 1998). Therefore, due to c48/80's mechanism of action, we were able to assess the possibility of arsenic targeting PLC, PLD, and calcium influx.

It is well established that Ca^{2+} influx is a crucial for mast cell degranulation. To explore whether the level of FcεRI-mediated cytoplasmic Ca^{2+} in RBL-2H3 mast cells is changed by arsenic exposure, we developed a microplate-based method to monitor the level of Ca^{2+} utilizing the fluorescent Ca^{2+} indicator. Using this method, we were able to measure the cytosolic Ca^{2+} levels in real time for over 2h after cells were stimulated and exposed to arsenic.

Finally, we evaluated the effect of arsenic on key phosphorylation events, crucial early signaling events in the mast cell degranulation pathway. It has previously been demonstrated that arsenic affects tyrosine phosphorylation events (Qian *et al*., 2003), including T cell signal transduction (Soto-Peña and Vega, 2008). Arsenic trioxide inhibits the PI3K/Akt pathway in chronic lymphocytic leukemia cells (Goussetis and Platanias, 2010). PI3K is a heterodimeric enzyme composed of a catalytic subunit (p110) and a regulatory subunit (p85) (Koyasu, 2003). PI3K is activated by Syk kinase (Okkenhaug and Vanhaesebroeck, 2003). Here we have examined the effect of arsenic on PI3K and Syk kinase by employing enzyme-linked immunosorbent assays (ELISA). The global phosphorylated Syk levels in the Ag-activated RBL cells were measured. For PI3K, both the phosphorylated p85 subunit of PI3K and the total PI3K p85 subunit were evaluated.

In this study, we unraveled the molecular mechanism used by Arsenite to inhibit mast cell function. We employed multiple experimental approaches in RBL-2H3 cells to determine

the mechanism of arsenic inhibition of mast cell degranulation. Here we present mechanistic data resulting from degranulation assays utilizing various stimulants, F-actin imaging, Ca^{2+} measurements, and ELISAs probing early phosphorylation events. We demonstrate that arsenic acts very early in the signaling pathway leading to degranulation, inhibiting the nearly immediate event of Syk kinase phosphorylation.

2.4 Materials and Methods

2.4.1 Chemicals and Reagents

A23187 ionophore, compound 48/80 (c48/80), quercetin, dimethyl sulfoxide (DMSO), sodium azide, and sulfinpyrazone were purchased from Sigma Aldrich (St. Louis, MO, USA). Thapsigargin (Tg) was obtained from Calbiochem/EMD Millipore (Billerica, MA, USA). Tyrodes buffer, bovine serum albumin (BSA)-Tyrodes (BT), sodium acetate buffer, and glycine carbonate buffer were prepared as previously described (Hutchinson *et al*., 2011). A low- Ca^{2+} Tyrodes (containing 0.9 mM rather than the typical 1.8 mM $CaCl_2$) was used in all c48/80 experiments. Chemicals of the highest possible purity were used. All buffers and media were sterile-filtered with VacuCap bottle-top filter devices (0.2 μM; Pall Life Sciences, Port Washington, NY, USA).

Arsenic was prepared under sterile conditions as 10 mM stocks of inorganic sodium (meta) arsenite (CAS no. 7784-46-5; manufactured by either JT Baker, Phillipsburg, NJ, USA; or Fluka, Seelze, Germany), and dissolved in sterile cell culture water (BioWhittaker Lonza, Walkersville, MD, USA). The stock was 0.2-μM filtered and stored as previously described by (Hutchinson *et al*., 2011).

Ca^{2+} ionophore A23187 was prepared by dissolving A23187 powder into 100% DMSO for a final concentration of 2.5 mg/ml. The solution was transferred to a microcentrifuge tube with a parafilmed lid and was wrapped in aluminum foil, for storage at -20 °C. On the day of an experiment, this stock was diluted directly into BT solution to create ionophore concentrations of 1.5×10^{-7} M and 2×10^{-7} M (0.004% DMSO).

Tg was prepared as described in (Weatherly *et al*., 2016). The highest DMSO vehicle concentration used in these experiments was 0.001 % (v/v).

Compound 48/80 was prepared using aseptic conditions as 30 mg/ ml stocks dissolved in cell culture water, aliquoted into sterile polypropylene microfuge tubes, and frozen at -20 °C until the day of use, so that each individual aliquot underwent only one freeze/thaw cycle. Quercetin was prepared as a 60 mM stock from anhydrous quercetin powder in 100% DMSO. Cells were treated with 20µM quercetin in RBL media (Hutchinson *et al*., 2011), resulting in a DMSO vehicle concentration of 0.033 % (v/v).

Fluo-4/AM (Life technologies, Grand Island, NY, USA) was dissolved in 100% DMSO to prepare a 911µM stock and stored at -20 °C until the day of use, so that each individual aliquot underwent only one freeze/thaw cycle.

2.4.2 RBL-2H3 Cell Culture

Cell culture methods were those of (Hutchinson *et al*., 2011)

2.4.3 Cytotoxicity Assays

Trypan blue exclusion assays were performed as previously described in detail by Hutchinson *et al*. (2011) and Palmer *et al*. (2012). In general, the details remained unchanged,

with the exception of the use of c48/80, which required a slightly different procedure in order to accommodate a 48h quercetin pre-treatment as well as the use of a low- Ca^{2+} Tyrodes buffer. Accordingly, RBL-2H3 cells were plated into sterile tissue culture treated, six-well plates (VWR, Radnor, PA, USA) at a density of 0.85 x 10^6 cells/well in RBL medium supplemented with 20 μM quercetin and incubated for 48 h at 37°C, 5% CO_2. After 48 h, spent medium was discarded, and fresh RBL medium was added to the cells for 30 min at 37°C, 5% CO_2. This liquid was then discarded, and low Ca^{2+} Tyrodes buffer ± 25 μg/ml c48/80 or vehicle ± arsenic was added to each well for 15 min at 37°C, 5% CO_2. This medium was removed, and wells were washed with 2 mL low Ca^{2+} Tyrodes to remove dead cells. Following removal of this wash, wells were rinsed with 1 mL trypsin. Plates were then incubated with 1 mL fresh trypsin for 10 minutes at 37°C, 5% CO_2 to allow cells to dislodge completely from the plates. Further removal of cells after this incubation was accomplished by repeated pipetting of the cell-containing trypsin into the wells, removing visible traces of cells from the surface of the well. The cell-containing trypsin was then quenched by addition into 1 mL of RBL media. Equal volumes of this mixture and trypan blue stain (Trypan Blue 0.4% solution in 0.85% NaCl; BioWhittaker Lonza) were then combined, and cell viability was assessed by counting those cells able to exclude the trypan blue stain using a hemocytometer (Bright-line, Hausser Scientific, Horsham, PA, USA). Values of living cells were then normalized to the vehicle values for any given assay before data compilation.

Lactate dehydrogenase (LDH) assay was performed as previously described (Hutchinson *et al*., 2011; Palmer *et al*., 2012).

ATP production and cytotoxicity were assayed via Promega (Madison, WI, USA) Toxglo kit instructions as described in (Weatherly *et al*., 2016). Arsenic exposures lasted 1 h.

2.4.4 Antigen-Mediated Degranulation Assay

Cells were sensitized by IgE, as described in (Weatherly *et al*., 2013). IgE-bound FcεRI receptors of RBL cells were aggregated by dinitrophenyl (DNP)-BSA multivalent Ag ± arsenic (for 1 h). Degranulation (release of β-hexosaminidase) was measured via a fluorescence-based 96-well microplate reader assay, as illustrated in (Weatherly *et al*., 2013).

2.4.5 Confocal Imaging of Membrane Ruffling

Experiments were performed as in (Palmer *et al*., 2012). Arsenic was used in place of triclosan; thus, vehicle in control samples was cell culture water.

2.4.6 Ca^{2+} Ionophore-Stimulated Degranulation in RBL-2H3 Cells

This assay was essentially performed as described by (Weatherly *et al*., 2013), except that two different Ca^{2+} ionophore A23187 doses (1.5×10^{-7} M and 2×10^{-7} M) were used, based on their ability to elicit a low-range and mid-range level of degranulation, respectively, with this lot of A23187. Additionally, arsenic (in place of triclosan) was diluted into A23187/BT solution at the noted concentrations (0.004% DMSO vehicle in all samples).

2.4.7 Thapsigargin-Induced Degranulation

To test the ability of arsenic to alter an earlier Ca^{2+} signaling event than that induced by A23187 Ca^{2+} ionophore, we used Tg, a known inhibitor of SERCA in mammalian cells. Degranulation experiments were conducted similarly to antigen-stimulated RBL-2H3 degranulation experiments (Weatherly *et al*., 2013), except that there was no IgE pretreatment and that RBL-2H3 cells were treated with 4.6 nM Tg for one hour (37 °C and 5% CO_2) in the

presence of 0-750 ppb arsenic. To combine multiple experiments, data were normalized to the response elicited by 4.6 nM Tg in the presence of arsenic vehicle only (cell culture water).

2.4.8 Compound 48/80-Mediated Degranulation

RBL cells were harvested after 2-5 days of growth via trypsinization, and were resuspended at a density of 0.25 x 10^6 cells/ml in fresh RBL medium ± 20μM quercetin. One hundred microliter of this suspension per well was plated in black flat-bottom, tissue culture-treated, sterile, 96-well plates (Greiner Bio-One, Monroe, NC, USA). After 48 h in a 5% CO_2 incubator at 37°C, spent RBL medium ± quercetin was removed by decanting. From here, sample wells were washed twice with 0.9 mM Ca^{2+} (low-calcium) Tyrodes, and 100 μl/well fresh RBL medium was added to cells for 30 min (Galli *et al*., 2008). Stimulated cell samples then received 200μl aliquots of c48/80, spontaneous release cells received plain low Ca^{2+} Tyrodes, and lysed cells received Triton-X 100 diluted to 0.2% (v/v) in low- Ca^{2+} Tyrodes. Degranulation (release of β-hexosaminidase) was quantified as previously described (Weatherly *et al*., 2013).

2.4.9 Calcium measurement assay

RBL-2H3 cells (100μL/well) were plated in a 96-well plate in RBL media at a density of 0.5 x 10^6 cells/ml and incubated overnight at 37°C and 5% CO_2. Also, 2 mM sulfinpyrazone solution in Tyrodes buffer was prepared, vortexed, and rotated at 37°C overnight. On the following day, cells were sensitized with 0.1 μg/ml anti-DNP IgE (Sigma) (in RBL media; 100μL per well) for 1 h at 37°C and 5% CO_2. Sulfinpyrazone solution (2mM) was sterilized using syringe filtration (0.2 μm), after its pH was adjusted to 7.4, and then was diluted to 0.6 mM

using BT (2 mg/mL BT). The stock of 911µM Fluo-4/AM dye was diluted to 4.55 µM using BT. For DMSO control samples, 0.5% DMSO-BT was also prepared. Some of the 4.55 µM Fluo-4/AM-BT was further diluted to be 2.5 µM using 0.6 mM sulfinpyrazone in BT (Fluo-4/AM-sulfinpyrazone-BT) and 0.27% DMSO-sulfinpyrazone- BT was also prepared as the corresponding vehicle control.

After 1h IgE-sensitization, cells were washed with warm BT (200 µL per well), followed by addition of 100 µL per well of 4.55 µM Fluo-4/AM-BT, 0.5% DMSO-BT, or BT (all in the absence of sulfinpyrazone), to the appropriate wells for 1 min. Immediately after 1 min, these solutions were discarded, and 200 µL per well of 2.5 µM Fluo-4/AM-sulfinpyrazone- BT, 0.27% DMSO-sulfinpyrazone-BT, or 0.6 mM sulfinpyrazone- BT was added for 30 min at 37°C. After 30 min of Fluo-4 incubation, cells were washed twice with 0.6 mM sulfinpyrazone - BT (200 µL per well), and then 250 µL per well of 0.6 mM sulfinpyrazone-BT were added for the baseline fluorescence reading at 485 nm excitation and 528 nm emission for 2 min (42 s intervals between readings). The sulfinpyrazone-BT solutions were discarded from the plate, and 240 µL per well of 0.6 mM sulfinpyrazone-BT ± 0.0002 µg/mL antigen ± 750 ppb arsenic were added to the corresponding wells. Fluorescence readings, at 485 nm excitation and 528 nm emission, were taken for 1 h post- stimulation (42 s intervals between readings).

After the hour, for maximal Ca^{2+} readings, which are a measurement of cell number per well, 10 µL of 10% Triton-X 100 (TX-100) was added to each well. The fluorescence reading was taken after a10 min incubation (with agitation) at 37°C. TX-100 fluorescent values for all replicates were averaged, and no differences among samples were determined by one-way ANOVA followed by Tukey's post- test (data not shown), indicating that all wells contained equal numbers of cells.

Finally, 50 µL of 0.5M EDTA (USB, Cleveland, OH, USA), which chelates Ca^{2+} and lowers the fluorescent signal to the background level, was added to each well, and the fluorescence reading was taken after a 5 min incubation. Fluorescence levels dropped to no-Fluo-4 background levels, and no statistically significant differences among samples were found (data not shown), indicating that measured fluorescence signals were due to the interaction of Fluo-4 dye and Ca^{2+}.

2.4.10 Phospho-p85 PI3K ELISA

A Fast Activated Cell-based ELISA Kit (Active Motif, Carlsbad, CA, USA) was used, to detect the levels of both phosphorylated and total PI3K p85 in the cell, according to the manufacturer's instructions. RBL-2H3 cells (100 µL per well) were plated in a clear 96-well plate at a density of 0.5 x 10^6 cells/ml and incubated for 12-16 h at 37°C and 5% CO_2. On the following day, after 1 h sensitization with 0.1 µg/ml anti-DNP IgE (Sigma), cells were stimulated with either 1µg/ml DNP-BSA antigen or BT (control) ± 750 ppb arsenic for 5 min at 37°C. Next, cells were fixed with 4% formaldehyde (Sigma) in PBS (Lonza, Rockland, ME, USA) solution at room temperature for 20 min. Once the formaldehyde mixture was discarded, cells were washed three times with 1X wash buffer provided in the kit (200 µL per well per wash; 5 min gentle shaking per wash). The remaining steps were carried out according to the manufacturer's directions. Absorbance was measured (at 450 nm) immediately after the addition of the "stop" solution. Cells were then stained with crystal violet, following the manufacturer's protocol, and absorbance was read at 595 nm. The measured OD_{450} reading was then corrected for cell number by dividing the OD_{450} value by the OD_{595} value for each well.

2.4.11 Phospho-Syk ELISA

PathScan® Phospho-Syk sandwich ELISA kit (Cell Signaling Technologies, Beverly, MA, USA) was used to detect endogenous levels of phosphorylated Syk according to the manufacturer's instructions. This is a pan-tyrosine ELISA, able to detect altered phosphorylation for all Syk's key Tyr residues. For this assay, RBL-2H3 (1.75×10^6 cells/mL) were plated on 10 cm^2 tissue-culture treated, sterile dishes (Cellstar, Greiner Bio-One, Monroe, NC, USA) at a volume of 6.5 mL per well (final cell density of 1.14×10^7 cells per dish), and were incubated overnight (12-16 h) at 5% CO_2 and 37°C. Cells were sensitized overnight by addition of 1µg/ml anti-DNP IgE (generously provided by Drs. Barbara Baird and David Holowka, Cornell University) in RBL media or the following day for 1 h with 0.1 µg/ml anti-DNP IgE (Sigma).

Following the overnight incubation, each dish was checked to ensure a cell confluence of 80-90%. After IgE-sensitization (37°C and 5% CO_2), spent IgE-media mixture was discarded, and dishes were washed twice with 5 ml BT to remove any unbound IgE. The 5 ml treatments added next included either BT for the unstimulated controls or DNP-BSA antigen at 1µg/ml for stimulated samples; all samples included arsenic or water vehicle (cell culture water, Lonza, Rockland, ME, USA). Dishes were incubated for exactly 5 min in a bacterial incubator at 37°C. Immediately, dishes were placed on ice, washed once with ice-cold PBS (~5 mL), and lysed with 0.4 mL of ice-cold 1X lysis buffer containing phenylmethanesulfonyl fluoride solution for 5 min. (The 10X lysis buffer provided in the kit was diluted with sterile water before use;100 mM phenylmethanesulfonyl fluoride [Sigma] stock dissolved in ethanol was added at a concentration of 1 mM immediately prior to buffer addition). Next, cells were harvested by scraping and were placed into pre-cooled 2mL microcentrifuge tubes. Cell suspensions were sonicated three times on ice by introducing a clean sonicating probe directly into the sample. The sonicator (Branson

Sonifier, Branson Ultrasonics Corporation, Danbury, CT, USA) was set at output control of 5, duty cycle of 30, Timer at 2, 1 s in duration, with a 10 s break on ice in between sonications (these sonicating conditions were found to result in complete cell lysis; data not shown). Finally, the sonicated lysates were spun down at 14400xg for 10 min at 4°C. A volume of 100 µL of clarified supernatant was transferred to new, pre-cooled tubes containing 100 µL sample diluent (provided in kit). After a brief vortex, 100 µL of each diluted sample was placed into an appropriate ELISA well, sealed with parafilm, and incubated for 16-20 h at 4°C. The remaining steps were carried out according to the manufacturer's directions. Absorbance was measured immediately after the addition of the "stop" solution.

2.4.12 Statistical analyses

Unless otherwise indicated in individual figures, results from degranulation experiments (using Ag ± A23187 Ca^{2+} ionophore, Tg, or c48/80) are reported as mean ± SEM, with significant differences determined using Graphpad Prism software (San Diego, CA, USA). For multiple-comparison testing, Tukey's *post hoc test* was used following one-way ANOVA. In several cases, data required normalization in order to control for day-to-day variation of cell culture; in these instances, Tukey's comparisons are reported with regard to a low dose of the agent used that was not significantly different from the 0 control to which all values were normalized. In the event that normalization was not required, significance was directly made to the 0 control.

For calcium measurement assay, the data were analyzed as areas under the curve (AUC), a measure of total calcium response over a 30 or 60 min period. First, the fluorescence values before antigen stimulation (baseline) were averaged, then subtracted from the corresponding

antigen-stimulated samples' fluorescence values. Next, those values were normalized to the last 0 ppb arsenic time point. These normalized values were used to determine AUC via Graphpad Prism software. The AUC values were further normalized to each day's 0 ppb arsenic AUC value, and the data from multiple days of experiments were expressed as a bar graph. The statistical significance was determined via one-way ANOVA with Tukey's *post hoc* test

For the phospho-p85 PI3K ELISA, the average value from the antigen + 750 ppb arsenic group was normalized to the average value from the antigen + 0 ppb arsenic group from each day before compiling multiple experiments, and significance was determined by one-sample unpaired t-test. For phospho-Syk ELISA, treatment samples (antigen ± 750 ppb arsenic) were expressed as a % increase over spontaneous control (no IgE/antigen) sample, and the statistical analysis was done by unpaired *t*-test.

2.5 Results

2.5.1 Short term exposure of arsenic inhibits antigen-mediated degranulation in RBL-2H3 mast cells without cytotoxicity

We have previously reported the ability of arsenic to inhibit degranulation in RBL-2H3 mast cells following 1 h exposure to DNP-BSA antigen (Ag) (Hutchinson *et al*., 2011) (Fig. 2.1).

We next tested whether degranulation is inhibited within 15min of antigen and arsenic exposure. Based on initial 15-min DNP-BSA antigen dose response data (not shown), 0.0004 μg/ml DNP-BSA antigen was chosen. This antigen dose was chosen because, in the absence of arsenic, it elicited a degranulation value of 9.4% ± 0.8% (SEM), which is similar to the response of the 0 ppb arsenic sample in Figure 2.1(Hutchinson *et al*., 2011). Arsenic (750 ppb) causes a

15% ± 2% (SEM) inhibition of the 0 ppb control value (Fig. A.1A). These data indicate the dampening effect of arsenic on antigen-mediated degranulation begins to occur quite rapidly in RBL mast cells. Arsenic has no significant effect on spontaneous degranulation (1.4% ± 0.1% [SEM]) during this time period (Fig. A.1B).

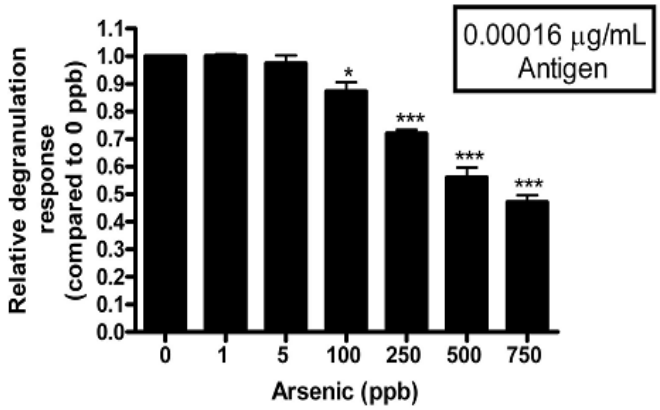

Figure 2.1. Arsenic inhibits RBL-2H3 cell degranulation following 1 h exposure to dinitrophenyl-bovine serum albumin antigen. Effects of various concentrations of arsenic on 1 h, 0.00016 μg/ml antigen-mediated degranulation were assessed as described (Hutchinson *et al*., 2011). In the absence of arsenic, this antigen dose elicited an average absolute degranulation response of 12 ± 2% (SEM; ~23% of the maximal response). Values represent means ± SEM for five independent experiments, where three replicates per dose were performed for each experiment. One-way ANOVA with Tukey's post-tests (compared to the 1 ppb sample) were performed using Graphpad Prism software; *p< 0.05, ***p< 0.001. Reprinted from (Hutchinson *et al*., 2011) (Copyright 2010 John Wiley & Sons, Ltd.)

To confirm the lack of cytotoxicity of high dose arsenic (up to 1500 ppb) seen in our previous work (Hutchinson *et al*., 2011), an additional cytotoxicity/mitochondrial function assay that measures both plasma membrane integrity and ATP production was performed. ATP is required for degranulation (Burgoyne and Morgan, 2003). Arsenic (up to 1500 ppb) is not only non-cytotoxic, but also does not disrupt ATP production (Fig. A2), even under buffer and timing conditions that allow for robust arsenic inhibition of antigen-stimulated degranulation (data not shown). Due to mammalian cell generation of ATP via both oxidative phosphorylation and glycolysis, glucose-free, galactose-containing media ("galactose media") was utilized to avoid

ATP production via glycolysis in this experiment (Fig. A2 A-B). In addition, neither cytotoxicity nor ATP depletion is observed in experiments utilizing glucose-containing media (Fig. A2 C-D), wherein cells produce sufficient ATP via glycolysis.

2.5.2 Membrane ruffling of F-actin in RBL-2H3 cells is not qualitatively affected by arsenic

RBL-2H3 cells were stained with Alexa 488-conjugated phalloidin to label F-actin and imaged with an Olympus confocal microscope. In the absence of FcεRI engagement (treatment with plain BT only, a "spontaneous release" control), cytoskeletal membrane ruffling is very limited or is not observed in cells (Fig. 2.2A). As seen in Fig. 2.2B, the addition of 750 ppb arsenic without an IgE-FcεRI crosslinking agent also does not lead to visible changes in F-actin distribution. Conversely, when IgE-bound FcεRI receptors were crosslinked by 0.00016 μg/ml DNP-BSA antigen, multiple membrane protrusions are observed (Fig. 2.2C). At this same antigen concentration (0.00016 μg/ml DNP-BSA) with the addition of 750 ppb arsenic, little or no qualitative difference is observed (Fig. 2.2D) compared to the no-arsenic control. Similar results are obtained with a mid-range dose of 0.0004 μg/ml Ag in the presence and absence of 750 ppb arsenic (Fig. A3). In summary, co-incubation of RBL-2H3 with DNP-BSA antigen and 750 ppb arsenic does not appear to substantially affect the extent of ruffling.

2.5.3 As does not inhibit degranulation of RBL-2H3 cells when stimulated with A23187 Ca^{2+} ionophore

Stimulation of RBL-2H3 cell degranulation using Ca^{2+} ionophore has been detailed in the scientific literature (Siraganian *et al*., 1975; Beaven *et al*., 1984; Hanson and Ziegler, 2002).

This method of degranulation bypasses engagement of FcεRI receptors, causing Ca^{2+} influx across the plasma membrane. Use of Ca^{2+} ionophore therefore allows identification of arsenic's cellular targets as being upstream or downstream of Ca^{2+} influx. Doses of A23187 ionophore were selected based on their non-cytotoxicity in a lactate dehydrogenase (LDH) assay (Fig. A4), in the presence of up to 750 ppb arsenic, which did not affect LDH enzyme activity (Fig. A5).

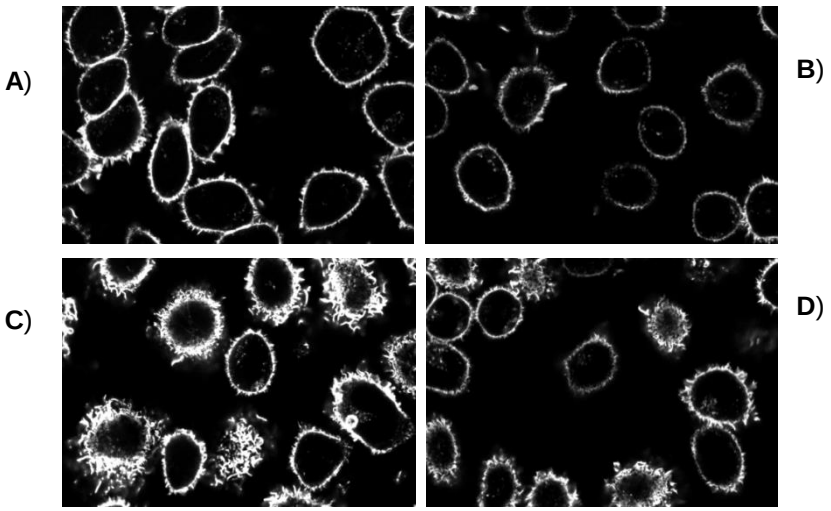

Figure 2 2. F-actin ruffling during antigen-stimulated degranulation of RBL-2H3 cells. F-actin was visualized using Alexa Fluor 488 conjugated phalloidin. RBL-2H3 cells were exposed to **(A)** no antigen; **(B)** no antigen+750 ppb arsenic; **(C)** 0.00016 μg/ml antigen; **(D)** 0.00016 μg/ml antigen+750 ppb arsenic for 1 h before being fixed. A representative set of images is shown.

DMSO has been linked to inhibition of interleukin-8 production (Deforge *et al*., 1992), decreased NF-κB activation in macrophage cells (Kelly *et al*., 1994), and has been shown to activate PKC and scavenge free radicals (Ogura *et al*., 1995). Arsenic an oxygen radical scavenger, DMSO has also been shown to inhibit the production of reactive oxygen species (ROS) in experimental studies (Hei *et al*., 1998; Liu *et al*., 2001). As ROS production has been shown to be vital to mast cell inflammatory responses (reviewed in (Swindle and Metcalfe, 2007)), and there is a strong relationship between ROS and degranulation in RBL-2H3 (Suzuki *et al*., 2003), it was important that we ensure the level of DMSO used in these ionophore

experiments does not impact degranulation in this way. We demonstrated that degranulation experiments containing 0.004% DMSO retain statistically significant inhibition, due to arsenic, of antigen-stimulated RBL-2H3 cells, and that DMSO at this concentration does not impact the cell's ability to degranulate. A two-way ANOVA in Prism was performed to compare antigen-stimulated degranulation experiments in the presence and absence of 0.004% DMSO: no statistically-significant difference was found (Fig. A6). These control data demonstrate that the degranulation values obtained from the A23187 Ca^{2+} ionophore tests are not impacted by the vehicle conditions.

We used the probe 2',7'-dichlorodihydrofluorescein diacetate (Cell Biolabs; San Diego, CA), which measures various intracellular ROS, in order to directly test whether arsenic modulates ROS under the treatment conditions of the degranulation experiments. Neither 500 nor 750 ppb arsenic affect intracellular ROS production at any time point measured for 1 h at 1-2 min intervals (data not shown).

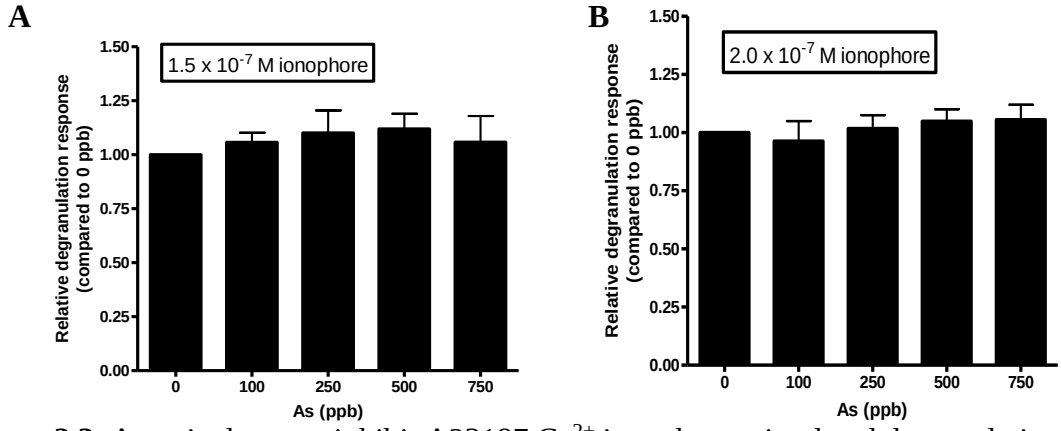

Figure 2.3. Arsenic does not inhibit A23187 Ca^{2+} ionophore-stimulated degranulation in RBL-2H3 cells. RBL-2H3 cells were harvested and plated as described in the "Methods" section. Cells were stimulated to degranulate for 1 h with either **(A)** 1.5 x 10^{-7} M (which caused an average absolute degranulation response of 11.5% ± 2.8% [SEM]) or **(B)** 2.0 x 10^{-7} M (which caused an average absolute degranulation response of 18.1% ± 3.2% [SEM]) A23187 Ca^{2+} ionophore. Resultant β-hexosaminidase was measured as described in "Methods." Values are means ± SEM from seven independent experiments per A23187 dose, each with three replicates per experiment. No statistical significance was determined by one-way ANOVA followed by Tukey's post- test, where multiple comparisons were made to the 100 ppb sample. As, arsenic.

Regarding the use of Ca^{2+} ionophore on RBL-2H3 cells, 1 h treatment of 1.5 x 10^{-7} M A23187 elicited an average absolute degranulation response of 11.5% ± 2.8% (SEM) in the absence of As (Fig.2.3A); exposure to 2.0 x 10^{-7} M A23187 resulted in a degranulation value of 18.1% ± 3.2% (SEM) (Fig.2.3B). Co-exposure to A23187 ionophore and arsenic (0-750 ppb) revealed no arsenic inhibition of degranulation (Fig.2.3). The lack of an inhibitory response due to As on Ca^{2+} ionophore-mediated degranulation strongly suggests a pathway target upstream of Ca^{2+} influx across the plasma membrane.

2.5.4 As does not inhibit degranulation of RBL-2H3 cells when stimulated with thapsigargin

There is a biphasic calcium modulation in RBL-2H3 cells. Before Ca^{2+} being shuttled across the plasma membrane in the degranulation pathway (which we facilitated, as detailed above, using A23187 ionophore), Ca^{2+} is released from internal ER stores. To investigate this earlier Ca^{2+} signaling event, we utilized the pharmacological agent Tg. We have found Tg to be extremely vulnerable to oxidation, requiring immediate use within 1-2 days of preparation. In the absence of arsenic, the average % degranulation response for 4.6 nM Tg was 11.9 + 3.9%; spontaneous release was 2.3 + 0.9% (mean ± SEM). As seen in Fig 2.4A, no significant difference in Tg-stimulated degranulation is caused by arsenic (Fig. 2.4A). A series of cytotoxicity experiments were performed to test whether 4.6 nM Tg ± arsenic is toxic to RBL-2H3 cells. Trypan blue exclusion (Fig. 2.4B) and LDH (Fig. 2.4C) data demonstrate no cytotoxicity for Tg and arsenic concentrations tested in degranulation experiments after 1 h exposure. Collectively, these results indicate that arsenic's cellular target is upstream of Ca^{2+} release from internal ER stores.

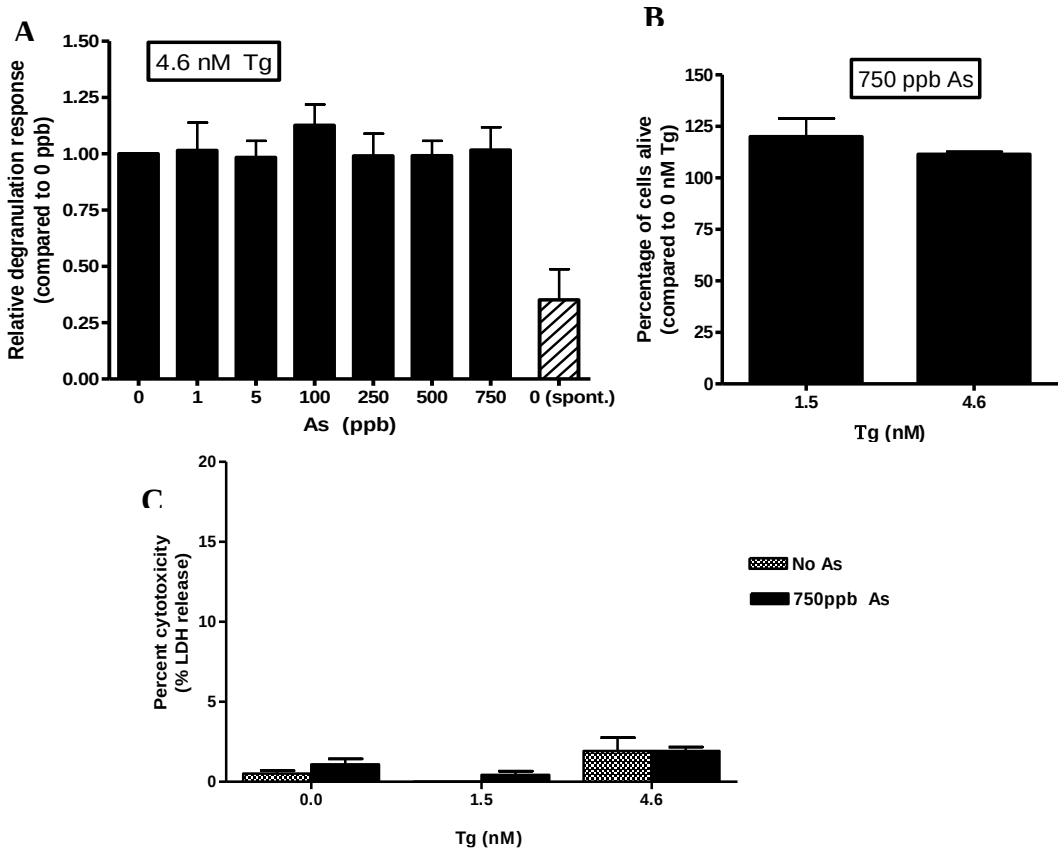

Figure 2.4. Arsenic does not inhibit Tg -induced degranulation. **(A)** Relative degranulation response of RBL-2H3 cells treated for 1hr with 4.6 nM Tg (which caused an average absolute degranulation response of 11.9 + 3.9% [SEM]), ± As. Values represent mean ± SEM of three to five experiments of triplicate samples per dose per experiment. A spontaneous release measurement (no Tg or As present) is depicted for reference. No significant difference was determined by one-way ANOVA. **(B)** trypan blue exclusion assays, the percentage of living cells present in the 0 nM Tg control is plotted against concentration of Tg (1.5 and 4.6 nM); all samples contain 750 ppb As. Values are means of two experiments, each with triplicate samples, where data were normalized to the 0 control (with no Tg and no As, but containing Tg vehicle of 0.001% dimethyl sulfoxide). No significant difference was determined by one-way ANOVA. **(C)** Short-term cytotoxicity was determined using an LDH cytotoxicity detection kit; concentration of Tg is plotted against the percentage LDH released in the absence or presence of 750 ppb As; values represent individual wells (n = 6-9), and error bars are SD. No significant difference was determined by one-way ANOVA. As: arsenic; LDH, lactic dehydrogenase; Tg, thapsigargin.

2.5.5 As does not affect c48/80-mediated degranulation in RBL-2H3 cells

To establish c48/80-mediated degranulation assays as a functional means to measure toxicant effects, it was first determined that 48 h treatment with quercetin (20 μM) followed by 15 min treatment with c48/80 (Senyshyn *et al*., 1998) induces statistically significant increases in

β-hexosaminidase release by RBL-2H3 cells in a dose-dependent manner (data not shown) and non-cytotoxic manner (Fig.2.5B). We additionally confirmed that treatment with c48/80 and quercetin has no effect on background fluorescence as measured in the degranulation assay (data not shown). Although we determined that 25 μg/ml c48/80 induces a non-cytotoxic increase in β-hexosaminidase release in the absence of quercetin pre-treatment, this modest response is enhanced by 48 h quercetin treatment (data not shown), allowing for greater dynamic range in which to study potential effects due to arsenic treatment.

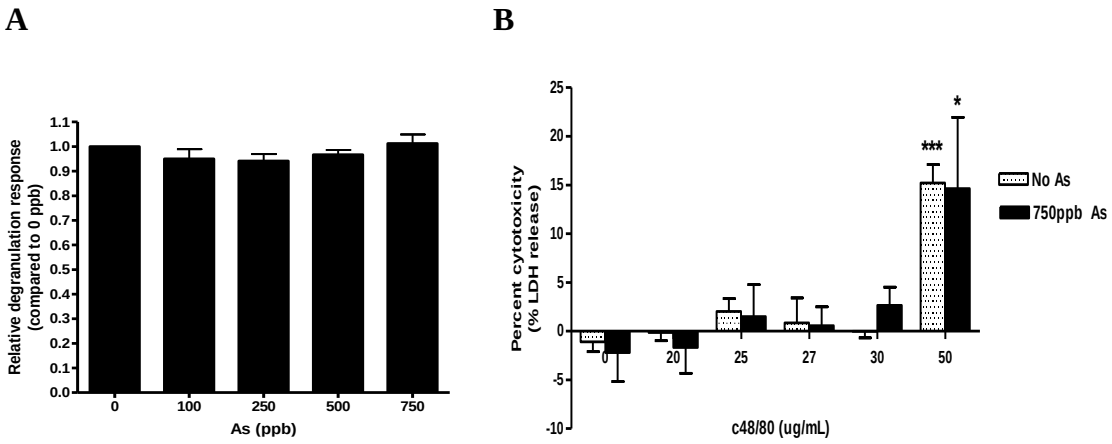

Figure 2.5. Arsenic does not affect c48/80-induced degranulation of RBL-2H3 cells. **(A)** Effect of As on c48/80-mediated degranulation. Cells were pre-treated with quercetin and then co-exposed to 25 μg/ml c48/80 (which caused an average absolute degranulation response of 7.7% ± 0.6% [SEM]) and varying concentrations of As (0-750 ppb) for 15 minutes, followed by β-hexosaminidase quantification as described in "Methods." Data were normalized to the 0 ppb As response value of each experiment (n = 5). **(B)** LDH cytotoxicity assay indicating non-cytotoxicity of 25 μg/ ml c48/80 treatment (n = 3). Cells were treated as in (A), and LDH release was measured as described in "Methods." (A-B) values represent means ± SEM; statistical significance was determined by one-way ANOVA followed by Tukey's post test (in A, comparison made to 100 ppb; in B, direct comparison is made to 0 μg/ml 48/80); *p< 0.05, ***p< 0.001. As, arsenic; LDH, lactic dehydrogenase.

In Fig. 2.5A, it is clear that arsenic does not affect c48/80-mediated degranulation responses, despite similar absolute levels of degranulation induced by c48/80 (7.7% ± 0.6% [SEM]) to the antigen used in the 15 min assay in Fig A.1A. The lack of inhibition is not due to synergistic cell membrane damage between compound 48/80 and arsenic, since the combination

of c48/80 and arsenic does not cause cytotoxicity (Fig. 2.5B). While 50 ug/mL c48/80 is cytotoxic (Fig. 2.5B), this concentration was not used in the degranulation experiments (Fig. 2.5A), which employed the non-cytotoxic dose of 25 μg/mL c48/80.

2.5.6 As inhibits antigen-stimulated Ca^{2+}influx

Ca^{2+} influx is a key event in the signal transduction pathway leading to mast cell degranulation. To directly measure cytosolic Ca^{2+} levels, RBL-2H3 cells were incubated with fluo 4/AM fluorescent dye for 30 min, to allow dye uptake, and then were exposed to 0.0002 μg/ml DNP-BSA antigen ± 750ppb arsenic. Next, fluorescence indicating levels of Ca^{2+} inside the cell were measured in a plate reader for 1 h post stimulation. Our data indicate that arsenic dampens Ca^{2+} influx into antigen-activated mast cells (Fig. 2.6). These results suggest that arsenic's target lies upstream of the Ca^{2+} influx event.

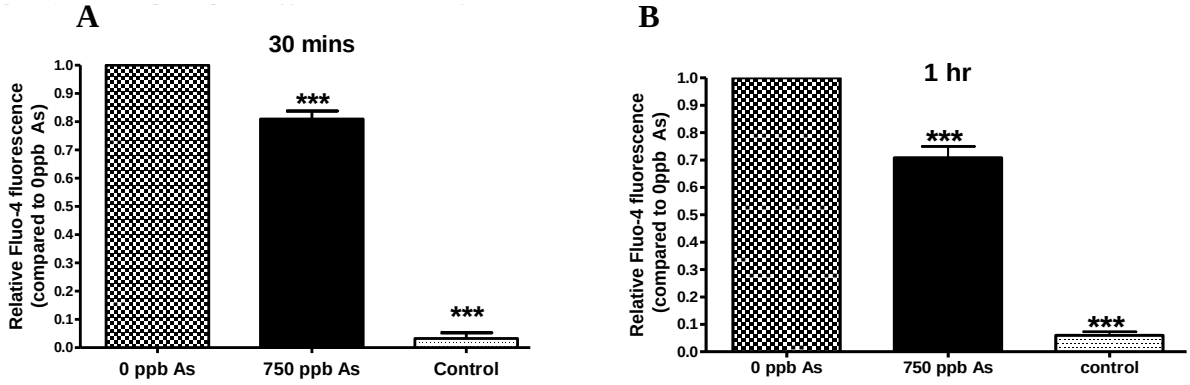

Figure 2.6. Arsenic dampens Ca^{2+} influx into antigen-activated RBL-2H3 cells. Fluo-4/AM was used to measure Ca^{2+} levels within RBL-2H3 cells which had been sensitized with anti-dinitrophenyl IgE (0.1μg/ml) for 1 h before exposure to ± 0.0002 μg/ml dinitrophenyl-bovine serum albumin antigen ± 750ppb As, at 30 min **(A)** or 1 h **(B)** post-antigen stimulation. Control samples received no As or antigen. Values represent mean (normalized to 0 ppb As) ± SEM of four experiments, with 8-16 replicates per dose per experiment. Statistical significance, as compared to the 0 ppb As sample, was determined by one-way ANOVA followed by Tukey's post test; ***$p<0.001$. As, arsenic.

2.5.7 As inhibits phosphorylation of phosphoinositide 3-kinase

PI3K is involved in a variety of cell functions because it catalyzes the production of many crucial lipid signaling molecules, including PIP_2. PIP_2 enables recruitment of a wide range of proteins containing Pleckstrin homology domains, thus drawing these proteins to the plasma membrane for activation (Abramson and Pecht, 2007). PIP_2 is used by PLC γ to generate IP_3, an important player in Ca^{2+} mobilization (Kalesnikoff and Galli, 2008). Overall, PI3K activation supports Ca^{2+} mobilization and degranulation. Therefore, we examined whether PI3K is affected by arsenic exposure. We utilized a commercially available Fast Activated Cell-based ELISA kit, which quantifies activated PI3K and/or total PI3K. Two primary antibodies provided from this ELISA kit recognize either phosphorylated p85, the regulatory subunit of PI3K or total PI3K p85 levels, respectively.

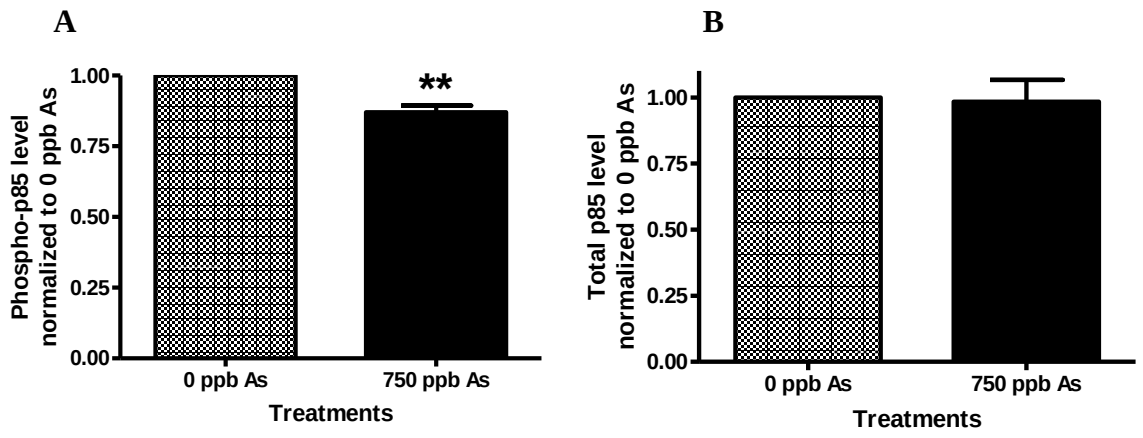

Figure 2.7. Arsenic inhibits phosphorylation of PI3K in RBL-2H3 cells. RBL-2H3 cells were sensitized with anti-dinitrophenyl IgE (0.1μg/ml) for 1 h before being treated with dinitrophenyl –bovine serum albumin antigen (1μg/ml) ± 750ppb As for 5 min. Levels of (A) phosphorylation of the p85 subunit of PI3K and (B) total p85 subunit of PI3K were measured with a Fast Activated Cell-based enzyme-linked immunosorbent assay kit. Data were plotted after correction for cell number (by use of crystal violet staining). Values represent mean (normalized to 0 ppb As) ± SEM of three to four experiments of triplicate samples. Statistical significance was determined by one sample t-test; **$p<0.01$. As, arsenic; PI3K, phosphoinositide 3-kinase.

Using this ELISA, we detected a significant decrease in phosphorylation of the p85 subunit of PI3K due to 750 ppb arsenic exposure, compared to the 0 ppb arsenic group (Fig. 2.7A). Because PI3K is constitutively associated with the kit receptor and because RBL-2H3 cells' kit receptor is known to be constitutively active, there is a high level of phosphorylated PI3K even in the absence of Ag stimulation in RBL-2H3 cells (Tsujimura *et al*., 1995). Thus, the data were normalized to the antigen-stimulated, 0 ppb arsenic samples, not to the unstimulated, 0 ppb arsenic sample. The level of total p85 protein was unchanged regardless of arsenic treatment (Fig. 2.7B). These results suggest that arsenic interferes with antigen-activated phosphorylation of PI3K.

2.5.8 As inhibits phosphorylation of Syk kinase

Previous studies report that the regulatory subunit (p85) of PI3K is one of the direct binding partners of Syk protein (Okkenhaug and Vanhaesebroeck, 2003; Mocsai *et al*., 2010). Since we observed the reduction of phosphorylation/activation level of PI3K (Fig. 2.7), we sought to investigate arsenic effects on phosphorylated Syk protein using a commercially available pan-tyrosine phosphorylated Syk ELISA. Using this ELISA, we detected significant changes in phosphorylated Syk protein between antigen-stimulated and spontaneous-release samples. Figure 2.8 compares antigen-stimulated samples ± 750 ppb arsenic and shows a significant decrease in phosphorylation of Syk protein due to arsenic treatment. Phospho-Syk ELISA data provide evidence that arsenic is interfering with early tyrosine phosphorylation events in the degranulation pathway in mast cells.

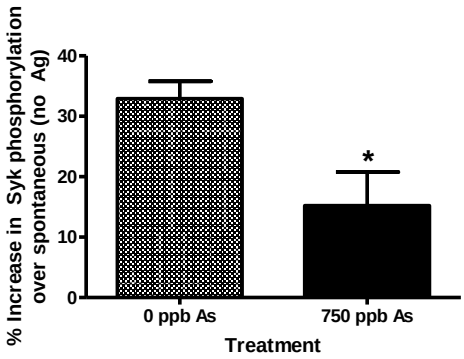

Figure 2.8. Arsenic inhibits phosphorylation of Syk kinase. RBL-2H3 cells were sensitized with dinitrophenyl IgE (0.1μg/ml) for 1 h before being treated with dinitrophenyl –bovine serum albumin antigen (1μg/ml) ± 750ppb As for 5 min. Phosphorylation of Syk was measured with a PathScan ® Phospho-Syk (panTyr) Sandwich enzyme-linked immunosorbent assay kit. Values are expressed as percent increase over spontaneous (no Ag) control samples and represent mean ± SEM of four experiments, each of triplicate samples. Statistical significance was determined by one sample t-test; *$p<0.05$. Ag, antigen; As, arsenic.

2.6 Discussion

Previously, we determined that arsenic's inhibition of mast degranulation, an important event in many physiological states and diseases, is not caused by its direct interference with the crosslinker-IgE interaction at the IgE-bound FcεRI receptors at the plasma membrane: the level of arsenic inhibition of crosslinker-stimulated degranulation was equivalent, regardless of the type of crosslinker used (i.e., DNP-BSA antigen or anti-IgE IgG; as long as the absolute level of degranulation triggered in the absence of arsenic was held constant) (Hutchinson *et al*., 2011). Additionally, arsenic showed no induction of degranulation response and no inhibition of spontaneous granule release in the absence of degranulation-triggering treatments such as IgE receptor crosslinking (Hutchinson *et al*., 2011). These data indicated that crosslinking of the FcεRI receptors is a necessary co-treatment for arsenic's inhibition of degranulation.

The main finding of the current study is that the cellular target for arsenic inhibition of mast cell degranulation lies early in the signaling pathway, likely involving altered phosphorylation of tyrosine kinase Syk (Fig. 2.8) and subsequently affecting the activation of

downstream target proteins of Syk, such as PI3K (Fig. 2.7). Syk and PI3K are both activated rapidly (within min) after antigen exposure. In our previously published study (Hutchinson *et al*., 2011), degranulation was inhibited by As in a 1 h treatment with DNP-BSA antigen. When we examined the same DNP-BSA antigen treatment in a shorter period (15 min), we found that As inhibits degranulation at this earlier time point as well, indicating that its effects are acute and rapid (Fig. A.1A). We also performed experiments with chronic arsenic exposure of mast cells and found that longer exposure of arsenic did not alter the extent of arsenic's inhibition of degranulation (data not shown).

Acute arsenic poisoning, at very high arsenic concentrations, can lead to inhibition of glycolysis and cellular ATP production, due to arsenic substitution for phosphate (DeMaster and Mitchell, 1973). While we earlier showed, via multiple methods, that arsenic is not cytotoxic to RBL-2H3 mast cells at the concentrations used in this study (Hutchinson *et al*., 2011), we had not yet determined whether arsenic affects ATP production under these experimental conditions. Here we show that arsenic doses up to 1500 ppb do not affect ATP production (Fig A2), suggesting that inhibition of catabolism and widespread phosphate substitution is not occurring. Under the same glucose-free conditions, the canonical mitochondrial uncoupler carbonyl cyanide 3-chlorophenylhydrazone, which also inhibits degranulation of RBL-2H3 cells, decreases ATP production, with an EC_{50} of 0.8μM – 1.6 μM (95% Cl),with no cytotoxicity (Weatherly *et al*., 2016).

To narrow down arsenic's target(s) in the mast cell signaling pathway, we investigated whether arsenic affects the F-actin rearrangement or "membrane ruffling" in RBL-2H3 cells, another phenotype of activated mast cells. This strategy tests for potential cellular targets for arsenic that are common to both the degranulation and membrane ruffling pathways, such as

PKC (Pfeiffer *et al*., 1985; Yanase *et al*., 2011). Our finding of no or a small arsenic effect on membrane ruffling (Fig 2.2) supports the conclusion that cellular targets that are downstream of Ca^{2+} influx and that are common to both degranulation and ruffling are unaffected by arsenic.

Ca^{2+} ionophore A23187 was utilized to bypass FcεRI and the early tyrosine phosphorylation events and to stimulate the release of granules through the influx of Ca^{2+} alone into the cell (Siraganian *et al*., 1975). In experiments utilizing A23187, we determined that arsenic does not inhibit degranulation (Fig 2.3), indicating that arsenic's pathway target is upstream of Ca^{2+} influx across the plasma membrane.

We also used the pharmacological agent Tg, which is a potent, cell permeable, IP_3-independent intracellular Ca^{2+} releaser/SERCA pump blocker that acts a mast cell secretagogue (Rasmussen and Christensen, 1978; Patkar *et al*., 1979). Like A23187 Ca^{2+} ionophore, Tg stimulates mast cell degranulation while by passing FcεRI crosslinking and early tyrosine phosphorylation events. However, unlike with A23187-induced cell activation, Tg stimulation does involve STIM-1 in the ER and the plasma membrane CRAC channels. Our data indicate that, with the use of the non-cytotoxic dose of 4.6 nM Tg to elicit degranulation, As does not inhibit degranulation (Fig 2.4). This concentration of Tg is within the documented IC_{50} for inhibiting SERCA (4-13 nM) (Calbiochem production information). Thus, these data show that arsenic's cellular target not only lies upstream of Ca^{2+} influx across the plasma membrane, but also is not STIM-1 or other players in ER Ca^{2+} mobilization.

In view of the fact that c48/80 activates degranulation via PLD in a Ca^{2+}- dependent manner, c48/80-mediated degranulation assays can be used to measure toxicant effects on these portions of the degranulation pathway. Because there is no arsenic effect on cells stimulated to degranulate with c48/80 (Fig. 2.5), arsenic's inhibitory actions on the degranulation pathway are

likely on some portion of the pathway that lies upstream of PLD and Ca^{2+} influx. Combined, the A23187 (Fig. 2.3), Tg (Fig. 2.4), and c48/80 (Fig. 2.5) data strongly suggest that arsenic's inhibitory action lies upstream of all calcium signaling in the degranulation pathway. In addition, these data indicate that PKC, PLD and other enzymes activated following Ca^{2+} mobilization are not arsenic's direct targets in RBL-2H3 mast cells.

To investigate arsenic effects on events upstream of Ca^{2+} influx, we developed a microplate-based assay to measure the level of cytoplasmic Ca^{2+} after antigen exposure, ± arsenic, in RBL-2H3 mast cells. We found a strong inhibition of the antigen-stimulated Ca^{2+} level in the cells due to arsenic exposure after both 30 min and 60 min of exposure (Fig. 2.6). The dampened Ca^{2+} influx into arsenic-exposed cells is another indicator that arsenic's target lies upstream of Ca^{2+} influx. Therefore, we investigated the effects of arsenic on early tyrosine phosphorylation events, which occur immediately after FcεRI receptor activation.

Previous researchers have reported that arsenic may interfere with phosphorylation events during signal transduction. For example, Cheng *et al*. (2004) found that sodium Arsenite inhibits the Janus kinase signal transducer and activator of transcription cascade, via inhibition of phosphorylation of STAT3 specifically at tyrosine resides (Cheng *et al*., 2004). Moreover, Soto-Peña *et al*. (2008) demonstrated that arsenic can interfere with phosphorylation of the kinases Lck and Fyn during T-cell signal transduction (Soto-Peña and Vega, 2008). In this study, we have found that arsenic inhibits phosphorylation of both PI3K and Syk kinases in antigen-activated RBL-2H3 cells (Fig. 2.7 and 2.8), thus providing a mechanism for arsenic inhibition of mast cell degranulation.

Arsenite has been shown in certain cases to interact with sulfhydryl groups of kinases and to form reactive oxygen species (ROS), which affect kinase activity (Liu *et al*., 2001). In this

study, we have found that arsenic does not affect ROS levels under the treatment conditions of these experiments. However, arsenic can directly bind to sulfhydryl groups of certain proteins, causing detrimental structural modification or denaturation (Chang *et al*., 2012). Syk kinase (both human and rat) contains numerous cysteine residues, five of which are located specifically in its kinase domain. Therefore, derangement of normal phosphorylation activity of Syk, via arsenic-sulfhydryl interactions, may be a mechanism underlying the inhibition of both antigen-stimulated Syk phosphorylation and degranulation of mast cells.

The implications of this mechanistic study can assist researchers to better understand a mode of arsenic toxicity that is likely to not be organism-specific or even mast-cell specific. Classic immunoreceptors, such as B cell receptors, T cell receptors, and Fc receptors, signal via similar mechanisms, and the signal transduction pathways present in mast cells share many similarities with those of T and B cells. Arsenic's inhibition of Syk activity (and, subsequently, PI3K) in mast cells suggests that arsenic inhibits Syk and similar proteins in the same manner in numerous cell types. Syk has garnered attention as a potentially novel target for treatment of allergic and inflammatory disorders (Wong *et al*., 2004; Ulanova *et al*., 2005; Bajpai *et al*., 2008). Because arsenic has now been shown to inhibit this vital process in allergy and asthma development, mast cell degranulation, our data strongly suggest that Syk could be a drug target to treat these diseases.

In fact, arsenic has been employed in Chinese medicine to treat asthma (ATSDR, 2007). While arsenic inhibition of mast cells *in vivo* has not yet been directly demonstrated, arsenic has been shown to block anaphylactic responses in guinea pigs (Poriadin *et al*., 1977) and to alleviate asthma responses in mice (Zhou *et al*., 2006; Chu *et al*., 2010). Also, arsenic-exposed, parasite-infected children in Bangladesh were found to be thinner than controls also exposed to parasites

but not to arsenic (Minamoto *et al*., 2005), a result that suggests that arsenic exposure could inhibit mast cells *in vivo*, thus increasing helminth burden and wasting. Inhibition of mast cell function by arsenic was not offered as an explanation for these findings but is a possible mechanism of the *in vivo* effects described in these studies.

In conclusion, we have shown that arsenic inhibits mast cell degranulation at environmentally relevant, non-cytotoxic doses, via inhibition of early tyrosine phosphorylation events. These data provide a molecular mechanism for arsenic's effects on this ubiquitous cell type and suggest that As will have similar molecular targets in many additional cell types.

CHAPTER 3

MOLECULAR MECHANISMS UNDERLYING ANTIMICROBIAL AGENT TRICLOSAN'S INHIBITION OF MAST CELL SIGNALING: ROLES OF PROTEIN KINASE C AND PHOSPHOLIPASE D

3.1 Abstract

Humans are exposed to antimicrobial agent triclosan (TCS) through use of TCS-containing products. Exposed tissues contain mast cells, which are involved in numerous biological functions and diseases by secreting various chemical mediators through a process termed degranulation. We previously demonstrated that TCS inhibits mast cell degranulation. Previously, we discovered that TCS inhibits Ca^{2+} influx into antigen (Ag)-stimulated mast cells. Here, we have investigated TCS effects on protein kinase C (PKC) and phospholipase D (PLD), crucial signaling enzymes that are activated downstream of Ca^{2+} rise. Using fluorescent constructs and confocal microscopy, we found that TCS delays the timing Ag-induced translocations of PKC βII, PKC δ, and PKC substrate MARCKS, even while the overall ability of these molecules to translocate is unaffected by TCS. Surprisingly, TCS does not inhibit PKC activity and actually increases PKC activity by 45 min post Ag. While TCS does not significantly affect the ability of PLD1 to translocate toward the plasma membrane in response to Ag stimulation, TCS does strongly inhibit overall PLD activity within 15 min post Ag. Our studies elucidate the biochemical mechanisms underlying triclosan's inhibition of degranulation and pinpoint the timing of defects by TCS on the mast cell signaling pathway. These results offer molecular predictions of triclosan's effects on other mammalian cell types which share these crucial signal transduction elements and provide explanations for recent epidemiological findings implicating TCS in human health problems.

3.2 Introduction

Triclosan (TCS) is a synthetic antimicrobial agent that was recently banned by the FDA from both consumer (Kux, 2016) and hospital soap products (Fischer, 2017). However, TCS still remains, at high concentrations, in other top-selling consumer products, such as toothpaste and in other "antibacterial" household products (*e.g.*, toys, kitchenware, etc.). TCS from consumer products is readily absorbed when applied to human tissues, where it is not rapidly metabolized or cleared. The resulting human tissue levels are comparable to exposure levels used in this current cell study (TCS exposure is reviewed in (Weatherly and Gosse, 2017)). Additionally, micromolar levels of TCS have been found in human body fluids in several published studies (also reviewed in (Weatherly and Gosse, 2017)). Thus, TCS dosages used in this current manuscript (10 μM in cell media for ≤ 1h) are directly relevant to actual human exposures to TCS products such as toothpaste.

Clinically, TCS has been used primarily as an antimicrobial (Daoud *et al*., 2014) and anti-gingival (Rover and Leu-Wai-See, 2014), and there have also been some potentially positive findings of TCS treatment of atopic dermatitis (Tan *et al*., 2010), which may be due to triclosan's ability to inhibit mast cell function (Palmer *et al*., 2012). However, numerous recent epidemiological studies report detrimental TCS effects on human health, including problems with thyroid function (Wang *et al*., 2017), reproduction (Hua *et al*., 2017), immune function, development (Wei *et al*., 2017) (reviewed in (Weatherly and Gosse, 2017)). Additional recent epidemiological studies have also revealed increased risks of gestational diabetes (Ouyang *et al*., 2018), abnormalities of sperm morphology (Jurewicz *et al*., 2018), and lowered cognitive test scores in children (Jackson-Browne *et al*., 2018), due to triclosan exposure. The cellular, molecular, and biochemical reasons for these health effects of TCS are not completely

understood but include mitochondrial toxicity (Ajao *et al*., 2015; Shim *et al*., 2016b; Weatherly *et al*., 2016), reactive oxygen species (ROS) generation (Lv *et al*., 2016), interference with cellular calcium dynamics (Ahn *et al*., 2008; Cherednichenko *et al*., 2012; Weatherly *et al*., 2018), endocrine disruption (Ruszkiewicz *et al*., 2017), and modulation of cytokine gene expression (Yueh *et al*., 2014; Marshall *et al*., 2015).

As noted above, TCS inhibits mast cell (MC) function (Palmer *et al*., 2012; Weatherly *et al*., 2013). MCs are found in nearly every human body tissue and in numerous other species (Kuby, 1997). They are particularly enriched in tissues subject to contact with outside environmental stimuli, such as the skin, gastrointestinal tract, oral mucosa (Walsh, 2003), and respiratory mucosa (Abraham and St John, 2010)—and thus are targets for exposure to chemicals from personal care product application. MCs are key players in many physiological and pathological processes including allergy, asthma, autoimmunity, infectious disease, cancer, and even many central nervous system disorders such as autism, anxiety, and multiple sclerosis (Metcalfe *et al*., 1997; Williams and Galli, 2000; Galli *et al*., 2005a; Silver and Curley, 2013; Girolamo *et al*., 2017). Therefore, inhibition of MC function has many potential consequences on human health. Many of the biochemical events crucial to MC function (such as cytoskeletal involvement, calcium signaling, protein kinase C, etc.) are also essential to signaling in numerous distinct cell types, including neurons and T cells. Thus, discovery of the biochemical mechanisms underlying TCS disruption of MCs leads to predictions of TCS effects in disparate cell types that share common signal transduction elements.

Mast cells are activated by binding of multivalent antigen (Ag) to immunoglobulin E (IgE)-bound cell surface FcεRI receptors (Kinet *et al*., 1983), resulting in secretion of cytoplasmic granules which contain mediators such as histamine, tryptase, β-hexosaminidase,

serotonin, cytokines, chemokines, and lipid mediators (Schwartz and Austen, 1980). This process is termed as mast cell degranulation. FcεRI crosslinking by Ag leads to a tyrosine phosphorylation cascade that activates phospholipase C (PLC) γ, which catalyzes the hydrolysis of phosphatidylinositol 4,5-bisphosphate (PIP_2) to yield diacylglycerol (DAG) and inositol 1,4,5-trisphosphate (IP_3). While DAG activates protein kinase C (PKC) (Steinberg, 2008), IP_3 binds to its receptor in the endoplasmic reticulum (ER) causes an efflux of Ca^{2+} from the ER (Berridge, 1993), into the cytosol and also into mitochondria (Takekawa *et al*., 2012; Furuno *et al*., 2015). Next, calcium release-activated calcium (CRAC) channels in the plasma membrane are activated, resulting in a flood of calcium into the cytosol (Putney *et al*., 2001).

Within the cytosol, this elevated Ca^{2+}, along with DAG and ROS (Swindle et al., 2004), binds to and activates the Ser/Thr family of protein kinase C (PKC) (Ozawa *et al*., 1993b; Steinberg, 2008). PKC isozymes are categorized into three subfamilies (classical [cPKC], novel [nPKC], and atypical [aPKC]), according to their biochemical and structural properties, such as their binding to DAG and/or Ca^{2+} (Ozawa *et al*., 1993b; Newton, 1995; Newton, 2001). Of particular importance in mast cells are certain cPKC isoforms (PKC α, βI, βII, and γ), which have conserved C1 domains (which bind DAG) (Newton, 2001) and C2 domains (which bind Ca^{2+} and acidic phospholipids). Also important to mast cell function are certain nPKC isoforms (PKC δ, ε, θ, and η), which are activated by DAG by binding to the C1 domain but which are lacking functional C2 domains and, thus, are lacking Ca^{2+} responsiveness (Newton, 1995). In addition to DAG, activators of PKC δ include various agents such as phorbol esters, UV or ionizing radiation, growth factors, and ROS (Yoshida, 2007; Lee and Yang, 2010). PKC β and δ, which belong to cPKC and nPKC, respectively, are particularly important in IgE–mediated mast cell degranulation (Nechushtan *et al*., 2000; Cho *et al*., 2004; Yanase *et al*., 2011).

Stimulation of RBL-2H3 cells with either Ag or Ca^{2+} ionophore causes a rapid translocation of PKC δ from the cytosol to the plasma membrane (Cho *et al*., 2004). Also, PKC δ translocation and degranulation are both activated by ROS generation in mast cells (Cho *et al*., 2004).

Activation of PKC causes its translocation from the cytosol to the plasma membrane, serving as a hallmark for PKC activation (Kraft and Anderson, 1983). Inactive PKC is located in the cytosol and autoinhibited by a pseudosubstrate (Nishizuka, 1995; Brown and Kholodenko, 1999). When Ca^{2+} binds to cytosolic PKC and alters its electrostatics and, hence, membrane lipid affinity (Codazzi *et al*., 2001), it can then bind DAG in the plasma membrane, leading to full activation of PKC by removal of pseudosubstrate from the active site. In other cases, DAG alone can recruit cytosolic PKC to the plasma membrane and induce conformational changes to activate PKC (Nishizuka, 1995; Jaken and Parker, 2000). Once PKC is translocated and active, it phosphorylates substrates in its proximity in or near the plasma membrane. One PKC substrate is myosin, the phosphorylation of which is important for actin cytoskeletal rearrangements ("membrane ruffling") and degranulation (Ludowyke *et al*., 1989; Choi *et al*., 1994).

Another of PKC's substrates is myristoylated alanine-rich C-kinase substrate (MARCKS) (Aderem, 1992). In unstimulated cells, MARCKS tightly binds to PIP_2 at the inner leaflet of the plasma membrane (Heo *et al*., 2006). When phosphorylated by activated/translocated PKC, MARCKS dissociates from the plasma membrane and enters the cytosol, thus exposing PIP_2 to be accessible to other proteins (such as PLC γ, for generation of more second messengers) for signaling leading to degranulation (Gadi *et al*., 2011). In addition, along with Ca^{2+}, PIP_2 is involved in the soluble N-ethylmaleimide–sensitive factor attachment protein receptor (SNARE)-mediated exocytotic machinery required for degranulation (Tadokoro *et al*., 2015).

Another major target of PKC is phospholipase D (PLD). Increases in intracellular Ca^{2+} and PKC translocation work in tandem to activate PLD in mast cells (Lin and Gilfillan, 1992) . Although there are many studies in other cell types showing that intracellular Ca^{2+} activates PLD activity (Exton, 1999; Qin *et al*., 2009), the mechanisms of PLD activation by Ca^{2+} remain to be elucidated. Structural analyses have shown that mammalian PLD does not contain a Ca^{2+} binding domain but does contain lipid (PIP_3 and PIP_2) -binding domains and a PKC-binding domain (Henage *et al*., 2006; Selvy *et al*., 2011). While a study showed that mammalian PLD activity is insensitive to changes in cytosolic Ca^{2+} concentration *in vitro* (Hammond *et al*., 1997), Ca^{2+} and PIP_2 act as essential cofactors for mammalian PLD activation within cells (Sciorra *et al*., 2002; Henage *et al*., 2006; Selvy *et al*., 2011). PLD activation involves Ca^{2+}-dependent PKC isoforms (Wakelam *et al*., 1997; Qin *et al*., 2009). A study using RBL-2H3 mast cells showed that PKC inhibitors decrease PLD activity and, subsequently, inhibit degranulation, suggesting a close relationship between PKC/PLD activation and degranulation in mast cells (Chahdi *et al*., 2002).

PLD hydrolyzes phosphatidylcholine, creating phosphatidic acid (PA), an important second messenger for numerous cellular functions (Wakelam *et al*., 1997; Cockcroft, 2001; O'Luanaigh *et al*., 2002; Zeniou-Meyer *et al*., 2007). PA stimulates PLC γ (Nishizuka, 1995) and also can be converted directly into DAG by PA phosphohydrolase—leading to a secondary rise in intracellular DAG levels (Nakashima *et al*., 1991). These increases in DAG are involved in activation of the DAG-dependent PKC isoforms (Baldassare *et al*., 1992; Nishizuka, 1995; Peng and Beaven, 2005), suggesting that PKC-PLD activation is closely regulated in a complementary manner between the two enzymes in mast cells. Additionally, PA plays a critical

role in regulating mast cell morphology (Marchini-Alves *et al*., 2012). Continual activity of PLD2 is required for membrane ruffling in mast cells (O'Luanaigh *et al*., 2002).

Two mammalian isoforms, PLD1 and PLD 2, are expressed in mast cells. PLD1 localizes to cytoplasmic granules and has low basal activity whereas PLD2 is constitutively expressed at a high level and is located at the plasma membrane (Choi *et al*., 2002; Lee *et al*., 2006). Stimulation of mast cells activates both PLD isoforms, but only PLD1 undergoes translocation to the plasma membrane and drastic upregulation of its activity (Brown *et al*., 1998). Even though many studies have agreed on the location and expression of PLD isoforms in mast cells, there have been controversial and conflicting data regarding the functions of these isoforms. Several studies have reported positive roles of both PLD isoforms in mast cell degranulation (Brown *et al*., 1998; Chahdi *et al*., 2002; Peng and Beaven, 2005; Lee *et al*., 2006), with PLD1 involved in granule translocation and with PLD2 involved in membrane fusion of these granules (Choi *et al*., 2002). However, one intriguing recent study using PLD1- and PLD2-knockout mice found that PLD1 positively regulates degranulation, while PLD2 is a negative regulator (PLD2 deficiency enhanced microtubule formation) (Zhu *et al*., 2015).

Microtubule polymerization is another essential player: granules are mobilized to the plasma membrane along microtubules for degranulation (Smith *et al*., 2003). Agents that inhibit microtubule polymerization inhibit degranulation (Urata and Siraganian, 1985; Tasaka *et al*., 1991; Marti-Verdeaux *et al*., 2003). Once granules are moved to the plasma membrane, they dock and fuse to the membrane with the help of PLD and multiple SNAREs in a Ca^{2+}-dependent process (Guo et al., 1998; Baram et al., 1999; Paumet et al., 2000; Blank et al., 2002; Woska and Gillespie, 2012), resulting in degranulation.

Previously, we discovered that non-cytotoxic doses of TCS (5-20 μM), within 1 hour (15 min-1 hour) cause strong, dose-dependent inhibition of degranulation (in either the rat mast cell model RBL-2H3 or the human mast cell line HMC-1) (Palmer *et al*., 2012; Weatherly *et al*., 2013; Weatherly *et al*., 2016), and here we have sought to determine the underlying molecular mechanisms. Recently, we discovered that TCS drastically interferes with mast cell Ca^{2+} dynamics, at the ER, mitochondria, and cytosolic influx across the plasma membrane (Weatherly *et al*., 2018). Therefore, we hypothesized that the cellular translocation and activity of Ca^{2+}-activated PKC and PLD enzymes, as well as the translocation of PKC substrate MARCKS, would be inhibited by TCS exposure.

Here, we report that the effects of TCS on PKC, MARCKS, and PLD localization and activity in Ag-stimulated RBL-2H3 mast cells using biochemical assays and live-cell/real-time confocal microscopy. We have discovered that TCS delays translocation of PKC βII and δ to the plasma membrane and subsequently delays MARCKS dissociation from the plasma membrane, even while, surprisingly, overall PKC activity is uninhibited by TCS. Furthermore, we found that PLD activity in Ag-stimulated RBL-2H3 mast cells is decreased even while PLD1 translocation is unaffected by TCS. Together with our earlier published findings, these results paint a mechanistic picture of triclosan's mode of action on mast cells and pinpoint the timing of TCS-induced defects in the mast cell signaling pathway.

3.3 Methods

3.3.1 Chemicals and reagents

TCS (99%; Sigma-Aldrich) was freshly prepared each day in aqueous Tyrodes buffer as described in (Weatherly *et al*., 2013) and was used at non-cytotoxic doses (Palmer *et al*., 2012).

5-Fluoro-2-indolyl des-chlorohalopemide (FIPI) (Calbiochem) was dissolved in 100% DMSO to obtain 1 mM stock. Further dilutions were made in bovine serum albumin (BSA)-Tyrodes (BT) buffer to make 75nM (0.0075% DMSO) and 150 nM (0.015% DMSO). Phenylmethanesulfonyl fluoride (PMSF; Sigma) was dissolved in 100% ethanol to be 200 mM and was stored at -20 °C.

3.3.2 Cell culture

RBL-2H3 ("RBL") mast cells were cultured as in (Hutchinson *et al*., 2011) and (Weatherly *et al*., 2013).

3.3.3 Protein kinase C activity assay (ELISA)

A PKC Kinase activity kit (Enzo Life Science) was used to simultaneously measure the activity of multiple PKC isoforms (PKC α, βI, βII, γ, δ, ε, η, and θ). RBL-2H3 cells were plated in 10 cm^2 tissue culture-treated sterile dishes (Greiner Bio-One) (1.14×10^7 cells per dish, in 6.5 mL media) and were incubated overnight (12–16 h) at 37 °C/5% CO_2. The following day, cells were sensitized with 0.1 μg/mL monoclonal anti-dinitrophenol (DNP) mouse immunoglobulin E (IgE; Sigma-Aldrich) for 1 hour at 37 °C/5% CO_2 in RBL media. After IgE sensitization, spent IgE media was discarded, and cells were washed with warm BT to remove excess IgE. Next, cells were exposed to either BT (control) or multivalent DNP–BSA antigen (Ag) in BT ± 10 μM TCS for 10 to 45 minutes at 37 °C. Cell lysis buffer (1X; Cell Signaling Technology) was prepared from 10X stock, via dilution in PBS. Immediately before use, PMSF was added to this 1X cell lysis buffer for a final concentration of 1mM PMSF. After incubation, cells were washed with ice-cold PBS, then incubated for 1.5 minutes on ice with 400μL of ice-cold 1X cell lysis buffer containing 1mM PMSF. Next, cells were harvested by cell scraper (Falcon) and were

placed into pre-chilled microcentrifuge tubes and further lysed using a sonicator (Branson Sonifier, Branson Ultrasonics Corporation; set at output control 5 Watts, duty cycle of 30, 1 sec duration per sonication pulse, with a 5 sec break on ice in between sonications). Finally, the sonicated cells were centrifuged at 14,400xg for 10 minutes at 4°C, and lysate supernatants (technical duplicates, 30 µL per ELISA well, from each cell lysate) were used in the ELISA following the manufacturer's protocol (except 1x lysis buffer was used as a background in place of the kinase assay dilution buffer included in the kit). PKC activity was determined by measuring the absorbance at 450 nm using a microplate reader (Synergy 2; Biotek). During the 90 min primary antibody incubation step of the PKC ELISA, a 25 µL aliquot of the remaining of cell supernatant of each sample was diverted for use in total protein concentration determination. The bicinchoninic acid (BCA) assay was performed, using Pierce BCA protein assay kit (Thermo), following the manufacturer's protocol.

Raw absorbance ELISA data were processed by first subtracting average background values (kit reagents in 1X lysis buffer with no cell supernatant) from each sample, and the background-subtracted duplicates were then averaged. These values were then divided by the total protein concentration of that particular sample, and finally were normalized to the unstimulated (no Ag) control for each experimental day. The percent increase of PKC activity over control was determined by subtracting the normalized control value from the normalized Ag or Ag + TCS values and dividing this number by the control value.

3.3.4 Confocal imaging

RBL-2H3 cells were transfected via electroporation using Amaxa Nucleofector kit T (Lonza) as described in (Weatherly *et al*., 2018). Constructs used were YFP-PKCβII-YFP (a gift

from Alexandra Newton; Addgene plasmid #14866; "PKC βII"; (Violin *et al*., 2003)), GFP-PKCδ -C1(2) (a gift from Tobias Meyer; Addgene plasmid # 21216; (Codazzi *et al*., 2001)), mRFP-MARCKS-ED (generously provided by Dr. Barbara Baird and Dr. David Holowka, Cornell University; "MARCKS"; (Gadi *et al*., 2011)), or PLD1-EGFP construct (generously provided by Dr. Michael Frohman of Stony Brook University and Dr. Shamshad Cockcroft of University College London; (O'Luanaigh *et al*., 2002; Du *et al*., 2003)). Regarding GFP-PKCδ-C1(2) (sometimes referred to herein as "PKC δ"), this short form of PKC δ, which only contains C1 (2) domains, has previously been employed to effectively investigate PKC δ translocation (Codazzi *et al*., 2001; Mogami *et al*., 2003). Both PKC constructs were cloned from *R. norvegicus* (rat) (Codazzi *et al*., 2001; Violin *et al*., 2003), and MARCKS-ED and PLD1 DNA were from human (Du *et al*., 2003; Gadi *et al*., 2011). The percent identities of PKC β, PKC δ, ED domain of MARCKS, and PLD1, between human and rat, from pairwise alignments using NIH Blast, are 98%, 90%, 96%, and 87%, respectively.

Following electroporation, cells were plated (100,000 or 125,000 cells/well in 8-well ibidi plates) for overnight incubation in phenol red-free media (recipe is found in (Weatherly *et al*., 2018)), then sensitized with IgE, stimulated with Ag, and imaged via confocal microscopy as detailed in (Weatherly *et al*., 2018). For YFP-PKCβII-YFP, GFP-PKCδ-C1(2), and PLD1-EGFP, a 30 milliwatt multi-argon laser (515nm excitation for YFP and 488 nm excitation for GFP and EGFP, emission 505-605 nm bandpass filter) was used. For mRFP-MARCKS-ED, a 1 milliwatt HeNe-Green laser (543 nm excitation, 560-660 nm emission filter) was used. Image acquisition speed was 10 µs/pixel.

Images were then analyzed using NIH Fiji ImageJ software to examine individual transfected cells from each experiment. Only cells that appeared healthy (in DIC images), in

focus, and fluorescent above background (autofluorescence) levels were utilized for analysis. To determine the "percentage translocation of transfected cells," each transfected cell with movement of the fluorescent construct to (or, for mRFP-MARCKS-ED, away from) the plasma membrane at any time point during the 10 min post-Ag exposure video acquisition was noted, and the total percentage of transfected cells that underwent this movement was calculated. For only transfected cells that underwent translocation, the "time to first translocation" was defined as the time stamp of first image frame in which PKC moved to the plasma membrane, exhibiting a clear complete ring formation around the plasma membrane (in the case of mRFP-MARCKS-ED, the time stamp utilized was that of the first image frame showing movement of the construct *away from* the plasma membrane).

As a control to verify triclosan's ability to inhibit mast cell function under these experimental conditions, the percentage of membrane ruffling, of transfected cells only, was calculated: differential interference contrast images were collected along with fluorescence images, and construct-transfected cells undergoing classical membrane ruffling (Palmer *et al*., 2012) post Ag exposure were noted, as a percentage of all transfected cells, ± TCS.

3.3.5 Phospholipase D Activity assay

To examine PLD activity, the Amplex® Red phospholipase D assay kit (Molecular Probes) (which measures activity of both isoforms PLD1 and PLD2 simultaneously) was utilized. The kit reagents were prepared as described in the manufacturer's protocol with the exception of using Tyrode's buffer in place of 1X Reaction Buffer.

RBL-2H3 cells (1.5×10^6 per well) were plated in tissue culture-treated, sterile 6-well plates (Greiner Bio-One) and incubated overnight (12–16 h) at 37 °C/5% CO_2. On the second

day, cells were sensitized with IgE, then washed with BT as described in the "Protein kinase C activity assay (ELISA)" section above. Cell samples were then exposed to either BT or Ag (0.1 or 0.001 μg/ mL), ± TCS or FIPI for 15 min at 37 °C. Immediately following this exposure, cells were placed on ice and washed with ice-cold PBS buffer. Triton-X 100 (Surfact-Amps X-100, 10%, low carbonyl and peroxide; Thermo; "TX") was diluted to 0.2% TX in PBS (Lonza). After removing all traces of the wash buffer, this 0.2% Triton-X (TX) buffer was added to the cells (300 μL/well). Next, cells were harvested by cell scraper (Falcon) into microcentrifuge tubes on ice, thoroughly vortexed and underwent a freeze-thaw cycle using liquid nitrogen immersion for 30 seconds, followed by room temperature thawing. Lysed cells were then centrifuged for 10 min at 14,400xg at 4°C. Each sample's supernatant (100 μL/well) was then transferred to a well within a black-side, clear-bottom, sterile 96-well plate (Greiner Bio-One), in technical duplicates. Background fluorescence was measured by preparing control samples with 0.2% TX in PBS. The remaining steps were carried out according to the manufacturer's directions. PLD activity was determined by measuring fluorescence intensity by microplate reader (Synergy 2; Biotek) at 530/25 nm excitation and 590/35 nm emission.

Raw data were processed by subtracting average background fluorescence (substrate and kit reagents in 0.2% TX-PBS with no cell supernatant) from each sample, and the background-subtracted duplicates were then averaged. These values were then normalized to the unstimulated (no Ag) control for each experimental day. The percent increase of PLD activity over control was determined by subtracting the normalized control value from the normalized Ag or Ag + TCS values and dividing this number by the control value.

The effect of TCS on the activity of purified PLD from *Arachis hypogaea* and *Streptomyces chromofuscus* was measured as described above, except these purified PLD

preparations were used in place of supernatant from the cell lysates. Purified PLD from *Streptomyces chromofuscus* (Sigma), purchased as a glycerol stock (50,000 units/mL), was diluted to be 0.125 units/mL in 0.2% TX-PBS before being used in the assay. Purified PLD from *Arachis hypogaea* (Sigma) was purchased as a lyophilized powder and first reconstituted in Tyrode's buffer to 500 units/mL and then further diluted in 0.2% TX-PBS to a final concentration to be 2.5 units/mL. Because the optimal temperature for *Arachis hypogaea* PLD is at 30°C, experiments with this PLD, which were carried out at 37°C in order to match the cellular experiments, were performed with extended exposure time with TCS: 1 hour, instead of 15 min.

3.3.6 Degranulation Assay

Degranulation was assayed via detection of β-hexosaminidase, a granule marker, as described in (Weatherly *et al*., 2013).

3.3.7 Statistical analyses

All analyses were done in Graphpad Prism. Numbers of technical replicates and independent days of experiments are noted each figure legend. Significance levels were assessed via one-tailed t-tests or one-way ANOVA with Tukey's *post-hoc* tests.

3.4 Results

We previously showed that, within a 60 minute co-exposure to TCS and antigen (Ag), non-cytotoxic TCS doses (5 μM and higher) inhibit RBL-2H3 mast cell degranulation elicited by a wide range of Ag doses (Palmer *et al*., 2012), including doses that elicit either minimal or

maximal degranulation responses. Additionally, modest amounts of degranulation (~7% absolute degranulation) elicited by short 15 min exposures to low Ag doses are inhibited by TCS during as few as 15 min of co-exposure (Palmer *et al*., 2012). However, the higher levels of degranulation (~35% absolute degranulation) elicited by high Ag doses (0.005 and 0.1μg/mL, used throughout much of this current manuscript) are not inhibited within the first 10 to 15 min of TCS exposure (data not shown) –even as degranulation is eventually and robustly inhibited by TCS within the full hour of co-exposure (Palmer *et al*., 2012). In this study, we have examined TCS effects on several of the biochemical events that lead to full degranulation within 60 min of Ag exposure in order to pinpoint the timing of the molecular mechanisms leading to TCS inhibition of mast cell degranulation.

3.4.1 Triclosan increases protein kinase C activity in Ag-stimulated RBL-2H3 mast cells.

PKC is a key signaling enzyme involved in mast cell degranulation (Ludowyke *et al*., 1989; Ozawa *et al*., 1993a; Gadi *et al*., 2011), and is activated by Ca^{2+} (Kang and Othmer, 2007; van Rossum and Patterson, 2009; Land and Rubin, 2017) and by diacylglycerol (Ozawa *et al*., 1993b; Steinberg, 2008). Because TCS decreases cytosolic Ca^{2+} mobilization (Weatherly *et al*., 2018), we hypothesized that TCS inhibits PKC activity, thereby inhibiting degranulation in mast cells. To probe this hypothesis, we utilized a PKC activity ELISA (Enzo life science) that measures the activity of eight PKC isoforms (α, βI, βII, γ, δ, ε, η, and θ) simultaneously.

RBL-2H3 (RBL) mast cells were stimulated by 0.1μg/mL DNP-BSA Ag for 10 min, or by 0.005 μg/mL DNP-BSA Ag for 15, 30, and 45 minutes, with and without 10 μM TCS. A control (no Ag stimulation) was also prepared. The lysates from each of the cell samples were used in the PKC activity ELISA. These data were normalized by the total protein concentration

values. Exposure of RBL cells to 0.1μg/ml Ag for 10 minutes causes a robust (~67%) increase in PKC activity over controls, as expected (Fig. 3.1A).

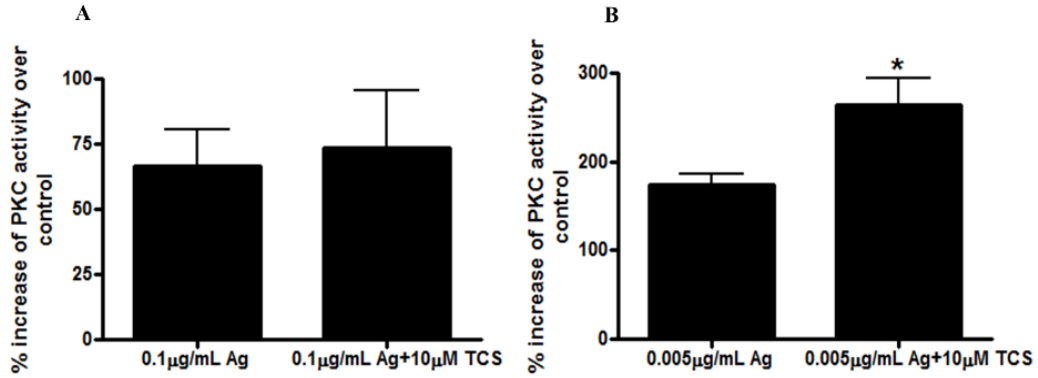

Figure 3.1. TCS effects on PKC activity in Ag-stimulated RBL-2H3 mast cells. Cells were stimulated with 0.1 μg/ml Ag ± 10 μM TCS for 10 min (A) or with 0.005 μg/ml Ag ± 10 μM TCS for 45 min (B) in BT. After exposure, PKC activity was measured via ELISA, and absorbance was read at 450 nm using a microplate reader. Raw data were processed as described in the Methods section to normalize to both total protein concentration and to unstimulated controls, in order to calculate percentage increase of PKC activity over unstimulated control. Data presented are means ± SEM of at least three independent experiments; duplicates per treatment per experiment. Statistically significant results, comparing Ag-stimulated cells ± TCS exposure, are represented by * $p < 0.05$, determined by one-tailed t-test.

Surprisingly, TCS has no effect on the ability of Ag to stimulate PKC activity at this 10 min timepoint (Fig.3.1A). Because cytosolic Ca^{2+} levels are only inhibited by ~10% by TCS within the first 10 min of Ag co-exposure, next we hypothesized that later time points would reveal TCS inhibition of PKC activity due to the greater reduction in cytosolic Ca^{2+} (compared to Ag-only control) caused by TCS at 15 min (~20% inhibition) and 60 min (~50% inhibition) post-Ag stimulation (Weatherly *et al*., 2018). However, similar results were found in 15 and 30 min exposure experiments (Fig. B1), which showed robust Ag-stimulated increases in PKC activity that are, again, unaffected by TCS (Fig. B1A-B). Interestingly, there is a significant TCS-induced *increase* in Ag-stimulated PKC activity at the 45 min time point (Fig 3.1B). Previous researchers showed that reactive oxygen species (ROS) can activate certain PKC isoforms

(thereby activating degranulation) (Bouwman *et al*., 2004; Lee and Yang, 2010). Also, we had previously found that ROS levels are increased by TCS exposure of Ag-stimulated RBL cells at this 45 min timepoint (Weatherly *et al*., 2018), which may explain triclosan's activation of PKC at 45 min (Fig. 3.1B).

3.4.2 Triclosan delays PKC βII and PKC δ translocation to plasma membrane in Ag-stimulated RBL-2H3 mast cells

Because the ELISA assay of PKC activation simultaneously measures eight PKC isoforms (Fig. 3.1), we hypothesized that potential TCS inhibition of key isoforms essential for degranulation may be masked by that measurement method. Previous studies have reported that PKC β and PKC δ isoforms are particularly important for mast cell degranulation (Nechushtan *et al*., 2000; Cho *et al*., 2004), so we investigated the activation of those individual key isoforms by monitoring their translocation using confocal microscopy. PKC translocation, to the plasma membrane, is known to be a hallmark of its activation (Mochly-Rosen *et al*., 1990). Thus, we utilized YFP-PKC βII-YFP and PKC δ C1 (2)-EGFP plasmids and transfected them via electroporation into RBL-2H3 mast cells, for transient expression. The translocation of PKC in real time in live cells over the course of 10 minutes was imaged by confocal microscopy.

In unstimulated RBL mast cells, the majority of PKC βII and PKC δ are located in the cytosol (as shown in representative still frame images from the videos; "Control [No Ag]" columns in Fig. 3.2A, 3.3A). Antigen (0.005μg/mL) stimulation causes both PKC isoforms to translocate rapidly to the plasma membrane (Fig. 3.2A, 3.2C, 3.3A, 3.3C). While addition of Ag+10 μM TCS does not affect the overall spatial translocation to the plasma membrane

compared to Ag-alone (Fig. 3.2A-B, 3.3A-B), temporal translocations of both PKC βII and PKC δ are delayed significantly by TCS (Fig. 3.2C, 3.3C, Table 3.1).

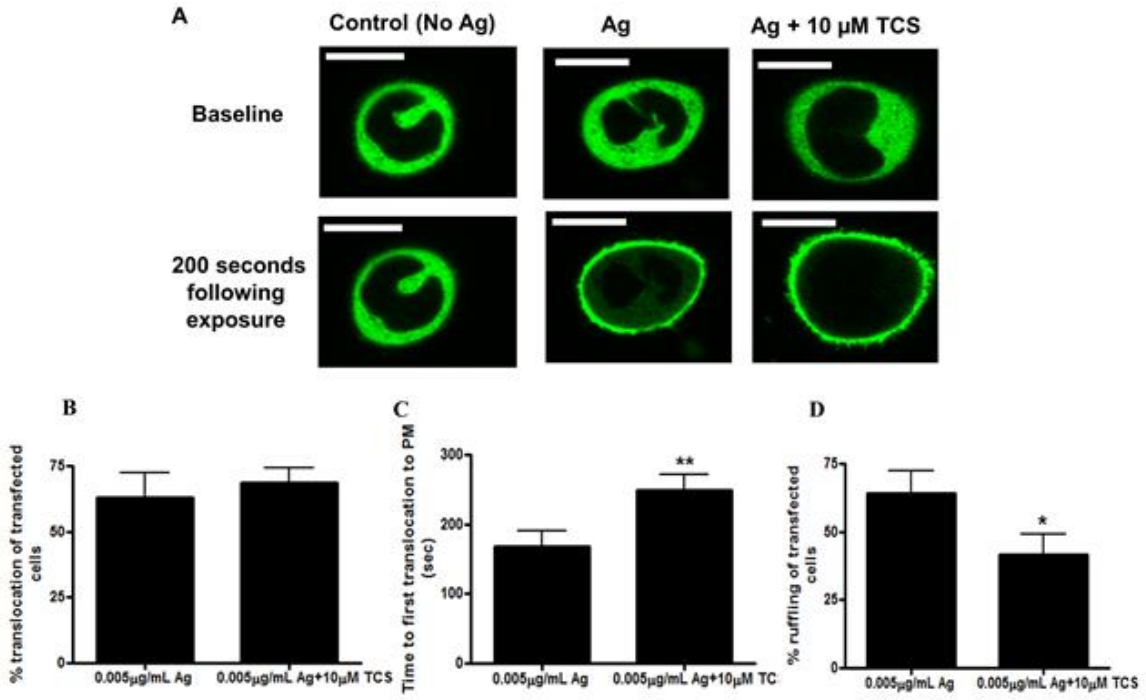

Figure 3.2. TCS effects on PKC βII translocation to the plasma membrane in Ag-stimulated RBL-2H3 cells. RBL cells were transfected with the YFP-PKC βII-YFP plasmid. Live cell time-lapse images were taken for 10 min immediately after addition of 0.005 μg/ml Ag or 0.005 μg/ml Ag + 10 μM TCS in the cells by confocal fluorescence microscopy. Representative images per group, pre-exposure and at ~200 sec post-exposure are shown in (A). Scale bar, 10 μm. As described in Methods, the percentage of transfected cells with PKC βII that translocated from the cytosol to the plasma membrane within 10 min post addition of Ag ± 10 μM TCS are plotted in (B); first time of this translocation is plotted in (C). As a control showing cellular inhibition by TCS, the percentage of transfected cells undergoing membrane ruffling within 10 min (D) was calculated using Fiji image J. For (B-D), values presented are derived from analysis of N= 43 for Ag-only cells and N=50 for Ag + 10 μM TCS cells. Percentage translocation and percentage ruffling values in (B) and (D) are from six independent days of imaging, ± SEM. Translocation time values in (C) are averages over the 43 (Ag) and 50 (Ag + 10 μM TCS) cells, ± SEM. Statistically significant results, comparing Ag-stimulated cells ± TCS exposure, are represented by * $p<0.05$, ** $p<0.01$, determined by one-tailed t-test.

Analyses of individual cells revealed that about two-thirds of transfected cells expressing PKC βII and nearly all cells expressing PKC δ undergo PKC translocation to the plasma membrane within 10 min of Ag stimulation, regardless of TCS exposure (Fig. 3.2B, 3.3B). Also

in both PKC βII- and PKC δ-transfected cells, following the first rapid translocation to the plasma membrane, periodic oscillations of PKC translocation between the plasma membrane and the cytosol were observed in Ag-stimulated cells, and were unaffected by TCS exposure (data not shown); these oscillations were previously documented for PKC βI in RBL cells (Gadi *et al*., 2011). However, the average time for PKC to translocate to the plasma membrane for the first time is increased significantly by TCS: a delay of about 80 sec for both PKC βII and PKC δ) (Fig. 3.2C, 3.3C, Table 3.1).

To verify that TCS does, indeed, inhibit mast cell function under these experimental conditions (10 min of imaging of individual PKC-transfected, Ag-stimulated RBLs), we utilized the previously-shown TCS inhibitory effect on mast cell ruffling (Palmer *et al*., 2012). We analyzed the percentage PKC-transfected cells that underwent cytoskeleton ruffling within 10 min of Ag addition, ± TCS, which showed both the expected robust stimulation of membrane ruffling by Ag and triclosan's inhibition (Fig. 3.2D, 3.3D). This ruffling analysis (Fig. 3.2D, 3.3D) also serves as a control showing that overexpression of the PKC constructs does not interfere with triclosan's ability to inhibit mast cell signaling.

Additionally, to further rule out unwanted effects of overexpression of PKC by transfection in RBLs, we measured the degranulation as described in (Weatherly *et al*., 2013), of PKC-transfected, Ag-stimulated RBLs, ± TCS. Exogenous overexpression of either PKC βII or PKC δ did not affect levels of mast cell degranulation compared to untransfected cells, and TCS inhibition of degranulation was, likewise, unaffected in these transfected cells (data not shown). Together, these controls confirm the validity of these transfection/confocal experiments for assessing TCS toxicity in mast cells.

Overall, Figures 3.2 and 3.3 indicate that TCS causes defects in PKC βII and PKC δ signaling by delaying their translocation to the plasma membrane. However, these PKC isoforms do (eventually) translocate and display oscillatory movement in the presence of TCS, suggesting that their activity is not the major target of TCS in its inhibition of mast cell function.

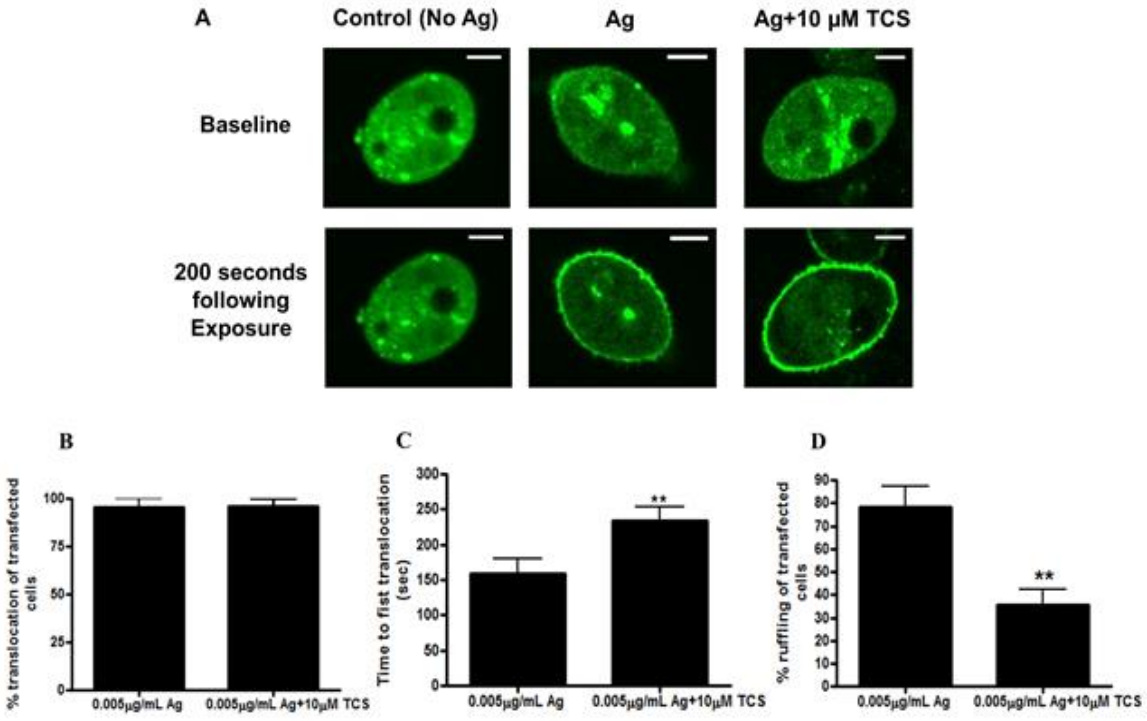

Figure 3.3. TCS effects on PKC δ C1 (2) translocation to the plasma membrane in Ag-stimulated RBL-2H3 cells. RBL cells were transfected with the PKC δ C1 (2)-EGFP plasmid. Live cell time-lapse images were taken for 10 min immediately after addition of 0.005 µg/ml Ag or 0.005 µg/ml Ag + 10 µM TCS in the cells by confocal fluorescence microscopy. Representative images per group, pre-exposure and at ~200 sec post-exposure are shown in (A). Scale bar, 5 µm. As described in Methods, the percentage of transfected cells with PKC δ C1 (2) that translocated from the cytosol to the plasma membrane within 10 min post addition of Ag ± 10 µM TCS are plotted in (B); first time of this translocation is plotted in (C). As a control showing cellular inhibition by TCS, the percentage of transfected cells undergoing membrane ruffling within 10 min (D) was calculated using Fiji image J. For (B-D), values presented are derived from analysis of N= 29 for Ag-only cells and N=47 for Ag + 10 µM TCS cells. Percentage translocation and percentage ruffling values in (B) and (D) are from five independent days of imaging, ± SEM. Translocation time values in (C) are averages over the 29 (Ag) and 47 (Ag + 10 µM TCS) cells, ± SEM. Statistically significant results, comparing Ag-stimulated cells ± TCS exposure, are represented by ** $p<0.01$, determined by one-tailed t-test.

3.4.3 Triclosan delays MARCKS translocation to the cytosol in Ag-stimulated RBL-2H3 mast cells

In order to directly assess whether PKC activity is affected by TCS in individual, living RBL cells, we assessed TCS effects on MARCKS. MARCKS is one of the most abundant substrates for PKC in mast cells (Blackshear, 1993; Gadi *et al*., 2011). In resting cells, MARCKS is held at the plasma membrane via specific electrostatic interactions with membrane phospholipids at its basic effector domain (ED) domain. Upon Ag stimulation, serine residues within the ED domain are phosphorylated by translocated PKC, resulting in MARCKS dissociation from the plasma membrane (Graff *et al*., 1989; Graff *et al*., 1989b). Thus, to determine whether TCS affects PKC kinase activity on its MARCKS substrate, we transfected the fluorescent construct mRFP-MARCKS-ED into RBL mast cells and monitored its translocation by confocal microscopy.

Upon Ag (0.005μg/mL) stimulation, mRFP-MARCKS-ED dissociates from the plasma membrane and moves into the cytoplasm (Fig. 3.4A). TCS (10μM) does not affect the overall ability of mRFP-MARCKS-ED to translocate to the cytosol (Fig 3.4A, 3.4B). Thus, these results indicate that overall PKC kinase activity is not hindered by TCS, in agreement with Fig. 3.1A and Fig. B1. Also, oscillatory behavior in which mRFP-MARCKS-ED dissociates from and re-associates with the plasma membrane in Ag-stimulated mast cells (Gadi *et al*., 2011) was observed, and the periodicity of mRFP-MARCKS-ED oscillations is not altered by TCS exposure (data not shown).

We analyzed the percentage MARCKS-transfected cells that underwent cytoskeleton ruffling within 10 min of Ag addition, ± TCS, which showed both the expected robust stimulation of membrane ruffling by Ag and triclosan's inhibition (Fig. 3.4D). This ruffling

analysis (Fig. 3.4D) also serves as a control showing that overexpression of the MARCKS constructs does not interfere with triclosan's ability to inhibit mast cell signaling.

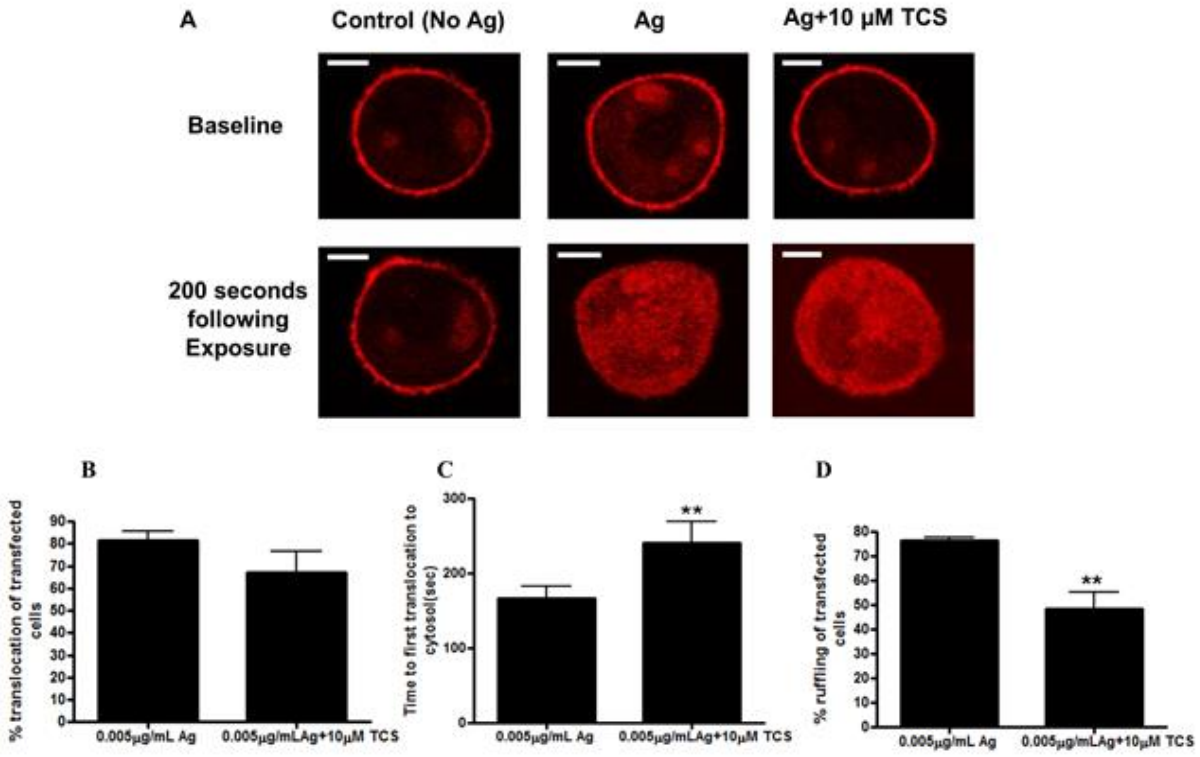

Figure 3.4. TCS effects on MARCKS translocation to the cytosol in Ag-stimulated RBL-2H3 cells. RBL cells were transfected with the mRFP-MARCKS-ED plasmid. Live cell time-lapse images were taken for 10 min immediately after addition of 0.005 µg/ml Ag or 0.005 µg/ml Ag + 10 µM TCS in the cells by confocal fluorescence microscopy. Representative images per group, pre-exposure and at ~200 sec post-exposure are shown in (A). Scale bar, 5 µm. As described in Methods, the percentage of transfected cells with MARCKS that translocated to the cytosol within 10 min post addition of Ag ± 10 µM TCS are plotted in (B); first time of this translocation is plotted in (C). As a control showing cellular inhibition by TCS, the percentage of transfected cells undergoing membrane ruffling within 10 min (D) was calculated using Fiji image J. For (B-D), values presented are derived from analysis of N= 80 for Ag-only cells and N=45 for Ag + 10 µM TCS cells. Percentage translocation and percentage ruffling values in (B) and (D) are from three independent days of imaging, ± SEM. Translocation time values in (C) are averages over the 80 (Ag) and 45 (Ag + 10 µM TCS) cells, ± SEM. Statistically significant results, comparing Ag-stimulated cells ± TCS exposure, are represented by ** $p<0.01$, determined by one-tailed t-test.

Further analyses of individual MARCKS-transfected, Ag-stimulated RBL cells revealed that TCS causes a defect in MARCKS signaling by delaying MARCKS dissociation from the

plasma membrane (by about 70 sec) (Fig 3.4C, Table 3.1). Overall, figure 3.4 data indicate that TCS causes a defect in PKC activity and MARCKS signaling, shown by delayed translocation to the plasma membrane. However, MARCKS does (eventually) translocate and displays normal oscillatory movement in the presence of TCS, suggesting that MARCKS is not the major target of TCS in its inhibition of mast cell function.

Table 3.1. Average time of first translocation of transfected cells

Sample	Ag exposure (sec)	# of cells (N)	Ag+ 10μM TCS exposure (sec)	# of cells (N)
PKC βII-YFP	170 ± 20	43	250 ± 20	50
PKC δ (C1)-EGFP	160 ± 20	29	240 ± 20	47
mRFP-MARCKS-ED	170 ± 20	80	240 ± 30	45

3.4.4 Triclosan and FIPI, a PLD inhibitor, decrease PLD activity in Ag-stimulated RBL-2H3 mast cells

Cytosolic Ca^{2+} and PKC translocation work in tandem to activate phospholipase D (PLD) (Lin and Gilfillan, 1992), which is another key player in the mast cell signaling pathway leading to degranulation (Chahdi *et al*., 2002). To examine whether TCS affects PLD activity, we utilized the fluorescence-based Amplex® Red phospholipase D assay kit, which measures the activity of both PLD1 and PLD2 isoforms at the same time.

First, we performed Ag-dose response assays measuring PLD activity by the Amplex® kit (data not shown). From these dose responses, we chose two Ag doses, 0.1μg/mL and 0.001μg/mL, which both produced robust activation of PLD activity, for further cellular PLD activity experiments with TCS exposure. With 0.1μg/mL Ag stimulation for 15 min, PLD activity is increased ~30% over the basal level in unstimulated control cells (Fig. 3.5A). This Ag-stimulated PLD activity is inhibited (decrease by ~50%) by 10μM TCS (Fig. 3.5A). A similar level of PLD inhibition was observed in cells stimulated by 0.001μg/mL Ag (data not shown).

These inhibitory effects of TCS on PLD activity were only observed in Ag-stimulated mast cells, not in resting RBL cells (data not shown).

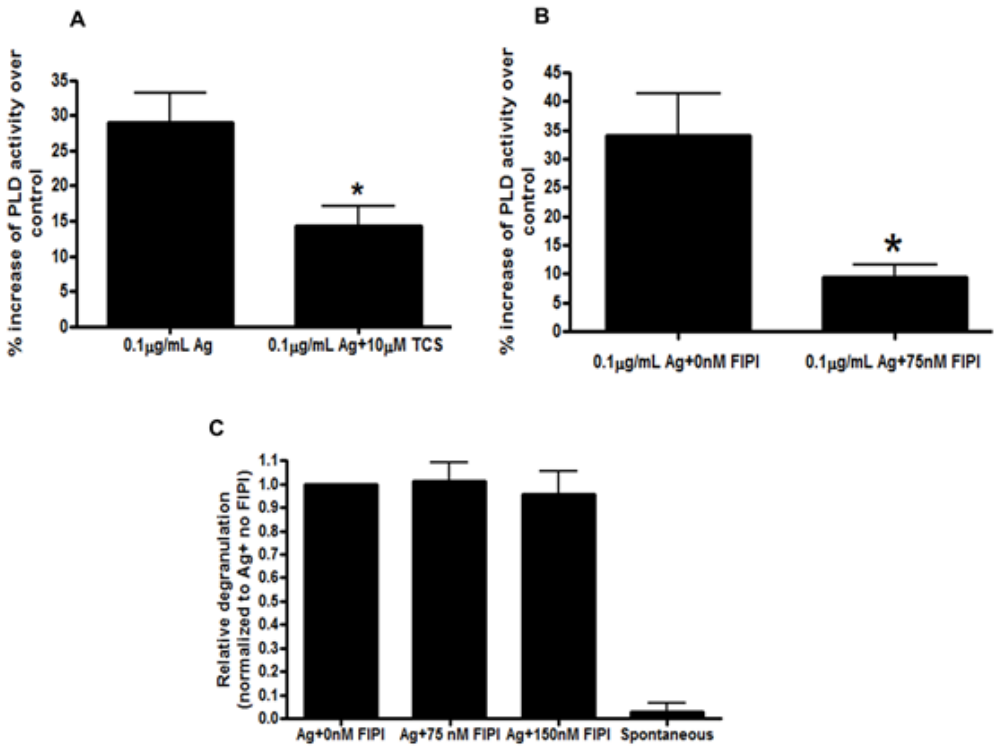

Figure 3.5. TCS effects on PLD activity in Ag-stimulated RBL-2H3 mast cells. Cells were stimulated with 0.1 µg/ml Ag ± 10 µM TCS for 15 min (A) or with 0.1 µg/ml Ag ± 75 nM FIPI for 15 min (B) in BT. After exposure, PLD activity was measured via Amplex® Red kit, and fluorescence was read using a microplate reader. Raw data were processed as described in the Methods section to normalize to unstimulated controls, in order to calculate percentage increase of PLD activity over unstimulated control. Data presented are means ± SEM of at least three independent experiments; triplicates per treatment per experiment. Statistically significant results, comparing Ag-stimulated cells ± TCS or FIPI exposure, are represented by * $p < 0.05$, determined by one-tailed t-test. (C) Degranulation was measured described in (Weatherly *et al.*, 2013) after cells were exposed to 0.1µg/ml Ag ± FIPI, for 1 hour. Spontaneous represents control cells that are not exposed to either antigen or FIPI. Values were then normalized to 0.1µg/ml Ag+ 0 nM FIPI. Data presented are means ±SEM of five independent experiments; three replicates per experiment. No significance among FIPI exposures was determined by one-way ANOVA followed by Tukey's *post-hoc* test.

As a control, degranulation was also measured under the same experimental conditions used for these cellular PLD assays: modest degranulation responses were stimulated by Ag (0.1µg/mL and 0.001µg/mL) and were inhibited by TCS within the 15 min timeframe of these

experiments (data not shown). We also confirmed that triclosan's inhibition of PLD activity is a true cellular effect and is not due to TCS interference with the components of the Amplex® kit (Fig. B2).

In another control experiment, we employed a known direct PLD inhibitor, FIPI, which irreversibly binds to the HKD (histidine, lysine, aspartic acid) domain in the catalytic site of PLD and inhibits both the PLD1 and the PLD2 isoforms (Su *et al*., 2009b). As expected, Ag-stimulated PLD activity is strongly inhibited by 75 nM FIPI (Fig. 3.5B). Interestingly, inhibition of PLD activity by 75 nM FIPI, and even higher doses of FIPI at 150 nM, did not lead to inhibition of degranulation (Fig. 3.5C), in agreement with a study done by Yanase *et al*. (Yanase *et al*., 2009).

3.4.5 Triclosan does not significantly affect PLD1 translocation to the plasma membrane in Ag-stimulated RBL-2H3 mast cells

Previous studies have shown that the PLD1 isoform, not PLD2, translocates toward the plasma membrane upon activation (Brown *et al*., 1998). Also, while activity of both PLD isoforms is measured simultaneously by the Amplex® kit, recent literature suggests that only the PLD1 isoform is positive regulator of degranulation (Zhu *et al*., 2015). Thus, we next performed real-time fluorescence imaging of PLD1-EGFP translocation to detect the spatiotemporal changes of PLD1 after co-exposure of Ag and TCS.

Upon Ag (0.1 μg/mL) stimulation, PLD1-EGFP translocates gradually to the plasma membrane, with variable onset times of ~2 to 10 minutes following Ag addition (Fig. 3.6A)—in contrast to the rapid and complete translocation patterns exhibited in the PKC βII, PKC δ, and MARCKS translocations. Further analyses showed that even though co-exposure of Ag with

TCS appears to modestly decrease PLD1 translocation toward the plasma membrane, the effect is not statistically significant (Fig. 3.6A-B).

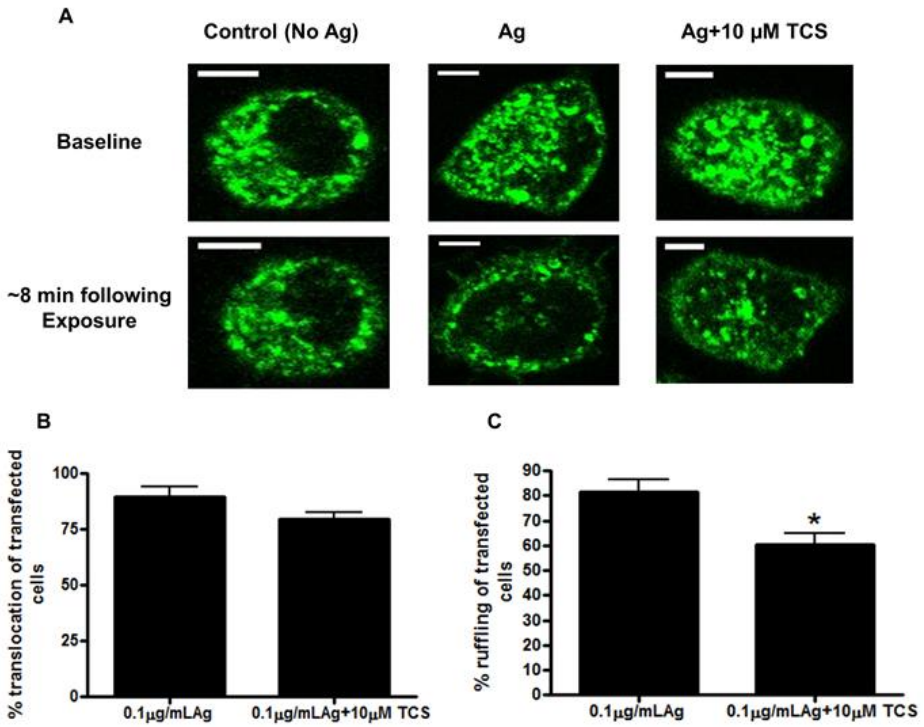

Figure 3.6. TCS effects on PLD1 translocation toward the plasma membrane in Ag-stimulated RBL-2H3 cells. RBL cells were transfected with the EGFP- PLD1 construct. Live cell time-lapse images were taken for 10 min immediately after addition of 0.1µg/ml Ag or 0.1µg/ml Ag + 10 µM TCS in the cells by confocal fluorescence microscopy. Representative images per group, pre-exposure and at ~8 min post-exposure are shown in (A). Scale bar, 5 µm. As described in Methods, the percentage of transfected cells with PLD1 that translocated toward the plasma membrane within 10 min post addition of Ag ± 10 µM TCS are plotted in (B). As a control showing cellular inhibition by TCS, the percentage of transfected cells undergoing membrane ruffling within 10 min (C) was calculated using Fiji image J. For (B and C), values presented are derived from analysis of four independent days of imaging, with 4-13 cells analyzed per treatment per day, with error shown as SEM. Statistically significant results, comparing Ag-stimulated cells ± TCS exposure, are represented by ** $p<0.05$, determined by one-tailed t-test.

No oscillatory behavior of PLD1-EGFP movement was displayed: PLD1 stayed at or near the plasma membrane once translocated, at least within the 10-15 min imaging period. As in Figures 3.2-3.4, we again analyzed the percentage PLD1-EGFP-transfected cells that underwent cytoskeleton ruffling within 10 min of Ag addition, ± TCS, which showed both the expected

robust stimulation of membrane ruffling by Ag and triclosan's inhibition of it (Fig. 3.6C). This ruffling analysis (Fig. 3.6C) shows that overexpression of the PLD1-EGFP construct does not interfere with triclosan's ability to inhibit mast cell signaling.

3.4.6 TCS does not directly inhibit PLD activity

To determine whether TCS directly binds to and inhibits PLD activity, we used purified PLD from *Arachis hypogaea* (peanut), which contains two HKD domains, similar to those found in mammalian PLD isoforms (Guo *et al*., 2006). Purified PLD was prepared in buffer conditions that mimic our cell-based PLD activity assays and then was exposed to varying concentrations of TCS (0 – 20 μM). There was no effect of TCS on PLD from *Arachis hypogaea* (Fig. 3.7), suggesting the triclosan's inhibition of mammalian PLD activity (Fig. 3.5A) may not be due to direct binding of TCS to PLD. A similar lack of direct TCS effect on PLD activity was found in experiments using a different purified PLD, from *Streptomyces chromofuscus* (Fig. B3).

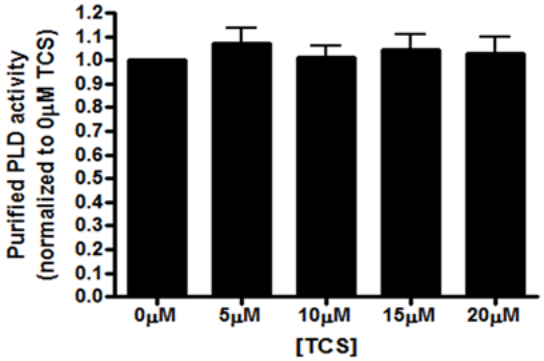

Figure 3.7. TCS effects on purified PLD from *Arachis hypogaea*. PLD activity was measured using the Amplex® Red PLD assay kit after incubating purified *Arachis hypogaea* PLD with 0 to 20 μM TCS for 1 hour. Values were normalized to the control (0μM TCS) and presented as means ± SEM of three independent days of experiments; with triplicates per treatment per experiment. No significance was determined by one-way ANOVA followed by Tukey's *post-hoc* test.

3.4.7 Structural analysis of triclosan's inhibition of mast cell degranulation: comparison to sucralose

In order to investigate the roles of triclosan's chemical structural features in its ability to inhibit mast cell degranulation, we assayed degranulation upon co-exposure of Ag with sucralose (main ingredient in Splenda®) which has structural similarities to TCS (Fig. B4). We found that sucralose, at doses relevant to human exposure, does not affect degranulation, at least during the one hour time frame assessed (Fig. B4). These data indicate that presence of two carbon rings (combined in ether linkage) decorated with three chlorines is insufficient to affect mast cell function. This result lends further support to the idea that the proton ionophore nature of TCS is the key structural determinant of its modulation of mast cells (Weatherly *et al*., 2016).

3.5 Discussion

In this investigation of the biochemical mechanisms underlying triclosan disruption of mast cell signaling, we have revealed triclosan's effects on activity and on spatial and temporal subcellular localization of crucial signaling molecules. We found that, although TCS surprisingly does not inhibit Ag-stimulated PKC activity, TCS delays the translocations of PKC isoforms βII and δ to the plasma membrane and dissociation of the PKC substrate MARCKS from the plasma membrane (events which occur during the 10 min period following Ag stimulation). Conversely, TCS inhibits Ag-stimulated PLD activity by 15 min post Ag stimulation but does not affect translocation of PLD1 toward the plasma membrane, movement which largely occurs within the first 10 min post Ag. Of interest, a previous study also found that inhibition of PLD activity (via primary alcohol treatment) suppresses mast cell degranulation but does not affect translocation of PLD1 (Brown *et al*., 1998).

An overarching finding of this mechanistic investigation of TCS degranulation suppression is that, during the first ~10 min following Ag stimulation, several of the major early biochemical events are not significantly inhibited by TCS, despite strong TCS inhibition of degranulation within 1 hour (Weatherly *et al*., 2013). Originally, we had hypothesized that PKC activity (measured by ELISA, Fig. 3.1 and by translocation of its substrate MARCKS, Fig. 3.4) would be inhibited because TCS reduces the cytosolic Ca^{2+} concentration following Ag stimulation (Weatherly *et al*., 2018). A PKC isoform key to mast cell degranulation (Yanase *et al*., 2011), βII, contains a C2 domain (Blobe *et al*., 1996) responsible for modulating Ca^{2+}-responsive activation of the enzyme. However, TCS actually increases efflux of Ca^{2+} out of the endoplasmic reticulum (and into the cytosol) within the first 3 min post-Ag and increases influx of Ca^{2+} into the mitochondria within the first 4 min post-Ag (Table 3.2 and (Weatherly *et al*., 2018)): changes that promote degranulation.

Additionally, intracellular levels of reactive oxygen species (ROS) are enhanced by TCS (Table 3.2 and (Weatherly *et al*., 2018)) — another TCS effect that is actually supportive of degranulation because ROS activates degranulation (Swindle et al., 2004). Reduction in the level of Ca^{2+} within the cytosol (the cellular compartment that contains PKC) does not occur until at least 10 min post Ag exposure (Weatherly *et al*., 2018) and does not reach ~20% inhibition (area under the curve) until 15 min (and ~50% inhibition until 1 hour). Thus, even though PKC activity is robustly stimulated by Ag within 10 min, it is unaffected by TCS (Fig. 3.1A), likely both due to the longer time frame required (>10 min) for TCS to robustly inhibit cytosolic Ca^{2+} (Weatherly *et al*., 2018) and due to triclosan's stimulation of ROS leading to stimulation of ROS-activated PKC isoforms such as PKCδ (Cho *et al*., 2004; Yoshida, 2007;

Lee and Yang, 2010)(Fig. 3.1B). Table 3.2 summarizes TCS effects on biochemical events in the mast cell degranulation pathway and their timing.

These data support the conclusion that PKC can still do its job (translocate to the plasma membrane, oscillate between the cytosol and plasma membrane, actively process its substrate MARCKS) during the first ~10 min of Ag and TCS co-exposure—even while the delays in PKC (from ~2.7 to 4.2 min) and MARCKS (from ~2.8 to 4 min) movement are early indicators of problems to come. The major disruptive events caused by TCS do not commence until ~15 min, including ~20% decrease in integrated cytosolic Ca^{2+} level, significantly inhibited PLD activity, and disruption in microtubule formation (Table 3.2): defects which are key to inhibiting degranulation.

Even though PLD activity is inhibited by TCS by 15 min post Ag, translocation of PLD1 is unaffected, likely because its movement toward the plasma membrane begins within ~2 min post-Ag and has occurred to a large degree with the first 10 min. However, after PLD has been largely re-located to or near the plasma membrane, its activity is inhibited. Taken together, these PKC and PLD studies strongly suggest that a significant accumulated decrease in cytosolic Ca^{2+} concentration, which does not occur until ~15 min post-Ag, is the key event leading to inhibition of degranulation. Below we discuss how dampened cytosolic Ca^{2+} could cause the inhibitory events in Table 2 (red arrows: translocation delays, decreased PLD activity, and inhibited microtubule polymerization).

Our lab and others previously demonstrated that TCS is a proton ionophore mitochondrial uncoupler, which disrupts mitochondrial function in multiple cell types (Ajao *et al*., 2015; Weatherly *et al*., 2016; Weatherly *et al*., 2018) and in zebrafish embryos (Shim *et al*., 2016b; Raftery *et al*., 2017). We previously showed, though, that mitochondrial uncoupling is not the

main mechanism causing triclosan's inhibition of degranulation (Weatherly *et al*., 2018). However, proton ionophoric effects of TCS on the mast cell plasma membrane may be the cause of degranulation inhibition. Support for this hypothesis includes findings of a recent study which demonstrated that TCS is a proton ionophore in artificial bilayer lipid membranes and can depolarize bacterial membrane potential (Popova *et al*., 2018). Because Ca^{2+} flows down its electrochemical gradient through mast cell plasma membrane CRAC channels following Ag stimulation, TCS perturbation of plasma membrane potential could be the mechanism underlying TCS disruption of Ca^{2+} influx into the cytosol. Future studies will address whether triclosan's proton ionophore nature perturbs the electrochemical potential of the mast cell plasma membrane (preliminary experiments using membrane potential sensitive organic dyes were inconclusive due to TCS interference with the dye's fluorescence (Weatherly *et al*., 2018)).

Sucralose, the active ingredient in artificial sweetener Splenda®, exhibits structural similarities to TCS: both molecules are comprised of two carbon rings combined in ether linkage and decorated with a total of three chlorines (Fig. B4). However, unlike TCS, sucralose does not affect degranulation, indicating that presence of the three chlorines on the two ether-linked rings is insufficient to affect mast cell function, at least during the one hour time frame assessed (Fig. B4). This result lends further support to the hypothesis that the proton ionophore nature of TCS is the key determinant of its modulation of mast cells (Weatherly *et al*., 2016).

While we suspect that TCS lowers Ag-stimulated cytosolic Ca^{2+} levels by disrupting the plasma membrane potential and, hence, by disrupting a driving force for Ca^{2+} influx, there are other potential mechanisms underlying TCS inhibition of cytosolic Ca^{2+}. One is that TCS could inhibit the early phosphorylation cascade that leads to PLC γ activation. PLC γ inhibition would lead to decreases in both DAG and IP_3 generation, which would subsequently result in hindered

IP_3-mediated ER Ca^{2+} release. However, TCS does the opposite: Ag-stimulated ER Ca^{2+} release is actually enhanced by TCS with Ag (Weatherly *et al*., 2018), and this result strongly suggests that biochemical events upstream of ER Ca^{2+} mobilization are uninhibited by TCS—hence our focus on effectors of Ca^{2+} influx, PKC and PLD, in this study.

Table 3.2. Triclosan effects on mast cell degranulation pathway: Time to first signaling defect, following co-exposure to Ag+ TCS

Signaling Event*	TCS Effect on this event**	Time of first defect caused by TCS***	References
Efflux of Ca^{2+} from ER	↑	3 min	(Weatherly *et al*., 2018)
Influx of Ca^{2+} into mitochondria	↑	4 min	(Weatherly *et al*., 2018)
Mitochondrial Ca^{2+} oscillations	↓	10 min	(Weatherly *et al*., 2018)
Influx of Ca^{2+} into cytosol	↓	10 min (~10% ↓) 15 min (~20%↓) 1 hr (~50%↓)	(Weatherly *et al*., 2018)
PKC βII and PKCδ translocation	**Delay**	Delayed from ~ 2.7 min (-TCS, + Ag) to ~ 4.2 min (+ TCS, +Ag)	Fig. 3.2C & 3.3C
PKC activity	↑	45 min	Fig. 3.1B
MARCKS translocation	**Delay**	Delayed from ~ 2.8 min (-TCS, + Ag) to ~ 4 min (+ TCS, +Ag)	Fig. 3.4C
Actin cytoskeleton ruffling	↓	10 min	Fig. 3.2D, 3.3D, 3.4D & 3.6C
PLD1 translocation	None	Within 10 min	Fig. 3.6B
PLD activity	↓	15 min	Fig. 3.5A
Microtubule polymerization	↓	15 min	(Weatherly *et al*., 2018)
ROS formation	↑	~45 min	(Weatherly *et al*., 2018)

* Ag concentration used:0.005 -0.1µg/mL(these doses caused roughly maximal degranulation in absence of TCS.

** Items in red indicate mechanisms of TCS inhibition of degranulation.

*** TCS concentration used: 10-20µM

Delays in PKC translocation caused by TCS may be due to attenuation of microtubule polymerization by TCS (Weatherly *et al*., 2018) at early time points after Ag stimulation. In CHO cells, microtubule integrity is required for translocation of PKC δ, in a complex with cytoskeletal protein Annexin V (Kheifets *et al*., 2006). Though drastic TCS inhibition of microtubule polymerization was documented at 15 min post Ag in (Weatherly *et al*., 2018), and that time point was chosen for its unambiguous TCS effects, defects in microtubule formation may potentially begin to accumulate at earlier time points and may thereby explain slowed PKC translocation. TCS may inhibit microtubule polymerization via its depression of cytosolic Ca^{2+}: Ag-stimulated elevation of cytosolic Ca^{2+} levels stimulates the association of the positive regulator protein GIT1 with tubulin, in turn leading to enhanced microtubule polymerization and degranulation (Sulimenko *et al*., 2015).

PKC βII phosphorylates myosin and also binds actin in mast cells (Ludowyke *et al*., 2006). Myosin phosphorylation is thought important for degranulation (Ludowyke *et al*., 1989; Choi *et al*., 1994). Moreover, the C2-like domain of PKC δ binds to F-actin to regulate actin redistribution in neutrophils (Lopez-Lluch *et al*., 2001) as well as in airway epithelial cells (Smallwood *et al*., 2005). Thus, inhibition of actin polymerization, as shown by inhibition of membrane ruffling, could be another explanation of triclosan's delay of PKC movement to the plasma membrane.

PLD plays important roles in mast cell degranulation (Brown *et al*., 1998; Cissel *et al*., 1998; Way *et al*., 2000), and its Ag-stimulated activity is inhibited by TCS (Table 3.2). Transient expression PLD experiments in RBL-2H3 cells show both isoforms are activated by Ag stimulation (Chahdi *et al*., 2002; O'Luanaigh *et al*., 2002). In mast cells, PLD1 is associated with granule membranes while PLD2 with the plasma membrane (Brown *et al*., 1998; Choi *et*

al., 2002). PLD1 has low basal activity, and its activation requires interactions with PKC and/or small GTPases such as ADP-ribosylation factor (ARF) and Rho family members (Liscovitch *et al*., 2000; Peng and Frohman, 2012). PLD1 is stimulated *in vitro* and *in vivo* directly by Ca^{2+}-dependent cPKC isoforms (PKCα and β) (Hammond *et al*., 1997; Kim *et al*., 1999; Zhang *et al*., 1999) in a PIP_2-dependent manner (Hammond *et al*., 1995; Rumenapp *et al*., 1995; Bae *et al*., 1998). In contrast, PLD2 is constitutively active and is more dependent on the presence of PIP_2 than other activators (Lopez *et al*., 1998; Sung *et al*., 1999). Background studies of basal PLD activity showed that TCS has no effect on constitutive PLD activity (data not shown), even as TCS strongly inhibits Ag-stimulated PLD activity (Fig. 3.5A). These results suggest that constitutively-active PLD2 is less of a target of TCS than is PLD1, due to PLD1's low basal activity and high activation potential.

FIPI, a potent dual inhibitor for PLD1 and PLD2, was employed in our study as a comparison to triclosan's inhibitory action on PLD activity and on degranulation. FIPI irreversibly binds to a serine residue within the HKD (histidine, lysine, aspartic acid) domain in the catalytic site of PLD, preventing the cleavage of phosphatidylcholine, thus blocking PA production (Su *et al*., 2009b). While we observed decreased PLD activity by FIPI, to our surprise, FIPI's inhibition of both PLD isoforms had no effect on overall degranulation in Ag-stimulated mast cells. Currently there is some controversy about the role of PLD1 and PLD2 in mast cells. It has been long believed that both PLD1 and PLD2 play a positive role in mast cell degranulation, in that PLD1 is involved in the granule transport to the plasma membrane (Chahdi *et al*., 2002; Hitomi *et al*., 2004; Peng and Beaven, 2005) and PLD2 is a fusogenic protein for granule's docking and fusion to the plasma membrane (Chahdi *et al*., 2002; Choi *et al*., 2002; Lee *et al*., 2006; Marchini-Alves *et al*., 2012). However, an intriguing recent study using PLD1-

and PLD2- knockout mice found that PLD1 positively regulates degranulation, while PLD2 is a negative regulator (Zhu *et al*., 2015). RhoA, which is directly affected by Ca^{2+} (though does not directly bind Ca^{2+}), interacts with PLD2 to play a negative role in microtubule formation. The authors also showed that mast cells isolated from double knockout mice ($PLD1^{-/-}$ and $PLD2^{-/-}$) exhibited normal degranulation compared to the control (Zhu *et al*., 2015), suggesting that PLD1 (positive) and PLD2 (negative) may effectively cancel out each other's roles in regulating degranulation. Another recent study from this group demonstrates the importance of PLD1, but not PLD2, in T cell activation (Zhu *et al*., 2018). Thus, our study using FIPI agrees with this finding that equally impeding the two PLD isoforms simultaneously yields no change in degranulation. Taken together with our results showing a lack of TCS effect on basal PLD activity, these findings provide further credence to the idea that triclosan's inhibitory action on PLD activity is targeted to PLD1, which is a positive regulator in degranulation--such that decreased PLD activity by TCS results in decreased degranulation.

Our study with purified PLD protein *in vitro* suggests that TCS does not directly bind to and inhibit activity of PLD; thus, PLD activity is more likely indirectly inhibited by TCS-induced decreases in cytosolic Ca^{2+} level. The PLD used in this study was derived from *Arachis hypogaea* and has an HKD domain which contains a serine residue and which is highly homologous to the HKD domains found in rat and human PLD1 and PLD2 proteins. Even though PLD does not directly interact with Ca^{2+}, the activities of its activation cofactors, such as small GTPase proteins, PKC, and PIP_2, are dependent on Ca^{2+} signaling (Wakelam *et al*., 1997). Moreover, several studies have demonstrated that degranulation requires activation of PLD accompanied by sustained cytosolic Ca^{2+} levels (Lin and Gilfillan, 1992; Ozawa et al., 1993a;

Cissel et al., 1998; Chahdi et al., 2002). Thus, the data suggest that PLD activity and, hence, degranulation, is inhibited by triclosan's inhibition of Ca^{2+} influx into the cytosol.

The role of PLD has been implicated in various essential cellular functions in various cell types: signal transduction in embryonic kidney cells (Fang *et al*., 2001), cell migration in breast cancer cells (Hui *et al*., 2006), membrane vesicular trafficking (Du *et al*., 2003) and cytoskeletal reorganization (Colley *et al*., 1997) in fibroblasts, autophagy (Dall'Armi *et al*., 2010) in cervical cancer cells, and viral infections (Oguin *et al*., 2014) in alveolar basal epithelial cells. Due to these diverse roles of PLD in biology, PLD is involved in numerous physiological and disease states, including cancer (Su *et al*., 2009a), neurodegenerative disorders (Cai *et al*., 2006), cardiovascular problems (Chiang, 1994), and infectious diseases (Taylor *et al*., 2015). Therefore, inhibition of PLD by TCS might affect these different health problems.

In conclusion, we have elucidated biochemical mechanisms underlying inhibition of mast cell function by TCS, at dosages relevant to human exposure, by interrogating the activity and localization of key signaling enzymes. Combined with our previous findings on triclosan's effects on calcium mobilization and microtubules, these results provide the temporal details of TCS-induced defects in PKC and PLD signaling steps, which lead to degranulation inhibition. In addition to TCS inhibition of mast cells, any cell type that depends on PLD function may be inhibited by TCS.

CHAPTER 4

SEARCHING FOR TRYPTASE IN THE RBL-2H3 MAST CELL MODEL: PREPARATION FOR COMPARATIVE MAST CELL TOXICOLOGY STUDIES WITH ZEBRAFISH[2]

4.1 Abstract

Mast cells comprise a physiologically and toxicologically important cell type that is ubiquitous among species and tissues. Mast cells undergo degranulation, in which characteristic intracellular granules fuse with the plasma membrane and release many bioactive substances, such as the enzymes β-hexosaminidase and tryptase. Activity of mast cells in the toxicology model organism zebrafish has been monitored via tryptase release and cleavage of substrate BAPNA. An extensively-used *in vitro* mast cell model for studying toxicant mechanisms is the RBL-2H3 cell line. However, instead of tryptase, granule contents such as β-hexosaminidase have usually been employed as RBL-2H3 degranulation markers. In order to align RBL-2H3 cell toxicological studies to *in vivo* mast cell studies using zebrafish, we aimed to develop an RBL-2H3 tryptase assay. Unexpectedly, we discovered that tryptase release from RBL-2H3 cells is not detectable, using BAPNA substrate, despite optimized assay that can detect as little as 1 ng tryptase. Additional studies performed with another substrate, tosyl-Gly-Pro-Lys-pNA, and with an ELISA also revealed a lack of tryptase protein released from stimulated RBL-2H3 cells. Furthermore, none of the eight rat tryptase genes (*Tpsb2, Tpsab1, Tpsg1, Prss34, Gzmk, Gzma, Prss29, Prss41*) are expressed in RBL-2H3 cells, even though all are found in RBL-2H3 genomic DNA and even though β-hexosaminidase mRNA is constitutively expressed. Therefore, mast cell researchers should utilize β-hexosaminidase or another reliable marker for RBL-2H3

[2] A portion (15%) of this work was performed by Rachel Kennedy with the remainder being performed by Juyoung Shim

degranulation studies, not tryptase. Comparative toxicity testing in RBL-2H3 cells *in vitro* and in zebrafish mast cells *in vivo* will require use of a degranulation reporter different from tryptase.

4.2 Short Abstract

Mast cells degranulate, releasing substances such as β-hexosaminidase and tryptase. Mast cell activity in zebrafish is monitored via tryptase release. To align *in vitro* RBL-2H3 mast cell line studies to *in vivo* mast cell zebrafish studies, we aimed to develop an RBL-2H3 tryptase assay. However, tryptase protein is not released from stimulated RBL-2H3 cells. Also, no rat tryptase gene is expressed in RBL-2H3s. Comparative toxicity testing in RBL-2H3 cells and in zebrafish mast cells will require a non-tryptase degranulation reporter.

4.3 Introduction

Mast cells (MCs) are highly granulated cells that are typically recognized for their role in allergies and asthma (Kuby, 1997). However, they are also involved in many helpful immune functions such as host defense (Galli *et al*., 2008; Abraham and St John, 2010), bacterial and parasitic clearance (Pawankar, 2005), and recruitment of neutrophils to sites of infection (Echtenacher *et al*., 1996; Malaviya *et al*., 1996). MCs possess additional immune-related functions that affect diseases such as cancer (Coussens *et al*., 1999; Gounaris *et al*., 2007), autoimmune disorders (Lee *et al*., 2002), and inflammatory bowel disease (Wilcz-Villega et al., 2013). Interestingly, MCs also have roles in neurological processes and diseases such autism (Theoharides *et al*., 2012b), anxiety disorders (Silver *et al*., 1996; Nautiyal *et al*., 2008), and multiple sclerosis (Rozniecki *et al*., 1995). MCs, found in nearly all human tissues, are prominent in tissues in contact with the external environment, such as skin, blood capillaries,

nerve terminals, gastrointestinal tract, respiratory mucosa, etc. (reviewed in (Galli *et al*., 2005b)). Also MCs are found in numerous different organisms (Baccari *et al*., 2011). Due to their physiological importance, ubiquity, and location near surface tissues, MCs are key toxicological targets.

MCs exhibit the unmistakably distinctive morphological feature of densely populated cytoplasmic granules, which get secreted upon MC stimulation: a process called degranulation (Kuby, 1997). Degranulation is typically initiated via multivalent antigen (Ag) crosslinking of immunoglobulin E (IgE) receptor-bound FcεRI receptors but can be stimulated in numerous ways, including via compound 48/80 (c48/80) or calcium ionophore application. The resulting signaling cascade culminates in degranulation, the release of granule-associated bioactive mediators, such as histamine, serotonin, β-hexosamindase (β-hex), and tryptase (Schwartz and Austen, 1980). Assays for release of these mediators (and more) have been extensively utilized to test mast cell function.

Thus, the presence of granules containing tryptase is considered a canonical marker of MCs, and release of tryptase (into cell supernatant *in vitro* or into the bloodstream *in vivo*) has often been utilized as a test of mast cell stimulation and function (Irani *et al*., 1986). Mast cell tryptase is a family of trypsin-like serine proteases that cleave sites after basic amino acids such as Arg and Lys (Lehninger *et al*., 2005). Tryptase requires the glycosaminoglycan heparin for its activity (Hallgren *et al*., 2001). In general, tryptases can be grouped into three main types, α (I-II), β (I-III), and γ (transmembrane). Most tryptase purified from human tissues is a mixture of β isoforms which are the products of two genes, TPSB2 and TPSAB1 (Caughey, 2011). Numerous distinct roles of mast cell tryptase have been reported: some protective/anti-inflammatory, and some pro-inflammatory (reviewed in (Caughey, 2011)). One example of a mechanism of action

of tryptase is cleavage and inactivation of calcitonin gene-related peptide, thus regulating vasodilation (Tam and Caughey, 1990; Walls *et al*., 1992). Tryptase acts upon many other substrates as well. Mast cell tryptase is also involved in angiogenesis (Stack and Johnson, 1994; Crivellato *et al*., 2004) and in development of multiple sclerosis (Rozniecki *et al*., 1995). In the laboratory, the presence of active tryptase in a solution can be detected by incubation with a chromogenic substrate such as N-α-benzoyl-DL-Arg-p-nitroanilide (BAPNA) or tosyl-Gly-Pro-Lys-p-nitroanilide: tryptase cleaves the bond between the Arg or Lys and the p-nitroaniline (pNA), releasing yellow-colored pNA, measurable in a plate reader (Lavens *et al*., 1993). Other chromogenic and fluorogenic tryptase substrates are also available.

Zebrafish (*Danio rerio*) (ZF) are a powerful, human-disease relevant (Ward and Lieschke, 2002; Lieschke and Currie, 2007) model organism for toxicology studies (Garcia *et al*., 2016). Zebrafish and humans share a highly conserved FcεRI receptor, and mast cells of both species share similarities in innate and adaptive immune responses (Dobson *et al*., 2008; Da'as *et al*., 2011; Da'as *et al*., 2015). Two methods for assessing mast cell function in zebrafish have recently been developed. Both methods use tryptase as the mast cell marker. First, a method has been developed to quantify mast cell degranulation in adult ZF, by assaying for tryptase in blood, using the substrate BAPNA (Dobson *et al*., 2008; Da'as *et al*., 2011). Intraperitoneal injection of adult zebrafish with an MC stimulant (such as c48/80) causes a large rise in blood plasma tryptase level (pNA production), as compared to saline-injected control animals (Dobson *et al*., 2008). Zebrafish have granzyme A (also known as granzyme K-like), a gene orthologue for human granzyme K (GZMK), which is conserved in rat (Gzmk), mouse, and ZF. Granzyme tryptases, including granzyme A and K, are serine proteases and shown to cleave after the basic residues Arg and Lys ((Plasman *et al*., 2014), so this ZF granzyme tryptase may be the enzyme

cleaving BAPNA in this ZF assay. Also, Dobson *et al*. (Dobson *et al*., 2008) and Balci *et al.* (Balci *et al*., 2014) detected staining of ZF tissues with a monoclonal anti-human MC tryptase antibody specific for TPSAB1, although an orthologue to this specific gene has not yet been cloned from ZF. Second, a tryptase assay using ZF embryos also has been developed (Yang *et al*., 2015). In this method, all the drugs and reagents, including stimulant (*e.g.*, c48/80) and substrate (*e.g.,* BAPNA), are directly added to the fish water.

In addition to animal models for studies of mast cells, *in vitro* mast cell models have contributed enormously to scientists' understanding of the biochemical details of mast cell signaling and of drug and toxicant modes of action on MCs. Among mast cell models, the rat basophilic leukemia - clone 2H3 (RBL-2H3) cell line has been used widely as a well-accepted model of mast cell signaling and function (Barsumian *et al*., 1981). RBL-2H3 cells, used extensively for over 40 years, are an important mast cell model for *in vitro* studies of MC toxicology and pharmacology. Other experimental mast cells exist, but each has advantages and disadvantages, such as human HMC-1 cells which lack FcεRI (Nilsson *et al*., 1994), human LAD2 cells which contain FcεRI but which require >2 weeks for each doubling (Jensen *et al*., 2005), P815 cells which are largely non-adherent, and primary bone marrow-derived mouse mast cells which senesce after a brief time in culture. RBL-2H3 ("RBL") cells are easy to quickly and continuously culture in large quantities, contain the core signaling machinery of mature human mast cells (Fewtrell, 1979; Metzger *et al*., 1982), and are functionally homologous to rodent mucosal mast cells (Seldin *et al*., 1985). Many molecular similarities between human and rodent mast cells have been detailed in (Abramson and Pecht, 2007). The pathway leading to degranulation in RBL cells is very well described, allowing for the identification of pathway targets for toxicants or drugs that affect this signaling system.

For many of the studies documented to date, RBL degranulation has been quantified via measurement of released β-hex: β-hex in the supernatant over stimulated cells is incubated with fluorogenic substrate 4-methylumbelliferyl-N-acetyl-β-D-glucosaminide (4-MU), and the resulting fluorescent product is detected in a microplate reader (Naal *et al*., 2004). β-hex enzyme catalyzes degradation of GM2 ganglioside, and mutations in this enzyme lead to neurodegenerative diseases (Bayleran *et al*., 1987; Tifft and Proia, 1997). β-hex has been successfully used as a MC function marker because it is released in parallel with canonical MC marker histamine (Schwartz *et al*., 1979). The homologs of β-hex genes have been identified in ZF (*hexa* and *hexb*)(Zizioli *et al.*, 2014). Of note, activated human primary lung mast cells secrete tryptase in parallel with histamine (Schwartz *et al*., 1981), but tryptase release has not typically been used as a RBL-2H3 degranulation marker.

Previously, we discovered that MC degranulation is disrupted by environmental toxicants, such as arsenic (Hutchinson *et al*., 2011; Shim *et al*., 2016a), and by the antimicrobial drug triclosan (TCS) (Palmer *et al*., 2012; Weatherly *et al*., 2013). Along with other cell types, these studies utilized RBL-2H3 cells and β-hex detection to quantify MC degranulation. However, all published studies of mast cells in ZF have, instead, utilized tryptase as the biochemical marker of mast cell function. Thus, in order to align our cell culture-based toxicological studies in this proven RBL mast cell model to *in vivo* toxicological studies of mast cells in the ZF model organism, we became interested in using tryptase as a marker for degranulation of RBL-2H3 cells. Measurement of tryptase release from RBL-2H3 cells would lay the groundwork for comparative/confirmative high-throughput toxicology assays of mast cell function and signaling that could use both ZF and this canonical mast cell model, RBL cells. For example, we are interested in studying and comparing effects of TCS on mast cells in ZF as a

whole organism follow-up to our findings that TCS inhibits function of RBL-2H3 cells (Palmer *et al*., 2012) and of human HMC-1 mast cells (Weatherly *et al*., 2016). Parallel studies of RBL-2H3 mast cells and ZF have already proven to be instructive in toxicology: for example, ZF mitochondrial function is inhibited by TCS (Shim *et al*., 2016b) at similar doses and time frames that also depress mitochondrial function in RBL-2H3 cells (Weatherly *et al*., 2016). Thus, we were motivated to develop a tryptase release assay from RBL-2H3 cells in order to design parallel assays of toxicant effects on MC function in both ZF and RBL-2H3, for applied toxicology investigations linking *in vitro* and *in vivo* systems. Background studies showing that TCS does not directly affect activity of purified tryptase (Kennedy, 2013) further bolstered our belief that it would be possible to use this degranulation marker for comparative mast cell toxicology studies of TCS.

In this study, we have optimized the conditions of a substrate-based assay for tryptase activity and have applied it to assess degranulation of RBL-2H3 cells. We report the results of three separate assay methods for detecting tryptase protein secreted from degranulated RBL-2H3 cells, as well as of PCRs performed to detect mRNA transcripts of eight distinct tryptase genes within these cells.

4.4 Materials and Methods

4.4.1 Chemicals and reagents

Purified human lung tryptase (E.C. Number 3.4.21.59; corresponds to human gene symbols TPSD1, TPSB2, TPSAB1) was purchased from Calbiochem /EMD Millipore (Billerica, MA, USA) and was stored as aliquots wrapped in aluminum foil at -20 °C. BAPNA (Nα -Benzoyl -D,L-arginine-*p*-nitroanilide • HCl) tryptase substrate (Bachem, Bubendorf,

Switzerland) was stored at -20°C in an amber bottle and wrapped in aluminum foil. Anti-dinitrophenyl (DNP) mouse Immunoglobulin E (IgE) (monoclonal, clone SPE-7), Ca^{2+} ionophore A23187, heparin, dimethyl sulfoxide (DMSO) were purchased through Sigma (St. Louis, MO, USA). Triton-X 100 (TX) was obtained from Thermo (Rockford, IL, USA).

Tryptase from human lung (TFHL) buffer was prepared to match the buffer contained in the purified tryptase purchased through Calbiochem, and contained 1 M NaCl, 50 mM acetate buffer, and 0.05 mM heparin (0.09% heparin), which was titrated to pH 5 with 10 N sodium hydroxide. 15-mL aliquots were frozen at -20 °C, and thawed as needed.

The components of Tyrodes buffer are that of (Hutchinson *et al*., 2011) and (Weatherly *et al*., 2013). Modified Tyrodes buffer (mT), pH 7.4, contained lower NaCl and lower $CaCl_2$ than typical Tyrodes, and was made by combining 100 mM NaCl, 5 mM KCl, 0.9 mM $CaCl_2$, 1 mM $MgCl_2$, 20 mM HEPES, and 5.6 mM glucose. As needed, bovine serum albumin (BSA) at 1 mg/ml was added to mT on the day of an experiment. BAPNA buffer solution I was prepared by first combining 1 mM $MgCl_2$, 0.1 M Trizma base (Sigma, St. Louis, MO, USA), and 1 M glycerol (Promega, Madison, WI, USA). After mixing well, 0.02% heparin (w/v) was added, and the pH of this solution was titrated to either 9 or 8, depending on the experiment. Similarly, BAPNA solution II was prepared in the same manner as solution I, only it contained the added component of 0.8 mM BAPNA (in assays, final concentration of BAPNA was 0.4 mM). These two buffer solutions were made fresh daily.

A23187 Ca^{2+} ionophore was prepared by dissolving A23187 powder into 100% DMSO for a final concentration of 2.5 mg mL^{-1} h and stored as aliquots wrapped in aluminum foil at -20 °C. On the day of an experiment, this stock was diluted directly into Tyrodes-BSA solution or mT-BSA to create necessary ionophore concentrations.

Cell harvest buffer (10X) was prepared with 1.35 M NaCl, 0.05 M KCl, 0.17 M HEPES, and 0.02 M EDTA, which was titrated to pH 7.6.

Chemicals of the highest possible purity were used. All buffers and media were sterile filtered using 0.2 μM VacuCap filters (Pall Corporation, Port Washington, NY, USA).

4.4.2 Purified tryptase assay

Purified tryptase working solutions containing 1-500 ng tryptase were prepared by making dilutions in TFHL buffer. Using a clear 96-well half-area plate (Grenier Bio-One, Monroe, NC, USA), 50 μL of 0.02% heparin (w/v) mT-BSA was added to each sample well. From all wells, 1 μL was removed, and tryptase (1 μL) at the varying levels indicated replaced this volume. To these 50-μL samples, 50 μL BAPNA solution II (containing BAPNA substrate) was added; controls lacking BAPNA substrate contained 50 μL BAPNA solution I (containing no BAPNA substrate). Tryptase activity was detected spectrophotometrically in a Synergy 2 plate reader (Biotek, Winooski, VT, USA) by measuring the colorimetric cleavage product p-nitroaniline (pNA) at 410 nm. The plate was read immediately (t = 0), as well as periodically, up to 72 h (Lavens *et al*., 1993). During incubation at 37 °C/5% CO_2, the plate was tightly sealed with parafilm, and the plate lid was weighted down by a lead ring; these methods, along with glycerol, aided in preventing sample loss over the 72-h time period.

4.4.3 Cell culture

RBL culture methods were those of (Hutchinson *et al*., 2011) and NIH-3T3 mouse fibroblast culture methods were those of (Weatherly *et al*., 2016).

4.4.4 Stimulation of RBL-2H3 cells induced via IgE-receptor crosslinking by antigen or Ca^{2+} ionophore

Cells were stimulated with either DNP-BSA multivalent antigen (Ag) (following IgE sensitization) or A23187 Ca^{2+} ionophore, essentially as described (Weatherly *et al*., 2013) except that mT-BSA buffer was used in place of BT buffer. DMSO (0.004% final) was also used in spontaneous, 0.2% TX, and background wells to control for vehicle effects.

Following cell stimulation for 1h at 37°C, resulting β-hex or tryptase released into cell supernatant was quantified as described in (Weatherly *et al*., 2013) or tryptase assay described in "RBL-2H3 cell degranulation assay for tryptase release, measured by BAPNA substrate," below. Additionally, to test the effects of heparin on this process, 0.02% heparin was added to A23187, spontaneous, 0.2% TX, and background samples.

4.4.5 RBL-2H3 cell degranulation assay for tryptase release, measured by BAPNA substrate

Following treatment for cell stimulation described above, cell supernatant (50 μL) was transferred to a 96-well half-area plate (Grenier Bio-One, Monroe, NC, USA) that contained 50 μL of BAPNA solution II. The absorbance of the colorimetric cleavage product pNA was detected over a 72-h period as with the purified tryptase experiments.

4.4.6 RBL-2H3 cell degranulation assay for tryptase release, measured by commercial kit utilizing tosyl-Gly-Pro-Lys-pNA substrate

All the reagents were prepared following manufacturer's protocol (EMD Millipore, Billerica, MA, USA) unless otherwise indicated in individual figure legends. RBL supernatant

were obtained as described in previous section. Lysates from RBL cells were obtained in 2 steps: first, RBL cells were harvested using 1X cell harvest buffer (diluted from 10X with cell culture water) and centrifuged for 8 min at 500xg. After removal of supernatant, cell pellet was washed with PBS and resuspended in 1X assay buffer. Next, the cell supernatant from the lysate was obtained as described under Syk ELISA assay in (Shim *et al*., 2016a) and incubated with tosyl-Gly-Pro-Lys-pNA substrate. For statistical analysis, first raw absorbance data from each treatment were processed by subtracting average background values (1X assay buffer with substrate) from each sample, and the background-adjusted triplicates were then averaged. These values were normalized to the unstimulated (no Ag or no ionophore) control for each experimental day when compared among supernatants. For comparison between RBL supernatant and RBL lysates, values were normalized to the RBL supernatant.

Lysates from NIH-3T3 cells were obtained in the same manner as the RBL cell lysis methods as described above. To determine total protein concentration from the RBL and NIH-3T3 cell lysates, the bicinchoninic acid (BCA) assay (Pierce BCA protein assay kit [Thermo]) was performed, following the manufacturer's protocol. Raw tryptase degranulation absorbance data obtained from lysate samples were averaged after subtracting average background values (1X assay buffer with substrate) from each sample. Background-subtracted values were then divided by the total protein concentration of that particular sample. Finally, these values were normalized to RBL lysates for each experimental day.

4.4.7 Tryptase (TPSAB1) ELISA

Tryptase ELISA kit (Cell Signaling Technologies, Beverly, MA, USA) was used to detect levels of rat (*Rattus norvegicus*) TPSAB1 protein according to the manufacturer's

instructions. For this assay, RBL-2H3 were cultured in 6-well plates, stimulated and lysed as described under Syk ELISA assay in (Shim *et al*., 2016a). A volume of 300 µL of cell lysate supernatant was placed into an appropriate ELISA well in duplicates per treatment. The remaining steps were carried out according to the manufacturer's directions.

4.4.8 RNA extraction and cDNA synthesis from RBL-2H3 cells

Total RNA was isolated from RBL-2H3 cells using Trizol® reagent (Life Technologies, Grand Island, NY, USA) following the manufacturer's instructions. The concentration and purity of the total RNA were determined by Nanodrop-1000 UV-Vis spectrometer (Thermo Scientific, Rockford, IL, USA). Total RNA (10 µg per sample) was treated with TURBO DNA-free kit (Ambion, Grand Island, NY, USA) to remove any contaminating genomic DNA. The RNA preparation was reverse-transcribed to cDNA using an iScript cDNA synthesis kit (Bio-Rad, Hercules, CA, USA) according to the manufacturer's protocol.

4.4.9 Genomic DNA extraction from RBL-2H3 cells

DNeasy Blood & Tissue Kit (Qiagen, Valencia, CA, USA) was used for genomic DNA extraction from RBL-2H3 cells by following the manufacturer's instructions. The concentration of genomic DNA was measured using Nanodrop-1000 UV-Vis spectrometer (Thermo scientific, Rockford, IL, USA).

4.4.10 Polymerase chain reaction (PCR) for rat tryptase genes

Primers for each *Rattus norvegicus* tryptase genes were inferred from NCBI (http://www.ncbi.nlm.nih.gov). Primers were designed using NCBI Primer Blast (http://www.ncbi.nlm.nih.gov/tools/primer-blast) and IDT Oligoanalyzer software

(https://www.idtdna.com/analyzer/Applications/OligoAnalyzer), and synthesized by Integrated DNA Technologies (Coralville, Iowa, USA). Sequences for PCR primer pairs, annealing temperatures, and size of the transcripts for tryptase genes are shown in Fig 4.6C and Fig 4.7B.

PCR was carried out in a 50uL reaction volume, utilizing 100ng of the cDNA or genomic DNA as a template and 0.4 μM of each primer. The amplicons were generated using a Phusion High-Fidelity DNA polymerase from New England Biolabs (Ipswich, MA, USA) and following PCR conditions: initial one cycle of 98°C for 30sec, then 35 cycles of 98°C for 10sec, 51.5-58.5C (depending on the genes) for 30sec, and 72°C for 30sec and followed by one cycle of a final 72°C extension for 5 min. A mock PCR, in which the DNA template was excluded, was also performed as a negative control. Amplification of rat β-actin, rat β-hexosaminidase A and B genes were used as positive controls.

For gel electrophoresis, Seakeam LE agarose (Cambrex, Rockland, ME, USA) and 1Kb plus DNA ladder (Life Technologies, Grand Island, NY, USA) were purchased. The PCR products were analyzed in a 1% agarose gel and stained with 0.5 μg/mL of ethidium bromide (Sigma, St Louis, MO, USA).

4.4.11 Sequencing analyses

To confirm the identity of amplified sequences, the PCR products were separated in a 1% agarose gel to extract the single specific band, which was subsequently purified using a Qiaquick Gel extraction kit (Qiagen, Valencia, CA, USA). Each purified product was then sequenced at the University of Maine Sequencing facility using an ABI 3730 DNA sequencer (Applied Biosystems, Foster City CA, USA). The obtained DNA sequences were confirmed by NCBI

BLAST search (http://blast.ncbi.nlm.nih.gov/Blast.cgi) and ClustalW2 alignment program (http://www.ebi.ac.uk/Tools/msa/clustalw2).

4.4.12 Statistical analysis

Unless otherwise indicated in individual figures, results from degranulation experiments are reported as mean ± SEM, with significant differences determined by either a One-Way ANOVA (Analysis of Variance) followed by Tukey's *post-hoc* test or One-sample t-test, using Graphpad Prism software (San Diego, CA, USA).

4.5 Results

4.5.1 The tryptase activity assay is optimized to detect as low as 1 ng of purified human lung tryptase using BAPNA (Nα-Benzoyl-D, L-Arg-*p*-nitroanilide) substrate.

Eight rat tryptase or tryptase-like genes were found in the rat genome database (RGD: http://rgd.mcw.edu) and were compared to their human orthologs (HGNC: http://www.genenames.org) (Table 4.1).

Before testing RBL-2H3 mast cells, we optimized the tryptase assay in cell-free system, based on the protocol developed by Lavens *et al*. (Lavens *et al*., 1993), which is able to detect tryptase by measuring the cleavage product (*p*-nitroanilide [pNA]) of a known tryptase substrate BAPNA and purified human lung tryptase. The purified human lung tryptase that was utilized contains three tryptase species: TPSAB1, TPSB2 and TPSD1.

When various doses of purified tryptase (0-500ng) were incubated with BAPNA and absorbance at 410 nm was read in a plate reader, detection of pNA plateaued within 72 hours (Fig. 4.1A). Following optimization of both timing (Fig. 4.1A; including modifying assay

parameters to minimize sample loss) and of buffer components (pH, heparin concentration, levels of Ca^{2+} and Na^{+}, addition of heparin and bovine serum albumin, etc), we successfully detected pNA production from as little as 1ng of purified tryptase tested (Fig. 4.1B). Previously, the lowest level of pNA detected by Lavens *et al.* was 10ng (Lavens *et al*., 1993).

Table 4.1. Tryptase and tryptase-like proteins in rats and human

Rat Gene Symbols	Alternative Names	Human Orthologs
Tpsab1	Mast cell protease-7; Tryptase βI; Tryptase α/β1;Skin tryptase	TPSAB1
Tpsb2	Mast cell protease-6; Tryptase-β2; Tryptase-2	TPSB2
Tpsg1	Transmembrane tryptase; Tryptase γ1	TPSG1
Gzmk	Granzyme K; Natural Killer (NK)-tryptase-2	GZMK
Prss29	Serine protease 29; tryptase δI	PRSS29P/ TPSD1
Prss41	Serine protease 41; testis serine protease 1	PRSS41
Gzma	Granzyme A	GZMA
Prss34	Mastin; Serine Protease 34	-

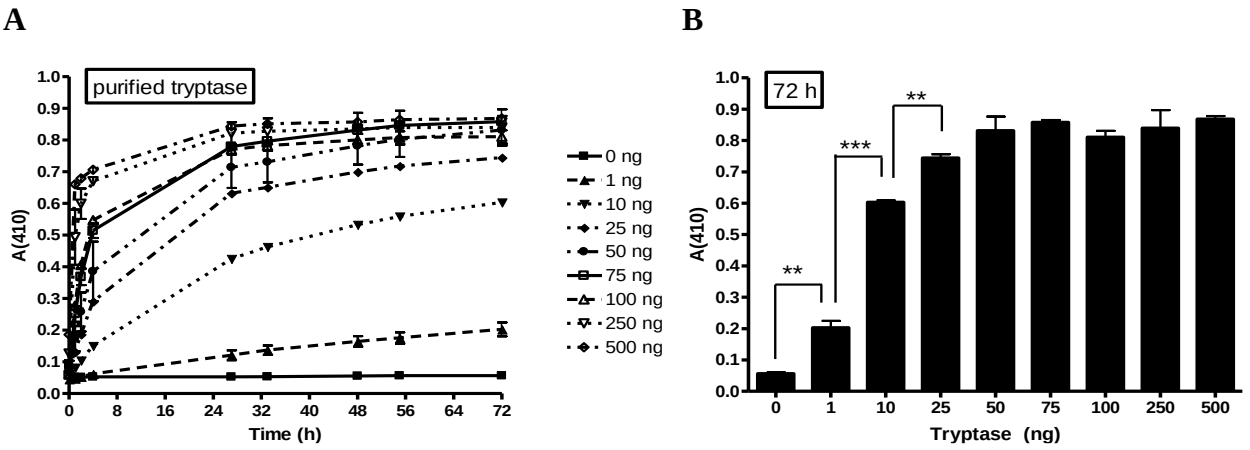

Figure 4.1. **Measurement of interaction of purified human lung tryptase (TPSAB1/TPSB2/TPSD1) with N-benzoyl-DL-arginine-p-nitroanilide (BAPNA) substrate**. (A) As described in Materials & Methods, purified tryptase was incubated at the concentrations indicated over 72 hours with BAPNA. A_{410} is plotted against the time in h. In (B) tryptase concentration is detected at a single, 72-h time point; tryptase (ng) is depicted versus the pNA signal. Statistical significance was determined GraphPad Prism using a one-way ANOVA followed by a Tukey's post test; ***p<0.001, **p<0.01.

4.5.2 Tryptase is not detectable in the supernatant from degranulated RBL-2H3 mast cells, using BAPNA substrate.

Following our purified tryptase experiments, our next goal was to detect tryptase released from a mast cell model line RBL-2H3 using the same tryptase substrate, BAPNA, incubated for a period of 72 h. Because the plan was to stimulate RBL-2H3 to degranulate for one hour with Ca^{2+} ionophore A23187 and to collect the cell supernatants to test for the presence of tryptase by measuring pNA production, we first tested the conditions of a modified Tyrodes buffer with no BSA on A23187 ionophore dose response degranulation curve in RBL-2H3. We monitored the release of β-hexosaminidase from these cells using 4-MU (4-methylumbelliferone) substrate.

As seen in Fig. 4.2A, we detected robust increases in β-hexosaminidase released from RBL-2H3 due to ionophore stimulation. Then we used the same exact conditions for stimulating RBL-2H3 to degranulate, with the exception that now we assayed the cell supernatant for tryptase activity (pNA) using BAPNA substrate.

Surprisingly, we were unable to detect any significant release of tryptase from RBL-2H3 cells (Fig. 4.2B). Importantly, we performed control studies in which 25 ng purified tryptase was incubated with BAPNA in a background of various reagents used in the degranulation assay (A23187 ionophore, DMSO [ionophore vehicle], TX, and BSA), and found that these variables do not significantly affect the ability of purified tryptase to cleave BAPNA substrate (Fig.C1).

Taken together, these data indicate that RBL-2H3 cells likely do not release active tryptase protein that is able to cleave the BAPNA substrate.

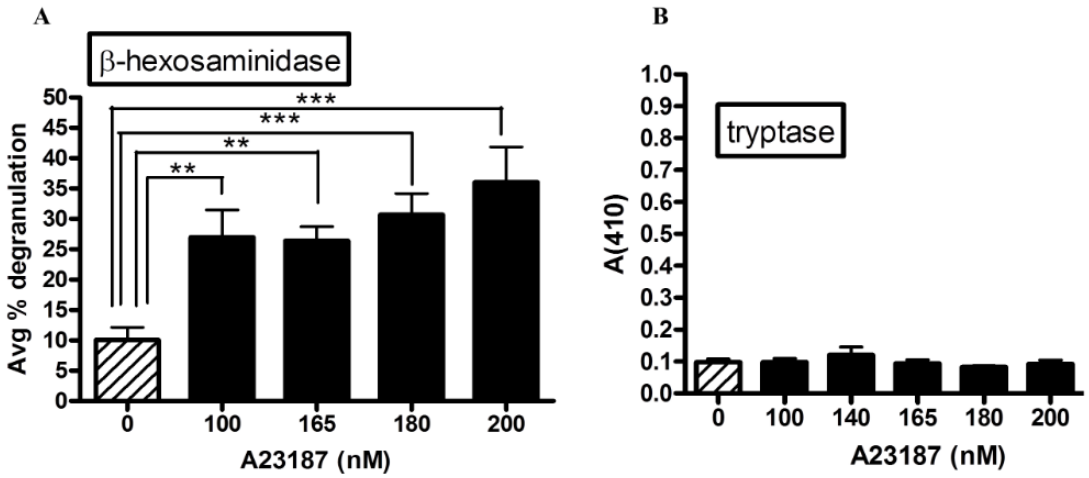

Figure 4.2. Measurement of β-hexosaminidase and tryptase in the supernatant of RBL-2H3 mast cells stimulated with calcium ionophore A23187. RBL-2H3 cells were incubated for one hour with A23187 ionophore in modified Tyrodes buffer, and degranulation was quantified after incubation with (A) 4-Methylumbelliferone (4MU) substrate for β-hexosaminidase or with (B) BAPNA substrate for tryptase. Data are from one representative experiment; values represent means ± SD of triplicate samples. Statistical significance was determined by one-way ANOVA followed by Tukey's post test.

4.5.3 Tryptase is not detectable in the supernatants from degranulated RBL-2H3 mast cells, using tosyl-Gly-Pro-Lys-pNA substrate.

After observing no tryptase detection from degranulated RBL cells using the BAPNA tryptase substrate, we utilized the commercially available tryptase degranulation kit from EMD Millipore, which contains another known tryptase substrate: tosyl-Gly-Pro-Lys-pNA, instead of BAPNA. First, a high dose of antigen (1μg/mL) in modified Tyrodes buffer (following IgE sensitization) was applied for RBL cell stimulation, but no tryptase was detected from the supernatants of stimulated RBL cells (Fig. 4.3A). Then we examined the release of tryptase after stimulating RBL cells with 1μg/mL antigen in the proprietary assay buffer which was provided in the kit, and, again, no tryptase was detected (Fig. 4.3B). Lastly, we stimulated RBL cells with A23187 ionophore, strictly following the manufacturer's protocol provided by EMD Millipore,

and measured the production of pNA from the cell supernatant. There was no significant difference compared to unstimulated control cells in this condition, either (Fig. 4.3C).

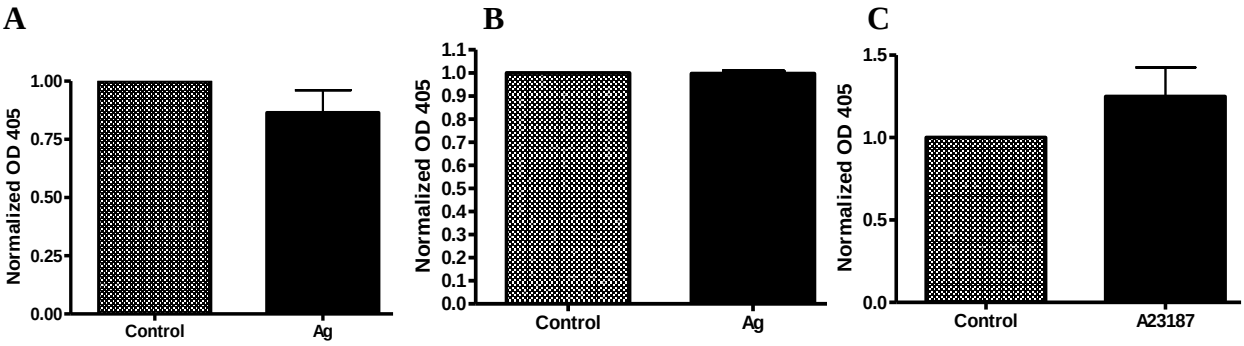

Figure 4.3. Measurement of tryptase in the supernatant of RBL-2H3 mast cells stimulated with antigen or A23187 ionophore using tosyl-gly-pro-lys-pNA tryptase substrate. RBL-2H3 cells were sensitized for one hour with 0.1μg mL^{-1}anti-DNP mouse IgE in RBL media (A and B). In (A), plated cells were treated with DNP-BSA Ag (1μg mL^{-1}) for 15 minutes in modified Tyrodes buffer. In (B), cells in suspension were treated with DNP-BSA Ag (1μg mL^{-1}) treatment for 1 hour in 1X Assay buffer provided in the Mast cell degranulation assay kit (EMD Millipore). In (C), cells in suspension were stimulated with 200nM A23187 ionophore for 1 hour. Degranulation was quantified with tosyl-gly-pro-lys-pNA tryptase substrate provided by the Mast cell degranulation assay kit (EMD Milipore). Error bars represent the standard error of the mean of the data from three experiments; triplicates per sample were done on each experimental day. No statistical significance was determined by one-sample t-tests.

4.5.4 Lysates from RBL-2H3 mast cells and from NIH-3T3 fibroblast cells contain a substance that can cleave the tosyl- Gly-Pro-Lys-pNA substrate.

Since tryptase release from RBL cells was not detectable using either of those tryptase substrates, we next tested RBL cell lysates. Compared to the signal from RBL cell supernatant, lysates from RBL cells displayed significantly higher readings when incubated with tosyl-Gly-Pro-Lys-pNA substrate (Fig. 4.4A). To test whether the signals obtained from the RBL lysates were due to the presence of tryptase, we also examined NIH-3T3 cell lysates because NIH-3T3 cells are non-granulated fibroblasts which do not contain mast cell markers. We found that there was no significant difference between NIH-3T3 lysates and RBL-2H3 lysates (Fig. 4.4B).

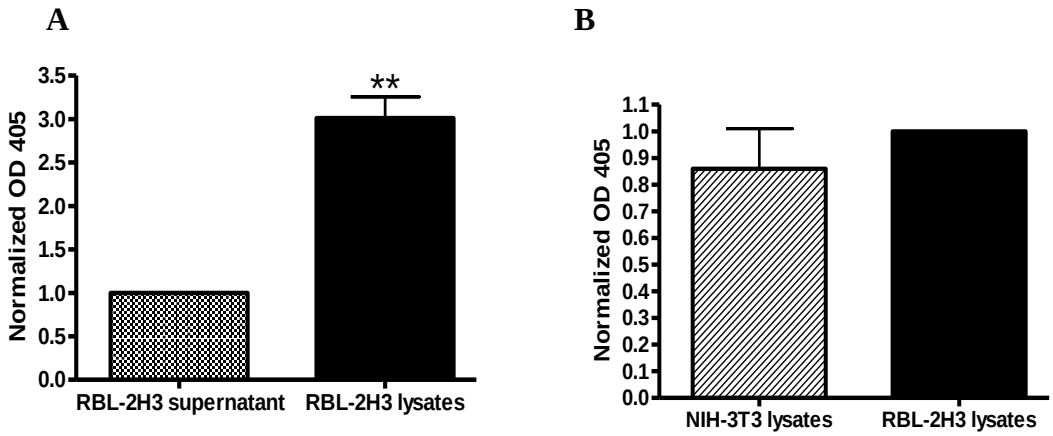

Figure 4.4. Measurement of tryptase from RBL-2H3 and NIH-3T3 cell lysates using tosyl-gly-pro-lys-pNA tryptase substrate. Lysates from RBL-2H3 cells (A) and NIH-3T3 cells (B) were collected as described in Materials & Methods and incubated with tosyl-gly-pro-lys-pNA tryptase substrate for 72 hours. Error bars represent the standard error of the mean of the data from three experiments; triplicates per sample were done on each experimental day. (A) Statistical significance, as compared to the RBL supernatant sample, was determined by one-sample t-tests. ***p<0.01* (B) No statistical significance was determined in comparing RBL-2H3 and NIH-3T3 lysates samples by one-sample t-test.

4.5.5 Tryptase is not detectable in the supernatants from degranulated RBL-2H3 mast cells, using rat TPSAB1 ELISA.

Using two different tryptase substrates, BAPNA (Fig. 4.2) and tosyl- Gly-Pro-Lys-pNA (Fig. 4.3), no active tryptase protein (capable of cleaving either of these substrates) was detected in the supernatants of degranulated RBL-2H3 mast cells. Those data suggest that no active tryptase protein is present in the RBL cells' granules. To further investigate whether degranulated RBL cell supernatants contain tryptase, regardless of protein activity level, we utilized a sandwich ELISA kit, which detects one of the key rat tryptase protein types, TPSAB1. This ELISA kit detects as little as 0.3 ng/mL tryptase (as shown in a standard curve generated using purified rat TPSAB1 protein [provided in the kit], Fig. C2). Again, no tryptase was detected in the supernatants of Ag-stimulated, degranulated RBL cells (compare "RBL control supernatant" to "RBL Ag supernatant" in Fig. 4.5), another indication that tryptase is not present in the granules of RBL cells. However, the phenomenon of apparent tryptase signal found in

RBL lysates, as in Fig. 4, was also found in RBL lysates via this ELISA measurement (Fig. 4.5). Again, though, the TPSAB1 ELISA signal from RBL lysates was equivalent to the ELISA signal arising from NIH-3T3 cell lysates (Fig. 4.5). Thus, the apparent TPSAB1 signal in RBL cell lysates is not a granule-associated protein.

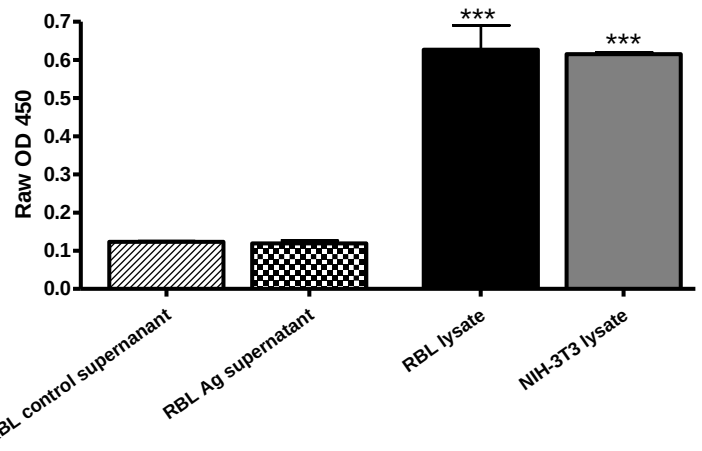

Figure 4.5. **Measurement of Tpsab1 tryptase from RBL and NIH cells by ELISA**. RBL-2H3 cells were sensitized with anti-DNP IgE (0.1μg mL^{-1}) for 1 hr before being treated with DNP-BSA Ag (1μg mL^{-1}) for 15 min. Rat tryptase protein (Tpsab1) was measured using a sandwich ELISA kit (Biomatik). Data are from one representative experiment; values represent means ± SD of duplicate samples. Statistical significance was determined as compared to the RBL control supernatant sample, by one-way ANOVA followed by Tukey's post test. ****p<0.001*

4.5.6 No rat tryptase mRNA was detected in RBL-2H3 cells using PCR.

Because three distinct methods of tryptase protein detection (Figs. 4.2, 4.3, and 4.5) failed to find tryptase protein released from degranulated RBL cells, we next used PCR to investigate whether tryptase mRNA transcripts are present in RBL cells. To generate cDNA template, total RNA was extracted from antigen-stimulated RBL-2H3 cells and was reverse-transcribed. Numerous cell treatment experimental conditions prior to the RNA extraction are listed in supplementary material Table C1, including several variations of IgE sensitization, antigen stimulation, and timeframe conditions. Primer pairs and the size of amplicons for eight

rat tryptase genes are shown in Fig. 4.6C. In addition, mRNA of two rat β-hexosaminidase genes (*Hexa* and *Hexb*) and of β-actin (*Actb*) were amplified as positive controls.

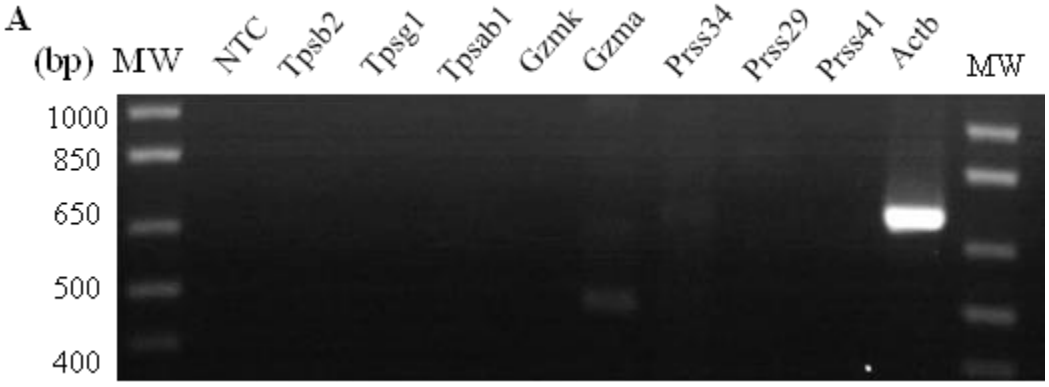

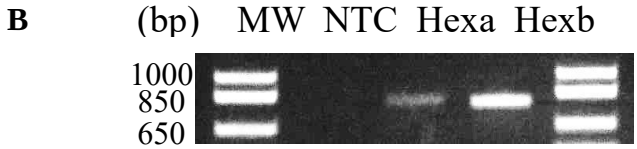

C

Gene symbols	Forward Primer	Reverse Primer	Annealing Temp (°C)	Product size (bp)
Tpsb2	5'-GTGTGGGACTGCACATCAAAAGC-3'	5'-ACATAGCGGTGAATCCAGTCCAGG-3'	58.5	589
Tpsg1	5'-CCACTGCTTCTCTGGGTCTGTGAACTC-3'	5'-CACCTCAGTCAGAACTCCAAGGCTG-3'	58.5	738
Tpsab1	5'-GAGAAGATCAAAGACAGCTGAGG-3'	5'-GAAGCTGTACCCTGAGCTTG-3'	55	480
Gzmk	5'-CAGTACCGCGGCAAGCATATTTGT-3'	5'-CAGAGTCACCCTTGCAGGAATCC-3'	58.5	494
Gzma	5'-GCTAATTCCTGAAGGTGGCTG-3'	5'-ACGGAGGTTTCCGGCACAAA-3'	56	547
Prss34	5'-CACTGTGTAGAGCTGAAAGAGATGGAG-3'	5'-CTGGGCTGGAAGAAGGAGTG-3'	55	703
Prss29	5'-TCAAGCCAGTCAAGCTGTCC-3'	5'-GAATGGTGACCAAAGCCGAC-3'	55	477
Prss41	5'-GCCCTATCACCTCCGAGAAGTAC -3'	5'-AGCTTGGGGAAGCAGGACATC-3'	56	482
Actb	5'-GACCCAGATCATGTTTGAGA-3'	5'-GCTTGCTGATCCACATCTGC-3'	55	772
Hexa	5'-CTACCGTAGCCTGCTCTTCG-3'	5'-ATGAAGGCCTGGATGTTGGG-3'	54.5	816
Hexb	5'-GTTTAACGTCCTTCACTGGC-3'	5'-GCATCCACATATTCTCCCCA-3'	51.5	795

Figure 4.6. Measurement of rat tryptase and β-hexosaminidase mRNA from RBL-2H3 cells using PCR. Eight target rat tryptase genes' mRNA (A) and two β-hexosaminidase genes' mRNA (B) were analyzed. Total RNA was extracted from RBL-2H3 cells, and reverse transcription was performed as described in Materials & Methods in order to generate cDNA, which was amplified by PCR. Actin was used as a positive control. The primer pairs and the size of PCR products are listed in the table (C). The PCR amplicons were subjected to electrophoresis in 1% agarose gels, and the target bands were extracted for sequencing to be confirmed (data not shown). Data shown are representative of all cell stimulation conditions and timeframes (supplement table S1). None of tryptase genes' mRNA was found in any of the stimulation conditions whereas actin and β-hexosaminidase genes' mRNA were always detected. NTC is no template control; MW is molecular weight marker.

In fifteen separate testing conditions, from unstimulated controls to cells treated with high Ag doses to various RNA collection timepoints up to 24 hours post Ag stimulation, none of the eight tested tryptase genes' mRNA was detected by PCR (Fig. 4.6A). This lack of tryptase transcript detection stands in contrast to consistent robust detection of actin transcripts (Fig. 4. 6A) and of both β-hexosaminidase mRNAs (Fig. 4.6B), over all fifteen cell-treatment conditions listed in Table C1. Therefore, these findings show that no tryptase genes are expressed in RBL-2H3 cells.

4.5.7 Genomic DNA of all rat tryptase genes was detected using PCR, in RBL-2H3 cells.

A

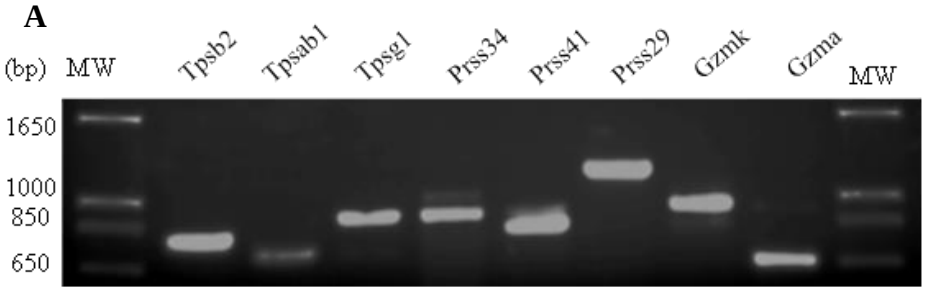

B

Gene symbols	Forward Primer	Reverse Primer	Annealing Temp (°C)	Product size (bp)
Tpsb2	5'-CGTGTACAGCTTCGTGAGCAGTATC-3'	5'-ACATAGCGGTGAATCCAGTCCAGG-3'	57	771
Tpsab1	5'-GAGAAGATCAAAGACAGCTGAGG-3'	5'-GAAGCTGTACCCTGAGCTTG-3'	53	703
Tpsg1	5'-GTGACAGGCTGGGGCTATACACA-3'	5'-CACCTCAGTCAGAACTCCAAGGCTG-3'	57	890
Prss34	5'-AAGAGATGGAGGCCAGTTGC-3'	5'-CTGGGCTGGAAGAAGGAGTG-3'	54.6	877
Prss41	5'-GCCCTATCACCTCCGAGAAGTAC-3'	5'-AGCTTGGGGAAGCAGGACATC-3'	56	819
Prss29	5'-TCAAGCCAGTCAAGCTGTCC-3'	5'-GAATGGTGACCAAAGCCGAC-3'	54	1154
Gzmk	5'-AGGCCAAAAGGATTCCTGCAAG-3'	5'-GATCAAAGGACCACCAGAGTC-3'	54.6	943
Gzma	5'-CCCTTCCACTGGTGCTCTTA-3'	5'-GGGTCTCCTGTCTCAACCAA-3'	56	649

Figure 4.7. **Measurement of rat tryptase genomic extracted from RBL-2H3 cells using PCR.** A) Eight target tryptase genes' genomic DNA were amplified by PCR as described in Materials & Methods. The primer pairs and the size of PCR products are listed in the table (B). PCR amplicons were subjected to electrophoresis in 1% agarose, and the target bands were extracted for sequencing confirmation (data not shown). MW is molecular weight marker.

Because none of the tryptase genes' mRNA was detected, we next questioned whether tryptase genomic DNA is present in this cell line. To determine whether these eight tryptase genes exist in the RBL genome, we extracted genomic DNA from RBL-2H3 cells and amplified with the gene-specific primer pairs shown in Fig. 4.7B. Genomic DNA from all eight tryptase genes was detected by PCR (Fig. 4.7A), and each band was excised, cleaned, sequenced, and confirmed as the correct gene (sequence data not shown). Overall, our results suggest that RBL-2H3 cells do not transcribe and translate tryptase genes even though all tryptase genes exist in the genomic DNA of RBL-2H3 cells.

4.6 Discussion

In this study, we optimized an assay, based upon cleavage of BAPNA substrate, for detection of as little as 1 ng active tryptase per sample. While this assay is 10-fold more sensitive than the BAPNA-based method published by Lavens *et al*. (which could pick up ≥10 ng tryptase) (Lavens *et al*., 1993), we were unable to find any tryptase released from stimulated, degranulated RBL-2H3 cells. In this assay, ~100,000 RBL-2H3 cells per well of a 96-well plate were stimulated under conditions causing robust degranulation and β-hex release, and one-quarter of the resulting cell supernatant (50 μL out of 200 μL supernatant in each well; equivalent to the contents released from ~25,000 RBL-2H3 cells) was incubated with BAPNA substrate.

According to Lavens *et al*. (1993), human lung mast cells contain 11.2 ± 0.7 pg tryptase per cell, so, if RBL-2H3 cells contained similar tryptase levels, we would expect ~280 ng tryptase per sample from fully-degranulated cells or perhaps 28 ng tryptase per sample from modestly-degranulated cells—levels far above the assay's sensitivity, 1 ng. Therefore, our results with the BAPNA substrate suggest that RBL-2H3 cells contain very little or no active tryptase

protein. Additional studies with an alternative tryptase substrate, tosyl-Gly-Pro-Lys-pNA, and with ELISA assays for TPSAB1 protein also revealed a lack of tryptase protein released from RBL-2H3 cells stimulated via multiple means.

Thus, we also investigated whether tryptase mRNA transcripts are found in RBL-2H3 cells. We found none of the mRNA transcripts of the rat tryptase genes (*Tpsb2, Tpsab1, Tpsg1, Prss34, Gzmk, Gzma, Prss29, Prss41*) in RBL-2H3 cells, whereas genomic DNA of all the tryptase genes was readily detected by PCR. Since these genes were found in genomic DNA, we looked for tryptase gene expression following a wide range of RBL-2H3 stimulation conditions, from 1 to 24 hours post antigen stimulation (Table C1), but no mRNA transcripts were found under any condition. The reason for testing at varied time points is that mast cells undergo recovery and regeneration/refilling of the granules after degranulation (Dvorak *et al*., 1986; Dvorak *et al*., 1988), so we had hypothesized that tryptase gene expression may fluctuate over time, before and after degranulation. Also, we performed clonogenic cytotoxicity assays and found that RBL-2H3 cells survive post-degranulation (data not shown), a necessary control for Table C1 experiments. We did find that mRNA levels of another MC granule component, β-hexosaminidase (both forms A and B), are constitutively robust in RBL-2H3 cells, regardless of time point or stimulation method: further evidence that, if any of these eight tryptase genes were expressed in RBL-2H3 cells, we would have been able to find its transcript in at least one of the sixteen cell stimulation conditions tested.

There were occasional, faint bands in gels assessing mRNA expression of tryptase genes (Fig. 4.6A), though these were not the correct product sizes of the expected tryptases (Fig. 4.6C). For example, from one gel, a faint band was excised from the Prss34 lane, purified, sequenced, and determined to be not tryptase but, rather, carboxypeptidase A3 (data not shown). The

nucleotide sequence homology between rat Prss34 and carboxypeptidase A3 is significant, so, most likely, the primers used for Prss34 accidentally amplified a small amount of this off-target gene after multiple rounds of PCR. Another time, a faint band from the Tpsab1 lane was sequenced and found to correspond to a histone deacetylase. Attempts to isolate and sequence a faint band, positioned below the expected *Gzma* size, from the *Gzma* lane were unsuccessful, likely because there was very little material present. Also, other researchers reported a lack of *Gzma* mRNA in RBL-2H3 cells (Nakajima *et al*., 1995). Overall, no tryptase mRNA was detected for any of the eight tested tryptase genes.

Other researchers have previously reported a lack of certain tryptases in RBLs. Similar to our Fig. 4.2 results, two other studies also observed a lack of tryptase via BAPNA assay in supernatants of degranulated RBL cells, even while β-hex release was readily measured in the same supernatants (Peng *et al*., 2011; Tang *et al*., 2012). Mass spectrometry analyses of cell supernatants from degranulated RBL-2H3s also found no tryptase proteins (Sadroddiny *et al*., 2012a; Sadroddiny *et al*., 2012b). Furthermore, Ide *et al.* reported that no mRNA of *Tpsb2* (noted as rMCT [rat mast cell tryptase] in the article) was located in RBL-2H3 cells (Ide *et al*., 1995). However, one publication did report high levels of tryptase (as measured by BAPNA reaction) released into the supernatants of unstimulated RBL-2H3 cells, with further increases due to hypoxia (Maxova *et al.*, 2010). This result is puzzling because, typically, very low levels of spontaneous degranulation occur in unstimulated (no antigen, no ionophore, etc) RBL-2H3 cells.

Two additional studies have reported detection of tryptase in RBL-2H3 cells (Small-Howard and Turner, 2005; Song *et al*., 2016). However, these two studies measured tryptase (via ELISA in Song *et al.* and via substrate activity assay in Small-Howard and Turner) within cell lysates, not

from the supernatants of stimulated intact cells. Since our current study demonstrated that lysates from both RBL-2H3 and NIH-3T3 cells processed tosyl-Gly-Pro-Lys-pNA substrate (Fig. 4.4) and yielded tryptase ELISA absorbance (Fig. 4.5), these signals are likely not from MC granule tryptases. Rather, other, non-granule-associated serine proteases may be picked up by these two studies and in Figs.4.4 and 4.5. For example, retinoid-inducible serine carboxypeptidase 1 (also known as carboxypeptidase C) is found in RBL-2H3 cells (Sadroddiny *et al*., 2012a). Also, the substrate tosyl-Gly-Pro-Lys-pNA can be cleaved by enzymes other than tryptase, including plasmin/plasminogen (Wiedow *et al*., 1997; Vakili *et al*., 2001; Drinane *et al*., 2006). The key mast cell function is release of granule contents from safe storage in intracellular granules, into extracellular fluids, via plasma membrane fusion; thus, analyzing the contents of MC whole-cell lysates is an erroneous measure of MC function.

Because tryptase is known to be localized within granules and exclusively expressed in mast cells (Schwartz *et al*., 1987; da Silva *et al*., 2014), we had anticipated to find tryptase released into the supernatants of degranulated RBL-2H3 cells in this study. One possible reason for our findings is that RBL cells are physiologically similar to rodent mucosal mast cells (Seldin *et al*., 1985). MCs display a high degree of heterogeneity in contents of granules, as a consequence of their ubiquitous location and a wide range of microenvironments they encounter (da Silva *et al*., 2014). Human MCs are divided into two subsets based on protease content: MC_{TC}, containing tryptase, chymase, and carboxypeptidases, or MC_T, containing only tryptase (Irani *et al*., 1986). Rodent MCs are subcategorized into mucosal mast cells (MMCs) and connective tissue mast cells (CTMCs) (Metcalfe *et al*., 1997). While tryptase is present in all human MCs (Irani *et al*., 1986), rodent MMCs do not express tryptase but, rather, predominantly express chymase (Le Trong *et al*., 1987; Reynolds *et al*., 1990; Serafin *et al*., 1990; Huang *et*

al., 1991; Lutzelschwab *et al*., 1997). Thus, RBL-2H3 cells' similarity to MMCs might explain the lack of tryptase expression.

In summary, this current study is the first comprehensive report on detection of tryptase protein and transcripts from RBL-2H3 cells. Multiple lines of experimental evidence indicate that mRNA from eight tryptase genes is not present and that tryptase protein is either not present or is below detection limits of the assay in supernatants from degranulated RBL-2H3 cells. Instead, mast cell researchers should utilize β-hex, histamine, serotonin, or other reliable markers for RBL-2H3 degranulation studies. Comparative studies of toxicant effects on RBL-2H3 mast cells *in vitro* and in zebrafish *in vivo* will require use of a degranulation reporter different from tryptase.

CHAPTER 5

TRICLOSAN IS A MITOCHONDRIAL UNCOUPLER IN LIVE ZEBRAFISH

5.1 Abstract

Triclosan (TCS) is a synthetic antimicrobial agent used in many consumer goods at millimolar concentrations. As a result of exposure, TCS has been detected widely in humans. We have recently discovered that TCS is a proton ionophore mitochondrial uncoupler in multiple types of living cells. Here we present novel data indicating that TCS is also a mitochondrial uncoupler in a living organism: 24 hour post fertilization zebrafish embryos. These experiments were conducted using a Seahorse Bioscience XF^e 96 Extracellular Flux Analyzer modified for bidirectional temperature control, using the XF96 spheroid plate to position and measure one zebrafish embryo per well. Using this method, following acute exposure to TCS, basal oxygen consumption rate (OCR) increases, without a decrease in survival or heartbeat rate. TCS also decreases ATP-linked respiration and spare respiratory capacity and increases proton leak: all indicators of mitochondrial uncoupling. Our data indicate, that TCS is a mitochondrial uncoupler *in vivo*, which should be taken into consideration when assessing the toxicity and/or pharmaceutical uses of TCS. This is the first example of usage of a Seahorse Extracellular Flux Analyzer to measure bioenergetic flux of a single zebrafish embryo per well in a 96 well assay format. The method developed in this study provides a high-throughput tool to identify previously-unknown mitochondrial uncouplers in a living organism.

5.2 Short Abstract

Antimicrobial agent triclosan (TCS) is a mitochondrial uncoupler in multiple cell types. Here we present data, obtained with a Seahorse Bioscience XF^e 96 Extracellular Flux Analyzer,

indicating that TCS is also a mitochondrial uncoupler in living zebrafish (24 hpf; 1 embryo/well). TCS increases oxygen consumption rate and proton leak and decreases ATP-linked respiration and spare respiratory capacity without affecting survival or heartbeat rate. These data indicate, for the first time, that TCS is a mitochondrial uncoupler *in vivo*.

5.3 Introduction

Triclosan (5-chloro-2-(2,4-dichlorophenoxy)phenol; TCS) is a synthetic antimicrobial agent (Lyman and Furia, 1968) that has been used in hospitals since the 1970's. TCS can be found in soaps, deodorants, mouthwashes, toothpastes, household cleaners, and more products typically at concentrations up to several mM (Jones *et al*., 2000; Rodricks *et al*., 2010). Most U.S. citizens are exposed to triclosan (Calafat *et al*., 2008). Chronic exposure of zebrafish embryo/larvae to TCS has been found to cause delayed development, malformations, delayed hatching and inhibition of growth (Oliveira *et al*., 2009).

Recently, it has been published that TCS is a proton ionophore mitochondrial uncoupler in living rat (RBL-2H3) and human (HMC-1) mast cells, mouse fibroblasts (NIH-3T3), and primary human keratinocytes (Weatherly *et al*., 2016). Without cytotoxicity, TCS reduces ATP production and increases oxygen consumption rate (OCR), while its non-protonated sister compound TCS-methyl causes no such effects (Weatherly *et al*., 2016). Triclosan has also been shown to impair mitochondrial function in isolated rat liver mitochondria (Newton *et al*., 2005; Ajao *et al*., 2015). Additionally, *in vitro* studies suggest that TCS inhibits mitochondrial membrane potential (Attene-Ramos *et al*., 2015), an indicator of proton ionophore mitochondrial uncoupling (Suzuki *et al*., 2006; Kuznetsov *et al*., 2011).

In the present study, we investigate whether TCS is a mitochondrial uncoupler in an intact living organism, the 24 hour post fertilization (hpf) zebrafish embryo. Carbonyl cyanide *p*-triflouromethoxyphenylhydrazone (FCCP) is an ionophore proton ion carrier which disrupts ATP synthesis by transporting hydrogen ions across the inner mitochondrial membrane, thus bypassing the proton channel of ATP synthase (Heytler and Prichard, 1962). In this study, we utilized FCCP, a known mitochondrial uncoupler, as a reference compound to compare the effects of TCS on mitochondrial fidelity. This study is the first demonstration of TCS's mitochondrial effects *in vivo*, and our results indicate that the previous *in vitro* findings are valid.

Recently, Seahorse Bioscience XF-24 Extracellular Flux Analyzers have been used successfully to assess the bioenergetics of zebrafish (Stackley *et al*., 2011; Gibert *et al*., 2013; Bestman *et al*., 2015). One of the studies measured OCR and bioenergetics of zebrafish from 3 to 48 hpf (Stackley *et al*., 2011). They also validated the XF^e 24 measurements with the Clark electrode method (Stackley *et al*., 2011). Another XF-24 study analyzed the bioenergetics effects of the known mitochondrial uncoupler 2,4-dinitrophenol (DNP) on 3-72 hpf zebrafish (Bestman *et al.*, 2015). However, these published studies have utilized relatively low-throughput 24-well plates, time-consuming placement of islet capture screens, and multiple fish per well (required to attain suitable signal-to-noise ratios). The present study is the first instance of using chorionated zebrafish in a custom-modified Seahorse Bioscience XF^e 96 Extracellular Flux Analyzer, which allows temperature-controlled, high-throughput (96-well) bioenergetic measurements with a single embryo per well, without a need of an islet capture screen.

5.4 Materials and Methods

5.4.1 Animals and Ethics Statement

The fertilized eggs of wild-type zebrafish (*Danio rerio,* AB strain) were obtained from the Zebrafish Facility at the University of Maine by natural crosses. Embryos were maintained in egg water (60µg/mL Instant Ocean sea salts [Aquarium Systems, Mentor, OH, USA]) at 28 ºC with a 14/10 hr light/dark cycle. All experiments were performed with 24 hpf zebrafish, which remain in the chorion at this stage. Animal studies were approved by the Institutional Animal Care and Use Committee (IACUC) at the University of Maine and performed in accordance with the defined guidelines for use of zebrafish embryos.

5.4.2 TCS preparation

Triclosan (TCS) was purchased from Sigma-Aldrich (St. Louis, MO, USA) ("irgasan," ≥97% by HPLC; CAS no. 3380-34-5). A starting TCS stock (22.5 or 45 µM) was freshly prepared for each experimental day by dissolving TCS in egg water, without use of organic solvents, following our published protocol (Weatherly *et al*., 2013). TCS concentration was determined by UV-Vis spectrophotometry (Weatherly *et al*., 2013).

5.4.3 Mitochondrial oxygen consumption assay

A modified XF^e 96 Extracellular Flux Analyzer (Seahorse Bioscience, North Billerica, MA, USA; details of the commercially-available instrument are found at http://www.seahorsebio.com/products/how-xf-works.php) was used to measure oxygen consumption rate (OCR). Three modifications of published methods were used for this study: 1.) instrument re-configuration to allow for bi-directional temperature control; 2.) use of chorionated

zebrafish embryos to obviate the need for islet capture screens; and 3.) the use of one embryo per well rather than the two or more embryos required per well in previous studies. A novel modification of this instrument was made to allow for bi-directional temperature control, in order to allow temperature stabilization at the moderate levels (28-29ºC) favored by zebrafish. Prior to each run, calibration was performed using XF Calibrant solution (200 µL per well) (Seahorse Bioscience) in a XF^e 96 Extracellular Flux assay kit (Seahorse Bioscience) using an automated process by the analyzer.

Live zebrafish embryos (24 hpf) were arrayed in XF^e 96 Spheroid microplate (Seahorse Bioscience) with 50 µL of egg water (1 embryo/well). These chorionated embryos were briefly checked to confirm that they had settled into the center of the wells. We found that the chorion provides enough mass to weigh down the embryos to keep them settled at the bottom centers of the wells, where they remained for the duration of the assays, thus obviating the need for time-consuming placement of islet capture screens. In contrast to the previously published zebrafish work utilizing the XF-24 Seahorse equipment (Bestman *et al.*, 2015; Gibert *et al.*, 2013; Stackley *et al.,* 2011), only one embryo per well (rather than multiple fish) were required to attain a robust signal-to-noise ratio. The XF-24 system's micro-chambers utilize a measurement volume of 7 µL, whereas the XF^e 96's flux measurements occur in a volume of <2 µL. This ~4X reduction in volume translates to improved sensitivity which allows for the use of a single embryo per well. OCR values resulting from one 24 hpf zebrafish embryo/well were 100-150 pmol/min, and OCR values resulting from background control wells which contained egg water but no fish were close to 0 pmol/min, ± 9-11 pmol/min (standard deviation). Thus, the signal from one chemically-untreated 24 hpf embryo is 10-15 times the noise, a robust signal-to-noise level.

Next, 100 µL of either 22.5 µM or 45 µM of TCS were added to the appropriate wells, for final concentrations of 15 and 30 µM TCS, respectively. FCCP (provided in the XF Mito Stress Test Kit, Seahorse Bioscience), at a final concentration of 0.5µM, was also added (100 µL) as a positive control to the appropriate wells. Measurements of total zebrafish OCR were started immediately and performed according to the manufacturer's instructions. Thirteen basal readings were performed, each with 2 minutes of mixing and 3 minutes of measuring. When the readings were completed, the mortality of each embryo was determined by heartbeat measurement manually by eye under the light microscope for 30 seconds per embryo (Oliveira *et al*., 2009; Nesan and Vijayan, 2012; Pylatiuk *et al*., 2014).

5.4.4 XF Cell Mito Stress Test Kit OCR assay

The XF Cell Mito Stress Test kit (Seahorse Bioscience) contains three inhibitors, oligomycin, FCCP, and rotenone/antimycin-A, which target the functions of ATP synthase, mitochondrial uncoupling, and complex I/III, respectively. Oligomycin is used to distinguish the percentage of oxygen consumption devoted to ATP synthesis and the percentage of oxygen consumption required to overcome the natural proton leak across the inner mitochondrial membrane. The OCR stimulated by FCCP treatment can be used to calculate the spare respiratory capacity of cells, which is highly effective for determining mitochondrial fidelity and function. Rotenone/antimycin-A shuts down mitochondrial respiration and enables the delineation of mitochondrial versus non-mitochondrial OCR fractions contributing to respiration.

All drugs were prepared following the manufacturer's recommendations and were dissolved in egg water. The inhibitors were then loaded into XF^{e} 96 extracellular flux assay plate (Seahorse Bioscience). Titrations were performed to determine the optimal concentration of each

inhibitor (data not shown). Before successive injections of these three drugs, basal OCR (± TCS) was measured for ~1 hour (12 cycles, each consisting of 1.5 min mixing and 3 min measurement). Then, sequential injections of 12.5 µM oligomycin, 2 µM FCCP, and 0.5 µM rotenone/antimycin-A were performed, and OCR measurements were recorded for 3 minutes (following 2 minutes of mixing) for 14, 3, and 14 times, respectively. Proton leak (which is defined as [lowest OCR measurement following oligomycin addition] - [OCR following rotenone/antimycin-A treatment]), ATP-linked respiration (which is defined as [final basal OCR measurement before oligomycin addition] - [lowest OCR measurement following oligomycin addition]), and spare respiratory capacity (which is defined as [maximal respiration following FCCP injection] - [final basal OCR measurement before oligomycin addition)] were calculated by the XF Cell Mito Stress Test Report Generator (Seahorse Bioscience). The applied concentrations of oligomycin and FCCP were previously found not to cause zebrafish embryo death (Stackley *et al*., 2011).

5.4.5 Statistical Analysis

OCR was calculated by the Seahorse Wave software (Seahorse Bioscience). For figure 5.1A, data from 16-22 embryo replicates per treatment group per experimental day were averaged at each time point. These averages were then normalized to the last time point of the 30 µM TCS sample average. These results were then further normalized by comparing them to the 0 µM TCS control from the corresponding experimental day and by multiplying by 100% to get the percent of control. Next, these normalized data from 3 independent biological replicate experiments performed on different days were averaged together and were plotted as mean ± standard error of the mean (SEM).

The data representing proton leak, ATP-linked respiration, and spare respiratory capacity from 4 independent biological replicate experiments performed on different days (each experiment consisted of 14-16 embryo replicates per treatment group per experimental day) were analyzed by the XF Cell Mito Stress Test Report Generator (Seahorse Bioscience). Next, each set of experimental data was normalized to either the 0 µM control or 30 µM TCS sample. These normalized data (4 experiments) were averaged together to generate the Figure 5.2 bar charts. The significance was assessed via one-way analysis of variance (ANOVA) with Tukey's or Dunnett's *post-hoc* test, using Prism software (Graphpad, San Diego, CA, USA).

5.5 Results

5.5.1 Triclosan increases oxygen consumption rate in living zebrafish.

One embryo at 24hpf was placed in each well with egg water. Various concentrations of TCS or FCCP were added right before the assay plate was placed in the analyzer for immediate OCR measurements for ~1 hour. The first OCR measurement of each experiment was recorded ~5 minutes after TCS or FCCP exposures began. Both 15 µM and 30 µM TCS cause significantly higher basal OCR compared to control (Fig. 5.1A). FCCP (0.5 µM) also displays higher OCR compared to the control group (Fig. 5.1A). Also, ANOVA with Tukey's post-test analysis indicates that the 15 µM TCS sample is different from the 0.5 µM FCCP sample ($p < 0.001$) and that the 30 µM TCS sample is different from the 0.5 µM FCCP sample ($p < 0.05$).

For each experiment, 4-6 wells were assigned as background wells, that contained egg water ± TCS, but no embryos. Background OCR levels were not significantly altered by 30 µM TCS compared to control (data not shown), indicating that the effect on OCR is due to a biological response to TCS. When the assay was completed, the heartbeat of each embryo was

measured for 30 seconds under a light microscope. No mortality was observed in any of the groups (Fig. 5.1B). Also, TCS exposure did not affect heartbeat rate; however, 0.5 µM FCCP seemed to slow heartbeat rate compared to control, although this effect was not statistically significant (Fig 5.1B).

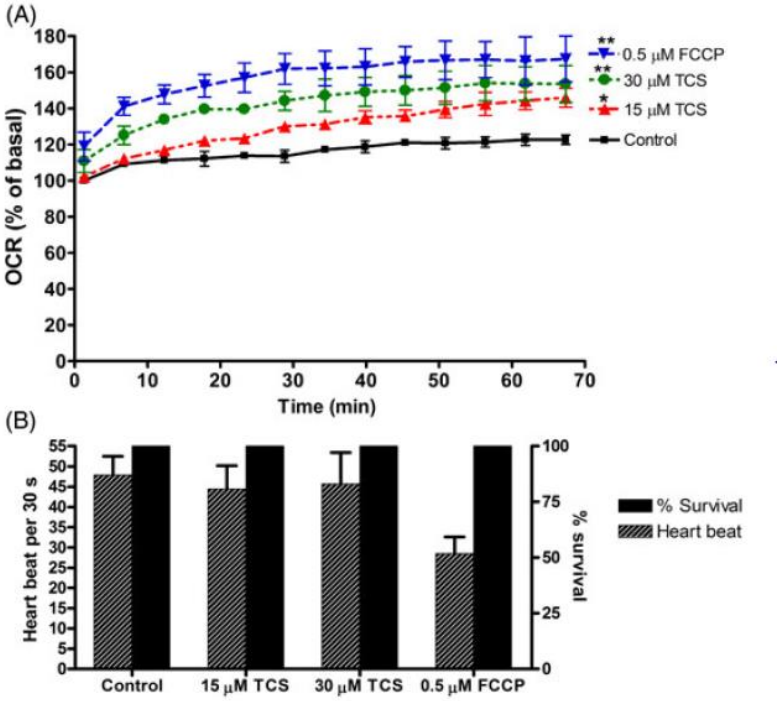

Figure 5.1. **Measurement of basal OCR of living zebrafish embryos exposed to TCS**. A) Basal OCR was measured for ~1 hour (13 readings), immediately after 24 hpf embryos were exposed to 0, 15, 30 µM TCS or 0.5 µM FCCP in egg water. At each timepoint, measurements were normalized to the first reading from the 0 µM control for that experimental day. Values represent means ± SEM for three independent experiments, where 16-22 embryos per treatment group were tested for each experiment. One-way ANOVA with Dunnett's post-tests (compared to the 0 µM control) were performed using Graphpad Prism software; *p< 0.05, **p< 0.01. B) Immediately after each basal OCR assay was completed, measurements of heartbeat of individual embryos were taken for 30 seconds, and the survival rate was determined. No significance was determined by one-way ANOVA with Dunnett's post-tests (compared to the 0 µM control).

5.5.2 Triclosan causes uncoupled mitochondrial respiration in living zebrafish

To further assess whether non-lethal doses of TCS disrupt mitochondrial function, the XF Cell Mito Stress Test Kit, which contains oligomycin, FCCP, and rotenone/antimycin-A, was utilized. Immediately following TCS or 0 µM control exposure, 12 measurements of basal OCR were taken before sequential injection of oligomycin (12.5 µM), FCCP (2 µM) and rotenone/antimycin-A (0.5 µM).

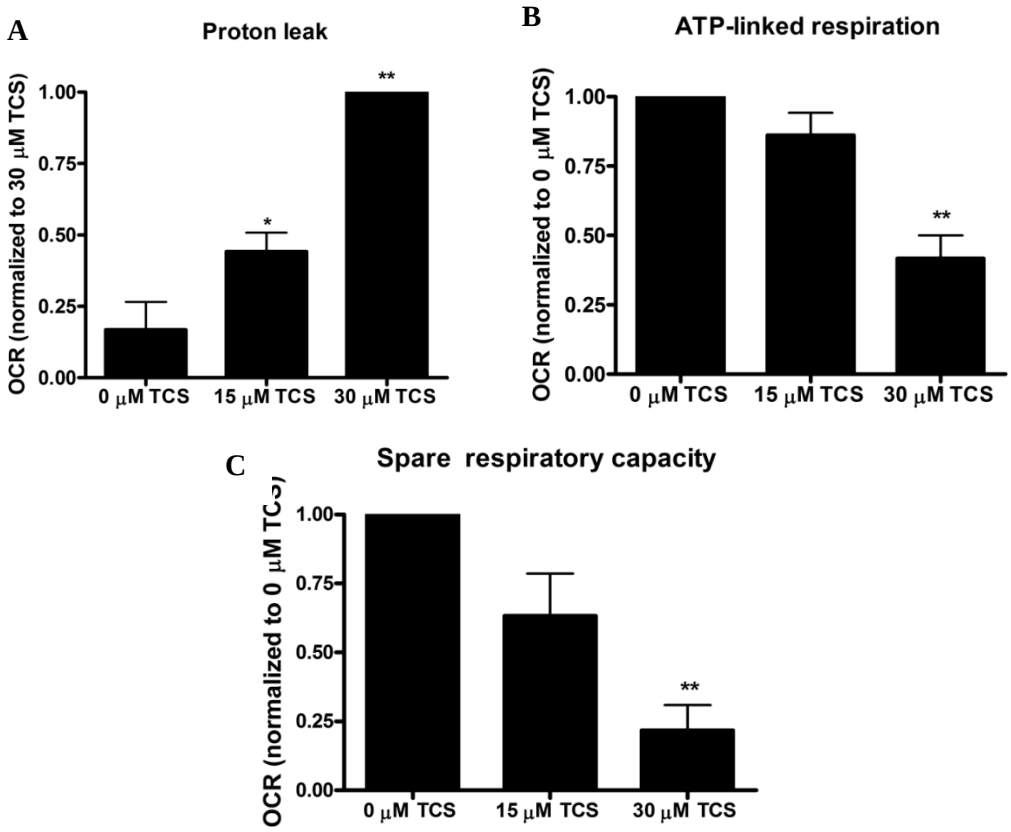

Figure 5.2. TCS as a mitochondrial uncoupler in living zebrafish. Zebrafish embryos (24 hpf) were exposed to TCS for ~1 hr (12 measurements of basal OCR), then the Mito Stress Test kit (Seahorse Bioscience) was performed. A) Proton leak, B) ATP-linked respiration, and C) Spare respiratory capacity were calculated using the Mito Stress Test Report Generator V2 (Seahorse Bioscience). Data from individual experimental days were normalized either to 30 µM TCS (A) or to 0 µM TCS (B and C) and values represent means ± SEM for four independent experiments, where 14-16 embryos per treatment group were tested in each experiment. One-way ANOVA with Dunnett's post-tests (compared to the 0 µM TCS) were performed using Graphpad Prism software; *$p < 0.05$, **$p < 0.01$

The proton leak, ATP-linked respiration and spare respiratory capacity were calculated as described before using the XF Cell Mito Stress Test Report Generator (Seahorse Bioscience). Both 15 and 30 µM TCS cause significant increases in proton leak, compared to 0 µM TCS control (Fig. 5.2A). High proton leak values indicate high levels of mitochondrial uncoupling and inefficient ATP production (Brand and Nicholls, 2011). ATP-linked respiration (that is, the respiration that is correlated with mitochondrial production of ATP) is inhibited by TCS (Fig. 5.2B). Spare respiratory capacity also decreases significantly at 30 µM TCS (Fig. 5.2C), indicating mitochondrial dysfunction during conditions of increased energy demand (Brand and Nicholls, 2011).

5.6 Discussion

Assessment of chemicals that can cause adverse human health and environmental effects needs to be conducted robustly and in a cost-effective manner. Zebrafish offer an effective, high-throughput low-cost alternative to mammalian testing. Zebrafish embryos have become a useful model in the field of toxicology (Nagel, 2002; Langheinrich, 2003; Braunbeck *et al*., 2005; Parng, 2005; McGrath and Li, 2008). This method we have developed could be a potential high-throughput *in vivo* assay to screen a variety of toxicants or drugs in order to identify novel mitochondrial uncoupler or other effectors of bioenergetic function.

Using zebrafish embryos, here we show that TCS is a mitochondrial uncoupler *in vivo*. We show that basal OCR increases with an increase in TCS and does not decrease survival or heartbeat rate at these concentrations. We also show TCS inhibition of ATP-linked respiration and spare respiratory capacity and TCS stimulation of proton leak. Triclosan's inhibition of ATP-linked respiration indicates that TCS inhibits mitochondrial ATP production. The increase

in proton leak indicates mitochondrial uncoupling (Brand and Nicholls, 2011) caused by TCS. Spare respiratory capacity is a measure of the organism's ability to respond to an increase in energy requirement (Yadava and Nicholls, 2007), and its inhibition by TCS indicates mitochondrial dysfunction (Brand and Nicholls, 2011). Decrease in ATP production and increase in OCR, both of which are shown here to be caused by TCS in 24 hpf zebrafish, are two of the main hallmarks of a mitochondrial uncoupler (Poe *et al*., 1967; Hanstein, 1976; Brand and Nicholls, 2011).

Zebrafish embryos (24-72 hpf) were previously used to assess the bioenergetics of a known mitochondrial uncoupler, 2,4-dinitrophenol (DNP), as an *in vivo* model (Bestman *et al*., 2015). This earlier study utilized the XF-24 Extracellular Flux Analyzer (Seahorse Bioscience). An islet capture screen was utilized to keep the zebrafish in place. As in a previous study, two embryos per well were necessary at the 7-30 hpf stages, and 3 embryos per well were required at the 3 hpf stages, in order to achieve sufficient OCR levels. With 3 hr exposure to 0.5 µM DNP, beginning at 3hpf, basal OCR levels were significantly increased in zebrafish embryos (Bestman *et al*., 2015). In comparison, we found that basal respiration of 24 hpf embryos is also increased due to TCS exposure for 1 hour at 15 and 30 µM (Fig. 5.1A). Proton leak in 24 hpf zebrafish embryos that had been treated with 0.5 µM DNP for total of 21 hours was increased (Bestman *et al*., 2015). Similar to this, at 24 hpf, 15 and 30 µM TCS exposure for 1 hour cause significant increases in proton leak (Fig. 5.2A). At 24-72 hpf, zebrafish embryos' ATP-linked respiration was decreased after exposure to 0.5 µM DNP for 21-69 hrs (Bestman *et al*, 2015). Similarly, 1 hour of TCS exposure inhibits ATP-linked respiration (Fig. 5.2B). Our finding that TCS causes similar effects on the key bioenergetic parameters basal OCR, ATP-linked respiration, and

proton leak, compared to the known mitochondrial uncoupler DNP, further support the idea that TCS is a mitochondrial uncoupler *in vivo*.

The robust effects of TCS (by immersion) on zebrafish bioenergetics that we report (Fig. 5.1A and Fig. 5.2) strongly suggest that TCS passes through the chorion. However, no complete assessment of the differential permeability of the chorion, which remains intact in 24 hpf embryos, has been performed, but the chorion has been shown to act as a barrier to various compounds (Braunbeck *et al*., 2005; Carlsson *et al*., 2013). The chorion discriminates against certain compounds depending on chemical structure (Harvey *et al*., 1983; Braunbeck *et al*., 2005; Sachidanandan *et al*., 2008; Kais *et al*., 2013). However, the exact nature of which compounds pass more easily through the chorion is contradictory. When TCS is in egg water (pH 7.0), ~90% of TCS molecules are protonated and, thus, lipophilic. The lipophilicity of the compound does seem to be a factor in the permeability across the chorion, but whether or not more lipophilic compounds increase or decrease the permeability remains up for debate (Braunbeck *et al.,* 2005; Sachidanandan *et al.,* 2008), and lipophilicity is likely only one of many structural factors determining chorion permeability of a particular chemical. A study found that exposure to 1.1 µM fipronil (a broad-use insecticide), starting at 1 hpf and ending at 48 hpf, caused notochord degeneration in zebrafish (Stehr *et al*., 2006). The exposure and subsequent notochord degeneration occurred while the embryos were still in the chorion, indicating that the fipronil most likely crossed the chorion barrier. Fipronil and TCS have similar two-ring organohalogen structures.

Thus, along with the fact that TCS caused extensive bioenergetic effects on the zebrafish, it is highly likely that at least some fraction of the applied TCS crossed the chorion during the treatment period. Size of the compound of interest also seems to be a factor in chorion

permeability. A study found that 3,000 Da fluorescent dextrans were able to pass through the chorion while 10,000 Da dextrans could not permeate the chorion (Creton, 2004). Because triclosan's molecular weight is ~289 Da, its size is likely not too large to penetrate the chorion. However, given the published data relating to the ability of the chorion to present a barrier to various xenobiotics (Braunbeck *et al.*, 2005), it is probable that TCS's potency is greater in dechorionated embryos.

The present investigation demonstrates that the ubiquitous antimicrobial TCS causes mitochondrial uncoupling, with no mortality, in a living organism at concentrations ~1000-fold lower than those used in personal care products. TCS at 30 μM is nearly as potent as 0.5 μM FCCP in 24 hpf zebrafish (Fig. 5.1A), and TCS's uncoupling effect is a biochemical mechanism that likely underlies many organismal health effects. Because triclosan's toxicity is currently being reviewed by U.S. and other government agencies, these live animal, mechanistic data are critical. This study was performed using a novel method, utilizing live, single, chorionated zebrafish embryos in a 96-well high-throughput format with bidirectional temperature control.

CHAPTER 6

SUMMARY AND CONCLUSIONS

Arsenic is an environmental toxicant which causes many human health problems. Arsenic exposure has been reported globally since its major route of exposure is via drinking water or diet. In some countries, large populations are exposed to high dosages of arsenic. Triclosan is an antimicrobial agent, which was found in nearly all the soap products in the late 2000s. Although the FDA recently banned its usage in most soap products (consumer and hospital settings), triclosan remains as an active ingredient in many consumer products, including a top-selling toothpaste, and in household products such as toys and kitchenware.

Mast cells are important immune cells that are involved in numerous physiological functions and diseases, including allergic reaction, inflammatory responses, host defense, neurological processes and more. Mast cells reside in nearly every tissue, particularly in where they interface with environment. Therefore, mast cells are easily targeted by toxicants.

Our lab has found that arsenic and triclosan inhibit mast cell degranulation, which is the release of granules containing many active biomediators to the extracellular space. Based on these findings, we have investigated the mechanisms underlying inhibitory action by arsenic and triclosan. In Chapter 2, we showed that one of arsenic's targets is phosphorylation of tyrosine kinase Syk, which is found in early mast cell signaling pathway. Additionally, we found that phosphorylation/activation of PI3K, one of the direct substrates of Syk, is also inhibited by arsenic. Inhibition of Syk and PI3K activation leads to decreased calcium mobilization, which is a critical step leading to MC degranulation.

Studies in Chapter 3 elucidated triclosan's effects two key molecules: phospholipase D (PLD) and protein kinase C (PKC). Even though we also revealed that triclosan dampens

cytosolic calcium levels as seen in arsenic studies, triclosan does not inhibit tyrosine phosphorylation-initiated events such as calcium efflux from the ER. PKC and PLD are central players in degranulation after cytosolic calcium rise. We have shown that triclosan decreases PLD activity while PKC activity is not inhibited. However, triclosan delays the translocation of PKC βII and PKC δ isoforms to the plasma membrane, and subsequently slows down dissociation of MARCKS, a substrate of PKC, from the plasma membrane to cytosol. The functions of PKC and PLD are shared in many other cell types and signaling pathways. Therefore, our findings on triclosan's effects on PKC and PLD provide mechanisms of the numerous human health problems reported in recent epidemiological studies.

In addition to revealing triclosan's targets in the mast cell signaling pathway, we have also investigated triclosan toxicity as a mitochondrial uncoupler (MU). Structural similarities between triclosan and other known MUs led us to explore this hypothesis. In previous work, we first identified that triclosan is indeed an MU *in vitro*, using several cell types, including mast cells, fibroblasts, and primary human skin cells. To compare this *in vitro* finding, we developed an *in vivo* assay to measure mitochondrial function using zebrafish embryos. Due to advantageous of utilizing zebrafish as a model organism, this assay is a high-throughput, 96 well-microplate based assay which can quickly evaluate a toxicant's effect in living organism. Using this assay, we have shown that mitochondrial toxicity is another mechanism of triclosan, *in vivo* (Chapter 5).

Finally, Chapter 4 reported our findings on tryptase detection in RBL-2H3 cells. The RBL-2H3 cell line has been extensively utilized as an *in vitro* mast cell model, but β-hexosaminidase or histamine have usually been employed as RBL-2H3 degranulation markers even though tryptase is considered a canonical marker of mast cells. Since mast cell activity in

zebrafish has been measured solely via tryptase release to date, we aimed to develop an RBL-2H3 tryptase assay in order to align RBL-2H3 cell toxicological studies to *in vivo* zebrafish mast cell studies. Unexpectedly, we have found that neither mRNA nor protein of rat tryptase genes are expressed in the RBL-2H3 cell line. Our comprehensive investigation to detect tryptase in RBL cells delivers an important message to the mast cell community and necessitates development of a separate marker for comparative studies between these two model systems.

Overall, the findings in this dissertation provide molecular and biochemical mechanisms for many human health problems due to arsenic and triclosan and establish groundwork for developing comparative toxicological studies using zebrafish to study mast cell toxicology and biology.

REFERENCES

Abdul, K.S., Jayasinghe, S.S., Chandana, E.P., Jayasumana, C., De Silva, P.M., 2015. Arsenic and human health effects: A review. Environmental toxicology and pharmacology 40, 828-846.

Abernathy, C.O., Liu, Y.P., Longfellow, D., Aposhian, H.V., Beck, B., Fowler, B., Goyer, R., Menzer, R., Rossman, T., Thompson, C., Waalkes, M., 1999. Arsenic: Health effects, mechanisms of actions, and research issues. Environmental Health Perspectives 107, 593-597.

Abhyankar, L.N., Jones, M.R., Guallar, E., Navas-Acien, A., 2012. Arsenic exposure and hypertension: a systematic review. Environ Health Perspect 120, 494-500.

Abou-Donia, M.B., El-Masry, E.M., Abdel-Rahman, A.A., McLendon, R.E., Schiffman, S.S., 2008. Splenda alters gut microflora and increases intestinal p-glycoprotein and cytochrome p-450 in male rats. J Toxicol Environ Health A 71, 1415-1429.

Abraham, S.N., St John, A.L., 2010. Mast cell-orchestrated immunity to pathogens. Nature Reviews Immunology 10, 440-452.

Abramson, J., Pecht, I., 2007. Regulation of the mast cell response to the type 1 Fc epsilon receptor. Immunological Reviews 217, 231-254.

Aderem, A., 1992. The MARCKS brothers: a family of protein kinase C substrates. Cell 71, 713-716.

Ahn, K.C., Zhao, B., Chen, J., Cherednichenko, G., Sanmarti, E., Denison, M.S., Lasley, B., Pessah, I.N., Kultz, D., Chang, D.P., Gee, S.J., Hammock, B.D., 2008. In vitro biologic activities of the antimicrobials triclocarban, its analogs, and triclosan in bioassay screens: receptor-based bioassay screens. Environ Health Perspect 116, 1203-1210.

Ajao, C., Andersson, M.A., Teplova, V.V., Nagy, S., Gahmberg, C.G., Andersson, L.C., Hautaniemi, M., Kakasi, B., Roivainen, M., Salkinoja-Salonen, M., 2015. Mitochondrial toxicity of triclosan on mammalian cells. Toxicol Rep 2, 624-637.

Akahoshi, M., Song, C.H., Piliponsky, A.M., Metz, M., Guzzetta, A., Abrink, M., Schlenner, S.M., Feyerabend, T.B., Rodewald, H.R., Pejler, G., Tsai, M., Galli, S.J., 2011. Mast cell chymase reduces the toxicity of Gila monster venom, scorpion venom, and vasoactive intestinal polypeptide in mice. The Journal of clinical investigation 121, 4180-4191.

Ali, H., Choi, O.H., Fraundorfer, P.F., Yamada, K., Gonzaga, H.M.S., Beaven, M.A., 1996. Sustained activation of phospholipase D via adenosine A(3) receptors is associated with enhancement of antigen- and Ca2+-ionophore-induced secretion in a rat mast cell line. Journal of Pharmacology and Experimental Therapeutics 276, 837-845.

Ali, H., Cunha-Melo, J.R., Saul, W.F., Beaven, M.A., 1990. Activation of phospholipase C via adenosine receptors provides synergistic signals for secretion in antigen-stimulated RBL-

2H3 cells. Evidence for a novel adenosine receptor. The Journal of biological chemistry 265, 745-753.

Aridor, M., Traub, L.M., Sagi-Eisenberg, R., 1990. Exocytosis in mast cells by basic secretagogues: evidence for direct activation of GTP-binding proteins. J Cell Biol 111, 909-917.

Arslan, B., Djamgoz, M.B.A., Akun, E., 2017. ARSENIC: A Review on Exposure Pathways, Accumulation, Mobility and Transmission into the Human Food Chain. Rev Environ Contam Toxicol 243, 27-51.

ATSDR, 2007. Toxicological profile for Arsenic. Agency for Toxic Substances and Disease Registry (ATSDR), Atlanta, GA.

Attene-Ramos, M.S., Huang, R., Michael, S., Witt, K.L., Richard, A., Tice, R.R., Simeonov, A., Austin, C.P., Xia, M., 2015. Profiling of the Tox21 Chemical Collection for Mitochondrial Function to Identify Compounds that Acutely Decrease Mitochondrial Membrane Potential. Environ Health Perspect 123, 49-56.

Baccari, G.C., Pinelli, C., Santillo, A., Minucci, S., Rastogi, R.K., 2011. Mast cells in nonmammalian vertebrates: an overview. International review of cell and molecular biology 290, 1-53.

Bae, C.D., Min, D.S., Fleming, I.N., Exton, J.H., 1998. Determination of interaction sites on the small G protein RhoA for phospholipase D. The Journal of biological chemistry 273, 11596-11604.

Bajpai, M., Chopra, P., Dastidar, S.G., Ray, A., 2008. Spleen tyrosine kinase: a novel target for therapeutic intervention of rheumatoid arthritis. Expert Opinion on Investigational Drugs 17, 641-659.

Balci, T.B., Coombs, A.J., Grondin, C., Da'as, S.I., Chute, I., Leger, D., Ferrando, A.A., Lewis, S., Berman, J.N., 2011. Using the Zebrafish As a Tool for Modeling Systemic Mastocytosis. Blood 118, 1385-1386.

Balci, T.B., Prykhozhij, S.V., Teh, E.M., Da'as, S.I., McBride, E., Liwski, R., Chute, I.C., Leger, D., Lewis, S.M., Berman, J.N., 2014. A transgenic zebrafish model expressing KIT-D816V recapitulates features of aggressive systemic mastocytosis. British journal of haematology 167, 48-61.

Baldassare, J.J., Henderson, P.A., Burns, D., Loomis, C., Fisher, G.J., 1992. Translocation of protein kinase C isozymes in thrombin-stimulated human platelets. Correlation with 1,2-diacylglycerol levels. The Journal of biological chemistry 267, 15585-15590.

Bambino, K., Chu, J., 2017. Zebrafish in Toxicology and Environmental Health. Curr Top Dev Biol 124, 331-367.

Baram, D., Adachi, R., Medalia, O., Tuvim, M., Dickey, B.F., Mekori, Y.A., Sagi-Eisenberg, R., 1999. Synaptotagmin II negatively regulates Ca2+-triggered exocytosis of lysosomes in mast cells. Journal of Experimental Medicine 189, 1649-1657.

Baram, D., Linial, M., Mekori, Y.A., Sagi-Eisenberg, R., 1998. Ca^{2+}-dependent exocytosis in mast cells is stimulated by the Ca2+ sensor, synaptotagmin I. J Immunol 161, 5120-5123.

Baram, D., Mekori, Y.A., Sagi-Eisenberg, R., 2001. Synaptotagmin regulates mast cell functions. Immunol Rev 179, 25-34.

Bardach, A.E., Ciapponi, A., Soto, N., Chaparro, M.R., Calderon, M., Briatore, A., Cadoppi, N., Tassara, R., Litter, M.I., 2015. Epidemiology of chronic disease related to arsenic in Argentina: A systematic review. Sci Total Environ 538, 802-816.

Barsumian, E.L., Isersky, C., Petrino, M.G., Siraganian, R.P., 1981. IgE-induced histamine release from rat basophilic leukemia cell lines: isolation of releasing and nonreleasing clones. European journal of immunology 11, 317-323.

Bayleran, J., Hechtman, P., Kolodny, E., Kaback, M., 1987. Tay-Sachs disease with hexosaminidase A: characterization of the defective enzyme in two patients. American Journal of Human Genetics 41, 532-548.

Beaven, M.A., Metzger, H., 1993. Signal-transduction by Fc-Receptors - The Fc-epsilon-RI case. Immunology Today 14, 222-226.

Beaven, M.A., Moore, J.P., Smith, G.A., Hesketh, T.R., Metcalfe, J.C., 1984. The calcium signal and phosphatidylinositol breakdown in 2H3 cells. Journal of Biological Chemistry 259, 7137-7142.

Benhamou, M., Ryba, N.J.P., Kihara, H., Nishikata, H., Siraganian, R.P., 1993. Protein-tyrosine kinase p72(Syk) in high-affinity IgE receptor signaling- Identification as a component of pp72 and association with the receptor gamma-chain after receptor aggregation. Journal of Biological Chemistry 268, 23318-23324.

Benhamou, M., Stephan, V., Robbins, K.C., Siraganian, R.P., 1992. High-affinity IgE receptor-mediated stimulation of rat basophilic leukemia (RBL-2H3) cells induces early and late protein-tyrosine phosphorylations. Journal of Biological Chemistry 267, 7310-7314.

Benramdane, L., Accominotti, M., Fanton, L., Malicier, D., Vallon, J.J., 1999. Arsenic speciation in human organs following fatal arsenic trioxide poisoning--a case report. Clin Chem 45, 301-306.

Bergamin, G., Cieri, D., Vazza, G., Argenton, F., Mostacciuolo, M.L., 2016. Zebrafish Tg(hb9:MTS-Kaede): a new in vivo tool for studying the axonal movement of mitochondria. Biochim Biophys Acta 1860, 1247-1255.

Berridge, M.J., 1993. Inositol trisphosphate and calcium signalling. Nature 361, 315-325.

Bestman, J.E., Stackley, K.D., Rahn, J.J., Williamson, T.J., Chan, S.S., 2015. The cellular and molecular progression of mitochondrial dysfunction induced by 2,4-dinitrophenol in developing zebrafish embryos. Differentiation 89, 51-69.

Blackshear, P.J., 1993. The MARCKS family of cellular protein kinase C substrates. The Journal of biological chemistry 268, 1501-1504.

Blank, U., Benhamou, M., 2013. Deciphering new molecular mechanisms of mast cell activation. Front Immunol 4, 100.

Blank, U., Cyprien, B., Martin-Verdeaux, S., Paumet, F., Pombo, I., Rivera, J., Roa, M., Varin-Blank, N., 2002. SNAREs and associated regulators in the control of exocytosis in the RBL-2H3 mast cell line. Molecular Immunology 38, 1341-1345.

Blobe, G.C., Stribling, D.S., Fabbro, D., Stabel, S., Hannun, Y.A., 1996. Protein kinase C beta II specifically binds to and is activated by F-actin. The Journal of biological chemistry 271, 15823-15830.

Borm, B., Requardt, R.P., Herzog, V., Kirfel, G., 2005. Membrane ruffles in cell migration: indicators of inefficient lamellipodia adhesion and compartments of actin filament reorganization. Exp Cell Res 302, 83-95.

Bouwman, R.A., Musters, R.J., van Beek-Harmsen, B.J., de Lange, J.J., Boer, C., 2004. Reactive oxygen species precede protein kinase C-delta activation independent of adenosine triphosphate-sensitive mitochondrial channel opening in sevoflurane-induced cardioprotection. Anesthesiology 100, 506-514.

Brand, M.D., Nicholls, D.G., 2011. Assessing mitochondrial dysfunction in cells. Biochem J 435, 297-312.

Braunbeck, T., Boettcher, M., Hollert, H., Kosmehl, T., Lammer, E., Leist, E., Rudolf, M., Seitz, N., 2005. Towards an alternative for the acute fish LC(50) test in chemical assessment: the fish embryo toxicity test goes multi-species -- an update. Altex 22, 87-102.

Brown, F.D., Thompson, N., Saqib, K.M., Clark, J.M., Powner, D., Thompson, N.T., Solari, R., Wakelam, M.J., 1998. Phospholipase D1 localises to secretory granules and lysosomes and is plasma-membrane translocated on cellular stimulation. Curr Biol 8, 835-838.

Brown, G.C., Kholodenko, B.N., 1999. Spatial gradients of cellular phospho-proteins. FEBS Lett 457, 452-454.

Burgoyne, R.D., Morgan, A., 2003. Secretory granule exocytosis. Physiol Rev 83, 581-632.

Bussmann, C., Hagemann, T., Hanfland, J., Haidl, G., Bieber, T., Novak, N., 2007. Flushing and increase of serum tryptase after mechanical irritation of a solitary mastocytoma. Eur J Dermatol 17, 332-334.

Cai, D., Zhong, M., Wang, R., Netzer, W.J., Shields, D., Zheng, H., Sisodia, S.S., Foster, D.A., Gorelick, F.S., Xu, H., Greengard, P., 2006. Phospholipase D1 corrects impaired betaAPP trafficking and neurite outgrowth in familial Alzheimer's disease-linked presenilin-1 mutant neurons. Proc Natl Acad Sci U S A 103, 1936-1940.

Calafat, A.M., Ye, X., Wong, L.Y., Reidy, J.A., Needham, L.L., 2008. Urinary concentrations of triclosan in the U.S. population: 2003-2004. Environ Health Perspect 116, 303-307.

Cambier, J.C., 1995. Antigen and Fc receptor signaling - the awesome power of the immunoreceptor tyrosine-based activation motif (ITAM). Journal of Immunology 155, 3281-3285.

Cardoso, P.G., Rodrigues, D., Madureira, T.V., Oliveira, N., Rocha, M.J., Rocha, E., 2017. Warming modulates the effects of the endocrine disruptor progestin levonorgestrel on the zebrafish fitness, ovary maturation kinetics and reproduction success. Environmental pollution (Barking, Essex : 1987) 229, 300-311.

Carlos, D., Sa-Nunes, A., de Paula, L., Matias-Peres, C., Jamur, M.C., Oliver, C., Serra, M.F., Martins, M.A., Faccioli, L.H., 2006. Histamine modulates mast cell degranulation through an indirect mechanism in a model IgE-mediated reaction. Eur J Immunol 36, 1494-1503.

Carlsson, G., Patring, J., Kreuger, J., Norrgren, L., Oskarsson, A., 2013. Toxicity of 15 veterinary pharmaceuticals in zebrafish (Danio rerio) embryos. Aquat Toxicol 126, 30-41.

Caughey, G.H., 2007. Mast cell tryptases and chymases in inflammation and host defense. Immunol Rev 217, 141-154.

Caughey, G.H., 2011. Mast cell proteases as protective and inflammatory mediators. Advances in Experimental Medicine and Biology 716, 212-234.

Chahdi, A., Choi, W.S., Kim, Y.M., Fraundorfer, P.F., Beaven, M.A., 2002. Serine/threonine protein kinases synergistically regulate phospholipase D1 and 2 and secretion in RBL-2H3 mast cells. Mol Immunol 38, 1269-1276.

Chahdi, A., Fraundorfer, P.F., Beaven, M.A., 2000. Compound 48/80 activates mast cell phospholipase D via heterotrimeric GTP-binding proteins. J Pharmacol Exp Ther 292, 122-130.

Chan, K.M., Ku, L.L., Chan, P.C., Cheuk, W.K., 2006. Metallothionein gene expression in zebrafish embryo-larvae and ZFL cell-line exposed to heavy metal ions. Mar Environ Res 62 Suppl, S83-87.

Chang, Y.Y., Kuo, T.C., Hsu, C.H., Hou, D.R., Kao, Y.H., Huang, R.N., 2012. Characterization of the role of protein-cysteine residues in the binding with sodium arsenite. Archives of toxicology 86, 911-922.

Chen, C.C., Grimbaldeston, M.A., Tsai, M., Weissman, I.L., Galli, S.J., 2005. Identification of mast cell progenitors in adult mice. Proc Natl Acad Sci U S A 102, 11408-11413.

Chen, L., Hu, C., Huang, C., Wang, Q., Wang, X., Yang, L., Zhou, B., 2012. Alterations in retinoid status after long-term exposure to PBDEs in zebrafish (Danio rerio). Aquat Toxicol 120-121, 11-18.

Chen, Y., Parvez, F., Gamble, M., Islam, T., Ahmed, A., Argos, M., Graziano, J.H., Ahsan, H., 2009. Arsenic exposure at low-to-moderate levels and skin lesions, arsenic metabolism, neurological functions, and biomarkers for respiratory and cardiovascular diseases: review of recent findings from the Health Effects of Arsenic Longitudinal Study (HEALS) in Bangladesh. Toxicol Appl Pharmacol 239, 184-192.

Cheng, H.Y.Y., Li, P., David, M., Smithgall, T.E., Feng, L.L., Lieberman, M.W., 2004. Arsenic inhibition of the JAK-STAT pathway. Oncogene 23, 3603-3612.

Cherednichenko, G., Zhang, R., Bannister, R.A., Timofeyev, V., Li, N., Fritsch, E.B., Feng, W., Barrientos, G.C., Schebb, N.H., Hammock, B.D., Beam, K.G., Chiamvimonvat, N., Pessah, I.N., 2012. Triclosan impairs excitation-contraction coupling and Ca2+ dynamics in striated muscle. Proc Natl Acad Sci U S A 109, 14158-14163.

Chiang, T.M., 1994. Activation of phospholipase D in human platelets by collagen and thrombin and its relationship to platelet aggregation. Biochim Biophys Acta 1224, 147-155.

Ching, T.T., Hsu, A.L., Johnson, A.J., Chen, C.S., 2001. Phosphoinositide 3-kinase facilitates antigen-stimulated Ca(2+) influx in RBL-2H3 mast cells via a phosphatidylinositol 3,4,5-trisphosphate-sensitive Ca(2+) entry mechanism. The Journal of biological chemistry 276, 14814-14820.

Chiu, H.F., Ho, S.C., Wang, L.Y., Wu, T.N., Yang, C.Y., 2004. Does arsenic exposure increase the risk for liver cancer? J Toxicol Environ Health A 67, 1491-1500.

Cho, S.H., Woo, C.H., Yoon, S.B., Kim, J.H., 2004. Protein kinase Cdelta functions downstream of Ca2+ mobilization in FcepsilonRI signaling to degranulation in mast cells. The Journal of allergy and clinical immunology 114, 1085-1092.

Choi, O.H., Adelstein, R.S., Beaven, M.A., 1994. Secretion from rat basophilic RBL-2H3 cells is associated with diphosphorylation of myosin light chains by myosin light chain kinase as well as phosphorylation by protein kinase C. The Journal of biological chemistry 269, 536-541.

Choi, O.H., Kim, J.H., Kinet, J.P., 1996. Calcium mobilization via sphingosine kinase in signalling by the Fc epsilon RI antigen receptor. Nature 380, 634-636.

Choi, W.S., Kim, Y.M., Combs, C., Frohman, M.A., Beaven, M.A., 2002. Phospholipases D1 and D2 regulate different phases of exocytosis in mast cells. J Immunol 168, 5682-5689.

Chu, K.H., Lee, C.C., Hsin, S.C., Cai, B.C., Wang, J.H., Chiang, B.L., 2010. Arsenic trioxide alleviates airway hyperresponsiveness and eosinophilia in a murine model of asthma. Cell Mol Immunol 7, 375-380.

Chung, E., Genco, M.C., Megrelis, L., Ruderman, J.V., 2011. Effects of bisphenol A and triclocarban on brain-specific expression of aromatase in early zebrafish embryos. Proc Natl Acad Sci U S A 108, 17732-17737.

Chung, J.S., Haque, R., Guha Mazumder, D.N., Moore, L.E., Ghosh, N., Samanta, S., Mitra, S., Hira-Smith, M.M., von Ehrenstein, O., Basu, A., Liaw, J., Smith, A.H., 2006. Blood concentrations of methionine, selenium, beta-carotene, and other micronutrients in a case-control study of arsenic-induced skin lesions in West Bengal, India. Environ Res 101, 230-237.

Cissel, D.S., Fraundorfer, P.F., Beaven, M.A., 1998. Thapsigargin-induced secretion is dependent on activation of a cholera toxin-sensitive and phosphatidylinositol-3-kinase-regulated phospholipase D in a mast cell line. J Pharmacol Exp Ther 285, 110-118.

Clapham, D.E., 1995. Intracellular calcium - replenishing the stores. Nature 375, 634-635.

Cockcroft, S., 2001. Signalling roles of mammalian phospholipase D1 and D2. Cell Mol Life Sci 58, 1674-1687.

Codazzi, F., Teruel, M.N., Meyer, T., 2001. Control of astrocyte Ca(2+) oscillations and waves by oscillating translocation and activation of protein kinase C. Curr Biol 11, 1089-1097.

Cohen, G.B., Ren, R.B., Baltimore, D., 1995. Modular binding domains in signal-transduction proteins. Cell 80, 237-248.

Colley, W.C., Sung, T.C., Roll, R., Jenco, J., Hammond, S.M., Altshuller, Y., Bar-Sagi, D., Morris, A.J., Frohman, M.A., 1997. Phospholipase D2, a distinct phospholipase D isoform with novel regulatory properties that provokes cytoskeletal reorganization. Curr Biol 7, 191-201.

Costello, P.S., Turner, M., Walters, A.E., Cunningham, C.N., Bauer, P.H., Downward, J., Tybulewicz, V.L., 1996. Critical role for the tyrosine kinase Syk in signalling through the high affinity IgE receptor of mast cells. Oncogene 13, 2595-2605.

Coussens, L.M., Raymond, W.W., Bergers, G., Laig-Webster, M., Behrendtsen, O., Werb, Z., Caughey, G.H., Hanahan, D., 1999. Inflammatory mast cells up-regulate angiogenesis during squamous epithelial carcinogenesis. Genes & development 13, 1382-1397.

Creton, R., 2004. The calcium pump of the endoplasmic reticulum plays a role in midline signaling during early zebrafish development. Brain research. Developmental brain research 151, 33-41.

Crivellato, E., Beltrami, C.A., Mallardi, F., Ribatti, D., 2004. The mast cell: an active participant or an innocent bystander? Histology and Histopathology 19, 259-270.

Da'as, S.I., Balci, T.B., Berman, J.N., 2015. Mast cell development and function in the zebrafish. Methods in molecular biology 1220, 29-57.

Da'as, S.I., Coombs, A.J., Balci, T.B., Grondin, C.A., Ferrando, A.A., Berman, J.N., 2012. The zebrafish reveals dependence of the mast cell lineage on Notch signaling in vivo. Blood 119, 3585-3594.

Da'as, S.I., Teh, E.M., Dobson, J.T., Nasrallah, G.K., McBride, E.R., Wang, H., Neuberg, D.S., Marshall, J.S., Lin, T.J., Berman, J.N., 2011. Zebrafish mast cells possess an FcepsilonRI-like receptor and participate in innate and adaptive immune responses. Developmental and Comparative Immunology 35, 125-134.

da Silva, E.Z., Jamur, M.C., Oliver, C., 2014. Mast cell function: a new vision of an old cell. Journal of Histochemistry and Cytochemistry 62, 698-738.

Daeron, M., 1997. Fc receptor biology. Annual Review of Immunology 15, 203-234.

Dai, H., Shen, N., Arac, D., Rizo, J., 2007a. A quaternary SNARE-synaptotagmin-Ca2+-phospholipid complex in neurotransmitter release. Journal of molecular biology 367, 848-863.

Dai, Y., Wang, S., Tominaga, M., Yamamoto, S., Fukuoka, T., Higashi, T., Kobayashi, K., Obata, K., Yamanaka, H., Noguchi, K., 2007b. Sensitization of TRPA1 by PAR2 contributes to the sensation of inflammatory pain. The Journal of clinical investigation 117, 1979-1987.

Dall'Armi, C., Hurtado-Lorenzo, A., Tian, H., Morel, E., Nezu, A., Chan, R.B., Yu, W.H., Robinson, K.S., Yeku, O., Small, S.A., Duff, K., Frohman, M.A., Wenk, M.R., Yamamoto, A., Di Paolo, G., 2010. The phospholipase D1 pathway modulates macroautophagy. Nat Commun 1, 142.

Daoud, F.C., Edmiston, C.E., Jr., Leaper, D., 2014. Meta-analysis of prevention of surgical site infections following incision closure with triclosan-coated sutures: robustness to new evidence. Surgical infections 15, 165-181.

Das, N., Paul, S., Chatterjee, D., Banerjee, N., Majumder, N.S., Sarma, N., Sau, T.J., Basu, S., Banerjee, S., Majumder, P., Bandyopadhyay, A.K., States, J.C., Giri, A.K., 2012. Arsenic exposure through drinking water increases the risk of liver and cardiovascular diseases in the population of West Bengal, India. BMC Public Health 12, 639.

de Castro, R.O., Zhang, J., Jamur, M.C., Oliver, C., Siraganian, R.P., 2010. Tyrosines in the Carboxyl Terminus Regulate Syk Kinase Activity and Function. Journal of Biological Chemistry 285, 26674-26684.

de Ruyter, J.C., Olthof, M.R., Seidell, J.C., Katan, M.B., 2012. A trial of sugar-free or sugar-sweetened beverages and body weight in children. N Engl J Med 367, 1397-1406.

Deforge, L.E., Fantone, J.C., Kenney, J.S., Remick, D.G., 1992. Oxygen radical scavengers selectively imhibit interleukin-8 production in human whole-blood. Journal of Clinical Investigation 90, 2123-2129.

DeMaster, E.G., Mitchell, A., 1973. A comparison of arsenate and vanadate as inhibitors or uncouplers of mitochondrial and glycolytic energy metabolism. Biochemistry 12, 3616-3621.

Dinh, T.T., Kennerly, D.A., 1991. Assessment of receptor-dependent activation of phosphatidylcholine hydrolysis by both phospholipase-D and phospholipase-C. Cell Regulation 2, 299-309.

Dobson, J.T., Seibert, J., Teh, E.M., Da'as, S., Fraser, R.B., Paw, B.H., Lin, T.J., Berman, J.N., 2008. Carboxypeptidase A5 identifies a novel mast cell lineage in the zebrafish providing new insight into mast cell fate determination. Blood 112, 2969-2972.

Drinane, M.C., Sherman, J.A., Hall, A.E., Simons, M., Mulligan-Kehoe, M.J., 2006. Plasminogen and plasmin activity in patients with coronary artery disease. Journal of Thrombosis Haemostasis 4, 1288-1295.

Du, G., Altshuller, Y.M., Vitale, N., Huang, P., Chasserot-Golaz, S., Morris, A.J., Bader, M.F., Frohman, M.A., 2003. Regulation of phospholipase D1 subcellular cycling through coordination of multiple membrane association motifs. J Cell Biol 162, 305-315.

Dvorak, A.M., Schleimer, R.P., Lichtenstein, L.M., 1988. Human mast cells synthesize new granules during recovery from degranulation. In vitro studies with mast cells purified from human lungs. Blood 71, 76-85.

Dvorak, A.M., Schleimer, R.P., Schulman, E.S., Lichtenstein, L.M., 1986. Human mast cells use conservation and condensation mechanisms during recovery from degranulation. In vitro studies with mast cells purified from human lungs. Laboratory Investigation 54, 663-678.

Echtenacher, B., Mannel, D.N., Hultner, L., 1996. Critical protective role of mast cells in a model of acute septic peritonitis. Nature 381, 75-77.

Ellett, F., Lieschke, G.J., 2010. Zebrafish as a model for vertebrate hematopoiesis. Curr Opin Pharmacol 10, 563-570.

Etzel, T.M., Calafat, A.M., Ye, X., Chen, A., Lanphear, B.P., Savitz, D.A., Yolton, K., Braun, J.M., 2017. Urinary triclosan concentrations during pregnancy and birth outcomes. Environ Res 156, 505-511.

Exton, J.H., 1999. Regulation of phospholipase D. Biochim Biophys Acta 1439, 121-133.

Fahrner, M., Derler, I., Jardin, I., Romanin, C., 2013. The STIM1/Orai signaling machinery. Channels (Austin) 7, 330-343.

Fang, Y., Vilella-Bach, M., Bachmann, R., Flanigan, A., Chen, J., 2001. Phosphatidic acid-mediated mitogenic activation of mTOR signaling. Science 294, 1942-1945.

FDA, 2013. Safety and Effectiveness of Consumer Antiseptics; Topical Antimicrobial Drug Products for Over-the-Counter Human Use; Proposed Amendment of the Tentative Final Monograph, pp.

Ferreccio, C., Gonzalez, C., Milosavjlevic, V., Marshall, G., Sancha, A.M., Smith, A.H., 2000. Lung cancer and arsenic concentrations in drinking water in Chile. Epidemiology 11, 673-679.

Ferris, C.D., Huganir, R.L., Supattapone, S., Snyder, S.H., 1989. Purified inositol 1,4,5-trisphosphate receptor mediates calcium flux in reconstituted lipid vesicles. Nature 342, 87-89.

Feske, S., Gwack, Y., Prakriya, M., Srikanth, S., Puppel, S.H., Tanasa, B., Hogan, P.G., Lewis, R.S., Daly, M., Rao, A., 2006. A mutation in Orai1 causes immune deficiency by abrogating CRAC channel function. Nature 441, 179-185.

Fewtrell, C., Kessler, A., Metzger, H.,, 1979. Comparative aspects of secretion from tumor and normal mast cells. Advances in Inflammmation Reserach, 205-221.

Fischer, A., 2017. FDA in Brief. https://www.fda.gov/NewsEvents/Newsroom/FDAInBrief/ucm589474.htm.

Fluckiger, A.C., Li, Z.M., Kato, R.M., Wahl, M.I., Ochs, H.D., Longnecker, R., Kinet, J.P., Witte, O.N., Scharenberg, A.M., Rawlings, D.J., 1998. Btk/Tec kinases regulate sustained increases in intracellular Ca2+ following B-cell receptor activation. Embo Journal 17, 1973-1985.

Frederiksen, H., Nielsen, J.K., Morck, T.A., Hansen, P.W., Jensen, J.F., Nielsen, O., Andersson, A.M., Knudsen, L.E., 2013. Urinary excretion of phthalate metabolites, phenols and parabens in rural and urban Danish mother-child pairs. Int J Hyg Environ Health 216, 772-783.

Furumoto, Y., Gonzalez-Espinosa, C., Gomez, G., Kovarova, M., Odom, S., Parravicini, V., Ryan, J.J., Rivera, J., 2004. Rethinking the role of Src family protein tyrosine kinases in the allergic response - New insights on the functional coupling of the high affinity IgE receptor. Immunologic Research 30, 241-253.

Furuno, T., Shinkai, N., Inoh, Y., Nakanishi, M., 2015. Impaired expression of the mitochondrial calcium uniporter suppresses mast cell degranulation. Molecular and cellular biochemistry 410, 215-221.

Gadi, D., Wagenknecht-Wiesner, A., Holowka, D., Baird, B., 2011. Sequestration of phosphoinositides by mutated MARCKS effector domain inhibits stimulated Ca(2+) mobilization and degranulation in mast cells. Mol Biol Cell 22, 4908-4917.

Galli, S.J., Grimbaldeston, M., Tsai, M., 2008. Immunomodulatory mast cells: negative, as well as positive, regulators of immunity. Nature Reviews Immunology 8, 478-486.

Galli, S.J., Kalesnikoff, J., Grimbaldeston, M.A., Piliponsky, A.M., Williams, C.M., Tsai, M., 2005a. Mast cells as "tunable" effector and immunoregulatory cells: recent advances. Annu Rev Immunol 23, 749-786.

Galli, S.J., Nakae, S., Tsai, M., 2005b. Mast cells in the development of adaptive immune responses. Nature Immunology 6, 135-142.

Garcia, G.R., Noyes, P.D., Tanguay, R.L., 2016. Advancements in zebrafish applications for 21st century toxicology. Pharmacology & Therapeutics 161, 11-21.

George, C.M., Brooks, W.A., Graziano, J.H., Nonyane, B.A., Hossain, L., Goswami, D., Zaman, K., Yunus, M., Khan, A.F., Jahan, Y., Ahmed, D., Slavkovich, V., Higdon, M., Deloria-Knoll, M., KL, O.B., 2015. Arsenic exposure is associated with pediatric pneumonia in rural Bangladesh: a case control study. Environ Health 14, 83.

Giannone, G., Dubin-Thaler, B.J., Rossier, O., Cai, Y., Chaga, O., Jiang, G., Beaver, W., Dobereiner, H.G., Freund, Y., Borisy, G., Sheetz, M.P., 2007. Lamellipodial actin mechanically links myosin activity with adhesion-site formation. Cell 128, 561-575.

Gibert, Y., McGee, S.L., Ward, A.C., 2013. Metabolic profile analysis of zebrafish embryos. Journal of visualized experiments : JoVE, e4300.

Gilbert-Diamond, D., Li, Z., Perry, A.E., Spencer, S.K., Gandolfi, A.J., Karagas, M.R., 2013. A population-based case-control study of urinary arsenic species and squamous cell carcinoma in New Hampshire, USA. Environ Health Perspect 121, 1154-1160.

Girolamo, F., Coppola, C., Ribatti, D., 2017. Immunoregulatory effect of mast cells influenced by microbes in neurodegenerative diseases. Brain Behav Immun 65, 68-89.

Gounaris, E., Erdman, S.E., Restaino, C., Gurish, M.F., Friend, D.S., Gounari, F., Lee, D.M., Zhang, G., Glickman, J.N., Shin, K., Rao, V.P., Poutahidis, T., Weissleder, R., McNagny, K.M., Khazaie, K., 2007. Mast cells are an essential hematopoietic component for polyp development. Proceedings of the National Academy of Sciences of the United States of America 104, 19977-19982.

Goussetis, D.J., Platanias, L.C., 2010. Arsenic trioxide and the phosphoinositide 3-kinase/akt pathway in chronic lymphocytic leukemia. Clin Cancer Res 16, 4311-4312.

Graff, J.M., Gordon, J.I., Blackshear, P.J., 1989. Myristoylated and nonmyristoylated forms of a protein are phosphorylated by protein kinase C. Science 246, 503-506.

Graff, J.M., Stumpo, D.J., Blackshear, P.J., 1989b. Characterization of the phosphorylation sites in the chicken and bovine myristoylated alanine-rich C kinase substrate protein, a prominent cellular substrate for protein kinase C. The Journal of biological chemistry 264, 11912-11919.

Grau-Perez, M., Kuo, C.C., Spratlen, M., Thayer, K.A., Mendez, M.A., Hamman, R.F., Dabelea, D., Adgate, J.L., Knowler, W.C., Bell, R.A., Miller, F.W., Liese, A.D., Zhang, C., Douillet, C., Drobna, Z., Mayer-Davis, E.J., Styblo, M., Navas-Acien, A., 2017. The Association of Arsenic Exposure and Metabolism With Type 1 and Type 2 Diabetes in Youth: The SEARCH Case-Control Study. Diabetes Care 40, 46-53.

Grice, H.C., Goldsmith, L.A., 2000. Sucralose--an overview of the toxicity data. Food Chem Toxicol 38 Suppl 2, S1-6.

Gruber, B.L., Marchese, M.J., Suzuki, K., Schwartz, L.B., Okada, Y., Nagase, H., Ramamurthy, N.S., 1989. Synovial procollagenase activation by human mast cell tryptase dependence upon matrix metalloproteinase 3 activation. The Journal of clinical investigation 84, 1657-1662.

Gu, H., Saito, K., Klaman, L.D., Shen, J., Fleming, T., Wang, Y., Pratt, J.C., Lin, G., Lim, B., Kinet, J.P., Neel, B.G., 2001. Essential role for Gab2 in the allergic response. Nature 412, 186-190.

Guha Mazumder, D., Purkayastha, I., Ghose, A., Mistry, G., Saha, C., Nandy, A.K., Das, A., Majumdar, K.K., 2012. Hypertension in chronic arsenic exposure: A case control study in West Bengal. Journal of environmental science and health. Part A, Toxic/hazardous substances & environmental engineering 47, 1514-1520.

Guillemot, J.C., Montcourrier, P., Vivier, E., Davoust, J., Chavrier, P., 1997. Selective control of membrane ruffling and actin plaque assembly by the Rho GTPases Rac1 and CDC42 in Fc epsilon RI-activated rat basophilic leukemia (RBL-2H3) cells. Journal of Cell Science 110, 2215-2225.

Guo, B.Z., Xu, G., Cao, Y.G., Holbrook, C.C., Lynch, R.E., 2006. Identification and characterization of phospholipase D and its association with drought susceptibilities in peanut (Arachis hypogaea). Planta 223, 512-520.

Guo, Z.H., Turner, C., Castle, D., 1998. Relocation of the t-SNARE SNAP-23 from lamellipodia-like cell surface projections regulates compound exocytosis in mast cells. Cell 94, 537-548.

Hallgren, J., Estrada, S., Karlson, U., Alving, K., Pejler, G., 2001. Heparin antagonists are potent inhibitors of mast cell tryptase. Biochemistry 40, 7342-7349.

Hammond, S.M., Altshuller, Y.M., Sung, T.C., Rudge, S.A., Rose, K., Engebrecht, J., Morris, A.J., Frohman, M.A., 1995. Human ADP-ribosylation factor-activated phosphatidylcholine-specific phospholipase D defines a new and highly conserved gene family. The Journal of biological chemistry 270, 29640-29643.

Hammond, S.M., Jenco, J.M., Nakashima, S., Cadwallader, K., Gu, Q., Cook, S., Nozawa, Y., Prestwich, G.D., Frohman, M.A., Morris, A.J., 1997. Characterization of two alternately spliced forms of phospholipase D1. Activation of the purified enzymes by phosphatidylinositol 4,5-bisphosphate, ADP-ribosylation factor, and Rho family

monomeric GTP-binding proteins and protein kinase C-alpha. The Journal of biological chemistry 272, 3860-3868.

Hanson, D.A., Ziegler, S.F., 2002. Regulation of ionomycin-mediated granule release from rat basophil leukemia cells. Molecular Immunology 38, 1329-1335.

Hanstein, W.G., 1976. Uncoupling of oxidative phosphorylation. Biochim Biophys Acta 456, 129-148.

Hartmann, T., Ruoss, S.J., Raymond, W.W., Seuwen, K., Caughey, G.H., 1992. Human tryptase as a potent, cell-specific mitogen: role of signaling pathways in synergistic responses. Am J Physiol 262, L528-534.

Harvey, B., Kelley, R.N., Ashwood-Smith, M.J., 1983. Permeability of intact and dechorionated zebra fish embryos to glycerol and dimethyl sulfoxide. Cryobiology 20, 432-439.

Hawkins, P.T., Eguinoa, A., Qiu, R.G., Stokoe, D., Cooke, F.T., Walters, R., Wennstrom, S., Claessonwelsh, L., Evans, T., Symons, M., Stephens, L., 1995. PDGF stimulates an increase in GTP-RAC via activation of phosphoinositide 3-kinase. Current Biology 5, 393-403.

Hawliczek, A., Nota, B., Cenijn, P., Kamstra, J., Pieterse, B., Winter, R., Winkens, K., Hollert, H., Segner, H., Legler, J., 2012. Developmental toxicity and endocrine disrupting potency of 4-azapyrene, benzo[b]fluorene and retene in the zebrafish Danio rerio. Reprod Toxicol 33, 213-223.

Heck, J.E., Andrew, A.S., Onega, T., Rigas, J.R., Jackson, B.P., Karagas, M.R., Duell, E.J., 2009. Lung cancer in a U.S. population with low to moderate arsenic exposure. Environ Health Perspect 117, 1718-1723.

Hei, T.K., Liu, S.X., Waldren, C., 1998. Mutagenicity of arsenic in mammalian cells: Role of reactive oxygen species. Proceedings of the National Academy of Sciences of the United States of America 95, 8103-8107.

Henage, L.G., Exton, J.H., Brown, H.A., 2006. Kinetic analysis of a mammalian phospholipase D: allosteric modulation by monomeric GTPases, protein kinase C, and polyphosphoinositides. The Journal of biological chemistry 281, 3408-3417.

Heo, W.D., Inoue, T., Park, W.S., Kim, M.L., Park, B.O., Wandless, T.J., Meyer, T., 2006. PI(3,4,5)P3 and PI(4,5)P2 lipids target proteins with polybasic clusters to the plasma membrane. Science 314, 1458-1461.

Heytler, P.G., Prichard, W.W., 1962. A new class of uncoupling agents--carbonyl cyanide phenylhydrazones. Biochem Biophys Res Commun 7, 272-275.

Hines, C., 2002. The diverse effects of mast cell mediators. Clinical reviews in allergy & immunology 22, 149-160.

Hirasawa, N., Santini, F., Beaven, M.A., 1995. Activation of the mitogen-activated protein kinase/cytosolic phospholipase A2 pathway in a rat mast cell line. Indications of different pathways for release of arachidonic acid and secretory granules. J Immunol 154, 5391-5402.

Hitomi, T., Zhang, J., Nicoletti, L.M., Grodzki, A.C., Jamur, M.C., Oliver, C., Siraganian, R.P., 2004. Phospholipase D1 regulates high-affinity IgE receptor-induced mast cell degranulation. Blood 104, 4122-4128.

Hogan, P.G., Lewis, R.S., Rao, A., 2010. Molecular Basis of Calcium Signaling in Lymphocytes: STIM and ORAI. In Paul, W.E., Littman, D.R., Yokoyama, W.M., (Eds.), Annual Review of Immunology, Vol 28, pp. 491-533.

Holowka, D., Sheets, E.D., Baird, B., 2000. Interactions between Fc epsilon RI and lipid raft components are regulated by the actin cytoskeleton. Journal of Cell Science 113, 1009-1019.

Hopenhayn-Rich, C., Biggs, M.L., Smith, A.H., 1998. Lung and kidney cancer mortality associated with arsenic in drinking water in Cordoba, Argentina. Int J Epidemiol 27, 561-569.

Howe, K., Clark, M.D., Torroja, C.F., Torrance, J., Berthelot, C., Muffato, M., Collins, J.E., Humphray, S., McLaren, K., Matthews, L., McLaren, S., Sealy, I., Caccamo, M., Churcher, C., Scott, C., Barrett, J.C., Koch, R., Rauch, G.J., White, S., Chow, W., Kilian, B., Quintais, L.T., Guerra-Assuncao, J.A., Zhou, Y., Gu, Y., Yen, J., Vogel, J.H., Eyre, T., Redmond, S., Banerjee, R., Chi, J., Fu, B., Langley, E., Maguire, S.F., Laird, G.K., Lloyd, D., Kenyon, E., Donaldson, S., Sehra, H., Almeida-King, J., Loveland, J., Trevanion, S., Jones, M., Quail, M., Willey, D., Hunt, A., Burton, J., Sims, S., McLay, K., Plumb, B., Davis, J., Clee, C., Oliver, K., Clark, R., Riddle, C., Elliot, D., Threadgold, G., Harden, G., Ware, D., Begum, S., Mortimore, B., Kerry, G., Heath, P., Phillimore, B., Tracey, A., Corby, N., Dunn, M., Johnson, C., Wood, J., Clark, S., Pelan, S., Griffiths, G., Smith, M., Glithero, R., Howden, P., Barker, N., Lloyd, C., Stevens, C., Harley, J., Holt, K., Panagiotidis, G., Lovell, J., Beasley, H., Henderson, C., Gordon, D., Auger, K., Wright, D., Collins, J., Raisen, C., Dyer, L., Leung, K., Robertson, L., Ambridge, K., Leongamornlert, D., McGuire, S., Gilderthorp, R., Griffiths, C., Manthravadi, D., Nichol, S., Barker, G., Whitehead, S., Kay, M., Brown, J., Murnane, C., Gray, E., Humphries, M., Sycamore, N., Barker, D., Saunders, D., Wallis, J., Babbage, A., Hammond, S., Mashreghi-Mohammadi, M., Barr, L., Martin, S., Wray, P., Ellington, A., Matthews, N., Ellwood, M., Woodmansey, R., Clark, G., Cooper, J., Tromans, A., Grafham, D., Skuce, C., Pandian, R., Andrews, R., Harrison, E., Kimberley, A., Garnett, J., Fosker, N., Hall, R., Garner, P., Kelly, D., Bird, C., Palmer, S., Gehring, I., Berger, A., Dooley, C.M., Ersan-Urun, Z., Eser, C., Geiger, H., Geisler, M., Karotki, L., Kirn, A., Konantz, J., Konantz, M., Oberlander, M., Rudolph-Geiger, S., Teucke, M., Lanz, C., Raddatz, G., Osoegawa, K., Zhu, B., Rapp, A., Widaa, S., Langford, C., Yang, F., Schuster, S.C., Carter, N.P., Harrow, J., Ning, Z., Herrero, J., Searle, S.M., Enright, A., Geisler, R., Plasterk, R.H., Lee, C., Westerfield, M., de Jong, P.J., Zon, L.I., Postlethwait, J.H., Nusslein-Volhard, C., Hubbard, T.J., Roest Crollius, H., Rogers, J., Stemple, D.L.,

2013. The zebrafish reference genome sequence and its relationship to the human genome. Nature 496, 498-503.

Hsueh, Y.M., Chung, C.J., Shiue, H.S., Chen, J.B., Chiang, S.S., Yang, M.H., Tai, C.W., Su, C.T., 2009. Urinary arsenic species and CKD in a Taiwanese population: a case-control study. Am J Kidney Dis 54, 859-870.

Hua, R., Zhou, Y., Wu, B., Huang, Z., Zhu, Y., Song, Y., Yu, Y., Li, H., Quan, S., 2017. Urinary triclosan concentrations and early outcomes of in vitro fertilization-embryo transfer. Reproduction 153, 319-325.

Huang, L., Wang, C., Zhang, Y., Li, J., Zhong, Y., Zhou, Y., Chen, Y., Zuo, Z., 2012. Benzo[a]pyrene exposure influences the cardiac development and the expression of cardiovascular relative genes in zebrafish (Danio rerio) embryos. Chemosphere 87, 369-375.

Huang, R.Y., Blom, T., Hellman, L., 1991. Cloning and structural analysis of MMCP-1, MMCP-4 and MMCP-5, three mouse mast cell-specific serine proteases. European journal of immunology 21, 1611-1621.

Huang, Y.L., Hsueh, Y.M., Huang, Y.K., Yip, P.K., Yang, M.H., Chen, C.J., 2009. Urinary arsenic methylation capability and carotid atherosclerosis risk in subjects living in arsenicosis-hyperendemic areas in southwestern Taiwan. Sci Total Environ 407, 2608-2614.

Hui, L., Zheng, Y., Yan, Y., Bargonetti, J., Foster, D.A., 2006. Mutant p53 in MDA-MB-231 breast cancer cells is stabilized by elevated phospholipase D activity and contributes to survival signals generated by phospholipase D. Oncogene 25, 7305-7310.

Hutchinson, L.M., Trinh, B.M., Palmer, R.K., Preziosi, C.A., Pelletier, J.H., Nelson, H.M., Gosse, J.A., 2011. Inorganic arsenite inhibits IgE receptor-mediated degranulation of mast cells. J Appl Toxicol 31, 231-241.

Hwang, J., Suh, S.S., Park, M., Park, S.Y., Lee, S., Lee, T.K., 2017. Differential gene expression patterns during embryonic development of sea urchin exposed to triclosan. Environ Toxicol 32, 426-433.

Ide, H., Itoh, H., Tomita, M., Murakumo, Y., Kobayashi, T., Maruyama, H., Osada, Y., Nawa, Y., 1995. cDNA sequencing and expression of rat mast cell tryptase. Journal of Biochemistry 118, 210-215.

Irani, A.A., Schechter, N.M., Craig, S.S., Deblois, G., Schwartz, L.B., 1986. Two types of human mast-cells that have distinct neutral protease compositions. Proceedings of the National Academy of Sciences of the United States of America 83, 4464-4468.

Ishiai, M., Kurosaki, M., Inabe, K., Chan, A.C., Sugamura, K., Kurosaki, T., 2000. Involvement of LAT, Gads, and Grb2 in compartmentation of SLP-76 to the plasma membrane. Journal of Experimental Medicine 192, 847-856.

Jackson-Browne, M.S., Papandonatos, G.D., Chen, A., Calafat, A.M., Yolton, K., Lanphear, B.P., Braun, J.M., 2018. Identifying Vulnerable Periods of Neurotoxicity to Triclosan Exposure in Children. Environ Health Perspect 126, 057001.

Jaken, S., Parker, P.J., 2000. Protein kinase C binding partners. BioEssays : news and reviews in molecular, cellular and developmental biology 22, 245-254.

James, K.A., Marshall, J.A., Hokanson, J.E., Meliker, J.R., Zerbe, G.O., Byers, T.E., 2013. A case-cohort study examining lifetime exposure to inorganic arsenic in drinking water and diabetes mellitus. Environ Res 123, 33-38.

Jensen, B.M., Dissing, S., Skov, P.S., Poulsen, L.K., 2005. A comparative study of the FcepsilonRI molecule on human mast cell and basophil cell lines. International archives of allergy and immunology 137, 93-103.

Johnson, A.R., Moran, N.C., 1969. Selective release of histamine from rat mast cells by compound 48-80 and anitgen. Am J Physiol 216, 453-459.

Jones, R.D., Jampani, H.B., Newman, J.L., Lee, A.S., 2000. Triclosan: A review of effectiveness and safety in health care settings. American Journal of Infection Control 28, 184-196.

Jurewicz, J., Radwan, M., Wielgomas, B., Kaluzny, P., Klimowska, A., Radwan, P., Hanke, W., 2018. Environmental levels of triclosan and male fertility. Environ Sci Pollut Res Int 25, 5484-5490.

Kais, B., Schneider, K.E., Keiter, S., Henn, K., Ackermann, C., Braunbeck, T., 2013. DMSO modifies the permeability of the zebrafish (Danio rerio) chorion-implications for the fish embryo test (FET). Aquat Toxicol 140-141, 229-238.

Kalesnikoff, J., Galli, S.J., 2008. New developments in mast cell biology. Nat Immunol 9, 1215-1223.

Kang, M., Othmer, H.G., 2007. The variety of cytosolic calcium responses and possible roles of PLC and PKC. Phys Biol 4, 325-343.

Kelly, K.A., Hill, M.R., Youkhana, K., Wanker, F., Gimble, J.M., 1994. Dimethyl-sulfoxide modulates NF-Kappa-B and cytokine activation in lipopolysaccharide-treated murine macrophages. Infect. Immun. 62, 3122-3128.

Kennedy, R.H., 2013. Effects of endocrine disrupting chemicals on mast cell function, Electronic Theses and Dissertations. University of Maine, pp.

Kettner, A., Pivniouk, V., Kumar, L., Falet, H., Lee, J.S., Mulligan, R., Geha, R.S., 2003. Structural requirements of SLP-76 in signaling via the high-affinity immunoglobulin E receptor (Fc epsilon RI) in mast cells. Molecular and Cellular Biology 23, 2395-2406.

Kheifets, V., Bright, R., Inagaki, K., Schechtman, D., Mochly-Rosen, D., 2006. Protein kinase C delta (deltaPKC)-annexin V interaction: a required step in deltaPKC translocation and function. The Journal of biological chemistry 281, 23218-23226.

Kienle, C., Kohler, H.R., Gerhardt, A., 2009. Behavioural and developmental toxicity of chlorpyrifos and nickel chloride to zebrafish (Danio rerio) embryos and larvae. Ecotoxicol Environ Saf 72, 1740-1747.

Kim, K., Park, H., Yang, W., Lee, J.H., 2011. Urinary concentrations of bisphenol A and triclosan and associations with demographic factors in the Korean population. Environ Res 111, 1280-1285.

Kim, M.J., Kang, K.H., Kim, C.H., Choi, S.Y., 2008. Real-time imaging of mitochondria in transgenic zebrafish expressing mitochondrially targeted GFP. Biotechniques 45, 331-334.

Kim, T.H., Seo, J.W., Hong, Y.S., Song, K.H., 2017. Case-control study of chronic low-level exposure of inorganic arsenic species and non-melanoma skin cancer. J Dermatol 44, 1374-1379.

Kim, Y., Han, J.M., Park, J.B., Lee, S.D., Oh, Y.S., Chung, C., Lee, T.G., Kim, J.H., Park, S.K., Yoo, J.S., Suh, P.G., Ryu, S.H., 1999. Phosphorylation and activation of phospholipase D1 by protein kinase C in vivo: determination of multiple phosphorylation sites. Biochemistry 38, 10344-10351.

Kimura, N., Shiraishi, S., Mizunashi, K., Ohtsu, H., Kimura, I., 2001. Synaptotagmin I expression in mast cells of normal human tissues, systemic mast cell disease, and a human mast cell leukemia cell line. J Histochem Cytochem 49, 341-346.

Kinet, J.P., 1999. The high-affinity IgE receptor (Fc epsilon RI): from physiology to pathology. Annu Rev Immunol 17, 931-972.

Kinet, J.P., Perez-Montfort, R., Metzger, H., 1983. Covalent cross-linking of subunits of the receptor for immunoglobulin E induced by immunoprecipitation. Biochemistry 22, 5729-5732.

Kitaura, J., Asai, K., Maeda-Yamamoto, M., Kawakami, Y., Kikkawa, U., Kawakami, T., 2000. Akt-dependent cytokine production in mast cells. Journal of Experimental Medicine 192, 729-739.

Kopeć, A., Panaszek, B., Fal, A.M., 2006. Intracellular signaling pathways in IgE-dependent mast cell activation. Archivum Immunologiae Et Therapiae Experimentalis 54, 393-401.

Koyasu, S., 2003. The role of PI3K in immune cells. Nat Immunol 4, 313-319.

Kraft, A.S., Anderson, W.B., 1983. Phorbol esters increase the amount of Ca2+, phospholipid-dependent protein kinase associated with plasma membrane. Nature 301, 621-623.

Kraft, S., Kinet, J.P., 2007. New developments in Fc epsilon RI regulation, function and inhibition. Nature Reviews Immunology 7, 365-378.

Kraus, T., Quidenus, G., Schaller, K.H., 2000. Normal values for arsenic and selenium concentrations in human lung tissue. Arch Environ Contam Toxicol 38, 384-389.

Kuby, J., 1997. Immunology. W.H. Freeman, New York.

Kux, L., 2016. Federal Register Vol. 81 No. 126.

Kuznetsov, A.V., Margreiter, R., Amberger, A., Saks, V., Grimm, M., 2011. Changes in mitochondrial redox state, membrane potential and calcium precede mitochondrial dysfunction in doxorubicin-induced cell death. Biochim Biophys Acta 1813, 1144-1152.

Lagunoff, D., Martin, T.W., Read, G., 1983. Agents that release histamine from mast cells. Annual review of pharmacology and toxicology 23, 331-351.

Lam, N.T., Currie, P.D., Lieschke, G.J., Rosenthal, N.A., Kaye, D.M., 2012. Nerve growth factor stimulates cardiac regeneration via cardiomyocyte proliferation in experimental heart failure. PLoS One 7, e53210.

Land, M., Rubin, C.S., 2017. A Calcium- and Diacylglycerol-Stimulated Protein Kinase C (PKC), Caenorhabditis elegans PKC-2, Links Thermal Signals to Learned Behavior by Acting in Sensory Neurons and Intestinal Cells. Mol Cell Biol 37.

Langheinrich, U., 2003. Zebrafish: a new model on the pharmaceutical catwalk. BioEssays : news and reviews in molecular, cellular and developmental biology 25, 904-912.

Lassen, T.H., Frederiksen, H., Kyhl, H.B., Swan, S.H., Main, K.M., Andersson, A.M., Lind, D.V., Husby, S., Wohlfahrt-Veje, C., Skakkebaek, N.E., Jensen, T.K., 2016. Prenatal Triclosan Exposure and Anthropometric Measures Including Anogenital Distance in Danish Infants. Environ Health Perspect 124, 1261-1268.

Lavens, S.E., Proud, D., Warner, J.A., 1993. A sensitive colorimetric assay for the release of tryptase from human lung mast-cells in-vitro. Journal of Immunological Methods 166, 93-102.

Le Trong, H., Parmelee, D.C., Walsh, K.A., Neurath, H., Woodbury, R.G., 1987. Amino acid sequence of rat mast cell protease I (chymase). Biochemistry 26, 6988-6994.

Lee, D.M., Friend, D.S., Gurish, M.F., Benoist, C., Mathis, D., Brenner, M.B., 2002. Mast cells: a cellular link between autoantibodies and inflammatory arthritis. Science 297, 1689-1692.

Lee, H.G., Yang, J.H., 2010. PKC-delta mediates TCDD-induced apoptosis of chondrocyte in ROS-dependent manner. Chemosphere 81, 1039-1044.

Lee, J.H., Kim, Y.M., Kim, N.W., Kim, J.W., Her, E., Kim, B.K., Kim, J.H., Ryu, S.H., Park, J.W., Seo, D.W., Han, J.W., Beaven, M.A., Choi, W.S., 2006. Phospholipase D2 acts as an essential adaptor protein in the activation of Syk in antigen-stimulated mast cells. Blood 108, 956-964.

Lehninger, A.L., Nelson, D.L., Cox, M.M., 2005. Lehninger Principles of Biochemistry. W.H. Freeman and Company, New York, New York.

Leonardi, G., Vahter, M., Clemens, F., Goessler, W., Gurzau, E., Hemminki, K., Hough, R., Koppova, K., Kumar, R., Rudnai, P., Surdu, S., Fletcher, T., 2012. Inorganic arsenic and basal cell carcinoma in areas of Hungary, Romania, and Slovakia: a case-control study. Environ Health Perspect 120, 721-726.

Li, S., Zhao, J., Wang, G., Zhu, Y., Rabito, F., Krousel-Wood, M., Chen, W., Whelton, P.K., 2015. Urinary triclosan concentrations are inversely associated with body mass index and waist circumference in the US general population: Experience in NHANES 2003-2010. Int J Hyg Environ Health 218, 401-406.

Li, X., Ying, G.G., Zhao, J.L., Chen, Z.F., Lai, H.J., Su, H.C., 2013. 4-Nonylphenol, bisphenol-A and triclosan levels in human urine of children and students in China, and the effects of drinking these bottled materials on the levels. Environ Int 52, 81-86.

Liaw, J., Marshall, G., Yuan, Y., Ferreccio, C., Steinmaus, C., Smith, A.H., 2008. Increased childhood liver cancer mortality and arsenic in drinking water in northern Chile. Cancer Epidemiol Biomarkers Prev 17, 1982-1987.

Lieschke, G.J., Currie, P.D., 2007. Animal models of human disease: zebrafish swim into view. Nature Reviews Genetics 8, 353-367.

Lin, P., Fung, W.J., Gilfillan, A.M., 1992. Phosphatidylcholine-specific phospholipase D-derived 1,2-diacylglycerol does not initiate protein kinase C activation in the RBL 2H3 mast-cell line. Biochem J 287 (Pt 1), 325-331.

Lin, P.Y., Gilfillan, A.M., 1992. The role of calcium and protein-kinase-C in the IgE-dependent activation of phosphatidylcholine-specific phospholipase-D in a rat mast (RBL 2H3) cell line. Eur J Biochem 207, 163-168.

Link, V., Shevchenko, A., Heisenberg, C.P., 2006. Proteomics of early zebrafish embryos. BMC developmental biology 6, 1.

Liou, J., Kim, M.L., Heo, W.D., Jones, J.T., Myers, J.W., Ferrell, J.E., Jr., Meyer, T., 2005. STIM is a Ca2+ sensor essential for Ca2+-store-depletion-triggered Ca2+ influx. Curr Biol 15, 1235-1241.

Liscovitch, M., Czarny, M., Fiucci, G., Tang, X., 2000. Phospholipase D: molecular and cell biology of a novel gene family. Biochem J 345 Pt 3, 401-415.

Liu-Mares, W., Mackinnon, J.A., Sherman, R., Fleming, L.E., Rocha-Lima, C., Hu, J.J., Lee, D.J., 2013. Pancreatic cancer clusters and arsenic-contaminated drinking water wells in Florida. BMC Cancer 13, 111.

Liu, S.X., Athar, M., Lippai, I., Waldren, C., Hei, T.K., 2001. Induction of oxyradicals by arsenic: Implication for mechanism of genotoxicity. Proceedings of the National Academy of Sciences of the United States of America 98, 1643-1648.

Logan, M.R., Odemuyiwa, S.O., Moqbel, R., 2003. Understanding exocytosis in immune and inflammatory cells: The molecular basis of mediator secretion. Journal of Allergy and Clinical Immunology 111, 923-932.

Lopez-Lluch, G., Bird, M.M., Canas, B., Godovac-Zimmerman, J., Ridley, A., Segal, A.W., Dekker, L.V., 2001. Protein kinase C-delta C2-like domain is a binding site for actin and enables actin redistribution in neutrophils. Biochem J 357, 39-47.

Lopez, I., Arnold, R.S., Lambeth, J.D., 1998. Cloning and initial characterization of a human phospholipase D2 (hPLD2). ADP-ribosylation factor regulates hPLD2. The Journal of biological chemistry 273, 12846-12852.

Ludowyke, R.I., Elgundi, Z., Kranenburg, T., Stehn, J.R., Schmitz-Peiffer, C., Hughes, W.E., Biden, T.J., 2006. Phosphorylation of nonmuscle myosin heavy chain IIA on Ser1917 is mediated by protein kinase C beta II and coincides with the onset of stimulated degranulation of RBL-2H3 mast cells. J Immunol 177, 1492-1499.

Ludowyke, R.I., Peleg, I., Beaven, M.A., Adelstein, R.S., 1989. Antigen-induced secretion of histamine and the phosphorylation of myosin by protein kinase C in rat basophilic leukemia cells. The Journal of biological chemistry 264, 12492-12501.

Lutzelschwab, C., Pejler, G., Aveskogh, M., Hellman, L., 1997. Secretory granule proteases in rat mast cells. Cloning of 10 different serine proteases and a carboxypeptidase A from various rat mast cell populations. Journal of Experimental Medicine 185, 13-29.

Lv, Y., Rui, C., Dai, Y., Pang, Q., Li, Y., Fan, R., Lu, S., 2016. Exposure of children to BPA through dust and the association of urinary BPA and triclosan with oxidative stress in Guangzhou, China. Environ Sci Process Impacts 18, 1492-1499.

Lyman, F.L., Furia, T.E., 1968. Toxicology of 2,4,4'-trichloro-2'-hydroxyphenyl ether. IMS Ind Med Surg 37, 546.

Lytton, J., Westlin, M., Hanley, M., 1991. Thapsigargin inhibits the sarcoplasmic or endoplasmic reticulum Ca-ATPase family of calcium pumps. The Journal of Biological Chemistry 266, 17067-17071.

Ma, H.T., Beaven, M.A., 2011. Regulators of Ca(2+) signaling in mast cells: Potential Targets for Treatment of Mast Cell-Related Diseases? Mast Cell Biology: Contemporary and Emerging Topics 716, 62-90.

Ma, Y., Han, J., Guo, Y., Lam, P.K., Wu, R.S., Giesy, J.P., Zhang, X., Zhou, B., 2012. Disruption of endocrine function in in vitro H295R cell-based and in in vivo assay in zebrafish by 2,4-dichlorophenol. Aquat Toxicol 106-107, 173-181.

Mahankali, M., Peng, H.J., Cox, D., Gomez-Cambronero, J., 2011. The mechanism of cell membrane ruffling relies on a phospholipase D2 (PLD2), Grb2 and Rac2 association. Cell Signal 23, 1291-1298.

Malaviya, R., Ikeda, T., Ross, E., Abraham, S.N., 1996. Mast cell modulation of neutrophil influx and bacterial clearance at sites of infection through TNF-alpha. Nature 381, 77-80.

Marchini-Alves, C.M., Nicoletti, L.M., Mazucato, V.M., de Souza, L.B., Hitomi, T., Alves Cde, P., Jamur, M.C., Oliver, C., 2012. Phospholipase D2: a pivotal player modulating RBL-2H3 mast cell structure. J Histochem Cytochem 60, 386-396.

Marshall, N.B., Lukomska, E., Long, C.M., Kashon, M.L., Sharpnack, D.D., Nayak, A.P., Anderson, K.L., Jean Meade, B., Anderson, S.E., 2015. Triclosan Induces Thymic Stromal Lymphopoietin in Skin Promoting Th2 Allergic Responses. Toxicol Sci 147, 127-139.

Marti-Verdeaux, S., Pombo, I., Iannascoli, B., Roa, M., Varin-Blank, N., Rivera, J., Blank, U., 2003. Evidence of a role for Munc18-2 and microtubules in mast cell granule exocytosis. Journal of Cell Science 116, 325-334.

Maull, E.A., Ahsan, H., Edwards, J., Longnecker, M.P., Navas-Acien, A., Pi, J.B., Silbergeld, E.K., Styblo, M., Tseng, C.H., Thayer, K.A., Loomis, D., 2012. Evaluation of the Association between Arsenic and Diabetes: A National Toxicology Program Workshop Review. Environmental Health Perspectives 120, 1658-1670.

Maurer, M., Wedemeyer, J., Metz, M., Piliponsky, A.M., Weller, K., Chatterjea, D., Clouthier, D.E., Yanagisawa, M.M., Tsai, M., Galli, S.J., 2004. Mast cells promote homeostasis by limiting endothelin-1-induced toxicity. Nature 432, 512-516.

Maxova, H., Bacakova, L., Lisa, V., Novotna, J., Tomasova, H., Vizek, M., Herget, J., 2010. Production of proteolytic enzymes in mast cells, fibroblasts, vascular smooth muscle and endothelial cells cultivated under normoxic or hypoxic conditions. Physiological Research 59, 711-719.

McGrath, P., Li, C.Q., 2008. Zebrafish: a predictive model for assessing drug-induced toxicity. Drug discovery today 13, 394-401.

Melak, D., Ferreccio, C., Kalman, D., Parra, R., Acevedo, J., Perez, L., Cortes, S., Smith, A.H., Yuan, Y., Liaw, J., Steinmaus, C., 2014. Arsenic methylation and lung and bladder cancer in a case-control study in northern Chile. Toxicol Appl Pharmacol 274, 225-231.

Melendez, A.J., Khaw, A.K., 2002. Dichotomy of Ca2+ signals triggered by different phospholipid pathways in antigen stimulation of human mast cells. Journal of Biological Chemistry 277, 17255-17262.

Metcalfe, D.D., 2008. Mast cells and mastocytosis. Blood 112, 946-956.

Metcalfe, D.D., Baram, D., Mekori, Y.A., 1997. Mast cells. Physiological Reviews 77, 1033-1079.

Metzger, H., Alcaraz, G., Hohman, R., Kinet, J.P., Pribluda, V., Quarto, R., 1986. The Receptor With High-Affinity For Immunoglobulin-E. 4, 419-470.

Metzger, H., Goetze, A., Kanellopoulos, J., Holowka, D., Fewtrell, C., 1982. Structure of the high-affinity mast cell receptor for IgE. Federation Proceedings 41, 8-11.

Millard, P.J., Ryan, T.A., Webb, W.W., Fewtrell, C., 1989. Immunoglobulin E receptor cross-linking induces oscillations in intracellular free ionized calcium in individual tumor mast cells. The Journal of biological chemistry 264, 19730-19739.

Milton, A.H., Shahidullah, S.M., Smith, W., Hossain, K.S., Hasan, Z., Ahmed, K.T., 2010. Association between chronic arsenic exposure and nutritional status among the women of child bearing age: a case-control study in Bangladesh. Int J Environ Res Public Health 7, 2811-2821.

Min, D., Shin, M.H., 2009. NADPH oxidase-derived ROS mediates mast cell degranulation induced by secretory products secreted by Trichomonas vaginalis. Journal of Immunology 182, 133.135.

Minamoto, K., Mascie-Taylor, C.G., Moji, K., Karim, E., Rahman, M., 2005. Arsenic-contaminated water and extent of acute childhood malnutrition (wasting) in rural Bangladesh. Environ Sci 12, 283-292.

Minoguchi, K., Benhamou, M., Swaim, W.D., Kawakami, Y., Kawakami, T., Siraganian, R.P., 1994. Activation of protein tyrosine kinase p72syk by Fc epsilon RI aggregation in rat basophilic leukemia cells. p72syk is a minor component but the major protein tyrosine kinase of pp72. The Journal of biological chemistry 269, 16902-16908.

Mizell, M., Romig, E.S., 1997. The aquatic vertebrate embryo as a sentinel for toxins: zebrafish embryo dechorionation and perivitelline space microinjection. Int J Dev Biol 41, 411-423.

Mochly-Rosen, D., Henrich, C.J., Cheever, L., Khaner, H., Simpson, P.C., 1990. A protein kinase C isozyme is translocated to cytoskeletal elements on activation. Cell Regul 1, 693-706.

Mocsai, A., Ruland, J., Tybulewicz, V.L., 2010. The SYK tyrosine kinase: a crucial player in diverse biological functions. Nat Rev Immunol 10, 387-402.

Mogami, H., Zhang, H., Suzuki, Y., Urano, T., Saito, N., Kojima, I., Petersen, O.H., 2003. Decoding of short-lived Ca2+ influx signals into long term substrate phosphorylation through activation of two distinct classes of protein kinase C. The Journal of biological chemistry 278, 9896-9904.

Mondal, D., Hasnain, M.G., Hossain, M.S., Ghosh, D., Ghosh, P., Hossain, H., Baker, J., Nath, R., Haque, R., Matlashewski, G., Hamano, S., 2016. Study on the safety and efficacy of miltefosine for the treatment of children and adolescents with post-kala-azar dermal leishmaniasis in Bangladesh, and an association of serum vitamin E and exposure to arsenic with post-kala-azar dermal leishmaniasis: an open clinical trial and case-control study protocol. BMJ Open 6, e010050.

Mostafa, M.G., Cherry, N., 2013. Arsenic in drinking water and renal cancers in rural Bangladesh. Occup Environ Med 70, 768-773.

Naal, R.M., Tabb, J., Holowka, D., Baird, B., 2004. In situ measurement of degranulation as a biosensor based on RBL-2H3 mast cells. Biosens Bioelectron 20, 791-796.

Nagel, R., 2002. DarT: The embryo test with the Zebrafish Danio rerio--a general model in ecotoxicology and toxicology. Altex 19 Suppl 1, 38-48.

Nakajima, H., Park, H.L., Henkart, P.A., 1995. Synergistic roles of granzymes A and B in mediating target cell death by rat basophilic leukemia mast cell tumors also expressing cytolysin/perforin. Journal of Experimental Medicine 181, 1037-1046.

Nakano, A., Kishi, F., Minami, K., Wakabayashi, H., Nakaya, Y., Kido, H., 1997. Selective conversion of big endothelins to tracheal smooth muscle-constricting 31-amino acid-length endothelins by chymase from human mast cells. J Immunol 159, 1987-1992.

Nakashima, S., Fujimiya, H., Miyata, H., Nozawa, Y., 1991. Antigen-induced biphasic diacylglycerol formation in RBL-2H3 cells: the late sustained phase due to phosphatidylcholine hydrolysis is dependent on protein kinase C. Biochem Biophys Res Commun 177, 336-342.

Naujokas, M.F., Anderson, B., Ahsan, H., Aposhian, H.V., Graziano, J.H., Thompson, C., Suk, W.A., 2013. The broad scope of health effects from chronic arsenic exposure: update on a worldwide public health problem. Environ Health Perspect 121, 295-302.

Nautiyal, K.M., Ribeiro, A.C., Pfaff, D.W., Silver, R., 2008. Brain mast cells link the immune system to anxiety-like behavior. Proceedings of the National Academy of Sciences of the United States of America 105, 18053-18057.

Nechushtan, H., Leitges, M., Cohen, C., Kay, G., Razin, E., 2000. Inhibition of degranulation and interleukin-6 production in mast cells derived from mice deficient in protein kinase Cbeta. Blood 95, 1752-1757.

Nesan, D., Vijayan, M.M., 2012. Embryo exposure to elevated cortisol level leads to cardiac performance dysfunction in zebrafish. Mol Cell Endocrinol 363, 85-91.

Newton, A.C., 1995. Protein kinase C: structure, function, and regulation. The Journal of biological chemistry 270, 28495-28498.

Newton, A.C., 2001. Protein kinase C: structural and spatial regulation by phosphorylation, cofactors, and macromolecular interactions. Chem Rev 101, 2353-2364.

Newton, A.C., 2010. Protein kinase C: poised to signal. Am J Physiol Endocrinol Metab 298, E395-402.

Newton, A.P., Cadena, S.M., Rocha, M.E., Carnieri, E.G., Martinelli de Oliveira, M.B., 2005. Effect of triclosan (TRN) on energy-linked functions of rat liver mitochondria. Toxicol Lett 160, 49-59.

Nilsson, G., Blom, T., Kusche-Gullberg, M., Kjellen, L., Butterfield, J.H., Sundstrom, C., Nilsson, K., Hellman, L., 1994. Phenotypic characterization of the human mast-cell line HMC-1. Scandinavian Journal of Immunology 39, 489-498.

Nishizuka, Y., 1995. Protein kinase C and lipid signaling for sustained cellular responses. Faseb J 9, 484-496.

Noble, S., Godoy, R., Affaticati, P., Ekker, M., 2015. Transgenic Zebrafish Expressing mCherry in the Mitochondria of Dopaminergic Neurons. Zebrafish 12, 349-356.

NRC, 2001. Subcommitte to update 1999 arsenic in drinking water, Arsenic in Drinking Water: 2001 update, National Academic Press, pp. 82-149.

O'Luanaigh, N., Pardo, R., Fensome, A., Allen-Baume, V., Jones, D., Holt, M.R., Cockcroft, S., 2002. Continual production of phosphatidic acid by phospholipase D is essential for antigen-stimulated membrane ruffling in cultured mast cells. Mol Biol Cell 13, 3730-3746.

Oguin, T.H., 3rd, Sharma, S., Stuart, A.D., Duan, S., Scott, S.A., Jones, C.K., Daniels, J.S., Lindsley, C.W., Thomas, P.G., Brown, H.A., 2014. Phospholipase D facilitates efficient entry of influenza virus, allowing escape from innate immune inhibition. The Journal of biological chemistry 289, 25405-25417.

Ogura, T., Shuba, L.M., McDonald, T.F., 1995. Action-potentials, ionic currents and cell water in guinea-pig ventricular preparations exposed to dimethyl-sulfoxide. Journal of Pharmacology and Experimental Therapeutics 273, 1273-1286.

Okkenhaug, K., Vanhaesebroeck, B., 2003. PI3K in lymphocyte development, differentiation and activation. Nat Rev Immunol 3, 317-330.

Oliveira, R., Domingues, I., Koppe Grisolia, C., Soares, A.M., 2009. Effects of triclosan on zebrafish early-life stages and adults. Environ Sci Pollut Res Int 16, 679-688.

Olivera, A., Mizugishi, K., Tikhonova, A., Ciaccia, L., Odom, S., Proia, R.L., Rivera, J., 2007. The sphingosine kinase-sphingosine-1-phosphate axis is a determinant of mast cell function and anaphylaxis. Immunity 26, 287-297.

Olszewski, M.B., Groot, A.J., Dastych, J., Knol, E.F., 2007. TNF trafficking to human mast cell granules: mature chain-dependent endocytosis. J Immunol 178, 5701-5709.

Olszewski, M.B., Trzaska, D., Knol, E.F., Adamczewska, V., Dastych, J., 2006. Efficient sorting of TNF-alpha to rodent mast cell granules is dependent on N-linked glycosylation. Eur J Immunol 36, 997-1008.

On, M., Billingsley, J.M., Jouvin, M.H., Kinet, J.P., 2004. Molecular dissection of the FcRbeta signaling amplifier. The Journal of biological chemistry 279, 45782-45790.

Ong, C.T., Khoo, Y.T., Mukhopadhyay, A., Masilamani, J., Do, D.V., Lim, I.J., Phan, T.T., 2010. Comparative proteomic analysis between normal skin and keloid scar. Br J Dermatol 162, 1302-1315.

Oppedal, D., Goldsmith, M.I., 2010. A chemical screen to identify novel inhibitors of fin regeneration in zebrafish. Zebrafish 7, 53-60.

Ouyang, F., Tang, N., Zhang, H.J., Wang, X., Zhao, S., Wang, W., Zhang, J., Cheng, W., 2018. Maternal urinary triclosan level, gestational diabetes mellitus and birth weight in Chinese women. Sci Total Environ 626, 451-457.

Ozawa, K., Szallasi, Z., Kazanietz, M.G., Blumberg, P.M., Mischak, H., Mushinski, J.F., Beaven, M.A., 1993a. Ca(2+)-dependent and Ca(2+)-independent isozymes of protein kinase C mediate exocytosis in antigen-stimulated rat basophilic RBL-2H3 cells. Reconstitution of secretory responses with Ca2+ and purified isozymes in washed permeabilized cells. The Journal of biological chemistry 268, 1749-1756.

Ozawa, K., Yamada, K., Kazanietz, M.G., Blumberg, P.M., Beaven, M.A., 1993b. Different isozymes of protein kinase C mediate feedback inhibition of phospholipase C and stimulatory signals for exocytosis in rat RBL-2H3 cells. The Journal of biological chemistry 268, 2280-2283.

Pacher, P., Csordas, P., Schneider, T., Hajnoczky, G., 2000. Quantification of calcium signal transmission from sarco-endoplasmic reticulum to the mitochondria. The Journal of physiology 529 Pt 3, 553-564.

Palmer, R.K., Hutchinson, L.M., Burpee, B.T., Tupper, E.J., Pelletier, J.H., Kormendy, Z., Hopke, A.R., Malay, E.T., Evans, B.L., Velez, A., Gosse, J.A., 2012. Antibacterial agent triclosan suppresses RBL-2H3 mast cell function. Toxicology and Applied Pharmacology 258, 99-108.

Paquet, D., Plucinska, G., Misgeld, T., 2014. In vivo imaging of mitochondria in intact zebrafish larvae. Methods in enzymology 547, 151-164.

Park, D.J., Min, H.K., Rhee, S.G., 1991. IgE-induced tyrosine phosphorylation of phospholipase C-gamma 1 in rat basophilic leukemia cells. The Journal of biological chemistry 266, 24237-24240.

Parker, P.J., 1995. Intracellular signaling - PI3-Kinase puts GTP on the Rac. Current Biology 5, 577-579.

Parng, C., 2005. In vivo zebrafish assays for toxicity testing. Current opinion in drug discovery & development 8, 100-106.

Passante, E., Ehrhardt, C., Sheridan, H., Frankish, N., 2009. Toll-like receptors and RBL-2H3 mast cells. Inflammation research : official journal of the European Histamine Research Society ... [et al.] 58 Suppl 1, 11-12.

Patkar, S.A., Rasmussen, U., Diamant, B., 1979. On the mechanism of histamine release induced by thapsigargin from *Thapsia garganica L*. Agents and Actions 9, 53-57.

Paul, S., Das, N., Bhattacharjee, P., Banerjee, M., Das, J.K., Sarma, N., Sarkar, A., Bandyopadhyay, A.K., Sau, T.J., Basu, S., Banerjee, S., Majumder, P., Giri, A.K., 2013. Arsenic-induced toxicity and carcinogenicity: a two-wave cross-sectional study in arsenicosis individuals in West Bengal, India. Journal of Exposure Science and Environmental Epidemiology 23, 156-162.

Paumet, F., Le Mao, J., Martin, S., Galli, T., David, B., Blank, U., Roa, M., 2000. Soluble NSF attachment protein receptors (SNAREs) in RBL-2H3 mast cells: Functional role of syntaxin 4 in exocytosis and identification of a vesicle-associated membrane protein 8-containing secretory compartment. Journal of Immunology 164, 5850-5857.

Pawankar, R., 2005. Mast cells in allergic airway disease and chronic rhinosinusitis. Chemical Immunology and Allergy 87, 111-129.

Pejler, G., Åbrink, M., Ringvall, M., Wernersson, S., 2007. Mast Cell Proteases. In Frederick W. Alt, K.F.A.T.H.F.M.J.W.U., Emil, R.U., (Eds.), Advances in Immunology. Academic Press, pp. 167-255.

Peng, B., He, R., Xu, Q., Gao, J., Lu, Y., Li, J., 2011. Comparison of RBL-2H3 and P815 cell lines for establishing *in vitro* model of mast cell degranulation. Chinese Journal of Natural Medicines 9, 227-231.

Peng, X., Frohman, M.A., 2012. Mammalian phospholipase D physiological and pathological roles. Acta Physiol (Oxf) 204, 219-226.

Peng, Z., Beaven, M.A., 2005. An essential role for phospholipase D in the activation of protein kinase C and degranulation in mast cells. J Immunol 174, 5201-5208.

Pfeiffer, J.R., Seagrave, J.C., Davis, B.H., Deanin, G.G., Oliver, J.M., 1985. Membrane and cytoskeletal changes associated with IgE-mediated serotonin release from rat basophilic leukemia-cells. Journal of Cell Biology 101, 2145-2155.

Pivniouk, V.I., Snapper, S.B., Kettner, A., Alenius, H., Laouini, D., Falet, H., Hartwig, J., Alt, F.W., Geha, R.S., 2003. Impaired signaling via the high-affinity IgE receptor in Wiskott-Aldrich syndrome protein-deficient mast cells. International immunology 15, 1431-1440.

Plasman, K., Demol, H., Bird, P.I., Gevaert, K., Van Damme, P., 2014. Substrate specificities of the granzyme tryptases A and K. Journal of Proteome Research 13, 6067-6077.

Poe, M., Gutfreund, H., Estabrook, R.W., 1967. Kinetic studies of temperature changes and oxygen uptake in a differential calorimeter: the heat of oxidation of NADH and succinate. Archives of biochemistry and biophysics 122, 204-211.

Popova, L.B., Nosikova, E.S., Kotova, E.A., Tarasova, E.O., Nazarov, P.A., Khailova, L.S., Balezina, O.P., Antonenko, Y.N., 2018. Protonophoric action of triclosan causes calcium efflux from mitochondria, plasma membrane depolarization and bursts of miniature end-plate potentials. Biochim Biophys Acta 1860, 1000-1007.

Poriadin, G.V., Baranov, A.P., Leskov, V.P., 1977. [Suppression of the anaphylactic response of isolated smooth muscle organs by potassium arsenite]. Biull Eksp Biol Med 84, 341-343.

Pribluda, V.S., Pribluda, C., Metzger, H., 1994. Transphosphorylation as the mechanism by which the high-affinity receptor for IgE is phosphorylated upon aggregation. Proceedings of the National Academy of Sciences of the United States of America 91, 11246-11250.

Prykhozhij, S.V., Berman, J.N., 2014. The progress and promise of zebrafish as a model to study mast cells. Dev Comp Immunol 46, 74-83.

Puri, N., Roche, P.A., 2008. Mast cells possess distinct secretory granule subsets whose exocytosis is regulated by different SNARE isoforms. Proc Natl Acad Sci U S A 105, 2580-2585.

Putila, J.J., Guo, N.L., 2011. Association of arsenic exposure with lung cancer incidence rates in the United States. PLoS One 6, e25886.

Putney, J.W., Jr., 1986. A model for receptor-regulated calcium entry. Cell Calcium 7, 1-12.

Putney, J.W., Jr., 1990. Capacitative calcium entry revisited. Cell Calcium 11, 611-624.

Putney, J.W., Jr., Broad, L.M., Braun, F.J., Lievremont, J.P., Bird, G.S., 2001. Mechanisms of capacitative calcium entry. J Cell Sci 114, 2223-2229.

Pylatiuk, C., Sanchez, D., Mikut, R., Alshut, R., Reischl, M., Hirth, S., Rottbauer, W., Just, S., 2014. Automatic zebrafish heartbeat detection and analysis for zebrafish embryos. Zebrafish 11, 379-383.

Qian, Y., Castranova, V., Shi, X.L., 2003. New perspectives in arsenic-induced cell signal transduction. Journal of Inorganic Biochemistry 96, 271-278.

Qin, H., Kent, P., Isales, C.M., Parker, P.M., Wilson, M.V., Bollag, W.B., 2009. The role of calcium influx pathways in phospholipase D activation in bovine adrenal glomerulosa cells. J Endocrinol 202, 77-86.

Raftery, T.D., Jayasundara, N., Di Giulio, R.T., 2017. A bioenergetics assay for studying the effects of environmental stressors on mitochondrial function in vivo in zebrafish larvae. Comparative biochemistry and physiology. Toxicology & pharmacology : CBP 192, 23-32.

Rahman, M., Vahter, M., Sohel, N., Yunus, M., Wahed, M.A., Streatfield, P.K., Ekstrom, E.C., Persson, L.A., 2006. Arsenic exposure and age and sex-specific risk for skin lesions: a population-based case-referent study in Bangladesh. Environ Health Perspect 114, 1847-1852.

Rasmussen, U., Christensen, S.B., 1978. Thapsigargine and thapsigargicine, two new histamine liberators from *Thapsia garganica*. Acta Pharmaceutica Suecica 15, 133-140.

Ravetch, J.V., Kinet, J.P., 1991. Fc-receptors. Annual Review of Immunology 9, 457-492.

Reth, M., 1989. Antigen receptor tail clue. Nature 338, 383-384.

Reynolds, D.S., Stevens, R.L., Lane, W.S., Carr, M.H., Austen, K.F., Serafin, W.E., 1990. Different mouse mast cell populations express various combinations of at least six distinct mast cell serine proteases. Proceedings of the National Academy of Sciences of the USA 87, 3230-3234.

Richetti, S.K., Rosemberg, D.B., Ventura-Lima, J., Monserrat, J.M., Bogo, M.R., Bonan, C.D., 2011. Acetylcholinesterase activity and antioxidant capacity of zebrafish brain is altered by heavy metal exposure. Neurotoxicology 32, 116-122.

Rivera, J., Gilfillan, A.M., 2006. Molecular regulation of mast cell activation. The Journal of allergy and clinical immunology 117, 1214-1225; quiz 1226.

Rodewald, H.R., Dessing, M., Dvorak, A.M., Galli, S.J., 1996. Identification of a committed precursor for the mast cell lineage. Science 271, 818-822.

Rodricks, J.V., Swenberg, J.A., Borzelleca, J.F., Maronpot, R.R., Shipp, A.M., 2010. Triclosan: a critical review of the experimental data and development of margins of safety for consumer products. Critical reviews in toxicology 40, 422-484.

Roos, J., DiGregorio, P.J., Yeromin, A.V., Ohlsen, K., Lioudyno, M., Zhang, S., Safrina, O., Kozak, J.A., Wagner, S.L., Cahalan, M.D., Velicelebi, G., Stauderman, K.A., 2005. STIM1, an essential and conserved component of store-operated Ca2+ channel function. J Cell Biol 169, 435-445.

Rother, K.I., Sylvetsky, A.C., Walter, P.J., Garraffo, H.M., Fields, D.A., 2018. Pharmacokinetics of Sucralose and Acesulfame-Potassium in Breast Milk Following Ingestion of Diet Soda. J Pediatr Gastroenterol Nutr 66, 466-470.

Rover, J.A., Leu-Wai-See, P., 2014. Role of Colgate Total toothpaste in helping control plaque and gingivitis. Am J Dent 27, 167-170.

Rozniecki, J.J., Hauser, S.L., Stein, M., Lincoln, R., Theoharides, T.C., 1995. Elevated mast cell tryptase in cerebrospinal fluid of multiple sclerosis patients. Annals of Neurology 37, 63-66.

Rumenapp, U., Geiszt, M., Wahn, F., Schmidt, M., Jakobs, K.H., 1995. Evidence for ADP-ribosylation-factor-mediated activation of phospholipase D by m3 muscarinic acetylcholine receptor. Eur J Biochem 234, 240-244.

Ruszkiewicz, J.A., Li, S., Rodriguez, M.B., Aschner, M., 2017. Is Triclosan a neurotoxic agent? J Toxicol Environ Health B Crit Rev 20, 104-117.

Sachidanandan, C., Yeh, J.R., Peterson, Q.P., Peterson, R.T., 2008. Identification of a novel retinoid by small molecule screening with zebrafish embryos. PLoS One 3, e1947.

Sadroddiny, E., Ai, J., Carroll, K., Pham, T.K., Wright, P., Pathak, A., Helm, B., 2012a. Protein profiling of the secretome of FcepsilonRI activated RBL-2H3.1 cells. Iranian Journal of Immunology 9, 1-31.

Sadroddiny, E., Moir, A.J., Helm, B.A., 2012b. A proteomics approach to the study of the molecular consequence of IgE-mediated cell signalling in RBL-2H3.1 cells and 2D reference map preparation for the RBL-2H3.1 cell line. Cell Biology International 36, 397-401.

Saint-Jacques, N., Parker, L., Brown, P., Dummer, T.J., 2014. Arsenic in drinking water and urinary tract cancers: a systematic review of 30 years of epidemiological evidence. Environ Health 13, 44.

Saitoh, S., Odom, S., Gomez, G., Sommers, C.L., Young, H.A., Rivera, J., Samelson, L.E., 2003. The four distal tyrosines are required for LAT-dependent signaling in Fc epsilon RI-mediated mast cell activation. Journal of Experimental Medicine 198, 831-843.

Scharenberg, A.M., Humphries, L.A., Rawlings, D.J., 2007. Calcium signalling and cell-fate choice in B cells. Nature Reviews Immunology 7, 778-789.

Scharenberg, A.M., Kinet, J.P., 1998. PtdIns-3,4,5-P3: a regulatory nexus between tyrosine kinases and sustained calcium signals. Cell 94, 5-8.

Scholz, S., Fischer, S., Gundel, U., Kuster, E., Luckenbach, T., Voelker, D., 2008. The zebrafish embryo model in environmental risk assessment--applications beyond acute toxicity testing. Environ Sci Pollut Res Int 15, 394-404.

Schroeder, H., Kanisawa, M., Frost, D.V., Mitchene.M, 1968. Germanium Tin And Arsenic In Rats - Effects On Growth Survival Pathological Lesions And Life Span. 96, 37-&.

Schwartz, L.B., 1990. Tryptase, a mediator of human mast cells. The Journal of allergy and clinical immunology 86, 594-598.

Schwartz, L.B., Austen, K.F., 1980. Enzymes of the mast cell granule. Journal of Investigative Dermatology 74, 349-353.

Schwartz, L.B., Austen, K.F., Wasserman, S.I., 1979. Immunologic release of beta-hexosaminidase and beta-glucuronidase from purified rat serosal mast cells. Journal of immunology 123, 1445-1450.

Schwartz, L.B., Irani, A.M., Roller, K., Castells, M.C., Schechter, N.M., 1987. Quantitation of histamine, tryptase, and chymase in dispersed human T and TC mast cells. Journal of immunology 138, 2611-2615.

Schwartz, L.B., Lewis, R.A., Seldin, D., Austen, K.F., 1981. Acid hydrolases and tryptase from secretory granules of dispersed human lung mast cells. Journal of immunology 126, 1290-1294.

Sciorra, V.A., Rudge, S.A., Wang, J., McLaughlin, S., Engebrecht, J., Morris, A.J., 2002. Dual role for phosphoinositides in regulation of yeast and mammalian phospholipase D enzymes. J Cell Biol 159, 1039-1049.

Seldin, D.C., Adelman, S., Austen, K.F., Stevens, R.L., Hein, A., Caulfield, J.P., Woodbury, R.G., 1985. Homology of the rat basophilic leukemia cell and the rat mucosal mast cell. Proceedings of the National Academy of Sciences of the USA 82, 3871-3875.

Selvy, P.E., Lavieri, R.R., Lindsley, C.W., Brown, H.A., 2011. Phospholipase D: enzymology, functionality, and chemical modulation. Chem Rev 111, 6064-6119.

Senger, M.R., Rosemberg, D.B., Seibt, K.J., Dias, R.D., Bogo, M.R., Bonan, C.D., 2010. Influence of mercury chloride on adenosine deaminase activity and gene expression in zebrafish (Danio rerio) brain. Neurotoxicology 31, 291-296.

Senyshyn, J., Baumgartner, R.A., Beaven, M.A., 1998. Quercetin sensitizes RBL-2H3 cells to polybasic mast cell secretagogues through increased expression of Gi GTP-binding proteins linked to a phospholipase C signaling pathway. J Immunol 160, 5136-5144.

Serafin, W.E., Reynolds, D.S., Rogelj, S., Lane, W.S., Conder, G.A., Johnson, S.S., Austen, K.F., Stevens, R.L., 1990. Identification and molecular cloning of a novel mouse mucosal mast cell serine protease. Jorunal of Biological Chemistry 265, 423-429.

Shao, B., Zhu, L., Dong, M., Wang, J., Wang, J., Xie, H., Zhang, Q., Du, Z., Zhu, S., 2012. DNA damage and oxidative stress induced by endosulfan exposure in zebrafish (Danio rerio). Ecotoxicology 21, 1533-1540.

Shelburne, C.P., Abraham, S.N., 2011. The mast cell in innate and adaptive immunity. Adv Exp Med Biol 716, 162-185.

Shim, J., Kennedy, R.H., Weatherly, L.M., Hutchinson, L.M., Pelletier, J.H., Hashmi, H.N., Blais, K., Velez, A., Gosse, J.A., 2016a. Arsenic inhibits mast cell degranulation via

suppression of early tyrosine phosphorylation events. Journal of Applied Toxicology 36, 1446-1459.

Shim, J., Weatherly, L.M., Luc, R.H., Dorman, M.T., Neilson, A., Ng, R., Kim, C.H., Millard, P.J., Gosse, J.A., 2016b. Triclosan is a mitochondrial uncoupler in live zebrafish. Jorunal of Applied Toxicology 36, 1662-1667.

Silver, R., Curley, J.P., 2013. Mast cells on the mind: new insights and opportunities. Trends Neurosci 36, 513-521.

Silver, R., Silverman, A.J., Vitkovic, L., Lederhendler, II, 1996. Mast cells in the brain: evidence and functional significance. Trends in Neurosciences 19, 25-31.

Siraganian, R.P., de Castro, R.O., Barbu, E.A., Zhang, J.A., 2010. Mast cell signaling: The role of protein tyrosine kinase Syk, its activation and screening methods for new pathway participants. Febs Letters 584, 4933-4940.

Siraganian, R.P., Kulczycki, A., Jr., Mendoza, G., Metzger, H., 1975. Ionophore A-23187 induced histamine release from rat mast cells and rat basophil leukemia (RBL-1) cells. J Immunol 115, 1599-1602.

Small-Howard, A., Turner, H., 2005. Exposure to tobacco-derived materials induces overproduction of secreted proteinases in mast cells. Toxicology and Applied Pharmacology 204, 152-163.

Smallwood, N.D., Hausman, B.S., Wang, X., Liedtke, C.M., 2005. Involvement of NH2 terminus of PKC-delta in binding to F-actin during activation of Calu-3 airway epithelial NKCC1. Am J Physiol Cell Physiol 288, C906-912.

Smith, A.H., Arroyo, A.P., Mazumder, D.N.G., Kosnett, M.J., Hernandez, A.L., Beeris, M., Smith, M.M., Moore, L.E., 2000. Arsenic-induced skin lesions among Atacameno people in Northern Chile despite good nutrition and centuries of exposure. Environmental Health Perspectives 108, 617-620.

Smith, A.H., Hopenhayn-Rich, C., Bates, M.N., Goeden, H.M., Hertz-Picciotto, I., Duggan, H.M., Wood, R., Kosnett, M.J., Smith, M.T., 1992. Cancer risks from arsenic in drinking water. Environ Health Perspect 97, 259-267.

Smith, A.H., Steinmaus, C.M., 2009. Health effects of arsenic and chromium in drinking water: recent human findings. Annu Rev Public Health 30, 107-122.

Smith, A.J., Pfeiffer, J.R., Zhang, J., Martinez, A.M., Griffiths, G.M., Wilson, B.S., 2003. Microtubule-dependent transport of secretory vesicles in RBL-2H3 cells. Traffic 4, 302-312.

Song, Y., Li, Z., Gao, Q., Pavase, T.R., Lin, H., 2016. Effect of malonaldehyde cross-linking on the ability of shrimp tropomyosin to elicit the release of inflammatory mediators and

cytokines from activated RBL-2H3 cells. Journal of the Science of Food and Agriculture 96, 4263-4267.

Soto-Peña, G.A., Vega, L., 2008. Arsenic interferes with the signaling transduction pathway of T cell receptor activation by increasing basal and induced phosphorylation of Lck and Fyn in spleen cells. Toxicology and Applied Pharmacology 230, 216-226.

Souder, J.P., Gorelick, D.A., 2018. Assaying uptake of endocrine disruptor compounds in zebrafish embryos and larvae. Comparative biochemistry and physiology. Toxicology & pharmacology : CBP 208, 105-113.

Spitsbergen, J.M., Kent, M.L., 2003. The state of the art of the zebrafish model for toxicology and toxicologic pathology research--advantages and current limitations. Toxicol Pathol 31 Suppl, 62-87.

Stack, M.S., Johnson, D.A., 1994. Human mast cell tryptase activates single-chain urinary-type plasminogen activator (pro-urokinase). Journal of Biological Chemistry 269, 9416-9419.

Stackley, K.D., Beeson, C.C., Rahn, J.J., Chan, S.S., 2011. Bioenergetic profiling of zebrafish embryonic development. PLoS One 6, e25652.

Stehr, C.M., Linbo, T.L., Incardona, J.P., Scholz, N.L., 2006. The developmental neurotoxicity of fipronil: notochord degeneration and locomotor defects in zebrafish embryos and larvae. Toxicol Sci 92, 270-278.

Steinberg, S.F., 2008. Structural basis of protein kinase C isoform function. Physiol Rev 88, 1341-1378.

Steinmaus, C., Yuan, Y., Kalman, D., Rey, O.A., Skibola, C.F., Dauphine, D., Basu, A., Porter, K.E., Hubbard, A., Bates, M.N., Smith, M.T., Smith, A.H., 2010. Individual differences in arsenic metabolism and lung cancer in a case-control study in Cordoba, Argentina. Toxicol Appl Pharmacol 247, 138-145.

Su, W., Chen, Q., Frohman, M.A., 2009a. Targeting phospholipase D with small-molecule inhibitors as a potential therapeutic approach for cancer metastasis. Future Oncol 5, 1477-1486.

Su, W., Yeku, O., Olepu, S., Genna, A., Park, J.S., Ren, H., Du, G., Gelb, M.H., Morris, A.J., Frohman, M.A., 2009b. 5-Fluoro-2-indolyl des-chlorohalopemide (FIPI), a phospholipase D pharmacological inhibitor that alters cell spreading and inhibits chemotaxis. Molecular pharmacology 75, 437-446.

Sukardi, H., Ung, C.Y., Gong, Z., Lam, S.H., 2010. Incorporating zebrafish omics into chemical biology and toxicology. Zebrafish 7, 41-52.

Sulimenko, V., Hajkova, Z., Cernohorska, M., Sulimenko, T., Sladkova, V., Draberova, L., Vinopal, S., Draberova, E., Draber, P., 2015. Microtubule nucleation in mouse bone

marrow-derived mast cells is regulated by the concerted action of GIT1/betaPIX proteins and calcium. J Immunol 194, 4099-4111.

Sullivan, C., Kim, C.H., 2008. Zebrafish as a model for infectious disease and immune function. Fish Shellfish Immunol 25, 341-350.

Sung, T.C., Altshuller, Y.M., Morris, A.J., Frohman, M.A., 1999. Molecular analysis of mammalian phospholipase D2. The Journal of biological chemistry 274, 494-502.

Suzuki, Y., Yoshimaru, T., Inoue, T., Ra, C., 2006. Mitochondrial Ca2+ flux is a critical determinant of the Ca2+ dependence of mast cell degranulation. Journal of leukocyte biology 79, 508-518.

Suzuki, Y., Yoshimaru, T., Matsui, T., Inoue, T., Niide, O., Nunomura, S., Ra, C., 2003. Fc epsilon RI signaling of mast cells activates intracellular production of hydrogren peroxide: Role in the regulation of calcium signals. Journal of Immunology 171, 6119-6127.

Swindle, E.J., Metcalfe, D.D., 2007. The role of reactive oxygen species and nitric oxide in mast cell-dependent inflammatory processes. Immunological Reviews 217, 186-205.

Swindle, E.J., Metcalfe, D.D., Coleman, J.W., 2004. Rodent and human mast cells produce functionally significant intracellular reactive oxygen species but not nitric oxide. The Journal of biological chemistry 279, 48751-48759.

Sylvetsky, A.C., Bauman, V., Blau, J.E., Garraffo, H.M., Walter, P.J., Rother, K.I., 2017a. Plasma concentrations of sucralose in children and adults. Toxicol Environ Chem 99, 535-542.

Sylvetsky, A.C., Walter, P.J., Garraffo, H.M., Robien, K., Rother, K.I., 2017b. Widespread sucralose exposure in a randomized clinical trial in healthy young adults. Am J Clin Nutr 105, 820-823.

Tadokoro, S., Inoh, Y., Nakanishi, M., Hirashima, N., 2015. Effects of PIP2 on membrane fusion between mast cell SNARE liposomes mediated by synaptotagmin 2. Biochim Biophys Acta 1848, 2290-2294.

Takekawa, M., Furuno, T., Hirashima, N., Nakanishi, M., 2012. Mitochondria take up Ca2+ in two steps dependently on store-operated Ca2+ entry in mast cells. Biol Pharm Bull 35, 1354-1360.

Tam, E.K., Caughey, G.H., 1990. Degradation of airway neuropeptides by human lung tryptase. American journal of respiratory cell and molecular biology 3, 27-32.

Tan, W.P., Suresh, S., Tey, H.L., Chiam, L.Y., Goon, A.T., 2010. A randomized double-blind controlled trial to compare a triclosan-containing emollient with vehicle for the treatment of atopic dermatitis. Clin Exp Dermatol 35, e109-112.

Tang, J.M., Lie, J., Wu, W., 2012. Studies on the degranulation of RBL-2H3 cells induced by traditional chinese medicine injections. Chinese medicine 3.

Tanguay, R.L., 2018. The Rise of Zebrafish as a Model for Toxicology. Toxicol Sci 163, 3-4.

Tasaka, K., Mio, M., Fujisawa, K., Aoki, I., 1991. Role of microtubules on Ca2+ release from the endoplasmic reticulum and associated histamine-release from rat peritoneal mast-cells. Biochemical Pharmacology 41, 1031-1037.

Taylor, C.W., Thorn, P., 2001. Calcium signalling: IP3 rises again ... and again. Current Biology 11, R352-R355.

Taylor, H.E., Simmons, G.E., Jr., Mathews, T.P., Khatua, A.K., Popik, W., Lindsley, C.W., D'Aquila, R.T., Brown, H.A., 2015. Phospholipase D1 Couples CD4+ T Cell Activation to c-Myc-Dependent Deoxyribonucleotide Pool Expansion and HIV-1 Replication. PLoS Pathog 11, e1004864.

Thastrup, O., Cullen, P.J., Drobak, B.K., Hanley, M.R., Dawson, A.P., 1990. Thapsigargin, a tumor promoter, discharges intracellular Ca2+ stores by specific inhibition of the endoplasmic reticulum Ca2+-ATPase. Proceedings of the National Academy of Sciences of the United States of America 87, 2466-2470.

Theoharides, T.C., Alysandratos, K.D., Angelidou, A., Delivanis, D.A., Sismanopoulos, N., Zhang, B., Asadi, S., Vasiadi, M., Weng, Z., Miniati, A., Kalogeromitros, D., 2012a. Mast cells and inflammation. Biochim Biophys Acta 1822, 21-33.

Theoharides, T.C., Angelidou, A., Alysandratos, K.D., Zhang, B., Asadi, S., Francis, K., Toniato, E., Kalogeromitros, D., 2012b. Mast cell activation and autism. Biochimica et Biophysica Acta 1822, 34-41.

Theoharides, T.C., Bondy, P.K., Tsakalos, N.D., Askenase, P.W., 1982. Differential release of serotonin and histamine from mast cells. Nature 297, 229-231.

Tifft, C.J., Proia, R.L., 1997. The beta-hexosaminidase deficiency disorders: development of a clinical paradigm in the mouse. Annals of Medicine 29, 557-561.

Tiwari, N., Wang, C.C., Brochetta, C., Ke, G., Vita, F., Qi, Z., Rivera, J., Soranzo, M.R., Zabucchi, G., Hong, W.J., Blank, U., 2008. VAWP-8 segregates mast cell-preformed mediator exocytosis from cytokine trafficking pathways. Blood 111, 3665-3674.

Trnovsky, J., Letourneau, R., Haggag, E., Boucher, W., Theoharides, T.C., 1993. Quercetin-induced expression of rat mast cell protease II and accumulation of secretory granules in rat basophilic leukemia cells. Biochem Pharmacol 46, 2315-2326.

Tsujimura, T., Furitsu, T., Morimoto, M., Kanayama, Y., Nomura, S., Matsuzawa, Y., Kitamura, Y., Kanakura, Y., 1995. Substitution of an aspartic acid results in constitutive activation of c-kit receptor tyrosine kinase in a rat tumor mast cell line RBL-2H3. Int Arch Allergy Immunol 106, 377-385.

Ulanova, M., Duta, F., Puttagunta, L., Schreiber, A.D., Befus, A.D., 2005. Spleen tyrosine kinase (Syk) as a novel target for allergic asthma and rhinitis. Expert Opinion on Therapeutic Targets 9, 901-921.

Urata, C., Siraganian, R.P., 1985. Pharmacologic modulation of the IgE or Ca2+-ionophore A23187 mediated Ca2+-influx, phospholipase activation, and histamine-release in rat basophilic leukemia-cells. International Archives of Allergy and Applied Immunology 78, 92-100.

Urtz, N., Olivera, A., Bofill-Cardona, E., Csonga, R., Billich, A., Mechtcheriakova, D., Bornancin, F., Woisetschlager, M., Rivera, J., Baumruker, T., 2004. Early activation of sphingosine kinase in mast cells and recruitment to Fc epsilon RI are mediated by its interaction with Lyn kinase. Molecular and Cellular Biology 24, 8765-8777.

Vakili, J., Standker, L., Detheux, M., Vassart, G., Forssmann, W.G., Parmentier, M., 2001. Urokinase plasminogen activator and plasmin efficiently convert hemofiltrate CC chemokine 1 into its active. Journal of immunology 167, 3406-3413.

van Rossum, D.B., Patterson, R.L., 2009. PKC and PLA2: probing the complexities of the calcium network. Cell Calcium 45, 535-545.

Velasco-Santamaria, Y.M., Korsgaard, B., Madsen, S.S., Bjerregaard, P., 2011. Bezafibrate, a lipid-lowering pharmaceutical, as a potential endocrine disruptor in male zebrafish (Danio rerio). Aquat Toxicol 105, 107-118.

Vig, M., Peinelt, C., Beck, A., Koomoa, D.L., Rabah, D., Koblan-Huberson, M., Kraft, S., Turner, H., Fleig, A., Penner, R., Kinet, J.P., 2006. CRACM1 is a plasma membrane protein essential for store-operated Ca2+ entry. Science 312, 1220-1223.

Violin, J.D., Zhang, J., Tsien, R.Y., Newton, A.C., 2003. A genetically encoded fluorescent reporter reveals oscillatory phosphorylation by protein kinase C. J Cell Biol 161, 899-909.

Wade, T.J., Xia, Y., Mumford, J., Wu, K., Le, X.C., Sams, E., Sanders, W.E., 2015. Cardiovascular disease and arsenic exposure in Inner Mongolia, China: a case control study. Environ Health 14, 35.

Wakelam, M.J., Martin, A., Hodgkin, M.N., Brown, F., Pettitt, T.R., Cross, M.J., De Takats, P.G., Reynolds, J.L., 1997. Role and regulation of phospholipase D activity in normal and cancer cells. Adv Enzyme Regul 37, 29-34.

Walls, A.F., Brain, S.D., Desai, A., Jose, P.J., Hawkings, E., Church, M.K., Williams, T.J., 1992. Human mast cell tryptase attenuates the vasodilator activity of calcitonin gene-related peptide. Biochem Pharmacol 43, 1243-1248.

Walsh, L.J., 2003. Mast cells and oral inflammation. Critical reviews in oral biology and medicine : an official publication of the American Association of Oral Biologists 14, 188-198.

Wang, C.F., Tian, Y., 2015. Reproductive endocrine-disrupting effects of triclosan: Population exposure, present evidence and potential mechanisms. Environmental pollution (Barking, Essex : 1987) 206, 195-201.

Wang, X., Chen, X., Feng, X., Chang, F., Chen, M., Xia, Y., Chen, L., 2015. Triclosan causes spontaneous abortion accompanied by decline of estrogen sulfotransferase activity in humans and mice. Scientific reports 5, 18252.

Wang, X., Ouyang, F., Feng, L., Wang, X., Liu, Z., Zhang, J., 2017. Maternal Urinary Triclosan Concentration in Relation to Maternal and Neonatal Thyroid Hormone Levels: A Prospective Study. Environ Health Perspect 125, 067017.

Ward, A.C., Lieschke, G.J., 2002. The zebrafish as a model system for human disease. Frontiers in Bioscience 7, d827-833.

Wasserman, G.A., Liu, X., Parvez, F., Ahsan, H., Factor-Litvak, P., Kline, J., van Geen, A., Slavkovich, V., Loiacono, N.J., Levy, D., Cheng, Z., Graziano, J.H., 2007. Water arsenic exposure and intellectual function in 6-year-old children in Araihazar, Bangladesh. Environ Health Perspect 115, 285-289.

Wasserman, G.A., Liu, X., Parvez, F., Ahsan, H., Factor-Litvak, P., van Geen, A., Slavkovich, V., LoIacono, N.J., Cheng, Z., Hussain, I., Momotaj, H., Graziano, J.H., 2004. Water arsenic exposure and children's intellectual function in Araihazar, Bangladesh. Environ Health Perspect 112, 1329-1333.

Way, G., O'Luanaigh, N., Cockcroft, S., 2000. Activation of exocytosis by cross-linking of the IgE receptor is dependent on ADP-ribosylation factor 1-regulated phospholipase D in RBL-2H3 mast cells: evidence that the mechanism of activation is via regulation of phosphatidylinositol 4,5-bisphosphate synthesis. Biochem J 346 Pt 1, 63-70.

Weatherly, L.M., Gosse, J.A., 2017. Triclosan exposure, transformation, and human health effects. J Toxicol Environ Health B Crit Rev 20, 447-469.

Weatherly, L.M., Kennedy, R.H., Shim, J., Gosse, J.A., 2013. A microplate assay to assess chemical effects on RBL-2H3 mast cell degranulation: effects of triclosan without use of an organic solvent. Journal of Visualized Expreiments, e50671.

Weatherly, L.M., Nelson, A.J., Shim, J., Riitano, A.M., Gerson, E.D., Hart, A.J., de Juan-Sanz, J., Ryan, T.A., Sher, R., Hess, S.T., Gosse, J.A., 2018. Antimicrobial agent triclosan disrupts mitochondrial structure, revealed by super-resolution microscopy, and inhibits mast cell signaling via calcium modulation. Toxicol Appl Pharmacol 349, 39-54.

Weatherly, L.M., Shim, J., Hashmi, H.N., Kennedy, R.H., Hess, S.T., Gosse, J.A., 2016. Antimicrobial agent triclosan is a proton ionophore uncoupler of mitochondria in living rat and human mast cells and in primary human keratinocytes. Journal of Appled Toxicology.

Wei, L., Qiao, P., Shi, Y., Ruan, Y., Yin, J., Wu, Q., Shao, B., 2017. Triclosan/triclocarban levels in maternal and umbilical blood samples and their association with fetal malformation. Clin Chim Acta 466, 133-137.

Wiedow, O., Weindler, F., Mrowietz, U., 1997. The effect of tamol on human mast cell chymase and plasmin. Skin Pharmacology 10, 90-96.

Wilcz-Villega, E.M., McClean, S., O'Sullivan, M.A., 2013. Mast cell tryptase reduces junctional adhesion molecule-A (JAM-A) expression in intestinal epithelial cells: implications for the mechanisms of barrier dysfunction in irritable bowel syndrome. The American Journal of Gastroenterology 108, 1140-1151.

Williams, C.M., Galli, S.J., 2000. The diverse potential effector and immunoregulatory roles of mast cells in allergic disease. The Journal of allergy and clinical immunology 105, 847-859.

Wilson, S.J., Shute, J.K., Holgate, S.T., Howarth, P.H., Bradding, P., 2000. Localization of interleukin (IL) -4 but not IL-5 to human mast cell secretory granules by immunoelectron microscopy. Clin Exp Allergy 30, 493-500.

Wong, B.R., Grossbard, E.B., Payan, D.G., Masuda, E.S., 2004. Targeting Syk as a treatment for allergic and and autoimmune disorders. Expert Opinion on Investigational Drugs 13, 743-762.

Woska, J.R., Gillespie, M.E., 2012. SNARE complex-mediated degranulation in mast cells. Journal of Cellular and Molecular Medicine 16, 649-656.

Wu, F., Jasmine, F., Kibriya, M.G., Liu, M., Cheng, X., Parvez, F., Islam, T., Ahmed, A., Rakibuz-Zaman, M., Jiang, J., Roy, S., Paul-Brutus, R., Slavkovich, V., Islam, T., Levy, D., VanderWeele, T.J., Pierce, B.L., Graziano, J.H., Ahsan, H., Chen, Y., 2015. Interaction between arsenic exposure from drinking water and genetic polymorphisms on cardiovascular disease in Bangladesh: a prospective case-cohort study. Environ Health Perspect 123, 451-457.

Wu, J., Chen, G., Liao, Y., Song, X., Pei, L., Wang, J., Zheng, X., 2011. Arsenic levels in the soil and risk of birth defects: a population-based case-control study using GIS technology. J Environ Health 74, 20-25.

Wu, S.M., Tsai, P.R., Yan, C.J., 2012. Maternal cadmium exposure induces mt2 and smtB mRNA expression in zebrafish (Danio rerio) females and their offspring. Comparative biochemistry and physiology. Toxicology & pharmacology : CBP 156, 1-6.

Xia, Y., Wade, T.J., Wu, K., Li, Y., Ning, Z., Le, X.C., He, X., Chen, B., Feng, Y., Mumford, J.L., 2009. Well water arsenic exposure, arsenic induced skin-lesions and self-reported morbidity in Inner Mongolia. Int J Environ Res Public Health 6, 1010-1025.

Xiao, W., Nishimoto, H., Hong, H., Kitaura, J., Nunomura, S., Maeda-Yamamoto, M., Kawakami, Y., Lowell, C.A., Ra, C., Kawakami, T., 2005. Positive and negative regulation of mast cell activation by Lyn via the FcepsilonRI. J Immunol 175, 6885-6892.

Xing, H., Li, S., Wang, Z., Gao, X., Xu, S., Wang, X., 2012. Histopathological changes and antioxidant response in brain and kidney of common carp exposed to atrazine and chlorpyrifos. Chemosphere 88, 377-383.

Yadava, N., Nicholls, D.G., 2007. Spare respiratory capacity rather than oxidative stress regulates glutamate excitotoxicity after partial respiratory inhibition of mitochondrial complex I with rotenone. J Neurosci 27, 7310-7317.

Yamada, K., Jelsema, C.L., Beaven, M.A., 1992. Certain inhibitors of protein serine/threonine kinases also inhibit tyrosine phosphorylation of phospholipase C gamma 1 and other proteins and reveal distinct roles for tyrosine kinase(s) and protein kinase C in stimulated, rat basophilic RBL-2H3 cells. J Immunol 149, 1031-1037.

Yanase, Y., Carvou, N., Frohman, M.A., Cockcroft, S., 2009. Reversible bleb formation in mast cells stimulated with antigen is Ca2+/calmodulin-dependent and bleb size is regulated by ARF6. Biochem J 425, 179-193.

Yanase, Y., Hide, I., Mihara, S., Shirai, Y., Saito, N., Nakata, Y., Hide, M., Sakai, N., 2011. A critical role of conventional protein kinase C in morphological changes of rodent mast cells. Immunology and Cell Biology 89, 149-159.

Yang, R., Lao, Q.C., Yu, H.P., Zhang, Y., Liu, H.C., Luan, L., Sun, H.M., Li, C.Q., 2015. Tween-80 and impurity induce anaphylactoid reaction in zebrafish. Journal of Applied toxicology 35, 295-301.

Yoder, J.A., Nielsen, M.E., Amemiya, C.T., Litman, G.W., 2002. Zebrafish as an immunological model system. Microbes and Infection 4, 1469-1478.

Yoshida, K., 2007. PKCdelta signaling: mechanisms of DNA damage response and apoptosis. Cell Signal 19, 892-901.

Yueh, M.F., Taniguchi, K., Chen, S., Evans, R.M., Hammock, B.D., Karin, M., Tukey, R.H., 2014. The commonly used antimicrobial additive triclosan is a liver tumor promoter. Proc Natl Acad Sci U S A 111, 17200-17205.

Zeng, R., Cannon, J.L., Abraham, R.T., Way, M., Billadeau, D.D., Bubeck-Wardenberg, J., Burkhardt, J.K., 2003. SLP-76 coordinates Nck-dependent Wiskott-Aldrich syndrome protein recruitment with Vav-1/Cdc42-dependent Wiskott-Aldrich syndrome protein activation at the T cell-APC contact site. Journal of Immunology 171, 1360-1368.

Zeniou-Meyer, M., Zabari, N., Ashery, U., Chasserot-Golaz, S., Haeberle, A.M., Demais, V., Bailly, Y., Gottfried, I., Nakanishi, H., Neiman, A.M., Du, G., Frohman, M.A., Bader, M.F., Vitale, N., 2007. Phospholipase D1 production of phosphatidic acid at the plasma

membrane promotes exocytosis of large dense-core granules at a late stage. The Journal of biological chemistry 282, 21746-21757.

Zhang, J., Berenstein, E.H., Evans, R.L., Siraganian, R.P., 1996. Transfection of Syk protein tyrosine kinase reconstitutes high affinity IgE receptor-mediated degranulation in a Syk-negative variant of rat basophilic leukemia RBL-2H3 cells. Jounal of Experimental Medicine 184, 71-79.

Zhang, J., Billingsley, M.L., Kincaid, R.L., Siraganian, R.P., 2000. Phosphorylation of Syk activation loop tyrosines is essential for Syk function. An in vivo study using a specific anti-Syk activation loop phosphotyrosine antibody. The Journal of biological chemistry 275, 35442-35447.

Zhang, S.L., Yu, Y., Roos, J., Kozak, J.A., Deerinck, T.J., Ellisman, M.H., Stauderman, K.A., Cahalan, M.D., 2005. STIM1 is a Ca2+ sensor that activates CRAC channels and migrates from the Ca2+ store to the plasma membrane. Nature 437, 902-905.

Zhang, Y., Altshuller, Y.M., Hammond, S.M., Hayes, F., Morris, A.J., Frohman, M.A., 1999. Loss of receptor regulation by a phospholipase D1 mutant unresponsive to protein kinase C. EMBO J 18, 6339-6348.

Zhao, W., Oskeritzian, C.A., Pozez, A.L., Schwartz, L.B., 2005. Cytokine production by skin-derived mast cells: endogenous proteases are responsible for degradation of cytokines. J Immunol 175, 2635-2642.

Zhou, L.F., Zhu, Y., Cui, X.F., Xie, W.P., Hu, A.H., Yin, K.S., 2006. Arsenic trioxide, a potent inhibitor of NF-kappaB, abrogates allergen-induced airway hyperresponsiveness and inflammation. Respiratory research 7, 146.

Zhou, W., Cao, L., Jeffries, J., Zhu, X., Staiger, C.J., Deng, Q., 2018. Neutrophil-specific knockout demonstrates a role for mitochondria in regulating neutrophil motility in zebrafish. Dis Model Mech 11.

Zhu, M., Foreman, D.P., O'Brien, S.A., Jin, Y., Zhang, W., 2018. Phospholipase D in TCR-Mediated Signaling and T Cell Activation. J Immunol 200, 2165-2173.

Zhu, M., Zou, J., Li, T., O'Brien, S.A., Zhang, Y., Ogden, S., Zhang, W., 2015. Differential Roles of Phospholipase D Proteins in FcepsilonRI-Mediated Signaling and Mast Cell Function. J Immunol 195, 4492-4502.

Zizioli, D., Guarienti, M., Tobia, C., Gariano, G., Borsani, G., Bresciani, R., Ronca, R., Giacopuzzi, E., Preti, A., Gaudenzi, G., Belleri, M., Di Salle, E., Fabrias, G., Casas, J., Ribatti, D., Monti, E., Presta, M., 2014. Molecular cloning and knockdown of galactocerebrosidase in zebrafish: new insights into the pathogenesis of Krabbe's disease. Biochim Biophys Acta 1842, 665-675.

APPENDIX A

SUPPLEMENTARY INFORMATION TO CHAPTER 2

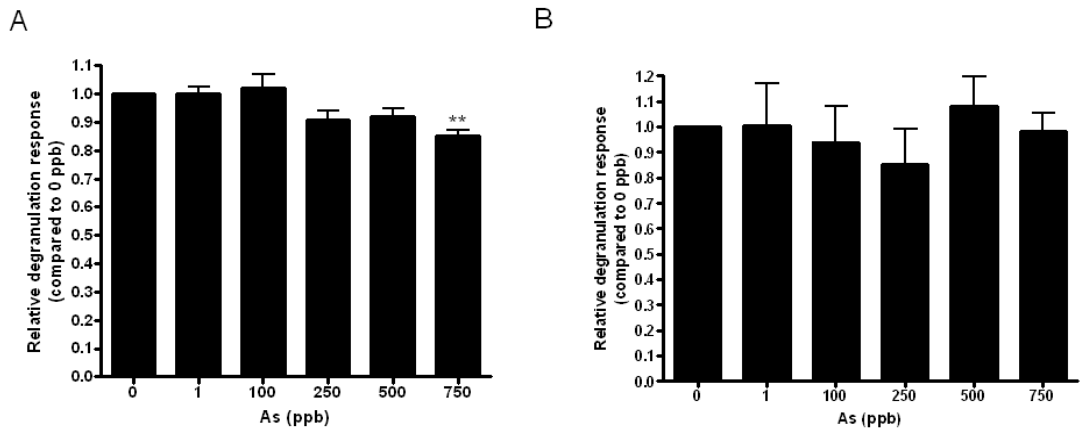

Figure A.1. As inhibits degranulation of RBL-2H3 cells following 15-min exposure to DNP-BSA antigen. Effect of As on **(A)** 15-min Ag-mediated degranulation (an average absolute degranulation response of 9.4% ± 0.8% [SEM] in the absence of As) or **(B)** 15-min spontaneous release (an average absolute degranulation response of 1.4% ± 0.1% [SEM] in the absence of As). Values represent means ± SEM for 5-11 experiments in (A) or n = 3 in (B), where three replicates were performed for each condition. Significance was determined by one-way ANOVA followed by Tukey's post test; ** indicates $p<0.01$, as compared to the 1 ppb column.

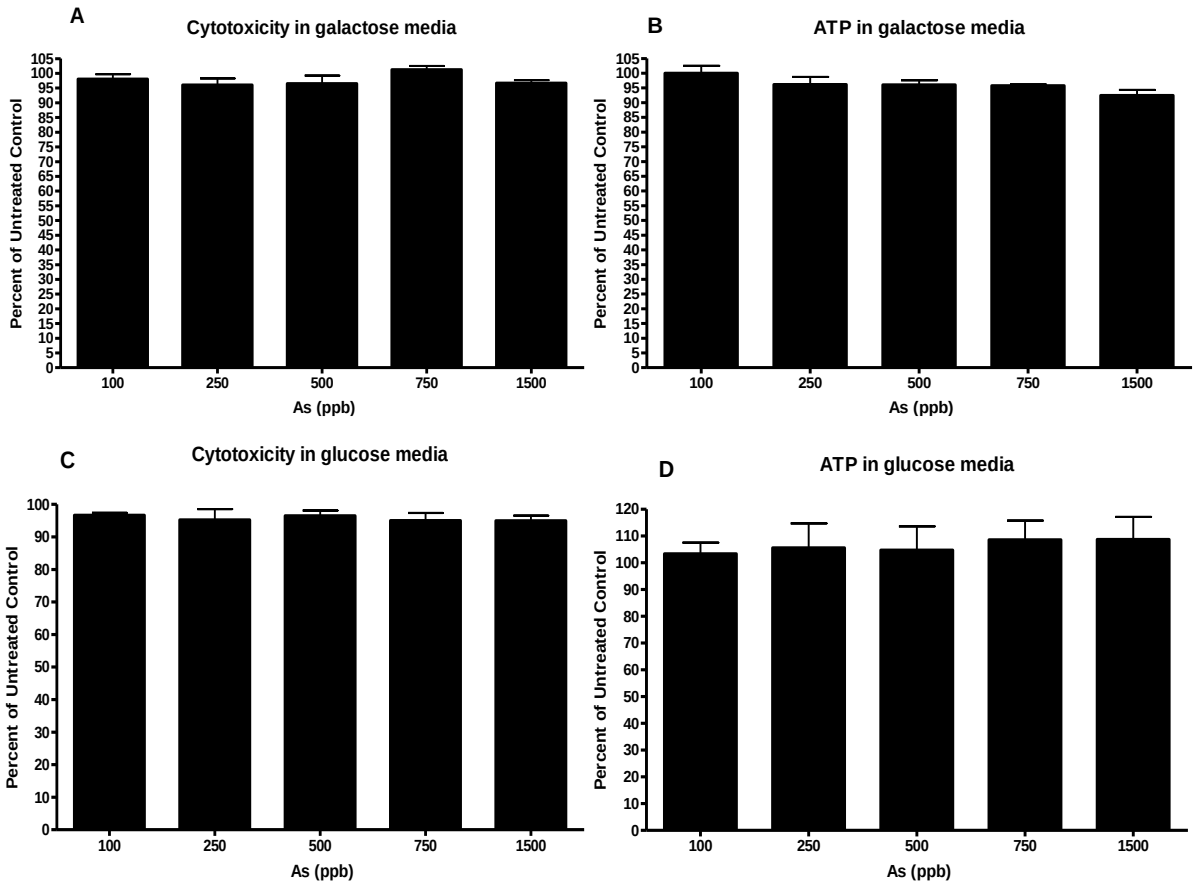

Figure A.2. ATP levels and cytotoxicity in RBL-2H3 cells exposed to As. **(A-B)** Exposure to various concentrations of As in galactose media and **(C-D)** in glucose media. Percent untreated control is 100% multiplied by the quotient of the fluorescence or luminescence value of each sample by the average value of the untreated control. Values are means ± SEM of three independent experiments (each with three replicates per dose). One-way ANOVA followed by Tukey's *post-hoc* test revealed no statistical significance.

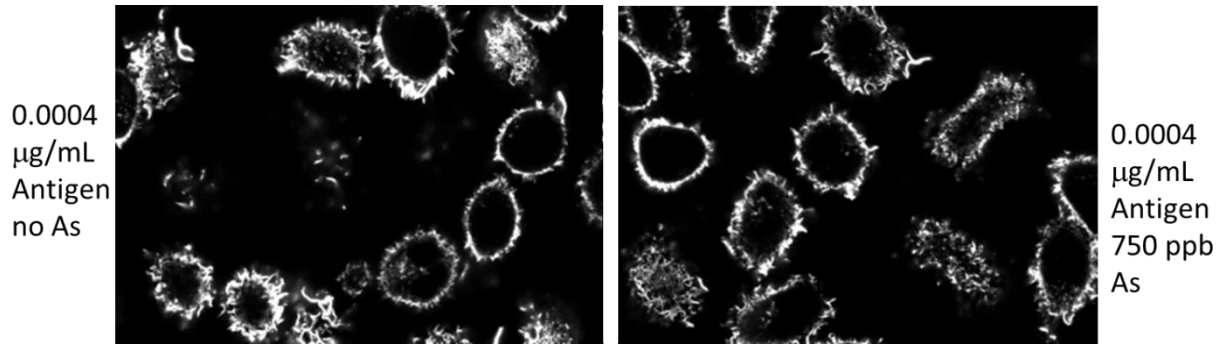

Figure A.3. F-actin ruffling during antigen-stimulated degranulation of RBL-2H3 cells. F-actin was visualized using Alexa Fluor 488 conjugated phalloidin. RBL-2H3 cells were exposed to 0.0004 µg mL^{-1} Ag (left) or to 0.0004 µg mL^{-1} Ag plus 750 ppb As (right) for one hour before being fixed. A representative set of images is shown.

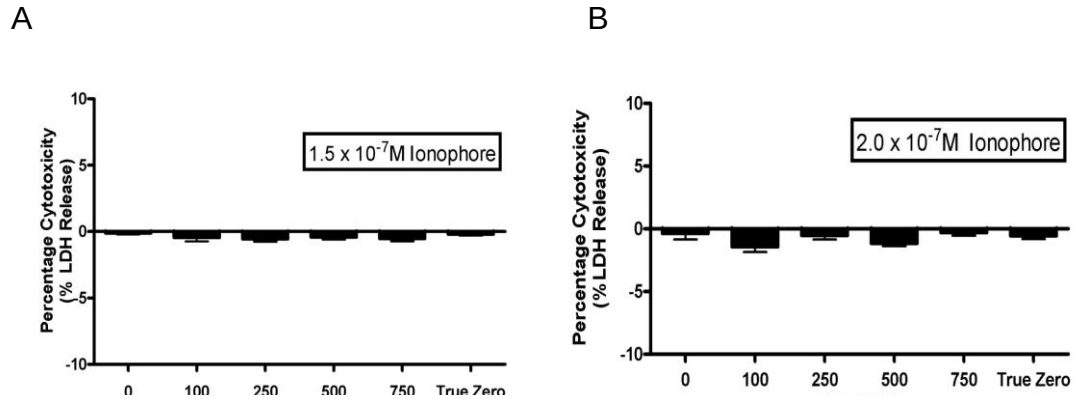

Figure A.4. Combined exposure of experimental As and A23187 ionophore doses causes no cytotoxicity in RBL-2H3 cells as determined by lactate dehydrogenase (LDH) cytotoxicity assay. To measure the impact of A23187 ionophore and As on viability of RBL-2H3 cells, an LDH assay kit was utilized as described in Methods. Arsenic was diluted into A23187 solutions of **(A)** 1.5 x 10^{-7} M or **(B)** 2 x 10^{-7} M to create 100-750 ppb As samples. "True zero" contains neither As nor ionophore but does contain the vehicle conditions of the experimental parameters. No statistically significant effects were found, by one-way ANOVA and Tukey's post test. Values represent means ± SEM of three experiments of three replicates per experiment.

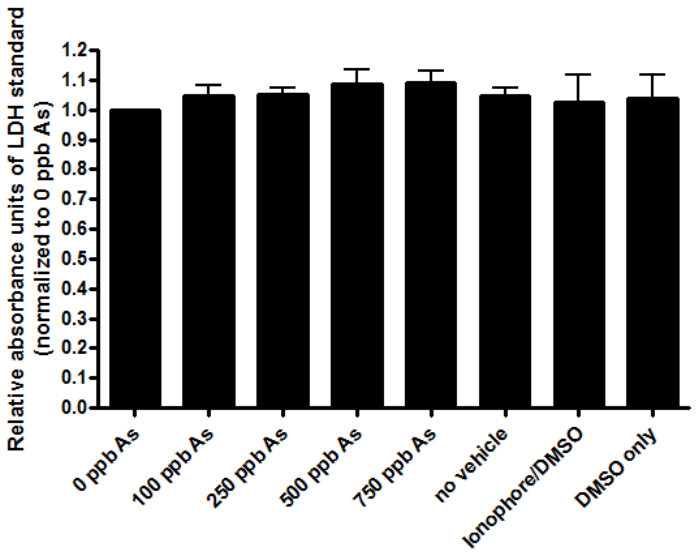

Figure A.5. LDH enzymatic activity is not affected by As and A23187 ionophore concentrations used in the degranulation assays. In order to test whether or not the LDH enzyme activity is altered by various chemical combinations used in the LDH experiment, LDH standard testing was performed in the presence of 2 x 10^{-7} M A23187, As, and vehicle conditions (0.004% DMSO). In a clear 96-well plate, a 50 µL sample of 0.000625 U/mL purified LDH enzyme standard (Cayman chemical company; Ann Arbor, MI, USA) was incubated with an equal volume of A23187/2x As, no A23187 or DMSO, A23187 only, or 0.002% DMSO (2x concentration of 0.004% DMSO vehicle) for one hour (37 °C/5% CO_2). The final A23187 concentration was 1.0 x 10^{-7} M; the final As concentrations represented a range from 100 to 750 ppb. The remainder of the experiment followed manufacturer's recommended protocol (Cytotoxicity detection kit LDH^{PLUS}; Roche Diagnostics). Absorbance values for experimental data sets were normalized against the 0 ppb As/LDH standard control, and plotted against treatment conditions. Statistical testing was performed in Prism using a one-way ANOVA and Tukey's post test. Values represent means ± SEM of two data sets (3 replicates per experiment) for each treatment condition.

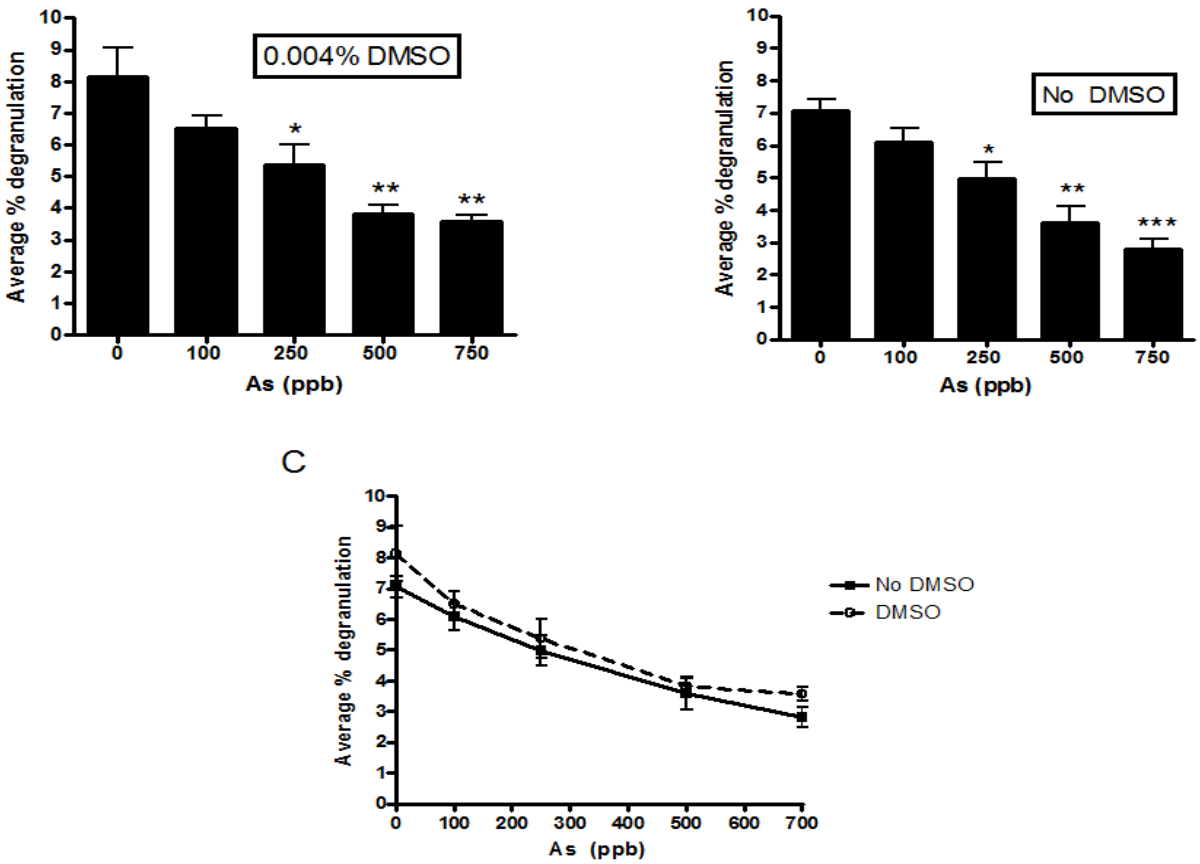

Figure A.6. DMSO vehicle concentration used for A23187 dilutions has no effect on antigen-stimulated degranulation of RBL-2H3 cells. Antigen-stimulated degranulation experiments were carried out to examine the effect of 0.004% DMSO vehicle used for A23187 dilutions. **(A-B)** IgE-sensitized mast cells were stimulated using a 0.00016 μg mL^{-1} dilution of DNP-BSA (no A23187 was utilized); in (A), all samples contained 0.004% DMSO. The plate was read in a fluorescence microplate reader (Synergy 2, Biotek), using 360/40 nm excitation and 460/40 nm emission filters. Data processing was performed as described by Palmer *et al*.(Palmer *et al*., 2012). Following one-way ANOVA, a Tukey's post test was used to assess significance (comparisons made to 0 ppb As). In (A-B) error bars represent means ± SD from three replicate data sets, and significance is indicated; ***p<0.001,**p<0.01, *p<0.05. In **(C)** a direct comparison of the data found separately in (A) and (B) is made. For these combined data, a two-way ANOVA with Bonferroni post test was performed to compare the Ag-stimulated degranulation in the presence and absence of 0.004% DMSO. No significant difference was found between either set of experiments.

APPENDIX B

SUPPLEMENTARY INFORMATION TO CHAPTER 3

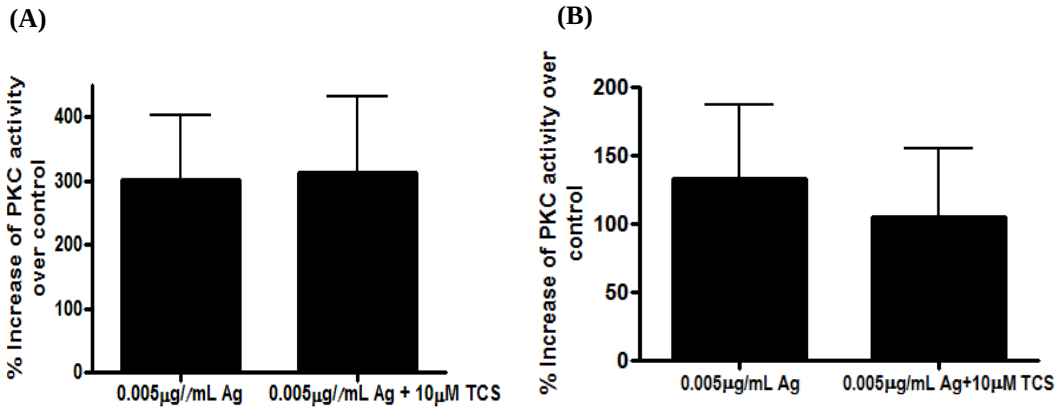

Figure. B.1. TCS does not affect PKC activity in Ag-stimulated RBL-2H3 mast cells within 15 (A) or 30 min (B). Cells were stimulated with 0.005 µg/ml Ag ± 10 µM TCS in BT. After exposure, PKC activity was measured via ELISA, and absorbance was read at 450 nm using a microplate reader. Raw data were processed as described in the main text Methods section to normalize to both total protein concentration and to unstimulated controls, in order to calculate percentage increase of PKC activity over unstimulated control. Data presented are means ± SEM of at least three independent experiments; duplicates per treatment per experiment. No statistical significance was determined by one tailed t-test (GraphPad prism).

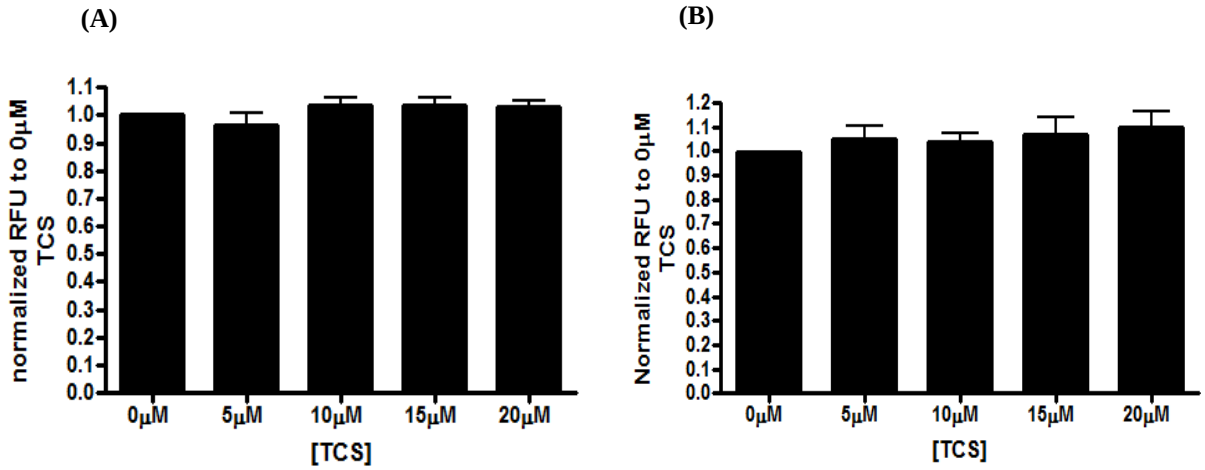

Figure. B.2. TCS does not interfere with components (choline oxidase [A] and horseradish peroxidase [B]) in the Amplex® Red phospholipase D assay kit. The Amplex® kit (Thermo Scientific), containing phosphatidylcholine, choline oxidase, horseradish peroxidase (HRP), and Amplex® Red reagent, works in the following process: PLD cleaves the substrate phosphatidylcholine into choline and phosphatidic acid. Choline is then oxidized by choline oxidase into betaine and hydrogen peroxide. HRP uses Amplex® red as an electron donor in the reduction of hydrogen peroxide to water, in a 1:1 stoichiometry to convert Amplex® red into resorufin whose fluorescence is measured at 530/25 excitation and 590/30 emission. To test the effects of TCS on the components of the kit, we initiated this process at different points and measured the fluorescence when exposed to varying TCS concentrations, from 0-20 μM. (A) We first examined the effect of TCS on choline oxidase activity. Choline chloride was purchased (MP Biomedicals) to initiate the cascade at the choline oxidase step. Choline chloride was prepared in 0.2% Triton-X (TX) and co-exposed with various concentrations of TCS (dissolved in BT) for 15 min. Next, 100 μL of the choline chloride ± TCS was added to 100 μL of master mix of the Amplex® Red kit for 30 min, followed by fluorescence measurement as described in the main text Methods section. Final choline chloride concentration was 1.5 μM, a level chosen to result in RFU readings similar to those obtained in the cellular PLD experiments. Overall, this control experiment's components were designed to utilize the same buffer conditions and concentrations as those found in cellular PLD experiments such as in main text Fig. 3.5A. (B) A similar experiment was used to determine whether TCS could inhibit HRP activity. This time the cascade was initiated by using hydrogen peroxide that was provided in the Amplex® kit. Fluorescence of resorufin was measured as in Methods. Values were normalized to 0 μM TCS of each experiment and represented as means ± SEM of three independent experiments; three replicates per treatment per experiment. No statistical significance was determined by one-way ANOVA followed by Tukey's *post-hoc* test (GraphPad Prism). Data show that TCS does not interfere with this PLD activity assay.

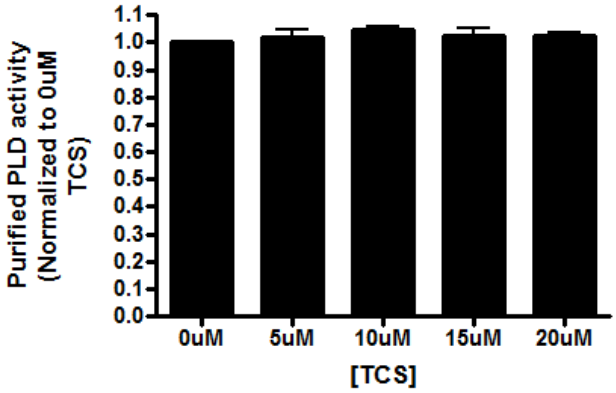

Figure. B.3. TCS has no effect on purified PLD from *Streptomyces chromofuscus*. Purified *Streptomyces chromofuscus* PLD (Sigma P0065) was diluted from glycerol stock in Tyrodes buffer and further diluted with 0.2% Triton X incubated with TCS ranging from 0- 20μM concentrations to be 0.125U/mL. After a 15 min exposure, PLD activity was measured using the Amplex® Red PLD assay kit (Thermo Scientific), which was prepared following the manufacturer's instructions. Overall, this experiment's components were designed to utilize the same buffer conditions and concentrations as those found in cellular PLD experiments such as in main text Fig. 3.5A. Values were normalized to 0 μM TCS of each experiment and represented as means ± SEM of three independent experiments; three replicates per treatment per experiment. No statistical significance was determined by one-way ANOVA followed by Tukey's *post-hoc* test (GraphPad Prism).

sucralose (CAS # 56038-13-2) **triclosan** (CAS # 3380-34-5)

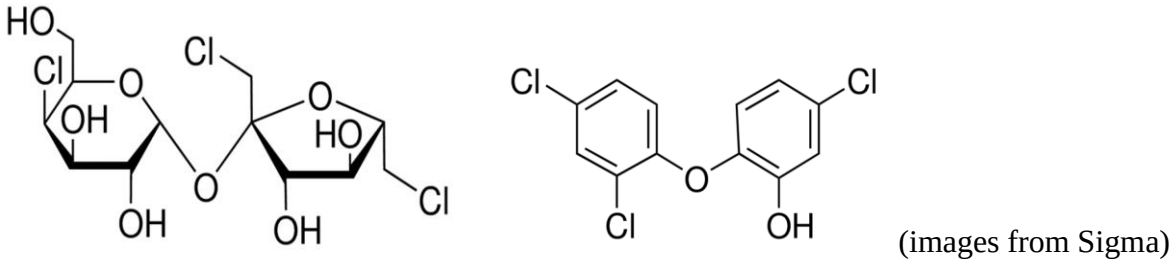

(images from Sigma)

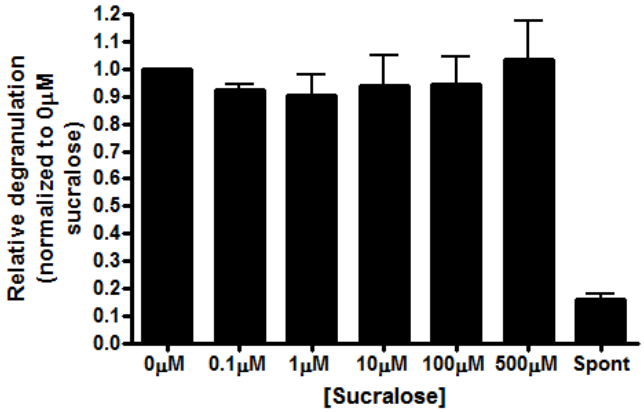

Figure. B.4. **Sucralose shares structural similarities with triclosan but does not affect degranulation of Ag-stimulated RBL-2H3 cells.** Similarities between triclosan and sucralose (both pictured above) include presence of two carbon rings combined in ether linkage, three chlorines decorating the two rings, and presence of hydroxyl groups on the rings. Sucralose (>98.0%) (TCI America) was dissolved for 20 min with stirring into Tyrodes buffer to prepare a 1 mM sucralose solution. Cells were sensitized with with 0.1μg/mL IgE for 1 hr, and stimulated with ± 0.0002 μg/mL Ag ± sucralose (0.1 to 500 μM) in BT buffer for 1 hr. Degranulation was assessed as a measurement of β-hexosaminisase release, described in (Weatherly *et al*., 2013), and the 0.0002 μg/mL Ag dose elicited a moderate absolute degranulation percentage response of ~18% in the absence of sucralose. Concentrations of sucralose tested were biologically relevant: these levels were detected in human blood plasma and urine samples following consumption of beverages containing sucralose at concentrations similar to those found in commercial products (de Ruyter *et al*., 2012; Sylvetsky *et al*., 2017a; Sylvetsky *et al*., 2017b; Rother *et al*., 2018). As an amphipathic molecule, sucralose is able to traverse cellular plasma membranes through simple diffusion, down its concentration gradient. Sucralose has been observed to passively diffuse from the gastro-intestinal tract into the blood (Grice and Goldsmith, 2000), though it can be metabolized by cytochrome p-450 and can be subject to efflux via p-glycoprotein (Abou-Donia *et al*., 2008). Values are normalized to the Ag control (no sucralose) and represented as means ± SEM from three independent experiments, with three replicates pre- treatment group per experiment. No statistical significance was determined by one-way ANOVA followed by Tukey's *post test* (GraphPad Prism). Thus, we conclude that the presence of two carbon rings in ether linkage and three chlorines positioned on the rings are insufficient for mast cell effects caused by triclosan, lending further evidence that the proton ionophoric properties of triclosan caused its effects.

APPENDIX C

SUPPLEMENTARY INFORMATION TO CHAPTER 4

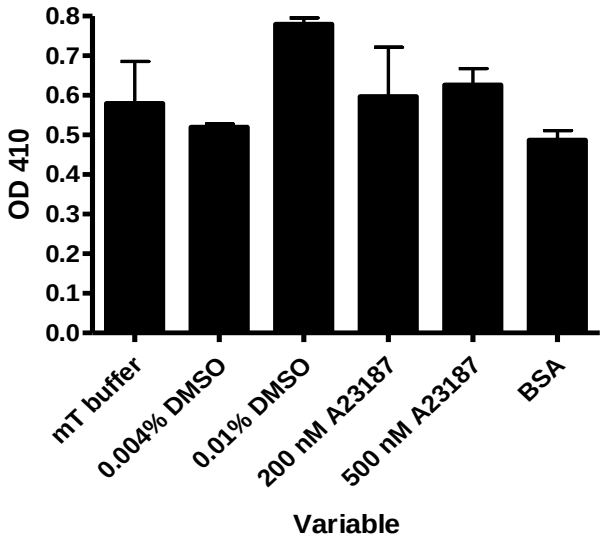

Figure C.1. Various buffer components do not interfere with BAPNA-tryptase substrate-enzyme reaction. Various buffer components, as indicated, were incubated with 25 ng tryptase for 72 h, after which absorbance at 410 nm was detected. Values represent triplicates replicates from one experiment (with the exception of 0.004% DMSO sample, which contains duplicates). No significant difference was determined by one-way ANOVA followed by Tukey's post test, with comparisons made to the mT buffer.

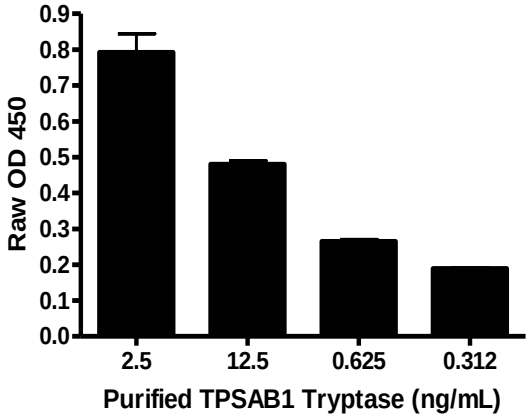

Figure C.2. TPSAB1 tryptase standard samples measured by ELISA. Rat TPSAB1 standard protein, provided in the tryptase ELISA kit (Biomatik), was measured. Values represent means ± SD of duplicate samples.

Table C.1. Various RBL-2H3 cell stimulation conditions before RNA extraction for PCR

Stimulation Conditions	Time of collection**	Tpsb2	Tpsab1	Tpsg1	Gzmk	Prss29	Prss41	Gzma	Prss34	Hexa	Hexb	Actb
No IgE, No Ag	24h	-	-	-	-	-	-	-	-	+	+	+
Overnight IgE, No Ag	24h	-	-	-	-	-	-	-	-	+	+	+
Overnight IgE+ 1h high*Ag	4h	-	-	-	-	-	-	-	-	+	+	+
1 hr IgE+ 1h low* Ag	24h	-	-	-	-	-	-	-	-	+	+	+
1 hr IgE+ 1h high Ag	1h	-	-	-	-	-	-	-	-	+	+	+
1 hr IgE+ 1h high Ag	4h	-	-	-	-	-	-	-	-	+	+	+
1 hr IgE+ 1h high Ag	16h	-	-	-	-	-	-	-	-	+	+	+
1 hr IgE+ 1h high Ag	24h	-	-	-	-	-	-	-	-	+	+	+
1 hr IgE, No Ag	immediately	-	-	-	-	-	-	-	-	+	+	+
1 hr IgE+ 5 min high Ag	immediately	-	-	-	-	-	-	-	-	+	+	+
1 hr IgE+ 10 min high Ag	immediately	-	-	-	-	-	-	-	-	+	+	+
1 hr IgE+ 15min high Ag	immediately	-	-	-	-	-	-	-	-	+	+	+
1 hr IgE+ 20 min high Ag	immediately	-	-	-	-	-	-	-	-	+	+	+
1 hr IgE+ 30 min high Ag	immediately	-	-	-	-	-	-	-	-	+	+	+
1 hr IgE+ 1h high Ag	immediately	-	-	-	-	-	-	-	-	+	+	+

*High Ag dose: 1 μg/mL; Low Ag dose: 0.1 μg/mL

**Time of collection: time between the end of Ag stimulation (stopped by washing) and cell harvest for Trizol® extraction.

APPENDIX D

SUPPLEMENTARY INFORMATION TO CHAPTER 5

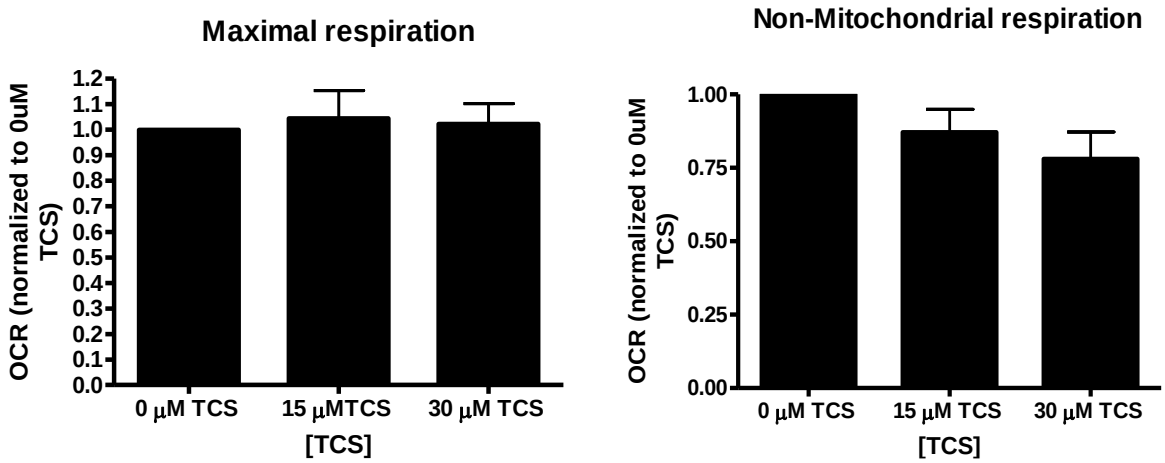

Figure D.1. Effects of TCS on maximal respiration and non-mitochondrial respiration in living zebrafish. Zebrafish embryos (24 hpf) were exposed to TCS for ~1 hr (12 measurements of basal OCR), then the Mito Stress Test kit (Seahorse Bioscience) was performed. A) Maximal respiration and B) Non-mitochondrial respiration were calculated using the Mito Stress Test Report Generator V2 (Seahorse Bioscience). Data from individual experimental days were normalized either to 0 μM TCS and values represent means ± SEM for four independent experiments, where 14-16 embryos per treatment group were tested in each experiment. One-way ANOVA with Dunnett's post-tests (compared to the 0 μM TCS) were performed using Graphpad Prism software.

Table D.1. Optimizing 24hpf ZF microinjection to measure the effect of TCS using Seahorse analyzer*

Injection conditions**	Results
Microinjection (of HSBB+ Phenol red dye["dye"] to visualize the droplet from the injector) to the yolk, which is ~80-90% of the body mass at 24hpf ZF	Needle is not readily going into the yolk. The droplets are stuck in the injection site, not being spread.
Microinjection (dye) to the vein	Impossible due to the lack of vein development at 24hpf
Microinjection(dye) to any parts of the body, excluding the yolk	Impossible due to the movement of fish (since they are not euthanized)
Microinjection(dye) into the chorion, not into the animal	More than 4nL/injection volume harms the chorion (either the chorion will be torn or ruptured when pulling off the needle). More than 40nL total (4nL/injection*10 times) leads to damage to the chorion.
Microinjection of FCCP into the chorion	40nL (4nL/injection x 10 times) of 1.7uM FCCP (final FCCP in the chorion is ~0.8uM) increased OCR with ~45% mortality. 20nL (4nL/injection x 5 times) of 2.4uM FCCP (final FCCP in the chorion is ~0.7uM) increased OCR without mortality.
Microinjection of TCS into the chorion	24nL (4nL/injection x 6 times) of 56.4uM TCS (final TCS concentration is ~19.6 uM TCS) causes ~17% mortality. 40nL (4nL/injection x 10 times) of 56.4uM TCS (final TCS concentration is ~26.5 uM TCS) causes ~25% mortality.

*Embryos are not euthanized during the injection.

** These microinjection to the ZF were also attempted by other students (Hina Hashmi and Denise Jay) in the Kim lab who are proficient in microinjection.

BIOGRAPHY OF THE AUTHOR

Juyoung Katherine Shim was born in the Republic of Korea on March 16, 1971, the first of four children born to Eui-Myung Shim and Yoem-Jun Kim. She attended Shin-Myung Girls' High School in Korea where she graduated as Valedictorian. During high school, Juyoung served as vice president of school government and won several award for Composition, English speaking, Math Olympiads, and Poetry in the regional and national levels.

Juyoung attended Hankook University of Foreign Studies (HUFS) in Seoul, Korea and graduated with a Bachelor of Arts in English and a minor in Education in March 1994. During her time in HUFS, she achieved her National Teachers Certification and served as an editor for the English department newspaper.

After Juyoung married to Changsu Lee in January 1994, they moved to Presque Isle, Maine where Changsu attended the University of Maine at Presque Isle (UMPI) in May 1994. She gave a birth to a daughter, Hana "Alexa" Lynn Lee in 1995.

After the family moved to Auburn, Maine, Juyoung attended Bates College in Lewiston, Maine and graduated *Summa cum laude* in May 2005 with a Bachelor of Science degree in Biochemistry. During her education at Bates College, she was inducted as a member of the *Phi Beta Kappa* Honor society and *Sigma Xi*. Also, she was awarded the Hoffman Research Support Grant in 2003 and the INBRE Undergraduate Research Fund in 2004 to support her scientific research.

In August 2005, she started working as scientific technician in the laboratory of Dr. Carol Kim in the University of Maine until she was promoted to research associate/lab manager in 2008. During her time in the Kim lab, she had three co-author publications and presented her

work at the American Society of Microbiology, North American Zebrafish Research Symposium, and Maine Biological and Medical Sciences Symposium.

In January 2013, Juyoung joined Dr. Julie Gosse's lab and became a PhD candidate in December 2015. During Graduate School, Juyoung taught the following courses as a Teaching Assistant: Biochemistry laboratory, Microbial genetics, Immunology laboratory, Genome Discovery I, Cell culture and techniques laboratory, and virology laboratory. She presented her work at several regional, national, and international conferences, including the Society of Toxicology (SOT) (2014-2018), Society for Environmental Toxicology and Chemistry (2016), North Atlantic Chapter of the Society for Environmental Toxicology and Chemistry (2015-2016), International Congress of Asian SOT (2015), and many others.

During her Ph.D. work, she published two first author papers and five co-author papers. Two manuscripts as a first author were submitted to *Toxicology and Applied Pharmacology* and *Journal of Applied Toxicology*. One manuscript is also being prepared from collaboration with Dr. Hayes' lab in the Psychology department.

Juyoung won the Ann Hanson Outstanding Graduate Teaching Assistant Award in 2014 and Edith M. Patch Outstanding Ph.D. student award in 2018. Nationally, she won the Mitzi and Prakash Nagarkatti Research Excellence in Immunotoxicology Award at SOT, Young Soo Choi Student scholarship award and Best Presentation award from Korean Toxicology Association in America, and Immunotoxicology specialty section Best Student Presentation award.

She lives in Bangor with her family. Juyoung became a US citizen in 2017. She is a candidate for the Doctor of Philosophy degree in Biochemistry and Molecular Biology from the University of Maine in August 2018.